NASA CR-72704
PWA FR-4000

SPACE STORABLE REGENERATIVE COOLING INVESTIGATION

Approved by J. P. Mitchell

PRATT & WHITNEY AIRCRAFT
FLORIDA RESEARCH AND DEVELOPMENT CENTER

Prepared for
NATIONAL AERONAUTICS AND SPACE ADMINISTRATION

NASA Lewis Research Center
Contract NAS3-11190
J. W. Gregory, Project Manager

Requests for copies of this report should be referred to

National Aeronautics and Space Administration
Scientific and Technical Information Facility
P.O. Box 33
College Park, Md. 20740

NASA CR-72704
PWA FR-4000

FINAL REPORT

SPACE STORABLE REGENERATIVE COOLING INVESTIGATION

Approved by J. P. Mitchell

PRATT & WHITNEY AIRCRAFT
FLORIDA RESEARCH AND DEVELOPMENT CENTER

Prepared for
NATIONAL AERONAUTICS AND SPACE ADMINISTRATION

8 OCTOBER 1971

Contract NAS3-11190

NASA Lewis Research Center
Cleveland, Ohio
J. W. Gregory, Project Manager
Liquid Rocket Technology Branch

FOREWORD

This final report for Contract NAS3-11190, "Space Storable Regenerative Cooling Investigation," was prepared by the Florida Research and Development Center of Pratt & Whitney Aircraft, Division of United Aircraft Corporation.

Engineers of the Applied Research Department at the Florida Research and Development Center who contributed to the technical effort include: A. W. Brooke, B. T. Brown, R. G. Browning, F. S. Inman, G. L. Koenig, L. Metz, T. B. Milam, J. P. Mitchell, J. W. Neal, D. J. Stout and B. C. Vennett.

The contract was administered by the Lewis Research Center of the National Aeronautics and Space Administration, Cleveland, Ohio. The NASA Project Manager was J. W. Gregory of the Chemical Rocket Division.

ABSTRACT

An experimental program was conducted to investigate performance and demonstrate regenerative cooling with flox/methane propellants at conditions suitable for a small pump-fed engine (5000-lbf thrust at 500 psia chamber pressure). Test hardware evaluated included fixed-thrust injectors, a throttling injector, water-cooled thrust chambers and regeneratively-cooled thrust chambers. The fixed-thrust injectors were tested in both water-cooled and regeneratively-cooled thrust chambers. The throttling injector was evaluated over a 5 to 1 thrust range using water-cooled chambers. Good durability was demonstrated in long duration firings by fixed-thrust and throttling injectors having concentric tube elements. Highest performance was obtained with a fixed-thrust injector using a 52-in. L* chamber; c* efficiency was above 96% over the 4 to 6 mixture ratio range and the peak measured specific impulse (with 60 to 1 expansion ratio) was slightly above 400 seconds. Regenerative cooling was demonstrated at 500 psia chamber pressure and over the 4.2 to 5.5 mixture ratio range. Good thrust chamber durability was obtained with an injector providing low thrust chamber heat fluxes. However, throat erosion occurred with a high heat flux, high-performance injector at combustion-side wall temperatures near the design value (1700° F). These results indicate that a wall temperature limit has been reached, and in future chambers, the throat station design wall temperatures will have to be decreased to obtain good durability.

CONTENTS

CONTENTS (Continued)

CONTENTS (Continued)

ILLUSTRATIONS

ILLUSTRATIONS (Continued)

ILLUSTRATIONS (Continued)

ILLUSTRATIONS (Continued)

ILLUSTRATIONS (Continued)

ILLUSTRATIONS (Continued)

ILLUSTRATIONS (Continued)

ILLUSTRATIONS (Continued)

ILLUSTRATIONS (Continued)

TABLES

TABLES (Continued)

NOMENCLATURE

Variable	Description	Units
A	Area	in.^{2}
A_{CD}	Effective area	in.^{2}
A_e	Nozzle exit area	in.^{2}
AR	Proportion of back wall that conducts heat (determines equivalent fin length)	Dimensionless
A_S	Nozzle hat band seal area	in.^{2}
A_t	Throat area	in.^{2}
$A(\epsilon^*)$	Friction similarity parameter	Dimensionless
B	Instrumentation bias limit	%
C	Coolant passage straight cut wall depth	in.
C_D	Discharge coefficient	Dimensionless
$C_{F_{vac}}$	Vacuum thrust coefficient	Dimensionless
C_{pb}	Coolant bulk specific heat	Btu/lb$_m$°R
C_S	Stream thrust coefficient	Dimensionless
c^*	Characteristic exhaust velocity	ft/sec
$c^*_{(Pc)}$	Characteristic exhaust velocity based on chamber pressure	ft/sec
$c^{*'}$	Theoretical characteristic exhaust velocity	ft/sec
D	Coolant passage depth	in.
DH	Coolant passage hydraulic diameter	in.
dQ/dA	Slope of heat transfer versus surface area curve	Btu/in.^{2}-sec

NOMENCLATURE (Continued)

Variable	Description	Units
E_1	Modulus of elasticity for combustion side wall	psi
E_2	Modulus of elasticity for structural back wall	psi
f	Fanning friction factor	Dimensionless
f_h	Friction factor with heat transfer	Dimensionless
F_{meas}	Measured thrust	lb_f
F_{vac}	Vacuum thrust	lb_f
g_c	Gravitational constant	$lb_m ft/sec^2 lb_f$
H	Coolant enthalpy	Btu/lb_m
h_c	Coolant side film coefficient	$Btu/hr\text{-}ft^2\text{-}°R$
h_g	Combustion side film coefficient	$Btu/hr\text{-}ft^2\text{-}°R$
ID	Internal diameter	in.
I_{vac}	Vacuum specific impulse	$lb_f\text{-}sec/lb_m$
I'_{vac}	Theoretical vacuum specific impulse	$lb_f\text{-}sec/lb_m$
J	Mechanical equivalent of heat (778.161)	$ft\text{-}lb_f/Btu$
K_w	Thermal conductivity of wall material	Btu/hr-ft-°R
ℓ	Combustion effective length	in.
L*	Combustion chamber characteristic length	in.
$\dot{M}$	Coolant fuel flowrate	lb_m/sec
N_s	Number of cooling passages	Dimensionless

NOMENCLATURE (Continued)

Variable	Description	Units
OD	External diameter	in.
P	Coolant pressure	psia
P_a	Ambient pressure	psia
P_c	Measured chamber pressure	psia
P_{diff}	Diffuser pressure	psia
Pr_b	Coolant bulk Prandtl number	Dimensionless
P_s	Nozzle separation pressure	psia
P_t	Throat total pressure	psia
ΔP	Pressure drop	psid
ΔP_f	Fuel injector pressure drop	psid
ΔP_p	Primary oxidizer injector pressure drop	psid
ΔP_s	Secondary oxidizer injector pressure drop	psid
ΔQ	Incremental heat transfer rate	Btu/hr
Q	Thrust chamber heat transfer rate	Btu/sec
q/A	Heat flux	Btu/ft^2-hr
Q_c	Combustion chamber heat transfer rate	Btu/sec
R	Chamber radius	in.
r	Mixture ratio	Dimensionless
Re_b	Coolant bulk Reynolds number	Dimensionless
s	Space between passages	in.
St	Stanton number	Dimensionless
S_{x_i}	Precision error associated with the ith variable	%

NOMENCLATURE (Continued)

Variable	Description	Units
S_ϕ	Precision	%
T	Temperature	°R
T_{aw}	Adiabatic wall temperature	°R
T_b	Coolant bulk temperature	°R
T_w	Chamber wall temperature	°R
$\bar{T}_{w_1}$	Average combustion-side hot wall temperature	°R
$\bar{T}_{w_2}$	Average structural back wall temperature	°R
T_{wc}	Coolant-side wall temperature	°R
T_{wg}	Combustion-side wall temperature	°R
U	Coolant velocity	ft/sec
U_ϕ	Uncertainty	%
VH	Velocity head	lb_f/ft^2
W	Passage width	in.
$\dot{W}$, $\dot{W}_c$	Total coolant flowrate	lb_m/sec
$\dot{W}_f$	Total fuel flowrate	lb_m/sec
$\dot{W}_p/\dot{W}_t$	Oxidizer flow split	Dimensionless
$\dot{W}_o$	Total oxidizer flowrate	lb_m/sec
X	Distance along coolant passage	in.
ΔX	Increment of length	in.
α_1	Coefficient of thermal expansion for combustion side wall	deg^{-1}
α_2	Structural back wall thickness	deg^{-1}

NOMENCLATURE (Continued)

Variable	Description	Units
δ	Wall thickness	in.
δ_1	Combustion side wall thickness	in.
δ_2	Structural back wall thickness	in.
ϵ	Nozzle expansion ratio, Absolute passage surface roughness	Dimensionless, in.
ϵ_c	Chamber contraction ratio	Dimensionless
ϵ^*	Friction similarity parameter	Dimensionless
$\eta_{CF_{vac}}$	Vacuum thrust coefficient efficiency	%
$\eta_{c^*(F)}$	Characteristic exhaust velocity efficiency based on thrust	%
$\eta_{c^*(P_c)}$	Characteristic exhaust velocity efficiency based on chamber pressure	%
η_{fin}	Fin efficiency	%
η_{Ivac}	Vacuum specific impulse efficiency	%
θ	Wall deflection angle	deg
μ_b	Coolant viscosity evaluated at bulk temperature	lb_m/ft-sec
μ_w	Coolant viscosity evaluated at wall temperature	lb_m/ft-sec
ρ_b	Coolant density evaluated at bulk temperature	lb_m/ft^3
ρ_w	Density evaluated at wall temperature	lb_m/ft^3
σ_B	Bending stress	psi
σ_S	Shear stress	psi
σ_T	Tensile stress	psi
σ_{TH}	Thermal stress	psi

NOMENCLATURE (Continued)

Variable	Description	Units
σ_y, σ	Yield strength	psi
σ_u	Ultimate strength	psi
χ	Pressure Load Parameter	Dimensionless

SECTION I
INTRODUCTION

The high energy space storable class of liquid propellants is very attractive for future long duration interplanetary missions because of the substantial payload increases offered when compared with earth storable propellants. Space storable propellants are dense, have high specific impulse, and provide hypergolic ignition characteristics. By definition, the fuel and oxidizers have high enough boiling points and sufficiently compatible liquid temperature ranges for long-term space storage. Typical space storable propellant combinations include: (1) the light hydrocarbon fuels such as methane, ethane, and propane, together with either oxygen difluride or fluorine-oxygen mixtures (flox), (2) diborane with oxygen difluoride and (3) the hydrazine base fuels with fluorine. Within this group the light hydrocarbon fuels are the only ones that can provide the active thrust chamber cooling capability required to permit reliable long duration operation. The hydrocarbon fuels are also good turbine working fluids and hence can be used in pump-fed systems operating at higher combustion chamber pressures than other space storable fuels. This characteristic results in a performance advantage for the light hydrocarbon fuels because, within a given envelope, expansion ratio can be increased directly with chamber pressure.

The objective of the work reported herein, which was conducted under Contract NAS3-11190, was to investigate the regenerative cooling capabilities and performance of the light hydrocarbon fuels when used with fluorinated oxidizers at chamber pressures suitable for low-thrust pump-fed engines. The program tasks are given in table I. The first task involved an analytical study to determine regenerative cooling limits for methane, ethane, propane, Butene-1, and a methane-ethane fuel blend when used with flox and OF_2. The chamber pressure range of 100 to 1000 psia and the thrust range from 1000 to 20, 000-lb were considered. Because methane was shown to have good regenerative cooling capabilities (and it has, when combined with flox, the highest theoretical specific impulse of the light hydrocarbon/fluorinated oxidizer propellant combinations), flox/methane was selected as the propellant combination for subsequent experimental evaluations under Tasks II through VII.

The results of the Task I analytical studies were presented in reference 1. Experimental work accomplished under Tasks II through VII is described in this report. The design point conditions for the program test hardware were 5000-lb_f thrust and 500-psia chamber pressure. Injectors and water-cooled thrust chambers were designed, fabricated, and test-fired in initial experimental efforts (Tasks II, III, and IV) to develop a high performance fixed-thrust injector and to obtain thrust chamber heat transfer data. A regeneratively cooled chamber was subsequently designed (using heat transfer data from the water-cooled chamber tests), fabricated, and tested under Task V. Under the remaining two tasks (Tasks VI and VII) a dual orifice throttling injector was designed, built, and tested.

Table I. Contract NAS3-11190 Program Tasks

Task	Description
I	Regenerative Cooling Analysis
II	Hardware Design and Analysis
III	Fixed Thrust Injector Development Tests
IV	Water-Cooled Chamber Altitude Tests
V	Regenerative Cooled Chamber Tests
VI	Throttling Injector Design and Fabrication
VII	Throttling Injector Tests

Detailed discussion of the program effort is provided in the remaining sections of this report. To facilitate presentation, it has been organized by hardware type rather than task item. The fixed-thrust injector hardware and water-cooled thrust chamber hardware are described in Sections IV and V respectively, and Section VI discusses the testing in which they were both evaluated. Regeneratively cooled thrust chamber hardware is described in Section VII, with testing covered in Section VIII. Sections IX and X are devoted to the throttling injector.

Both the water-cooled and regeneratively cooled thrust chambers built under the program were of THERMAL SKIN® construction. THERMAL SKIN is a registered trade name for an advanced nontubular thrust chamber concept developed by P&WA. THERMAL SKIN chambers consist of circumferential segments like barrel staves (figure 1) each of which is a bonded sandwich of two or more plates into which coolant passages are chemically etched. Details of the design and fabrication of the THERMAL SKIN chambers are given in this report.

The dual orifice injector evaluated in the program uses a throttling concept that P&WA evolved from turbojet fuel injection systems. The feasibility of dual orifice injectors for rocket engine applications has been demonstrated in past Air Force sponsored contracts and independent P&WA research programs. The injector designed in this program was based heavily on this previous experience. The dual orifice injection principle and P&WA's experience are described in Section IX.

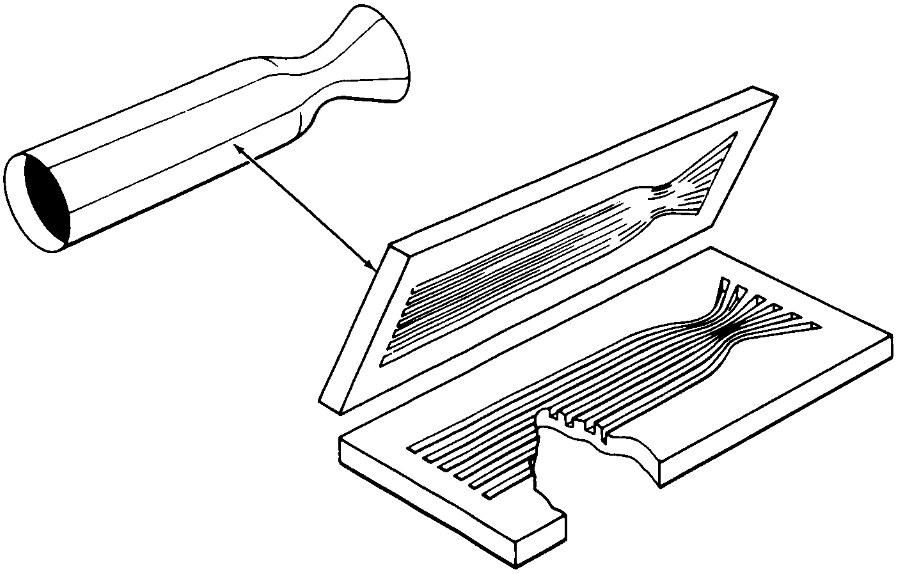

Figure 1. THERMAL SKIN® Thrust Chamber Construction

FD 27348

SECTION II
SUMMARY

This report describes the results of an experimental program conducted to demonstrate high performance injectors, for fixed-thrust and throttling, and regenerative thrust chamber cooling with flox/methane propellants at conditions of interest to NASA for a small pump-fed engine (5000-lb_f thrust at 500-psia chamber pressure).

In initial experimental efforts, fixed-thrust injectors were designed and tested in a water-cooled thrust chamber instrumented to permit determination of axial and circumferential heat flux profiles. Two injector types, a concentric-element and a four-oxidizer-on-one-fuel, pentad-element were evaluated in the effort. Because the intended use of these injectors was with a regeneratively cooled thrust chamber, both were designed for injection of the methane fuel as a gas. The concentric-element injector had swirlers for the liquid oxidizer and concentric fuel orifices configured to provide "converging fuel streams." Both of these features were provided to enhance flox atomization.

The pentad was eroded severely in its first test and no performance data were obtained with it. The converging fuel stream injector was tested with three different fuel faceplates, with two different combustion chamber characteristic lengths (L*'s of 30 and 52 in.), and over the 4 to 6 mixture ratio range. It proved to be very durable and, with a low porosity (40 scfm) Rigimesh faceplate in the longer L* chamber, provided a c* efficiency of 96.2% at a mixture ratio of 5.75, to slightly exceed the performance goal of the contract. Performance increased with decreasing mixture ratios, but decreased with (1) a reduction in chamber L* from 52 to 30 in. and (2) an increase in the faceplate porosity.

Thermal data obtained in the initial injector tests showed that heat transfer rates for a given injector configuration were nearly independent of mixture ratio but that the level can be changed dramatically by modifications to the injector. For example, the converging fuel stream injector with a low porosity (40-scfm) Rigimesh faceplate demonstrated a chamber heat transfer rate that was 90% of the theoretical level* at a mixture ratio of 5.0, whereas with a higher porosity (100-scfm) Rigimesh faceplate, the heat transfer was decreased to 65% of the theoretical level. This reduction was realized with only about a 1% performance degradation.

Later in the program, another concentric-element injector in which the spuds near the OD were "scarfed" to divert the oxidizer spray away from the chamber wall was designed and two configurations, with different extents of scarfing were tested. Reductions in chamber heat fluxes from those demonstrated by the converging fuel stream injector were realized as a result of the scarfing and furthermore, the reductions were a direct function of the degree of spud scarfing. The degree of scarfing had no significant effect on performance. Essentially the same performance was demonstrated by both scarfed configurations; however, the level was lower than that of the converging fuel stream configuration. These results, together with those obtained with the converging fuel

---

*Based on Bartz Short-form Prediction

stream injector, illustrate the type of injector modifications that can be employed to tailor chamber heat transfer rates in future regenerative thrust chamber work.

Regenerative cooled thrust chambers tested in the program were designed for the heat transfer rates measured in the water-cooled chamber tests with the highest performance injector configuration. THERMAL SKIN® construction was used exclusively. One chamber was fabricated as part of the contracted program and two chambers were fabricated independently. Because the chambers fabricated independently by P&WA were tested with contract injectors, the results obtained are included herein. Fabrication methods and techniques were progressively improved while constructing the three chambers. Two improvements made in fabrication methods that are noteworthy are those used for joining etched plates and for joining the circumferential elements (or staves) on their edges. Initially the etched plates were brazed together; however, diffusion bonding was ultimately used as a means of eliminating the relatively low temperature braze joint. Braze joints are vulnerable to overheating in subsequent welding operations and contribute to coolant passage-to-passage flow variations because the braze filler material fillets indiscriminately in coolant passage corners. Regarding the stave edge joining methods, the edges were manually Tungsten-Inert-Gas (TIG) welded in the first chamber. Electron Beam (EB) welding was demonstrated for the application and eventually substituted in later chambers because it is more controllable, provides a narrow full penetration weld, and results in less heat input to the part.

In tests with the first two thrust chamber assemblies, seam erosion problems were encountered. The erosion was attributed to abnormally large distances between passages at the seams, aggravated by low coolant flow in some of the passages adjacent to the seams. Additional cooling was provided in the seam areas at the throat of the third thrust chamber assembly (which was of sectional construction). With this latter chamber, good durability was demonstrated at mixture ratios up to 5.5 using a lower-heat-flux, scarfed element injector configuration. However, throat erosion did occur in a later test with the converging fuel stream injector that produced wall temperatures nearly equal to the maximum design value (1700° F). These results indicate that a wall temperature limit for the nickel combustion-side material in the flox/methane combustion environment has been reached and that, in future chamber designs, wall temperatures will have to be reduced to achieve good durability with high performance injectors. Since good durability was demonstrated at wall temperatures of 1400°F in the program, the safe design wall temperature has at least been bracketed.

High specific impulse levels and thrust coefficient efficiencies were demonstrated in simulated altitude tests with water-cooled and regeneratively-cooled thrust chambers of 60 to 1 expansion ratios. The converging fuel stream injector with the 40-scfm Rigimesh faceplate provided highest performance. In water-cooled chamber tests with this injector, the measured vacuum specific impulse was above 389 sec over the 4 to 6 mixture ratio range and the peak value was 396 sec at a mixture ratio of 5.0. At approximately the same mixture ratio, but in a regenerative chamber test with the same injector, the measured specific impulse was 400.3 sec. With this injector and others, thrust coefficient efficiency data obtained in the program indicate that nozzle kinetic losses are approximately 1% or less at 500 psia chamber pressure.

A dual orifice throttling injector was designed, fabricated and tested with a water-cooled chamber as the final part of the program. The injector was a concentric-tube design into which dual orifice elements were incorporated to provide the throttling feature. The dual orifice injector was evaluated in long duration firings at chamber pressures of 500, 250, and 100 psia. Stable combustion was achieved at all chamber pressures, but performance was low at 100-psia chamber pressure. At the 100 psia chamber pressure level and a mixture ratio of approximately 5.0, c* efficiency was only 88%. At a comparable mixture ratio, but at higher chamber pressures (500 and 250 psia), c* efficiency was at a respectable level (96%). These results indicate that additional work is required to achieve acceptable performance for throttling with the flox/methane propellant combination.

SECTION III
CONCLUSIONS

1. High delivered impulse performance can be obtained with the flox/methane propellant combination. High c* efficiencies are achievable with good injector design; furthermore, nozzle kinetic losses are approximately 1% or less and thus high thrust coefficient efficiencies are also obtainable.

2. Injector design has a dramatic effect on thrust chamber heat transfer rates. Injector features that reduce local mixture ratios near the thrust chamber wall in relation to the nominal operating value can effect significant reductions in heat transfer from the theoretical level.

3. Regenerative cooling using methane at the low thrust (5000-lb_f), moderately high chamber pressure (500-psia) conditions evaluated in the program is feasible. With chamber heat fluxes near theoretical values in some chamber locations (using the highest performance injector), the methane fuel had sufficient heat capacity to maintain the coolant exit temperature at a tolerable level.

4. A regeneratively cooled THERMAL SKIN® thrust chamber is practical with flox/methane propellants. Good chamber durability was demonstrated in the program with combustion-side wall temperatures up to 1400° R, but throat erosion was noted at wall temperatures near the design value of 1700° R. Thus these temperature levels bracket the safe design wall temperature for THERMAL SKIN chambers constructed using nickel as the combustion-side wall material, and a lower design value must be used.

5. Dual orifice injectors can provide throttling capability with flox/methane propellants. Stable combustion was achieved over a 5 to 1 thrust (and chamber pressure) range in the program. Performance was at acceptable levels at the higher chamber pressures (500 and 250 psia), but it dropped to a low level at 100-psia chamber pressure and thus additional throttling injector work is needed to overcome this deficiency.

SECTION IV
FIXED THRUST INJECTOR HARDWARE

A. GENERAL

Three fixed-thrust injectors were designed, fabricated and tested in the program. The objective of the effort was the development of an injector that would be suitable for use with a regenerative cooled thrust chamber. The design point thrust and chamber pressure levels were 5000 lb_f thrust and 500 psia chamber pressure. The performance goal for the injector was a characteristic exhaust velocity efficiency of 96% of the theoretical shifting equilibrium value at the optimum mixture ratio (5.75) for the highest theoretical specific impulse performance for flox/methane propellants. Because of their intended use with a regenerative thrust chamber, the injectors were designed for injection of the methane fuel as a gas. In this section, the fixed-thrust injectors are described, and injector design considerations and water flow tests made during the program are discussed.

B. DESCRIPTION

Two of the injectors had concentric-tube type injection elements and the third had four-oxidizer-on-one-fuel pentad elements. The concentric element injectors (figures 2 and 3) had 65 elements and the pentad injector (figure 4) had 68 elements. Injector characteristic dimensions and operating conditions are summarized in table II.

Fuel gap spacers and hydraulic swirler caps were utilized on both concentric tube injectors. The spacers keep the oxidizer spuds concentric with the fuel orifices. The hydraulic swirlers represent an adaptation of a design that has been used successfully by P&WA in high pressure O_2/H_2 injectors. The swirler caps have three slots that are machined from their OD to meet the ID tangentially. The cap ID is equal to the spud ID and hence the flox flow through the slots sets up a strong vortex flow in the spud, which in turn provides a spray of finely atomized droplets of uniform size upon injection. Each of the swirler caps is an individual part brazed into the back of the spud plate. Use of separately fabricated caps facilitates flow distribution control through selective assembly, since each cap can be flow checked before being used in an injector. By fabricating more caps than required it was possible to select caps whose flow calibrations matched within ±2% for the first assembly (converging fuel injector). In the second (scarfed element) assembly, the variation was reduced to ±1%.

In the converging fuel stream injector (figure 2), the fuel is injected so that it converges onto the oxidizer stream to enhance atomization. In the scarfed element injector, the fuel is injected axially. Spud scarfing was used as a means of altering spray patterns so that the oxidizer from the outer row elements was diverted away from the chamber wall to reduce heat transfer rates. Two configurations of the scarfed spud injector were evaluated. Originally (configuration I) the spuds in the outer two rows were scarfed; the scarf angle for the outer row (fourth row) was 45 deg while that for the third row was 22.5 deg. For configuration II, the injector was reworked to reduce the spud scarf angles. The scarf angle of the outside row was reduced from 45 deg to 22.5 deg and spud scarfing of the third row was eliminated (i.e., the spuds in the third row were machined flush).

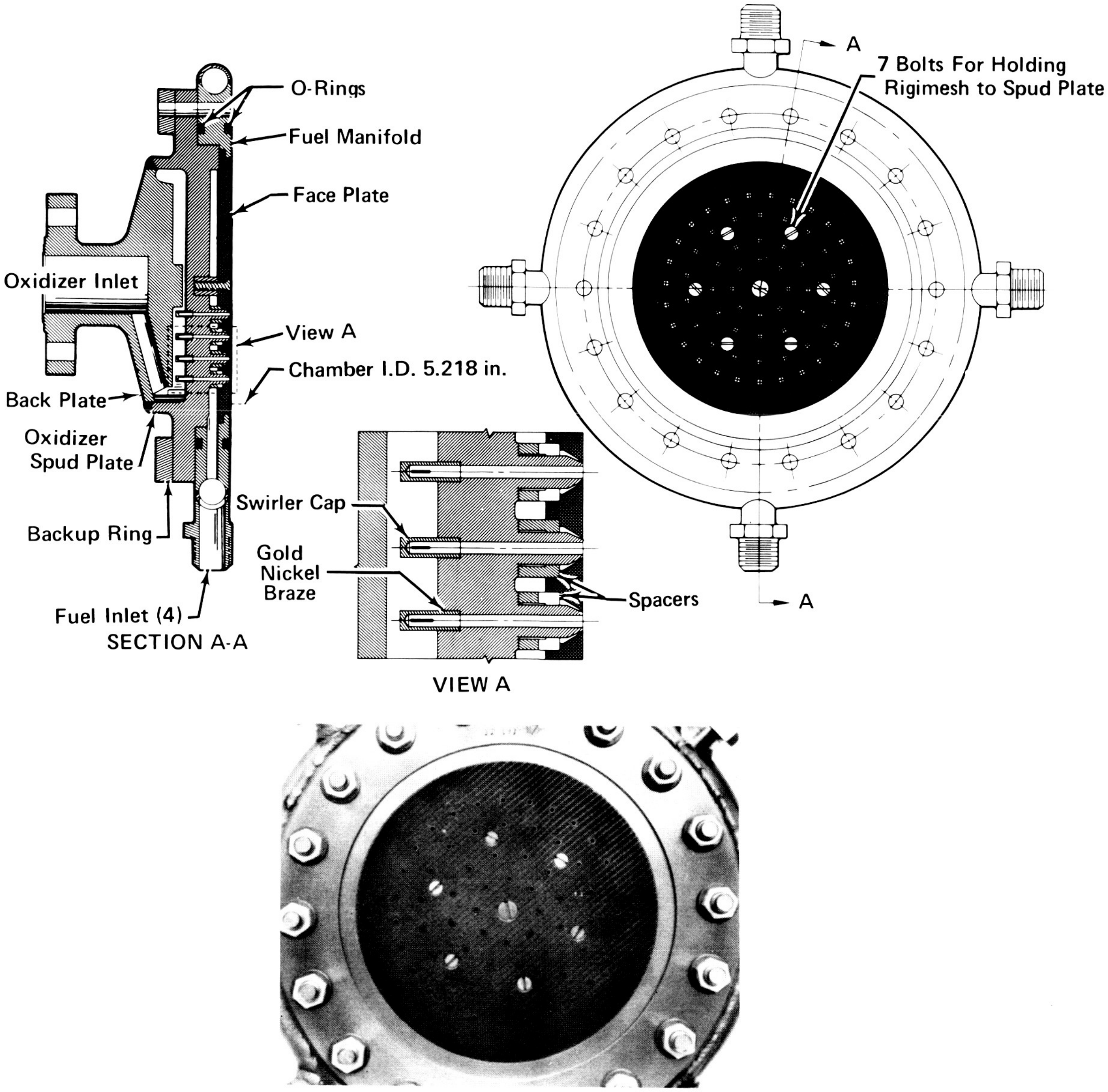

Figure 2. Converging Fuel Stream Injector FD 23566A

For all injectors, the oxidizer spud plates were constructed of nickel because of its good fluorine compatibility. The backplates were constructed of Inconel for strength and were welded to the spud plate with a circumferential weld.

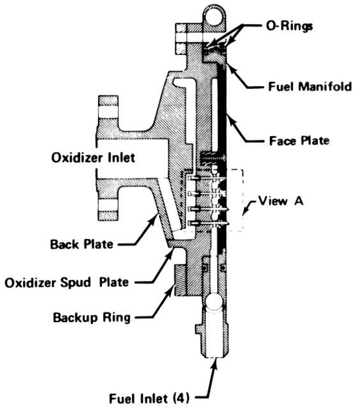

SECTION A-A

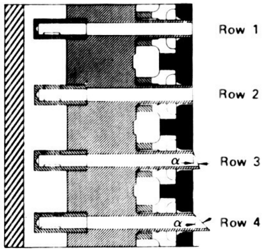

View A

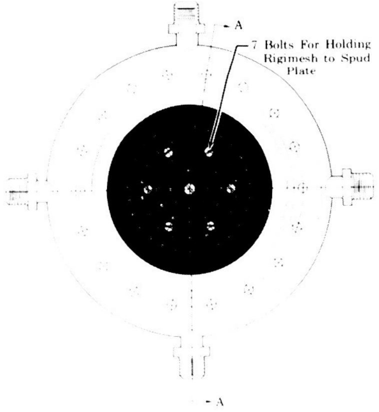

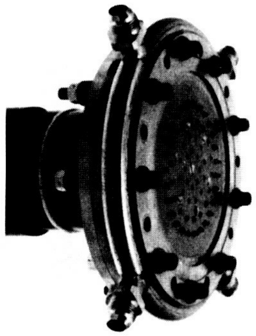

Configuration I

Scarf Angle (α)

Configuration	Row			
	1	2	3	4
I (Original Build)	0*	0	22.5	45
II	0	0	0	22.5

* α = 0 Is Equivalent to Spud Ends Being Flush to Faceplate.

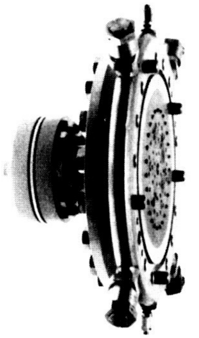

Configuration II

Figure 3. Scarfed Element Injector

FD 27943

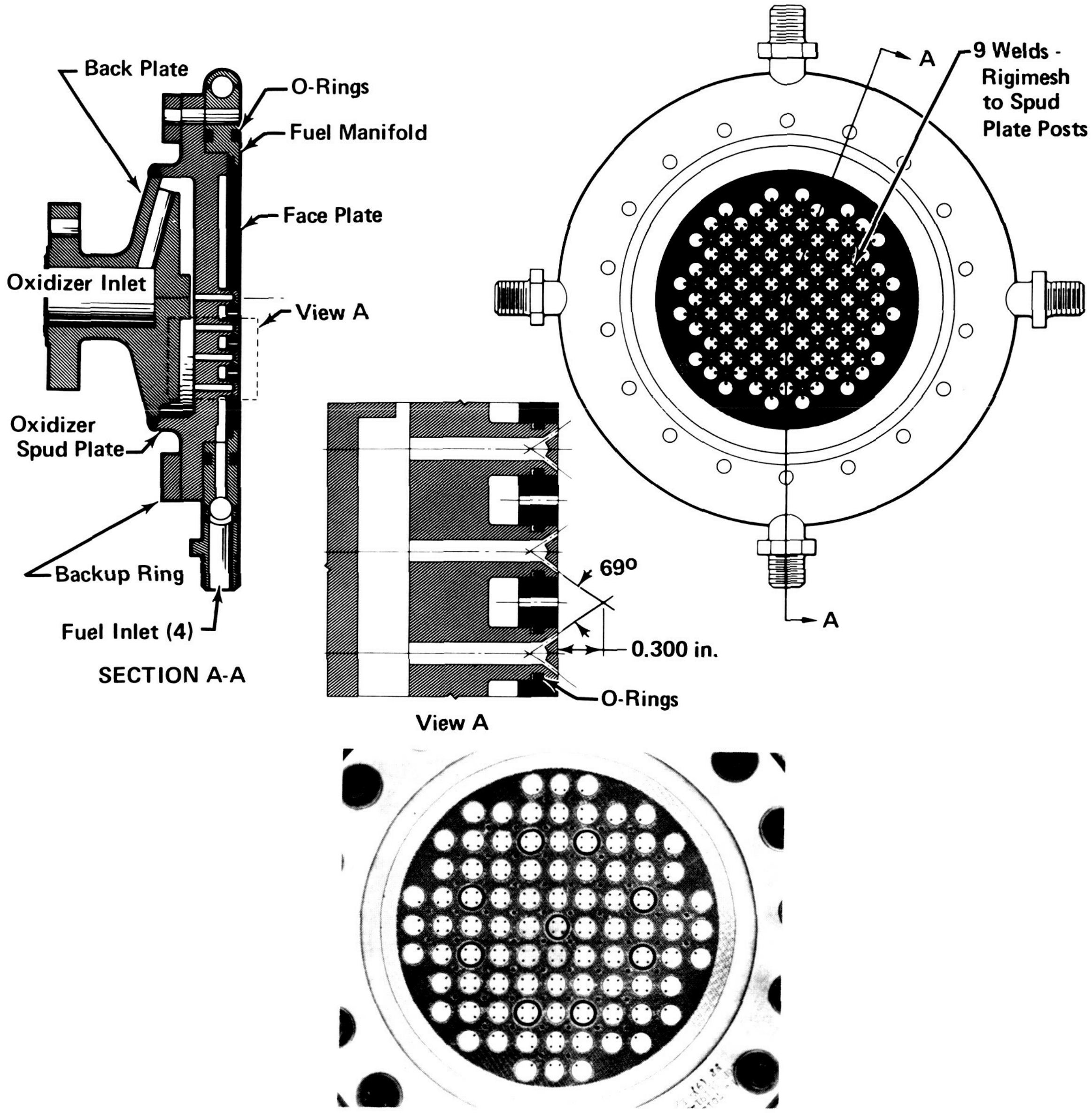

Figure 4. Pentad Injector FD 23567A

Mechanical features differed with respect to the method of attachment of the faceplate to the oxidizer spud plate. In the concentric element injectors, seven screws were used for the attachment, while in the pentad injector, welds around nine of the oxidizer posts provided attachment. Thus in the swirler injectors, the fuel parts can be disassembled from the oxidizer to facilitate cleaning and passivation. The fuel manifold, the fuel faceplate, and the fuel gap spacers are a bolt-on type. In the pentad injector, because the faceplate is welded to the oxidizer posts, disassembly requires machining.

Table II. Fixed-Thrust Characteristics, Dimensions, and Operating Conditions

	Converging Fuel Stream	Scarfed Element	Pentad
Oxidizer orifice diameter, in.	0.082	0.095	0.032
Oxidizer swirler slot area to orifice area ratio	1.0	1.0	-
Fuel orifice dimension, in.	0.007 (gap)	0.009 (gap)	0.060 (diameter)
Number of elements	65	65	68
Design oxidizer injector pressure drop*, psi	135	65	135
Design fuel injector pressure drop*, psi	200	100	200
Design fuel-to-oxidizer momentum*	2.0	2.0	2.0

*Mixture ratio = 5.75

The design was intended primarily for use of porous faceplates, although an alternate solid copper faceplate was tested. The porous material used was Rigimesh*, which is available in varying porosities. Table III lists the faceplates that were built for each injector. The alloy, from which the Rigimesh was formed was N-155 Multimet (an iron base alloy), which is the same material that has been used successfully in RL10 injectors. With the 40-scfm faceplates, approximately 15% of the fuel is injected through the Rigimesh for transpiration cooling. The flow is proportionally higher for the 100-scfm faceplate. All faceplates have a machined step at their OD which fits into a mating step at the fuel manifold ID. A tight fit between the two parts minimizes leakage at the faceplate OD.

C. DESIGN

Several injector design guidelines were established, based on experience obtained in previous injector research programs involving the flox/light hydrocarbon fuel propellant combinations, at lower chamber pressures and fluorine/hydrogen at comparable to, or higher than, the design chamber pressure (500 psia). These guidelines were:

1. The oxidizer injector should be designed to utilize the flox injection momentum for self-atomization. In flox/methane tests using RL10

---

*Rigimesh is a registered trade name for a woven and sintered wire mesh material made by Aircraft Porous Media, Inc., Glen Cove, N.Y.

injectors at 250-psia chamber pressure, significant improvements were achieved by incorporation of swirlers in the oxidizer orifices of the concentric tube elements to enhance atomization (reference 2).

2. The maximum number of injection elements that can be incorporated into the injector face should be used to minimize the flox orifice size, thereby enhancing atomization. A maximum injector element density configuration also minimizes element spacing which, in turn, leads to good interelement gas phase mixing (reference 3).

3. The fuel-to-oxidizer injection momentum ratio should be high. High momentum ratios, and hence high-velocity-fuel streams, enhance flox atomization and intra-element mixing. In practically all past programs with both fluorine/hydrogen and flox/light hydrocarbon propellants, involving liquid-liquid and gas-liquid injection and both impingement and concentric tube injectors, a general trend of increasing performance with increasing fuel-to-oxidizer injection momentum ratio has been observed (references 2, 4, 5, 6, 7, 8, and 9).

4. The injector should have a flat injection mixture ratio profile. A uniform mixture ratio distribution at the injection plane improves performance and reduces the requirements for downstream interelement mixing. With F_2/H_2 propellants (reference 9), it was found that tailoring of the fuel and oxidizer injection orifice discharge coefficients, to ensure a flat mixture ratio profile, is a prerequisite for achievement of high c* performance at high mixture ratios. A flat injection mixture ratio profile is considered to be even more important for flox/methane at its optimum mixture ratio (5.75), because the theoretical characteristic exhaust velocity curve peaks rather sharply at this mixture ratio value and, therefore, deviations in either an oxidizer-rich or oxidizer-lean direction will produce a performance loss.

Table III. Fixed-Thrust Injector Faceplates

Injector	Faceplates
Converging Fuel Stream	40-scfm* Rigimesh 100-scfm Rigimesh Solid Copper
Scarfed Element	40-scfm Rigimesh 100-scfm Rigimesh 40-100-scfm Rigimesh Solid Copper
Pentad	40-scfm Rigimesh 100-scfm Rigimesh

*Flowrate of air per square foot at a pressure drop of 2 psid.

The concentric tube and pentad injection elements were selected based on the foregoing design guidelines and single-element water flow tests (the results of which are given in paragraph E below). For these configurations, preliminary injector layouts were then accomplished to determine the maximum element density that could be achieved. It was found that because of the combined effect of a moderately high chamber pressure (500 psia) and a relatively low thrust level (5000 lb$_f$), the maximum injector element density that could be achieved in the small-face-area injector would be approximately 3 elements/in.^{2}. Based on these results and the Task I heat transfer studies, that showed the chamber heat transfer to be reduced at higher contraction ratios, a contraction ratio of 4 (and a corresponding face diameter of 5.20 in.) was subsequently selected. With this contraction ratio, the thrust/element size can be kept at a low level (approximately 75 lb$_f$ thrust/element), and thus in a range conducive to high performance. Figure 5 illustrates the design point.

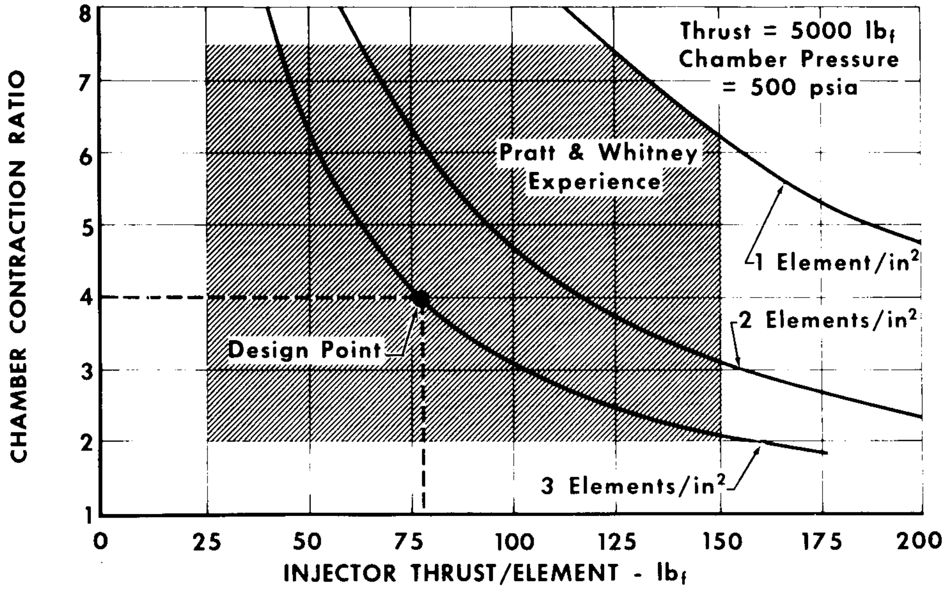

Figure 5. Relationship Between Chamber Contraction Ratio, Injector Element Density and Injector Thrust/Element GS 10674

The injector pressure drops were set based on stability and atomization considerations, and the desire to have a high fuel-to-oxidizer injection momentum ratio. Since the intended application for these injectors was in a pump-fed engine, pressure drops could be higher than those in pressure-fed engine injectors. The oxidizer injector design pressure drop was 135 psi at a mixture ratio of 5.75 for the converging fuel element injector and the pentad injectors. The corresponding design pressure drop for the oxidizer side of the scarfed-element injector was 65 psi. It was set at a lower level to accommodate operation at chamber pressures up to 1000 psia. With these relatively high pressure drops, chugging-type instability should not occur; furthermore, as will be shown below, atomization should be adequate. The fuel injector drop was set so that the fuel-to-oxidizer injection momentum ratio would be 2.0 at a mixture ratio of 5.75. This resulted in a design fuel pressure drop of approximately 200 psi for the converging fuel stream and pentad injectors and 100 psi for the scarfed-element injector.

The levels of atomization provided by the selected injector elements were calculated using the relationships compiled by Northern Research for P&WA. A correlation derived for two impinging streams (a doublet) was used to provide a representative atomization level for the pentad element, which had four liquid streams impinging. The calculated mean droplet diameters for the injectors at design point conditions were:

Converging fuel stream injector	80 microns
Scarfed-element injector	108 microns
Pentad injector	116 microns

All of these values were derived neglecting the atomizing effect of the gaseous fuel. The atomization requirements for complete vaporization of the flow were established using the effective length vaporization criterion of Priem and Heidmann (reference 10). From this reference, the vaporization curves given in figure 6 were derived as a function of mean droplet size and drop size distribution; the latter factor is characterized by standard deviation, σ .* The droplet size distribution for hydraulic swirlers has been measured by the Delavan Manufacturing Company for P&WA. The results show that the distribution corresponds to that described by a standard deviation of 1.5. From this result and from figure 6, it can be concluded that the hydraulic swirlers used on the converging fuel stream and scarfed-element injectors will provide adequate atomization. Although the drop size distribution for impingement elements has not been measured by P&WA, reference 10 indicates that these sprays have σ's between 1.5 and 3.7. For this range of standard deviations, the mean droplet size is small enough, (figure 6) that complete vaporization should also be obtained with the pentad element.

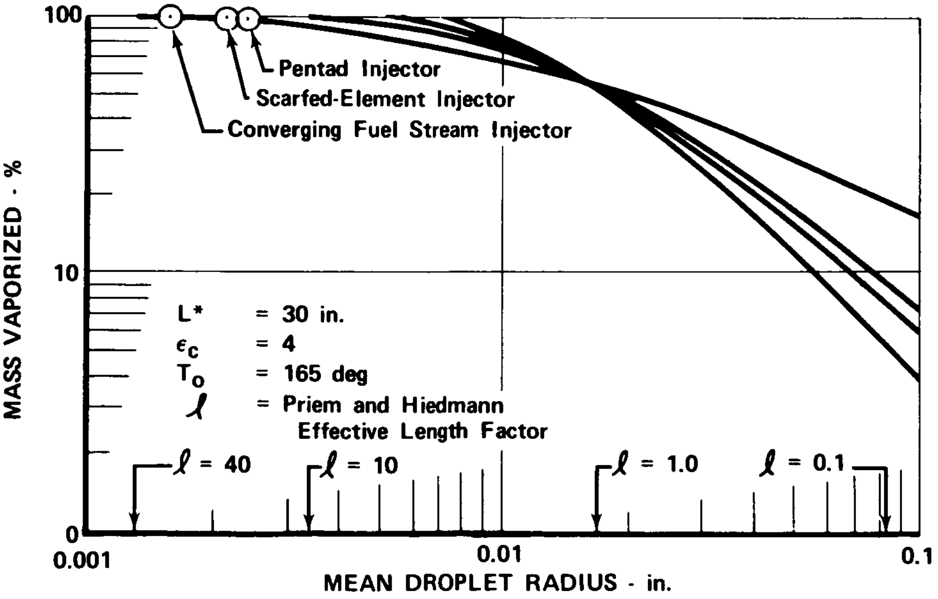

Figure 6. Vaporization Curves for Flox GS 10676B

---

*With a standard deviation (σ) of 1.0, all droplets in the spray would be the same size. Larger values of σ correspond to a larger range of droplet sizes. For example, with a spray distribution of $\sigma = 3.7$, an appreciable portion of the total mass (4%) is in droplets that are 10 times the median droplet size.

A flat mixture ratio injection profile was another desirable feature for the injectors. To achieve flat mixture ratio profiles in the concentric element injectors, the swirler caps on the outer row near the chamber wall were designed with slightly higher (10%) discharge coefficients (C_D) than those on the inner rows. These larger C_D swirlers inject proportionally more flox flow through the outer row, which compensates for the fuel flow that is injected through the permeable faceplate between the outer row and the chamber wall. In the pentad injector, special tailoring of the orifice sizes was not required to achieve a nearly flat injection mixture ratio profile.

D. INJECTOR COLD FLOW TESTS

Injector cold flow tests were made to obtain spray pattern photographs, calibration data, and mass and mixture ratio profiles. Figure 7 shows photographs of the injector spray patterns at approximately operating pressure drops. Included are (1) photographs of the injectors with water flow through the oxidizer sides only and (2) photographs of spray patterns obtained with gaseous nitrogen flowing through the fuel side and water flowing through the oxidizer sides of the injectors. These photographs illustrate (1) the enhancement of atomization by gas injection and (2) the effect of spud scarfing on the spray pattern.

The injectors were calibrated to determine the effective flow areas of (1) the oxidizer injector, (2) the fuel injector, and (3) the Rigimesh faceplates. Oxidizer injector calibration was accomplished using water; gaseous nitrogen was used to calibrate the fuel injector and the Rigimesh. In the Rigimesh calibrations, the fuel injector orifices were plugged. The effective flow areas determined during the calibration tests are given in table IV. Variations of the measured values from the design values are due to deviations in discharge coefficients, dimensions and Rigimesh permeability from design values.

The measured discharge coefficients for the swirler caps used in the concentric tube injectors were about 10% lower than the design values. (See table V.) The design values were obtained from measured discharge coefficients for swirler caps having the same slot-to-orifice (cap ID) area ratio, but different slot and orifice dimensions, which apparently caused the design and actual coefficients to disagree. Figure 8 presents a correlation of the swirler discharge coefficients with swirler slot-to-orifice area ratio obtained in this program.

On the fuel side, differences between design and actual effective flow areas are the result of variations in fuel gap size, Rigimesh porosities, and discharge coefficients from design values. For example, in the converging fuel stream injector, the OD of the oxidizer spuds were machined to the small side of the tolerance, resulting in the average fuel gap being slightly larger than the design value.

A patternator (figure 9) was used in the cold flow tests to investigate mass and mixture ratio profiles. The patternator has 20 sections formed by five concentric rings, each divided into four 90-deg segments. Mass flow profiles were obtained by injecting water through the oxidizer and fuel sides of the injector in separate tests. Figures 10 and 11 show the oxidizer and fuel injection profiles obtained at the injection plane for the three injectors. In most cases, the profiles compare favorably with the constant mass flux design curve. The mixture ratio profiles (figure 12) were obtained from the fuel and oxidizer mass flux profiles.

Converging Fuel Stream Injector

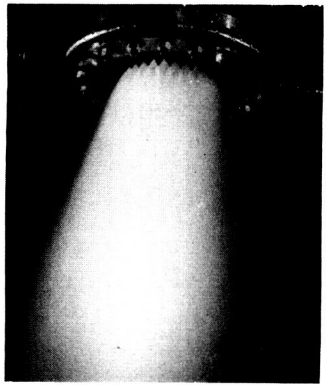
FE 76315

Oxidizer Injector, Water Flow
(ΔP = 150 psid)

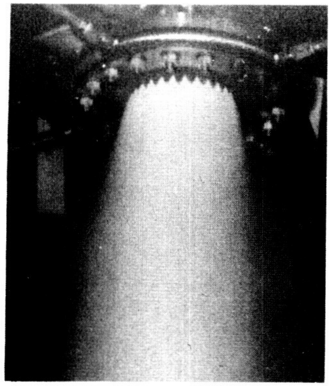
FE 76725

Combined Flow
(Oxidizer Injector ΔP = 150 psid,
Fuel Injector ΔP = 150 psid)

Pentad Injector

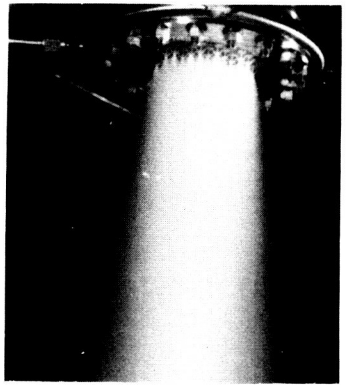
FE 76892

Oxidizer Injector, Water Flow
(ΔP = 150 psid)

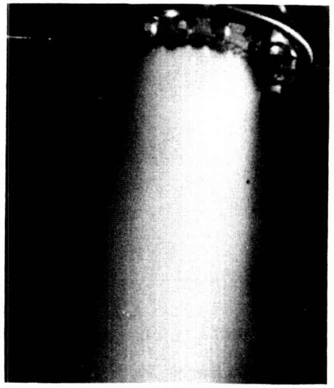
FE 76928

Combined Flow
(Oxidizer Injector ΔP = 150 psid
Fuel Injector ΔP = 150 psid)

Scarfed Element Injector (Configuration I)

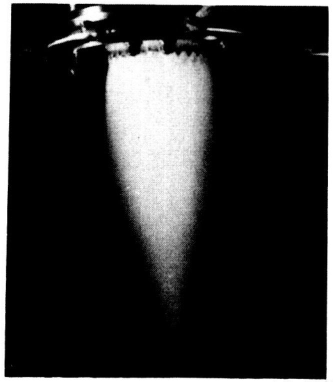
FE 85601

Oxidizer Injector, Water Flow
(ΔP = 50 psid)

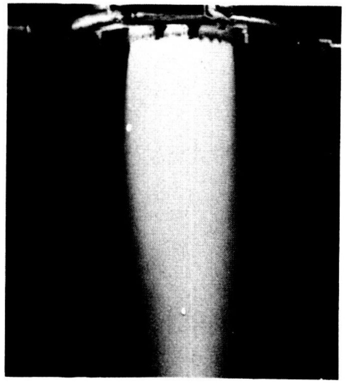
FE 85603

Combined Flow
(Oxidizer Injector ΔP = 50 psid,
Fuel Injector ΔP = 100 psid)

Scarfed Element Injector (Configuration II)

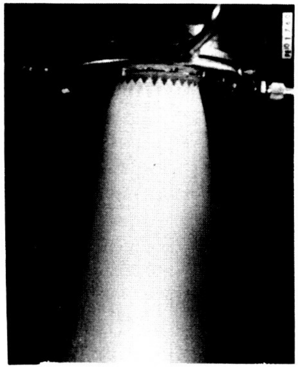
FE 101760

Oxidizer Injector, Water Flow
(ΔP = 50 psid)

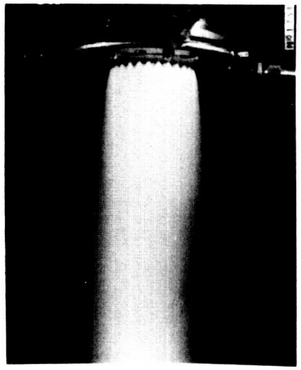
FE 101758

Combined Flow
(Oxidizer Injector ΔP = 50 psid,
Fuel Injector ΔP = 100 psid)

Figure 7. Injector Spray Patterns

FD 44784A

Table IV. Fixed-Thrust Injector Effective Flow Areas

Injector	Oxidizer AC_D - in.^{2}	Faceplate	Fuel AC_D - in.^{2}	Rigimesh AC_D - in.^{2}	Rigimesh Flow - %
Converging Fuel Stream	0.134 [0.146]**	40 scfm	0.244 [0.212]**	0.0454 [0.0325]	18.5 [17.2]
		100 scfm	0.244* [0.261]	0.106* [0.0814]	43.4* [31.2]
		Copper	0.167 [0.180]	- -	- -
Scarfed	0.180 [0.210]	40 scfm	0.331 [0.296]	0.040 [0.0325]	12.1 [11.0]
		100 scfm	0.307 [0.296]	0.106 [0.0814]	34.6 [23.6]
		40-100 scfm	0.329 [0.333]	0.058 [0.0695]	17.6 [20.9]
Pentad	0.141 [0.146]	40 scfm	NA [0.212]	NA [0.0233]	NA [11.0]
		100 scfm	0.232 [0.247]	0.0675 [0.0582]	29.1 [23.6]

*Based on hot run data
**Bracketed terms are design values.

Table V. Fixed-Thrust Injector Swirler Cap Characteristics

Injector	Injector Row	Cap ID, in.	Slot Dimensions*, in.	Cap Slot-to-Orifice Area Ratio	C_D
Converging Fuel Stream	Inner	0.0785	0.016 by 0.120	1.19	0.390 [0.435]**
	Outer	0.0785	0.016 by 0.148	1.47	0.434 [0.484]
Scarfed	Inner	0.0910	0.0155 by 0.178	1.27	0.400 [0.450]
	Outer	0.0910	0.0155 by 0.219	1.57	0.451 [0.495]

*Note: There are three slots per cap.
**Bracketed terms are design values.

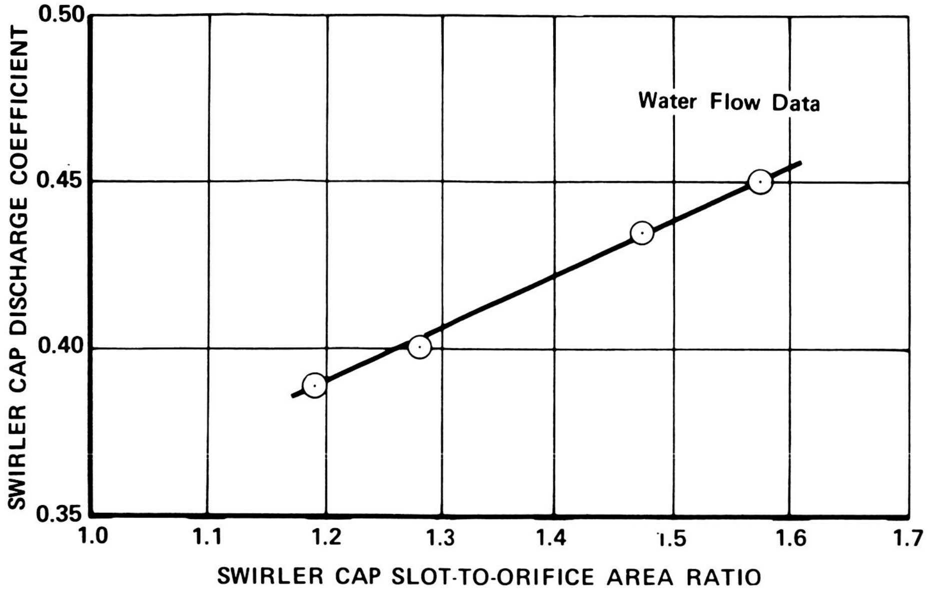

Figure 8. Swirler Cap Discharge Coefficient vs Swirler Cap Slot-to-Orifice Area Ratio FD 44783

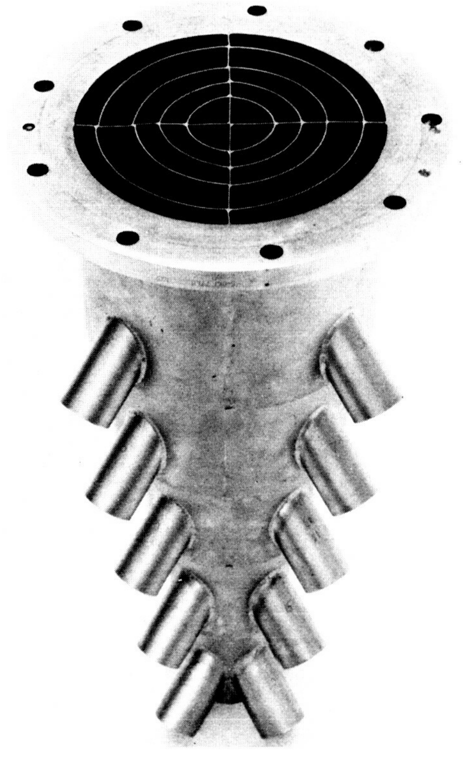

Figure 9. Injector Patternator FE 77724

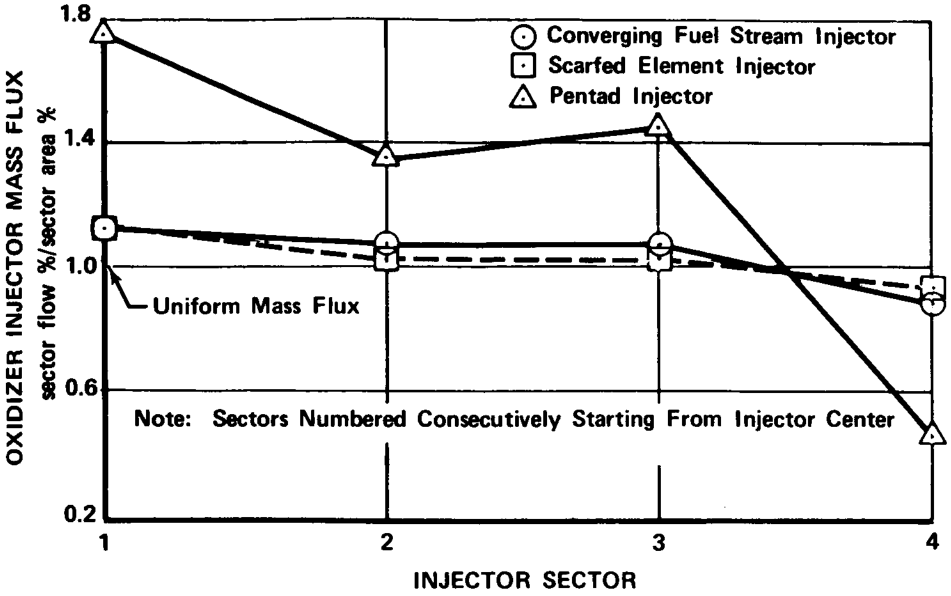

Figure 10. Oxidizer Injector Mass Flux Profiles FD 44782

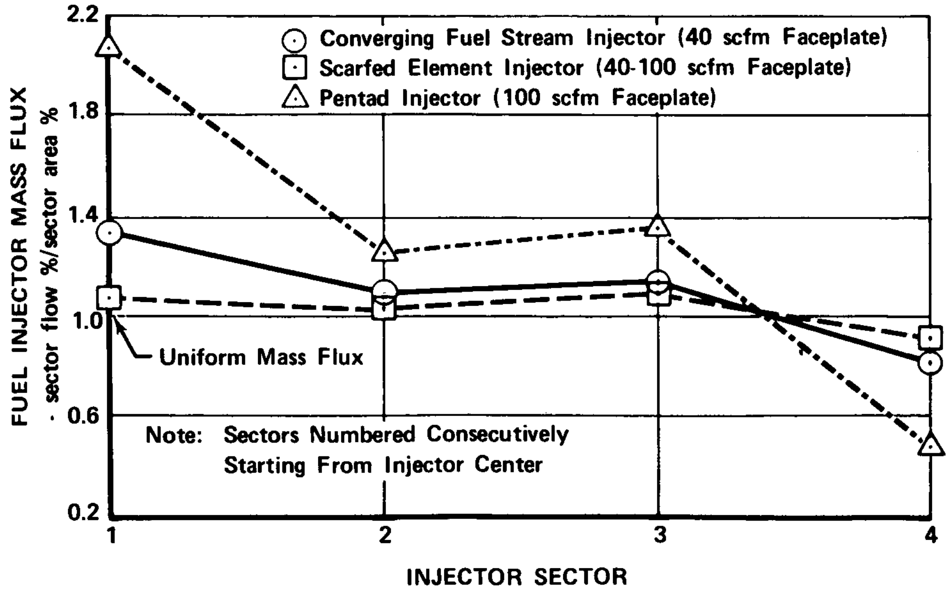

Figure 11. Fuel Injector Mass Flux Profiles FD 44781

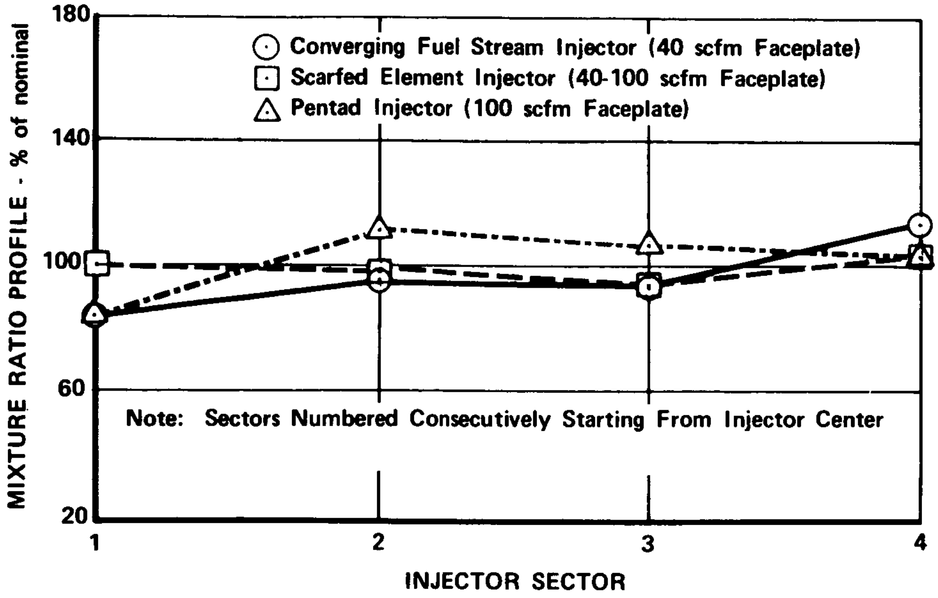

Figure 12. Mixture Ratio Profiles FD 44729A

E. SINGLE ELEMENT INJECTOR COLD FLOW TESTS

At the beginning of the program, several injector elements were evaluated in cold flow tests. The objective was to investigate atomization and mixing characteristics provided by different elements and to select the two most promising element configurations for incorporation into the first two injectors to be designed and built under the contract. Concentric tube and impingement type elements were evaluated.

Figures 13 and 14 illustrate the elements and present photographs of the spray patterns obtained with each. The elements include:

1. Concentric tube, no swirler, axial fuel injection
2. Concentric tube, ribbon swirler, axial fuel injection
3. Concentric tube, hydraulic swirler, axial fuel injection
4. Concentric tube, hydraulic swirler, diverging fuel stream
5. Concentric tube, hydraulic swirler, converging fuel stream
6. 60-deg triplet, two oxidizers on one fuel
7. 90-deg triplet, two oxidizers on one fuel
8. Triplet fan, two oxidizer fans on one fuel
9. Quadruplet, two opposing oxidizers on two opposing fuels
10. Pentad, four oxidizers on one fuel.

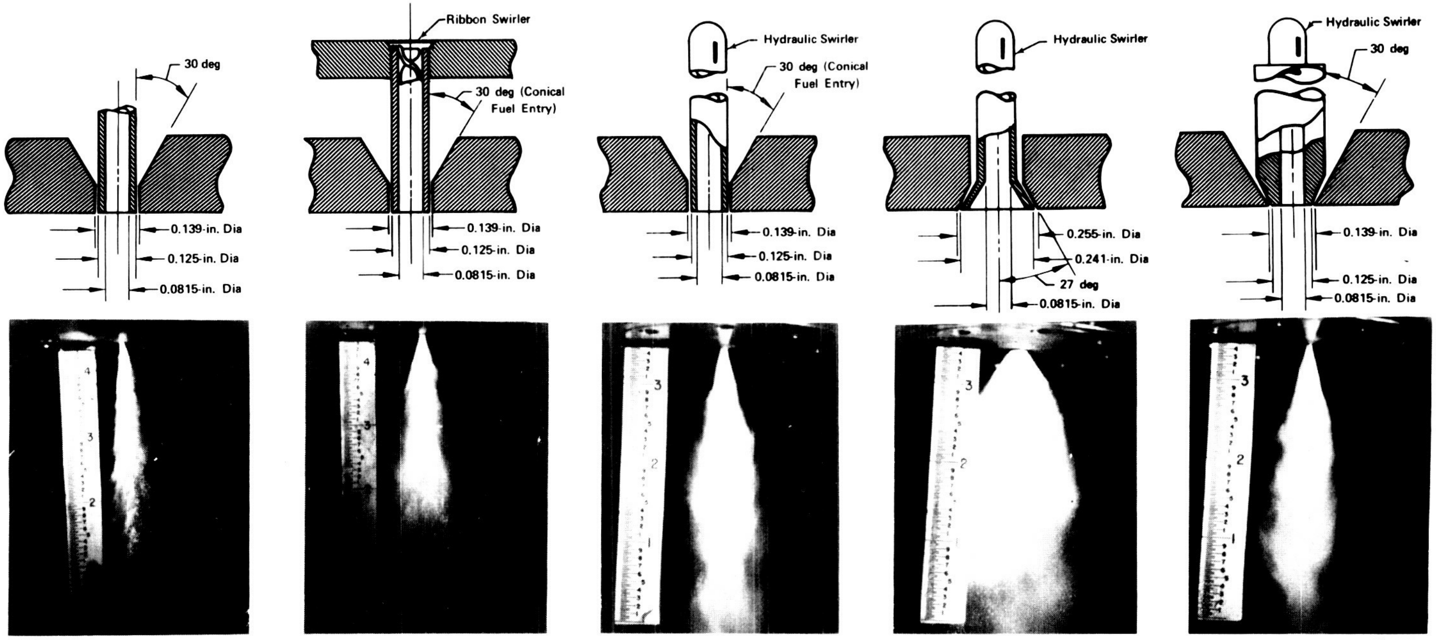

(a) Concentric Tube, No Swirler, Axial Fuel Injection

(b) Concentric Tube, Ribbon Swirler, Axial Fuel Injection

(c) Concentric Tube, Hydraulic Swirler, Axial Fuel Injection

(d) Concentric Tube, Hydraulic Swirler, Diverging Fuel Injection

(e) Concentric Tube, Hydraulic Swirler, Converging Fuel Injection

Figure 13. Concentric Tube Injector Elements and Spray Patterns

FD 44786A

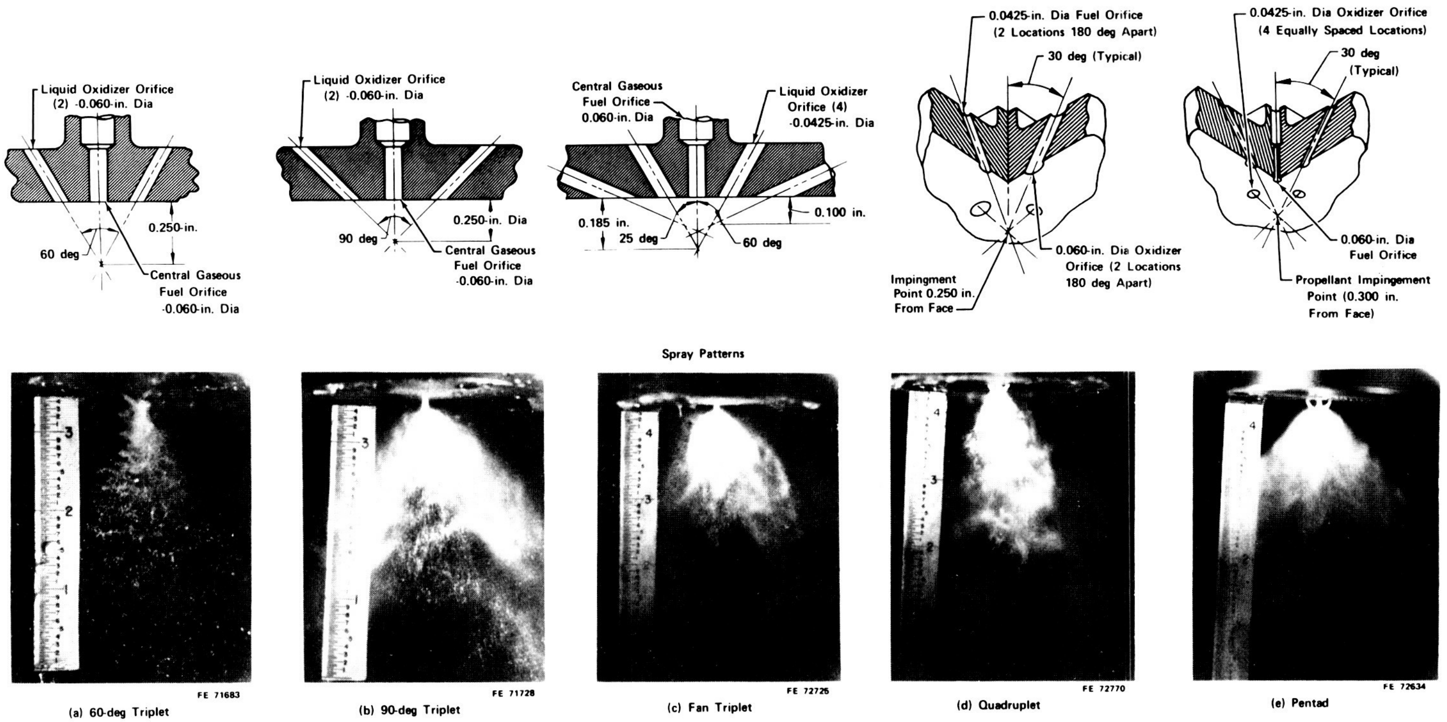

(a) 60-deg Triplet (b) 90-deg Triplet (c) Fan Triplet (d) Quadruplet (e) Pentad

Figure 14. Impingement Injector Elements and Spray Patterns

FD 44785A

All of the injection elements were sized to have a thrust/element of approximately 75 lb_f. In the cold flow tests, water and gaseous nitrogen were used to simulate the oxidizer and fuel respectively.

The spray patterns shown in figures 13 and 14 were photographed using an open shutter camera and a short flash duration (0.8 μsec). This microflash camera technique provides a more critical photograph of the spray pattern than that obtained with a low-shutter-speed camera, which reflects visually observed spray patterns.

Figure 13 shows spray patterns obtained with concentric tube injectors. The pattern obtained with a conventional concentric tube element, i.e., one that has axial fuel injection and no oxidizer swirler, indicates that both atomization and mixing are poor. Improvement is achieved by adding a ribbon swirler (figure 13b). The last three photographs in figure 13 show patterns obtained with hydraulic swirler elements using axial, diverging fuel and converging fuel injection. Some improvement in the spray pattern is achieved when a hydraulic swirler rather than the ribbon swirler is used. (Compare figures 13b and 13c.) However, the best mixing and atomization was obtained with the hydraulic swirler using converging fuel injection (figure 13e), and consequently it was selected as the first element configuration to be evaluated in the contract.

Figure 14 shows spray patterns obtained with the impingement type elements. The spray pattern obtained with the triplet elements indicates that the nitrogen did not penetrate the liquid impingement point and thus the droplet size distribution and mixing are not uniform across the spray pattern. The spray patterns obtained with the triplet fan, quadruplet and pentad elements indicated improved mixing and droplet size uniformity. Furthermore, of the three, the pentad element appeared to be the best and thus it was selected as the second element configuration to be evaluated in the contract.

In initial combustion firing tests with the converging fuel stream injector, good performance was obtained, but the chamber heat transfer rates were undesirably high. Consequently, injector elements that reduced chamber heat transfer rates were sought. The approach selected was to scarf the outer row spuds of the injector so that the oxidizer spray would be directed away from the wall. To verify that the scarfing technique would be effective, single-element tests were made. The photographs in figure 15 show the results. The effects of two scarf angles (45 deg and 22.5 deg) are illustrated. In both cases the spray is deflected from the orifice centerline which is indicated by the rod in the background of the photographs. Based on these results the following spud configurations were selected for the configuration I of the scarfed element injector.

1. For the outer element row, a scarfed spud cut so that its exit plane is 45 degrees from the injector faceplate plane

2. For the second element row in from the chamber wall, a 22.5 degree scarfed spud

3. For the two inside element rows, unscarfed spuds.

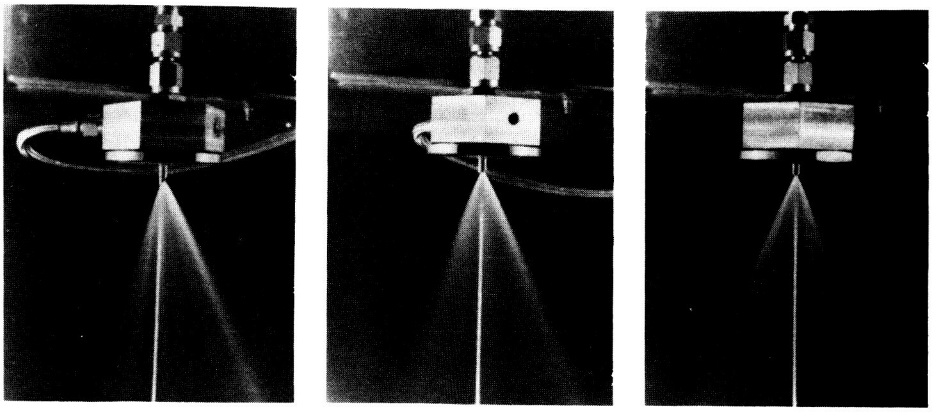

FE 82964

a. **45-deg Scarfed Spud Spray Pattern (ΔP = 90 psi)**

FE 82962

b. **22.5-deg Scarfed Spud Spray Pattern (ΔP = 90 psi)**

FE 82958

c. **Unscarfed Spud Spray Pattern (ΔP = 90 psi)**

Figure 15. Effect of Spud Scarfing on Spray Pattern

FD 44728A

SECTION V
WATER-COOLED THRUST CHAMBER HARDWARE

A. GENERAL

A water-cooled thrust chamber was designed, fabricated and used in the program during initial fixed-thrust injector tests and later in the throttling injector tests to determine performance and chamber heat transfer data. In this section the water-cooled chamber is described and design considerations are presented.

B. DESCRIPTION

The water-cooled thrust chamber assembly is shown in figure 16. The chamber was sized for 5000-lb_f thrust at 500-psia chamber pressure. It consists of three axial sections bolted together to provide a thrust chamber having a combustion chamber characteristic length (L*) of 30 in. and an expansion ratio of 60 to 1. The combustion chamber contraction ratio is 4 to 1. A segmented design was selected for the thrust chamber to permit: (1) the evaluation of the effect of combustion chamber length on performance and (2) the use of the thrust chamber hardware in both sea level and simulated altitude testing. Addition of another cylindrical combustion chamber section increases L* to 52 in. and removal of the nozzle extension reduces the expansion ratio to 6.5 for sea level testing.

THERMAL SKIN ® construction was selected for the water-cooled chamber because it could be incorporated easily in the segmented design. Also it was the preferred construction approach for the regenerative thrust chamber because of its design flexibility and relatively low cost, and thus its use in the water-cooled chamber provided additional experience with THERMAL SKIN fabrication techniques that was helpful in the subsequent regenerative thrust chamber construction effort.

Each of the four water-cooled thrust chamber sections has six 60-deg circumferential THERMAL SKIN staves. As described in Section I, a stave consists of a brazed sandwich structure of two plates. The coolant passages were etched in the inner (combustion side) plate. Initially, copper was selected for the inner plate material because of its high thermal conductivity and good etching qualities. It was used in the chamber and throat sections, but nickel was substituted in the nozzle extension because of temporary unavailability of copper plates of the size required.

The outer plate materials were selected so that their coefficients of thermal expansion (α) would be nearly equal to that of the inner plate materials to satisfy requirements for a good braze joint. In the chamber and throat sections, where copper was the combustion side plate material, stainless steel was used for the outer plate; in the nozzle extension, Inconel 600 was selected for use with the nickel combustion-side plate.

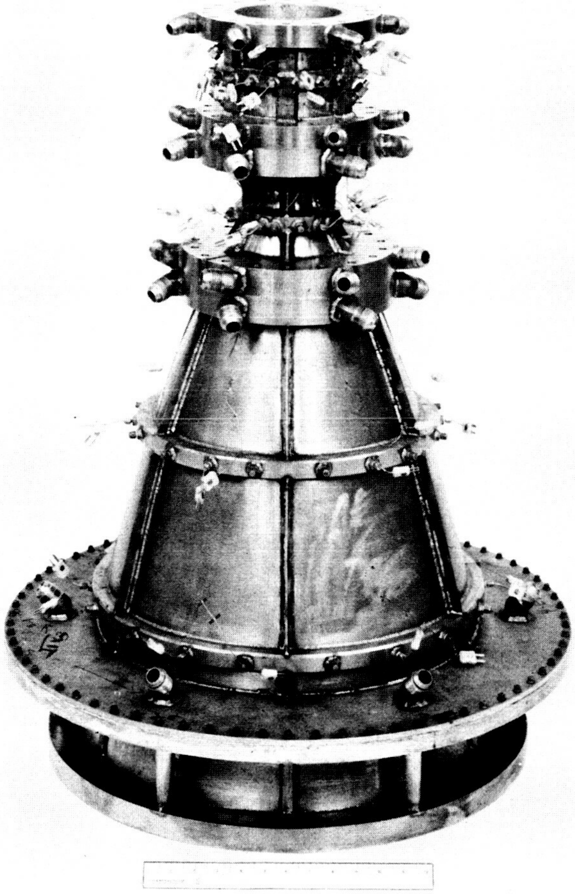

Figure 16. Water-Cooled Thrust Chamber Assembly FE 81182

The thickness of the outer plates was established to obtain adequate strength for operation at chamber pressures up to 1000 psia; therefore outer pressure shells were not required for any of the sections. The staves were not welded on the chamber ID and small seal welds rather than structural welds were used for joining the staves at the chamber OD to minimize the possibility of melting the braze between the THERMAL SKIN plates at their edges. Reinforcement strips attached to the outer plate material (see figure 17) by structural welds were provided to carry hoop loads. To increase the rigidity of the structure between the flanges, 1-in. deep stiffeners were welded to the reinforcement strips in the throat and nozzle sections as shown in the illustration. In the chamber sections, 1-in. thick reinforcement strips were used without stiffeners.

The inlet and exit coolant manifolds were machined in the flanges of all sections. The flanges were designed to provide separate manifolds for each stave element by using dams between the individual stave manifolds. (See figure 17.) Separate inlet and exit stave manifolds permitted control and measurement of the coolant flow to each stave and, ultimately, the determination of circumferential heat transfer variations within a given chamber section.

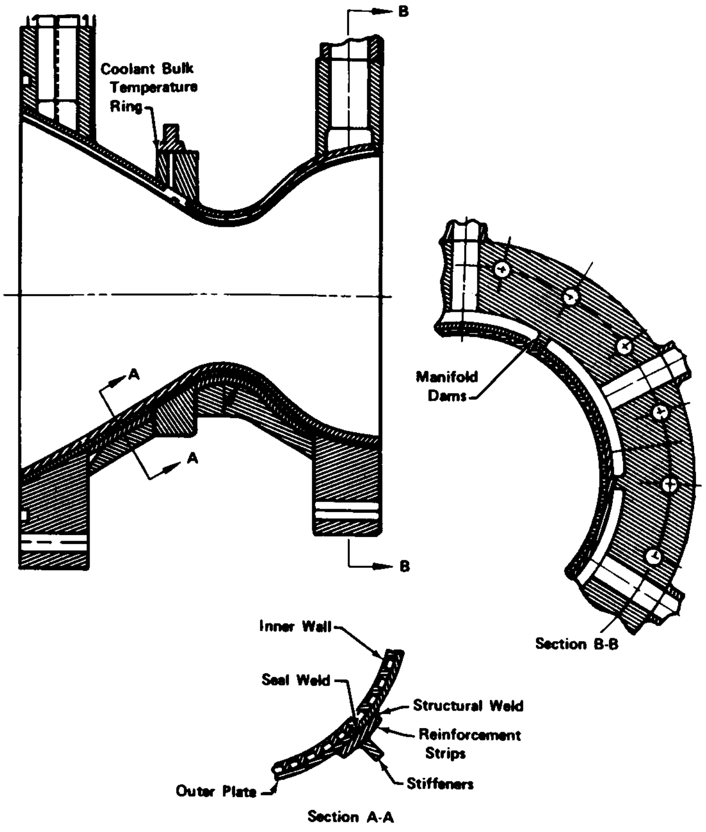

Figure 17. Water-Cooled Thrust Chamber Construction Details FD 44542

Each water-cooled chamber section had intermediate coolant manifold rings in which the midsection coolant bulk temperature measurements were obtained to facilitate the computation of an axial heat flux profile for individual stave elements. Twelve wall temperature thermocouples were also installed in each section. Table VI summarizes the instrumentation provided in each section; the locations of water-cooled chamber instrumentation are indicated in figure 18.

C. DESIGN

1. Contour Selection

The design contour for the water-cooled thrust chamber is shown in figure 19. The 2.6-in. throat diameter was sized for the design conditions of 5000-lb_f vacuum thrust, 500-psia chamber pressure, flox/methane propellants, 5.75 mixture ratio, and 60 to 1 expansion ratio. The combustion chamber is cylindrical, the shape being selected over a tapered configuration to facilitate changes in L*. The contraction ratio of 4 to 1 produces a chamber diameter of 5.2 in. The ratio was selected based on the desire to keep the injector thrust/element size in a range conducive to high performance, and to facilitate cooling. Analytical studies under Task I of the contract for the contraction ratio range of 2 to 4 has shown that, because of their lower heat fluxes and lower surface areas for a given chamber L*, higher contraction ratio chambers are easier to cool regeneratively (reference 1).

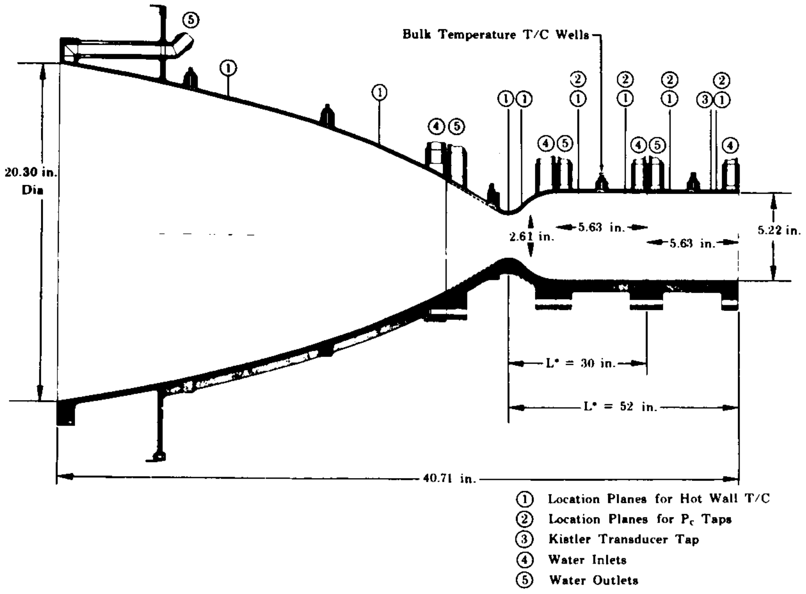

Figure 18. Water-Cooled Thrust Chamber Schematic FD 24639

Table VI. Water-Cooled Thrust Chamber Instrumentation

	Chamber Section	Throat Section	Nozzle Section
Chamber pressure taps	4	--	--
Hot wall thermocouples	12	12	12
Coolant bulk thermocouples	6	6	12
Coolant inlet thermocouples*	(one for all sections)		
Coolant outlet thermocouples	6	6	6

*All of the thrust chamber sections were supplied from one main supply manifold, and therefore only one inlet temperature was required for all sections.

The contour in the converging region of the throat section, described by the chamber and throat radius in figure 19 was selected to minimize chamber length. Downstream of the throat, the wall contour also has a radius of curvature equal to the throat radius. This radius of curvature was selected for ease of forming after an analysis of chemical kinetics, using a two-dimensional axisymmetric computer program (reference 11), indicated no performance advantage for a sharper radius of curvature.

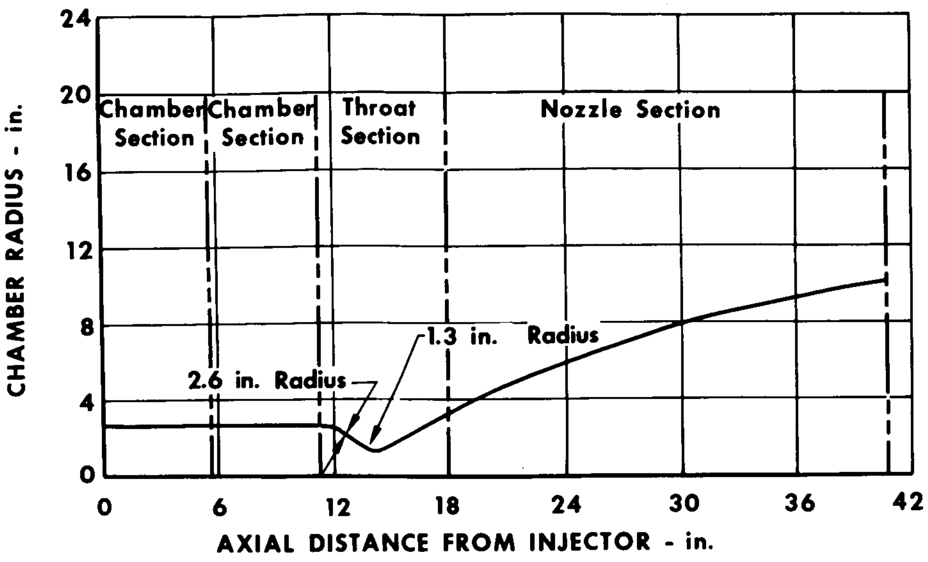

Figure 19. Thrust Chamber Contour GS 10977

The supersonic nozzle contour was determined using a method of characteristics solution. It was established for combustion gas properties based on equalibrium flow conditions. The contour corresponds to that for a minimum surface area design (reference 12); it is an ideal expansion ratio contour of 110 to 1, truncated to 60 to 1. The exit divergence angle is 9.5-deg. Considering divergence, friction, and flow nonuniformity in the transonic region, a nozzle stream thrust coefficient of 97.3% was computed for the contour.

Consideration of the ideal area ratio for sea level expansion established the truncation area ratio of the throat section. This section terminates at an area ratio of 6.5 to 1 to provide an exhaust pressure approximately equal to ambient and, hence, a low-expansion ratio that would not separate or overexpand in sea level tests. By use of the theoretical thrust coefficient for the low-expansion ratio throat section and sea level thrust measurements, an independent check on chamber-pressure-based c* data was provided.

2. Coolant Passage Design

The coolant passages were sized using the methods described in Appendix A. The water flowrate and the coolant pressure level were preselected. The water flowrate for each chamber section was set so that the temperature rise would be approximately 120°F. This temperature rise is high enough to minimize the effect of thermocouple error on the calculated heat transfer results, and low enough to maintain sufficient margin against bulk boiling at the coolant pressure level used.

The coolant pressure level was set as high as possible, considering test stand limitations, so that the coolant saturation temperature would also be high. Hence, relatively high wall temperatures could be tolerated without the occurrence of film boiling. High operating combustion side wall temperatures were desired to simulate those to be used in the regenerative thrust chamber and therefore to nullify the effect (if any) of wall temperature on carbon deposition and the latter's resulting effect on combustion side heat transfer. The passages were sized so that with forced convection cooling, the maximum coolant side wall temperature would be below the local saturation temperature.

The coolant passage geometry is summarized in figure 20. The chamber section had 54 passages (9 passages per 60-deg segment or stave) that were approximately square: 0.105 in. wide by 0.095 in. deep. In the throat section there were 48 passages (8/stave) which were 0.076 in. square at the throat station. On both sides of the throat, the passage depth was held constant and the passage width was increased proportionally with increases in thrust chamber diameter. The nozzle extension had 84 passages that were 0.125 in. wide by 0.030 in. deep at its inlet. The passage depth was constant throughout the section, but the number of passages was doubled by splitting (to keep the passage width less then 0.200 in. as dictated by stress considerations) at the point illustrated in figure 20.

Figure 21 presents the predicted operating conditions for the chamber sections using the design water flowrates. The maximum coolant side and combustion side wall temperatures are 960 and 1130°F respectively at the throat section. This former value is approximately equal to the water saturation temperature at that point.

The wall temperatures presented in figure 21 are one-dimensional values that were computed assuming the wall temperature was constant across the base of the web. In checking the validity of this assumption and determining if the combustion side wall temperature in the web area would be excessive, a two-dimensional analysis was made to establish temperature profiles in this area. Figure 22 shows the wall temperature profiles (and nodal system used in the analysis) for the throat station passage and web. The two-dimensional combustion side wall temperature on the passage center line is 1160°F. This compares favorably with a one-dimensional value of 1130°F from figure 21. Also, the maximum two-dimensional wall temperature of figure 22 is 1190°F, indicating that the gradient due to the web thickness is negligible.

The chamber heat flux profile predicted using the Bartz short form technique is compared with curves reflecting burnout heat fluxes, i.e., the upper limit heat flux for nucleate boiling, in figure 23. The burnout heat flux curves were computed by the correlation of Bernath presented in reference 13. As the illustration shows, a large safety margin against burnout was predicted.

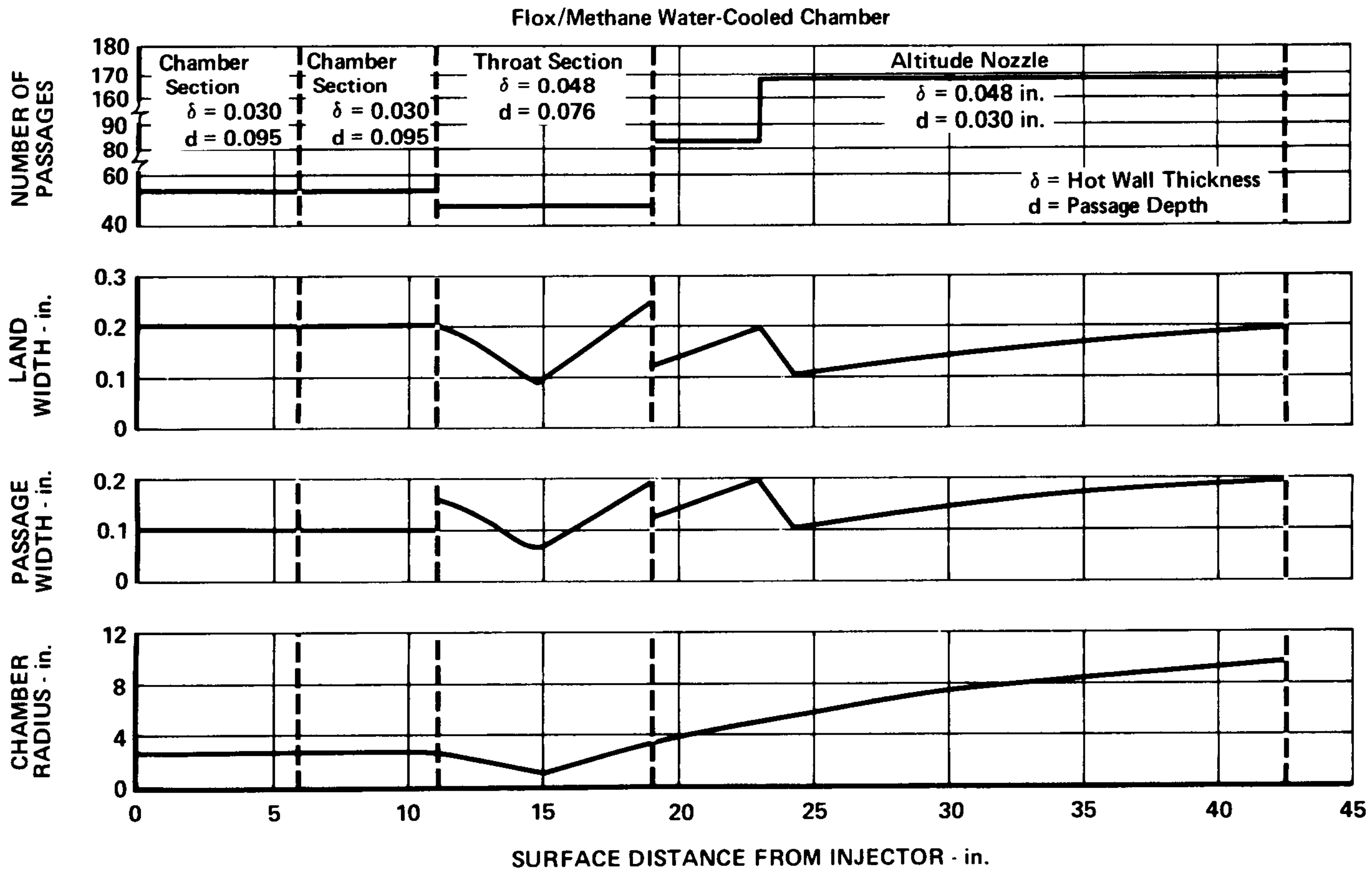

Figure 20. Cooling Passage Geometry (Water-Cooled Chamber)

GS 10979A

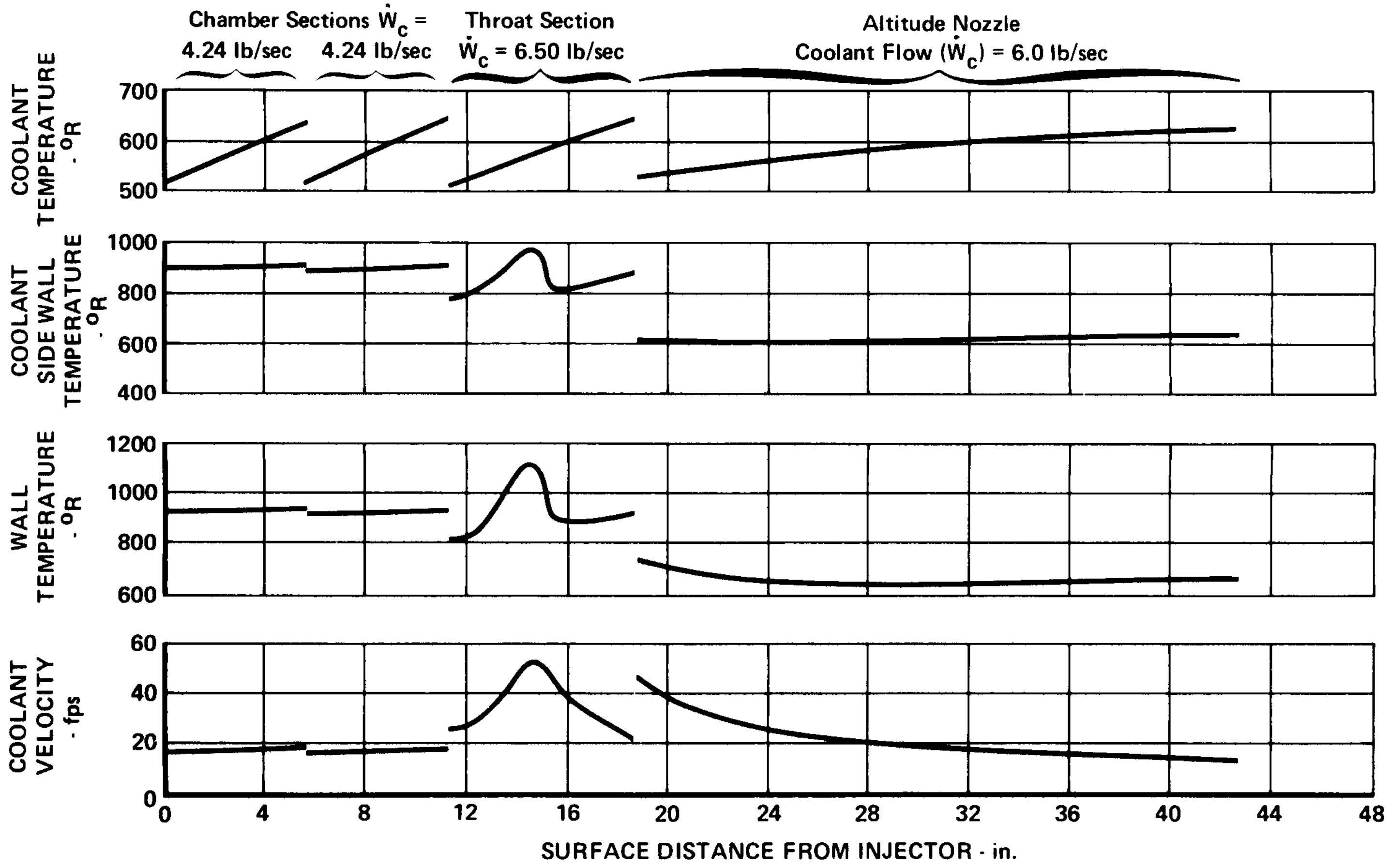

Figure 21. Design Operating Conditions (Water-Cooled Chamber)

FD 44543A

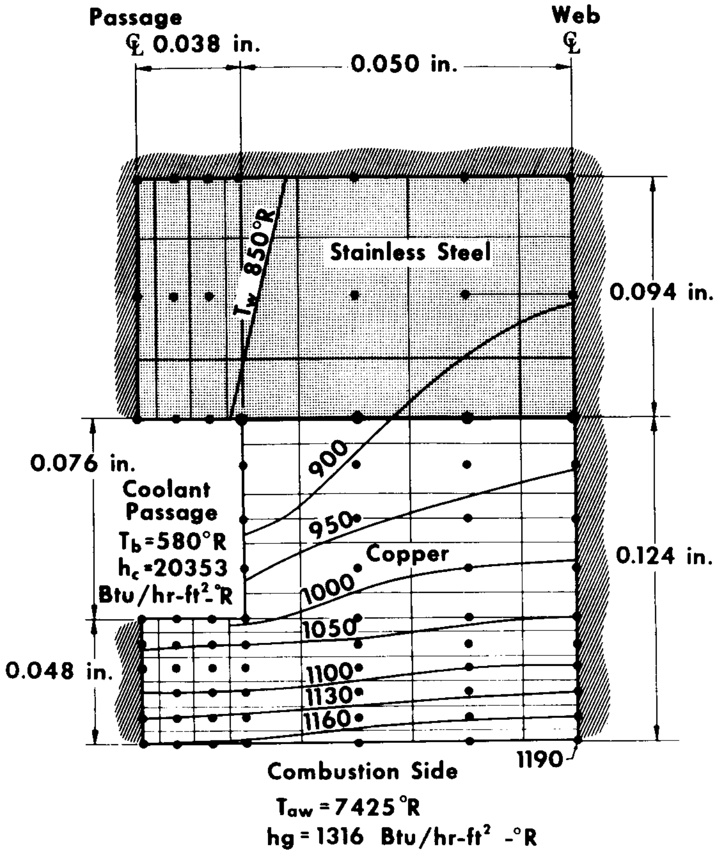

Figure 22. Two-Dimensional Model of Throat Station (Water-Cooled Chamber) GS 10827A

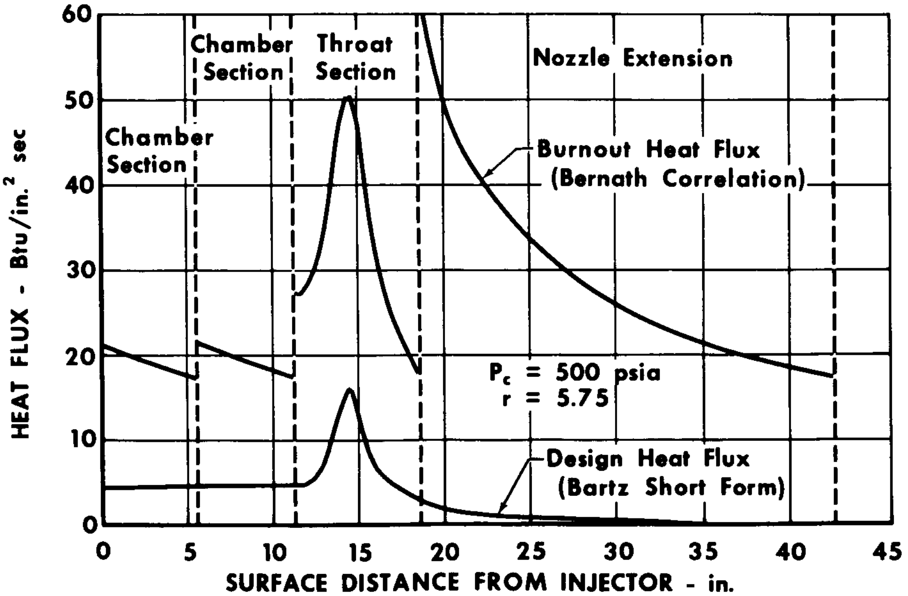

Figure 23. Heat Flux Profile (Water-Cooled Chamber) GS 10978

SECTION VI
FIXED-THRUST INJECTOR, WATER-COOLED CHAMBER TESTS

A. GENERAL

Fourteen water-cooled thrust chamber tests were made in the program with fixed-thrust injectors. Total firing time accumulated was 384 seconds. All of the tests were accomplished with flox/methane propellants; nominal test conditions were 5000-lb_f thrust and 500-psia chamber pressure. The three fixed-thrust injectors described in Section IV were evaluated in the tests; highest performance was obtained with the converging fuel stream injector using a 40-scfm Rigimesh faceplate. In this section the water-cooled chamber tests are discussed, performance and heat transfer data are presented, and hardware durability is described.

B. TEST SUMMARY

Table VII presents a summary of the water-cooled chamber tests. Initial tests (Nos. 1.10 through 7.02) and test No. 11.01 were made with only the combustion chamber and throat sections of the water-cooled chamber, expanding to sea level exhaust conditions. In remaining tests, the 60 to 1 expansion ratio nozzle extension was installed and the firings were made at simulated altitude exhaust conditions. All of the tests were made in the B-29 test stand of the Liquid Propellant Research Center at P&WA's Florida Research and Development Center. The test stand is described in Appendix B. Because the objective of the testing was development of an injector for subsequent use with a regenerative chamber, the methane gas supplied to the injector was heated to approximately 840° R to simulate the fuel injector inlet temperature for the regenerative mode of operation.

Typically, long duration firing tests were made to obtain performance data at several mixture ratios while operating at 500 psia chamber pressure. The concentric tube injectors proved to be very durable and extensive data were obtained with both the converging fuel stream and scarfed element configurations. However, in the only test made with the pentad injector (test No. 4.02), severe face burning occurred early in the test and steady-state performance data were not obtained. The durability of the pentad injector is discussed in subsection E.

C. PERFORMANCE DATA

1. General

Tables VIII and IX present the measured and derived data obtained in the water-cooled chamber tests. The equations used to determine performance parameters given in table IX are described in detail in Appendix C. Before discussing the performance data, several general comments are noteworthy; these are given in the following paragraphs.

Table VII. Fixed-Thrust Injector, Water-Cooled Chamber Test Summary

P&WA Ref. Test No.	Type	Injector	Characteristic Chamber Length, L* - in.	Mixture Ratio, r	Chamber Pressure, P_c - psia	Duration - sec	Remarks
1.10*	Sea Level	Converging fuel stream, 40 scfm Faceplate	30	4.0	500	13.0	Successful checkout firing test. Injector and chamber were in good condition after the test, except that some nickel plating was gone from the chamber ID. (Copper was not damaged.) The chamber was pressure-tested after the firing. There were no leaks.
2.01	Sea Level	Converging fuel stream, 40 scfm Faceplate	30	5.0	150	3.0	Planned 60-sec mixture ratio excursion. Test was prematuraly advanced to shutdown by faulty ignition burnwire circuit. Burnwire circuit repaired after test.
3.01	Sea Level	Converging fuel stream, 40 scfm Faceplate	30	4.0 to 5.0	500	32.3	Planned 60-sec mixture ratio excursion. Test was terminated when exit coolant pressure drop indicated a chamber leak. Post-test inspection revealed damage to both the chamber and throat section.
4.02	Sea Level	Pentad, 100 scfm Faceplate	30	4 and 5.75	500	13.3	Checkout firing with pentad injector. Post-test inspection showed that chamber was in good condition but that there was severe injector face erosion. Data records indicate that oxidizer injector ΔP dropped to a low level approximately 6 sec into test. Thus injector damage occurred just after reaching 500 psia chamber pressure.
5.01	Sea Level	Converging fuel stream, 40 scfm Faceplate	30	3.0	220	4.1	Planned 60-sec mixture ratio excursion with converging fuel stream injector. Control system noise caused high mixture ratio advance. Test hardware was not damaged. A faulty amplifier in the control system was replaced.
6.01	Sea Level	Converging fuel stream, 40 scfm Faceplate	30	---	---	---	Planned high mixture ratio checkout test with converging fuel stream injector. A power failure occurred just before starting the test, which caused the sequencer to malfunction and open the oxidizer and fuel control valves, but not the coolant valves. The throat section was severely damaged; four of six staves were burned.
7.02	Sea Level	Converging fuel stream, 40 scfm Faceplate	30	4 and 5.75	500	13.8	Test to obtain high mixture ratio performance data with 30-in. L* chamber. Post-test inspection of the faceplate indicated very slight erosion at outer-spud location. Problems attributed to partial fuel flow blockage by spacers. Spacers reworked to prevent flow blockage. Faceplate repaired.
8.04	Altitude	Converging fuel stream, 100 scfm Faceplate	52	4.0	100	0.5	Planned 60-sec test was advanced because of malfunction of power supply for nozzle coolant exit pressure advance system. Power supply replaced.
9.01	Altitude	Converging fuel stream, 100 scfm Faceplate	52	4.0 to 6.0	500	60.0	Successful mixture ratio excursion test with 52-in. L* chamber and nozzle extension at altitude conditions. Post-test inspection revealed no damage to test hardware.
10.01	Altitude	Converging fuel stream, 40 scfm Faceplate	52	4.0 to 6.0	500	60.0	Successful mixture ratio excursion test. Post-test inspection of test hardware revealed three small leaks in nozzle extension. Nozzle extension removed for 52-in. L* sea level test with copper faceplate.
11.01	Sea Level	Converging fuel stream, Copper Faceplate	52	4.0 to 6.0	500	60.0	Successful mixture ratio excursion test. Post-test inspection revealed small burnout in throat section. Test records indicate burnout occurred just before shutdown.
12.04	Altitude	Scarfed (Conf. II), 100-40 scfm Composite Faceplate	52	4.0	500	4.0	Planned checkout test was prematurely advanced because altitude system steam ejector was not pumping efficiently, resulting in a high nozzle exit pressure.
14.01	Altitude	Scarfed (Conf. II), 100-40 scfm Composite Faceplate	52	4.0 to 5.75	500	60.0	Successful test.
17.02	Altitude	Scarfed (Conf. II), 40 scfm Faceplate	52	4.0 to 5.75	500	60.0	Successful test.

*All tests are for Rig No. F-35114

Table VIII. Measured Data for Fixed-Thrust Injector, Water-Cooled Chamber Tests

Test Description			Thrust Chamber							Oxidizer Injector		Fuel Injector	
P&WA Reference Test No.	Injector	Test Type	Mixture Ratio	Chamber Pressure, psia	$\dot{W}_o$ lbm/sec	$\dot{W}_f$ lbm/sec	Thrust Net, lb	Ambient Pressure, psia	Diffuser Pressure, psia	Inlet Temperature, °R	Inlet Pressure, psia	Inlet Temperature, °R	Inlet Pressure, psia
1.10	Converging fuel stream, 40 scfm Faceplate	Sea level, L* = 30 in.	4.03	496.0	9.86	2.45	3538	14.69		154.6	648.0	777.7	766.3
			4.05	498.0	10.00	2.47	3548			155.9	652.0	782.8	774.8
3.01	Converging fuel stream, 40-scfm Faceplate	Sea level, L* = 30 in.	4.06	499.8	9.94	2.45	3543	14.72		156.1	650.3	795.8	764.4
			4.07	499.9	9.99	2.45	3544			155.7	651.2	799.3	767.4
			4.52	502.6	10.17	2.25	3568			154.3	656.1	806.9	736.1
			4.96	498.0	10.20	2.06	3521			152.3	647.5	807.4	697.3
			5.00	499.5	10.24	2.05	3532			152.0	649.8	807.4	697.4
7.02	Converging fuel stream, 40-scfm Faceplate	Sea level, L* = 30 in.	4.14	503.3	10.06	2.43	3689	14.72		156.5	650.6	780.1	724.9
			5.81	496.9	10.81	1.86	3470			161.0	656.9	784.3	637.4
			5.83	499.9	10.86	1.86	3490			160.0	660.9	785.6	640.7
			5.86	500.0	10.92	1.87	3502			159.6	662.2	787.1	640.8
9.01	Converging fuel stream, 100-scfm Faceplate	Altitude, L* = 52 in.	4.32	495.9	10.09	2.34	-3835	14.79	0.410	152.8	644.6	791.3	719.2
			5.26	496.1	10.31	1.96	-3900		0.410	150.5	643.7	799.8	662.7
			5.77	497.8	10.63	1.84	-3876		0.410	150.4	652.4	801.7	644.6
			5.99	496.3	10.71	1.79	-3896		0.410	150.3	654.5	801.5	637.9
			6.25	496.4	10.80	1.73	-3945		0.410	150.5	656.1	801.8	628.8
10.01	Converging fuel stream, 40-scfm Faceplate	Altitude, L* = 52 in.	4.17	496.0	10.00	2.40	-3822	14.78	0.410	153.8	644.9	800.8	746.3
			4.59	496.0	10.15	2.21	-3806		0.410	153.1	645.1	808.6	716.4
			5.00	496.2	10.20	2.04	-3806		0.410	151.2	644.5	811.7	688.1
			5.50	495.9	10.36	1.89	-3817		0.410	151.7	646.5	812.6	663.6
			5.76	495.6	10.51	1.83	-3823		0.410	152.0	649.2	813.5	653.7
			5.97	495.7	10.60	1.78	-3830		0.410	152.4	654.0	813.7	646.3
11.01	Converging fuel stream, Copper Faceplate	Sea level, L* = 52 in.	3.98	495.7	10.00	2.51	3521	14.72	0.410	158.4	658.4	784.5	842.7
			4.40	496.1	10.16	2.31	3525		0.410	155.1	653.7	796.7	797.6
			5.43	496.5	10.48	1.93	3521		0.410	154.4	651.1	798.2	716.7
			5.73	496.5	10.67	1.86	3523			154.8	651.9	797.9	702.8
14.01	Scarfed Element (Conf. II), 40-100 scfm Faceplate	Altitude, L* = 52 in.	3.94	505.3	10.43	2.65	-3628	14.75	0.368	155.0	578.7	779.6	694.2
			3.95	506.0	10.45	2.65	-3629		0.373	154.6	578.9	785.3	695.7
			4.67	506.3	10.79	2.31	-3640		0.397	151.8	580.7	795.3	654.9
			4.68	506.5	10.78	2.30	-3642		0.396	151.4	580.7	796.0	654.7
			4.95	506.5	10.90	2.20	-3659		0.400	150.1	582.2	799.2	642.5
			4.95	506.5	10.91	2.20	-3660		0.400	150.1	582.0	799.5	642.8
			5.16	506.1	11.00	2.13	-3676		0.401	150.3	582.4	800.8	634.0
			5.17	506.2	11.01	2.13	-3677		0.400	150.3	582.4	801.0	634.4
			5.44	506.1	11.12	2.04	-3692		0.402	150.5	584.5	801.5	624.8
			5.44	506.0	11.13	2.05	-3693		0.402	150.5	584.2	801.5	625.1
			5.62	506.2	11.27	2.01	-3692		0.403	150.7	585.8	801.9	620.4
			5.62	506.1	11.28	2.01	-3690		0.404	150.8	585.9	801.9	620.6
17.02	Scarfed element (Conf. II), 40-scfm Faceplate	Altitude, L* - 52 in.	3.95	506.5	10.45	2.64	-3670	14.83	0.399	152.5	578.4	785.1	720.0
			3.96	506.9	10.49	2.65	-3673		0.400	151.9	578.3	787.5	722.3
			4.70	507.1	10.79	2.30	-3686		0.411	150.3	580.2	797.3	672.6
			4.71	507.3	10.80	2.29	-3683		0.412	149.9	580.3	798.2	672.8
			4.94	507.2	10.89	2.20	-3694		0.418	150.8	582.0	802.6	661.3
			4.94	507.2	10.90	2.21	-3689		0.421	150.9	582.3	803.0	661.5
			5.14	507.3	10.99	2.14	-3698		0.418	152.4	583.9	804.9	653.1
			5.14	506.9	10.99	2.14	-3701		0.418	152.5	583.4	805.0	653.1
			5.41	506.7	11.12	2.06	-3714		0.422	153.2	584.9	805.5	642.2
			5.41	507.0	11.15	2.06	-3710		0.424	153.3	585.5	805.6	642.8
			5.60	507.1	11.24	2.01	-3715		0.420	153.9	586.9	806.6	636.6
			5.60	507.0	11.24	2.01	-3713		0.420	154.0	586.9	806.8	636.5

Table IX. Derived Data for Fixed-Thrust Injector, Water-Cooled Chamber Tests

P&WA Reference Test No.	Injector	Test Type	L*, in.	Mixture Ratio	Chamber Pressure, Throat Total, psia	Vacuum Thrust, lb.	I_{vac}, sec	c^*(Pc) ft/sec	$C_{F_{vac}}$	$\eta_{I_{vac}}$, %	$\eta_{c^*}(P_c)$, %	η_{c^*} (F), %	$\eta C_{F_{vac}}$, %
1.10	Converging fuel stream, 40-scfm faceplate	Sea level	30	4.03	503.3	4041	364.6	6830	1.55	90.06	99.12	98.65	90.86
				4.05	505.3	4052	364.8	6766	1.54	89.04	98.13	97.53	90.74
3.01	Converging fuel stream, 40-scfm faceplate	Sea level	30	4.06	507.2	4048	365.7	6836	1.54	89.31	98.00	97.83	91.13
				4.07	507.3	4048	365.8	6810	1.54	88.95	97.60	97.43	91.14
				4.52	510.0	4072	370.4	6859	1.54	88.54	97.02	96.99	91.26
				4.96	505.3	4025	374.4	6885	1.53	87.71	96.36	96.07	91.02
				5.00	506.8	4036	374.9	6890	1.53	87.64	96.32	95.99	90.99
7.02	Converging fuel stream, 40-scfm faceplate	Sea level	30	4.14	510.7	4094	327.8	6845	1.54	89.51	98.22	98.02	91.13
				5.81	504.2	3974	313.7	6662	1.52	83.55	93.40	91.49	89.43
				5.83	507.2	3994	314.1	6677	1.51	83.70	93.58	91.67	89.42
				5.86	507.4	4006	313.4	6643	1.52	83.52	93.10	91.48	89.72
9.01	Converging fuel stream, 100-scfm faceplate	Altitude	52	4.32	503.2	4836	389.1	6778	1.85	94.20	97.41		96.70
				5.26	503.4	4769	388.8	6870	1.82	92.00	96.76		95.08
				5.77	505.1	4792	384.4	6782	1.82	90.39	95.29		94.86
				5.99	503.6	4773	381.8	6743	1.82	90.75	95.01		95.52
				6.25	504.7	4725	377.1	6730	1.80	90.99	95.50		95.27
10.01	Converging fuel stream, 40-scfm faceplate	Altitude	52	4.17	503.3	4835	390.1	6796	1.85	95.28	98.33		96.89
				4.59	503.3	4851	392.7	6820	1.85	94.80	97.61		97.12
				5.00	503.5	4851	396.3	6886	1.85	94.71	97.64		97.00
				5.50	503.2	4840	395.2	6879	1.85	93.56	97.02		96.44
				5.76	502.9	4834	392.0	6826	1.85	92.49	96.15		96.18
				5.97	503.0	4828	390.1	6805	1.84	93.11	96.12		96.85
11.01	Converging fuel stream, copper faceplate	Sea level	52	3.98	503.0	4025	321.8	6732	1.54	88.70	97.77	97.16	90.72
				4.40	503.4	4030	323.2	6758	1.54	88.13	97.13	96.53	90.73
				5.43	503.8	4026	324.3	6792	1.54	86.58	95.97	94.83	90.22
				5.73	503.8	4027	321.3	6727	1.54	85.92	95.22	94.11	90.23
14.01	Scarfed element (Conf. II), 40-100 scfm faceplate	Altitude	52	3.94	498.3	5015	383.4	6688	1.84	93.91	96.83		96.98
				3.95	499.0	5014	382.8	6689	1.84	93.75	96.83		96.82
				4.67	499.3	4996	381.3	6691	1.83	91.66	94.83		96.65
				4.68	499.4	4995	381.8	6702	1.83	91.76	94.98		96.60
				4.95	499.4	4976	379.8	6693	1.83	90.61	94.31		96.07
				4.95	499.4	4975	379.3	6685	1.83	90.51	94.21		96.07
				5.16	499.1	4959	377.7	6674	1.82	89.52	93.76		95.47
				5.17	499.1	4959	377.4	6669	1.82	89.44	93.69		95.46
				5.44	499.0	4942	375.5	6658	1.81	88.51	93.35		94.81
				5.44	498.9	4942	375.0	6647	1.82	88.36	93.20		94.80
				5.62	499.1	4942	372.2	6599	1.81	87.64	92.52		94.73
				5.62	499.1	4944	372.1	6594	1.82	87.61	92.45		94.76
17.02	Scarfed element (Conf. II), 40-scfm faceplate	Altitude	52	3.95	499.5	5017	383.2	6698	1.84	93.88	96.95		96.82
				3.96	499.9	5014	381.5	6678	1.84	93.42	96.62		96.68
				4.70	500.0	4998	382.0	6709	1.83	91.82	95.04		96.61
				4.71	500.3	5000	382.0	6709	1.83	91.81	95.03		96.61
				4.94	500.1	4988	380.8	6704	1.83	90.92	94.50		96.20
				4.94	500.2	4992	380.9	6700	1.83	90.94	94.45		96.28
				5.14	500.3	4983	379.7	6693	1.83	90.16	94.06		95.85
				5.14	499.9	4981	379.5	6687	1.83	90.10	93.99		95.86
				5.41	499.6	4966	376.9	6656	1.82	88.94	93.36		95.27
				5.41	499.9	4971	376.3	6645	1.82	88.77	93.20		95.25
				5.60	500.0	4967	374.9	6627	1.82	88.35	92.91		95.09
				5.60	500.0	4969	375.0	6624	1.82	88.38	92.88		95.15

All of the measured data represent average values for 2-sec steady-state periods in the tests. To illustrate the steadiness of parameters during the data average periods, a typical oscillograph trace for one of the tests is shown in figure 24. This trace also indicates the combustion stability provided by the concentric-tube injectors. Peak-to-peak chamber pressure oscillations indicated by the Kistler transducer were only 3 psi.

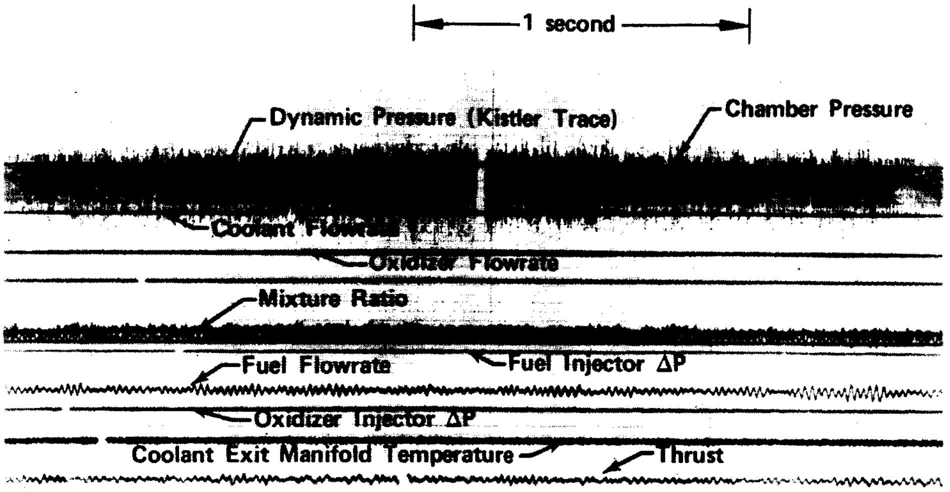

Figure 24. Oscillograph Trace for Water-Cooled Chamber Test No. 17.02 (P_c = 500, r = 5.62) FD 49501

Throat total pressures were determined from two chamber pressure tap locations. In the initial tests (tests 1.10 through 11.01), a chamber tap located just upstream of the throat was used. In tests 14.01 and 17.02, which were made later in the program, an injector face tap was also available. The face tap was installed primarily for use when testing the regenerative chamber; in that chamber the downstream tap had to be made so small that there was concern about it becoming plugged with carbon.

Determination of throat total pressures from the two taps involved different methods. For the downstream tap, the measured value corresponds to a static pressure which was converted to a total pressure by multiplying by 1.015 (the total-to-static pressure ratio from one-dimensional isentropic flow relationships for the chamber contraction ratio of 4). The pressure measurement at the injector face tap represents a total pressure before combustion. It was reduced to a throat total pressure by multiplying by 0.9862 to account for a momentum loss of 1.38% determined using the method described in reference 14. Throat total pressures calculated using measurements at the two separate taps are compared in table X for test 17.02. The two sets of data agree quite well; the largest difference is 2.9 psia, or about 0.6%.

Table X. Comparison of Throat Total Pressures (Test 17.02)

	Throat Total Pressure	
Time After Test Start, sec	Calculated Using Injector Face Tap Measurements	Calculated Using Chamber Tap Measurements
11	499.5*	502.0*
21	500.3	502.8
30	500.2	499.4
39	499.9	499.2
48	499.9	498.0
57	500.0	502.9

*All data represent 2-sec averages for time period starting at the time shown.

The characteristic exhaust velocity $c^*_{(Pc)}$ and the thrust coefficient $C_{F_{vac}}$, were calculated using standard equations; however, the throat area term used in the equations was the product of the measured area multiplied by a discharge coefficient of 0.985. This value was calculated for the geometry of the throat and combustion chamber using methods described in Appendix B. The effect of using a discharge coefficient less than 1.0 is to lower $c^*_{(Pc)}$ and raise $C_{F_{vac}}$.

The theoretical values used in calculating the vacuum specific impulse efficiency ($\eta_{I_{vac}}$) and the c* efficiency $\eta_{c^*(Pc)}$ were established for the measured inlet propellant conditions and corrected to account for the measured chamber heat losses. The thrust coefficient efficiency, $\eta_{C_{F_{vac}}}$, was determined by dividing $\eta_{I_{vac}}$ by $\eta_{c^*(Pc)}$. The parameter $\eta_{c^*(F)}$, shown in the table, represents a c* efficiency determined from thrust measurements during sea level tests. It was obtained by dividing the $\eta_{I_{vac}}$ values for the sea level tests by a theoretical thrust coefficient efficiency of 91.3% for the 6.5 to 1 expansion ratio sea level nozzle.

2. Performance Comparisons

Performance data were obtained with the concentric-tube injectors using different faceplates. During the course of the program tests were made with two different chamber characteristic lengths, and at both sea level and altitude-simulated exhaust conditions. The mixture ratio range covered was 4 to 6; data obtained are discussed below.

Figure 25 compares the c* efficiency data computed from thrust and chamber pressure measurements for sea level tests of the converging fuel stream injector. Good agreement was obtained at mixture ratios below approximately 5.0.

Above this mixture ratio level, the thrust-based data are lower than the P_c-based data. The cause for this disagreement is shown in the lower curve of the illustration: the measured thrust coefficient efficiency decreased at higher mixture ratios while the theoretical thrust coefficient efficiency did not. The theoretical value of 91.3% accounts for divergence, frictional, and subsonic losses, but not for chemical kinetic effects which are a function of mixture ratio. Therefore it is possible that this phenomenon caused the disagreement.

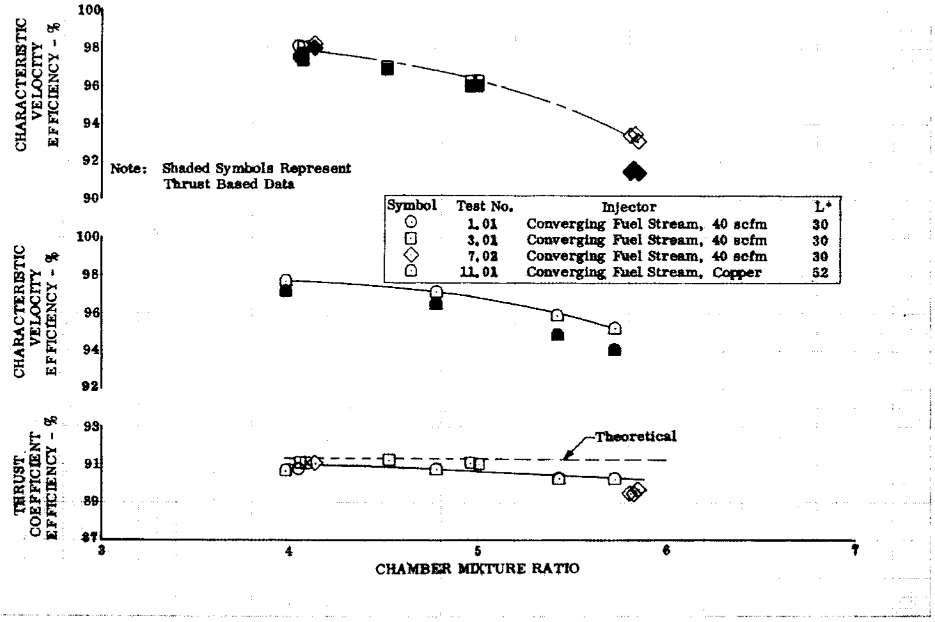

Figure 25. Comparison of Thrust and Chamber Pressure Based Injector Performance DF 83161A

Figure 26 presents a comparison of the c* efficiency data obtained with the converging fuel stream injector in 30-in. and 52-in. L* chambers. In both chambers, performance decreased with increasing mixture ratio. However, the degradation is less severe in the 52-in. L* chamber. Furthermore, at higher mixture ratios, performance was significantly higher in the longer chamber. At a mixture ratio of 5.75, an increase in chamber L* from 30 to 52-in. provided an increase in c* efficiency of 2.5%.

The c* efficiency data obtained with the 40-scfm Rigimesh, 100-scfm Rigimesh, and solid copper faceplates on the converging fuel stream injector, using the 52-in. L* chamber, are compared in figure 27. Performance was highest with the 40-scfm faceplate at all mixture ratios. The reason for the reduced c* performance with the 100-scfm and the copper faceplates is attributed to mixture ratio distribution. With the 100-scfm faceplate, more fuel was injected through the permeable faceplate than with the 40-scfm faceplate, thus reducing the proportion of the fuel injected through the fuel orifices, and raising the injection element mixture ratio relative to the nominal value. The copper faceplate warped sufficiently during testing to alter the fuel gaps at several elements, which in turn caused mixture ratio variations across the injector face.

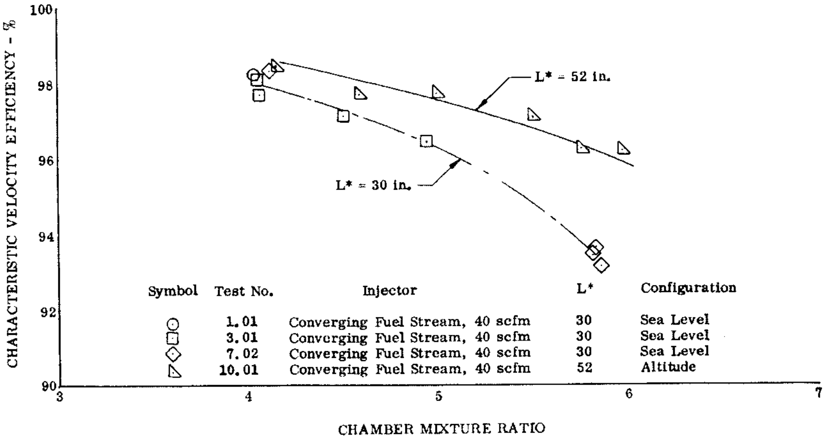

Figure 26. Variation of c* Performance for the Converging Fuel Stream Injector with Chamber L* and Mixture Ratio

DF 83160A

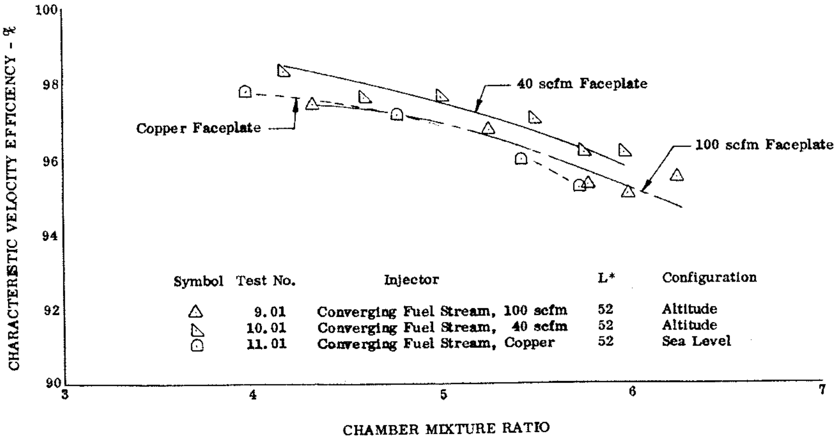

Figure 27. Variation of c* Performance for the Converging Fuel Stream Injector with Different Faceplates and Mixture Ratio

DF 83159A

Performance data from altitude tests made with the converging fuel stream and scarfed element injectors are presented in figure 28. Vacuum impulse and vacuum impulse efficiency, as well as c* efficiency, are highest with the 40-scfm faceplate on the converging fuel stream injector. With this injector configuration the measured specific impulse exceeded 389 sec over the 4 to 6 mixture ratio range, peaking at a level of 396 sec at a mixture ratio of 5.0.

D. CHAMBER HEAT TRANSFER DATA

Table XI presents the measured heat transfer data obtained in the water-cooled chamber tests. For each mixture ratio data point, the table presents measured values of coolant flowrate ($\dot{w}$), coolant exit temperature (T_{B0}), intermediate bulk temperatures (T_{B1} and T_{B2}), wall temperatures (T_{W1} and T_{W2}) and calculated heat transfer (Q) for each 60-deg stave of each thrust chamber section. (The location of the thermocouples in the thrust chamber are illustrated in figure 29.) In tests 14.01 and 17.02, a throat section from a three-piece regenerative thrust chamber was used instead of the water-cooled throat section. Because this piece of hardware did not include provisions for intermediate station instrumentation or individual stave instrumentation, only overall throat section heat transfer was obtained. For consistence in the data table, the overall throat heat transfer was divided by the number of staves (six) to determine an average stave heat transfer. Typical measured heat transfer data are presented and discussed below.

Figure 30 presents for selected tests of the converging fuel stream injector average temperature data measured in each axial section as a function of surface distance from the injector. For the same tests figure 31 presents measured circumferential temperature data for the throat section staves.

The total (i.e., overall) chamber heat transfer rates obtained for the various injector configurations are presented in figure 32 as a function of mixture ratio. The lower curve in this figure shows measured-to-predicted* heat transfer ratios. The heat transfer rates are nearly constant with mixture ratio for all injector configurations. The measured-to-predicted values increase with increasing mixture ratio because the theoretical (predicted) heat transfer curve decreases with increasing mixture ratio. Figure 33 presents the variation of the measured heat transfer with mixture ratio for the separate thrust chamber sections. In both figures 32 and 33 the effect of spud scarfing and fuel injector faceplate porosity can be seen. Heat transfer is lower with the higher porosity faceplates and with the scarfed element injector. Heat transfer rates for the throat and nozzle sections are not shown for tests 14 and 17 in figure 33 because the thermocouples used to measure coolant discharge temperature from these sections were inoperative in the aforementioned tests.

To use the measured heat transfer data from the water-cooled chamber tests as design data for the regenerative thrust chamber, combustion side heat transfer coefficient profiles were computed. The method used in these calculations warrants some explanation.

---

*Predicted or theoretical heat transfer was obtained using the Bartz short form equation.

Symbol	Test No.	Injector	L*
△	9.01	Converging Fuel Stream, 100 scfm	52
◺	10.01	Converging Fuel Stream, 40 scfm	52
⊙	14.01	Scarfed (Configuration II), 100-40 scfm	52
⊡	17.02	Scarfed (Configuration II), 40 scfm	52

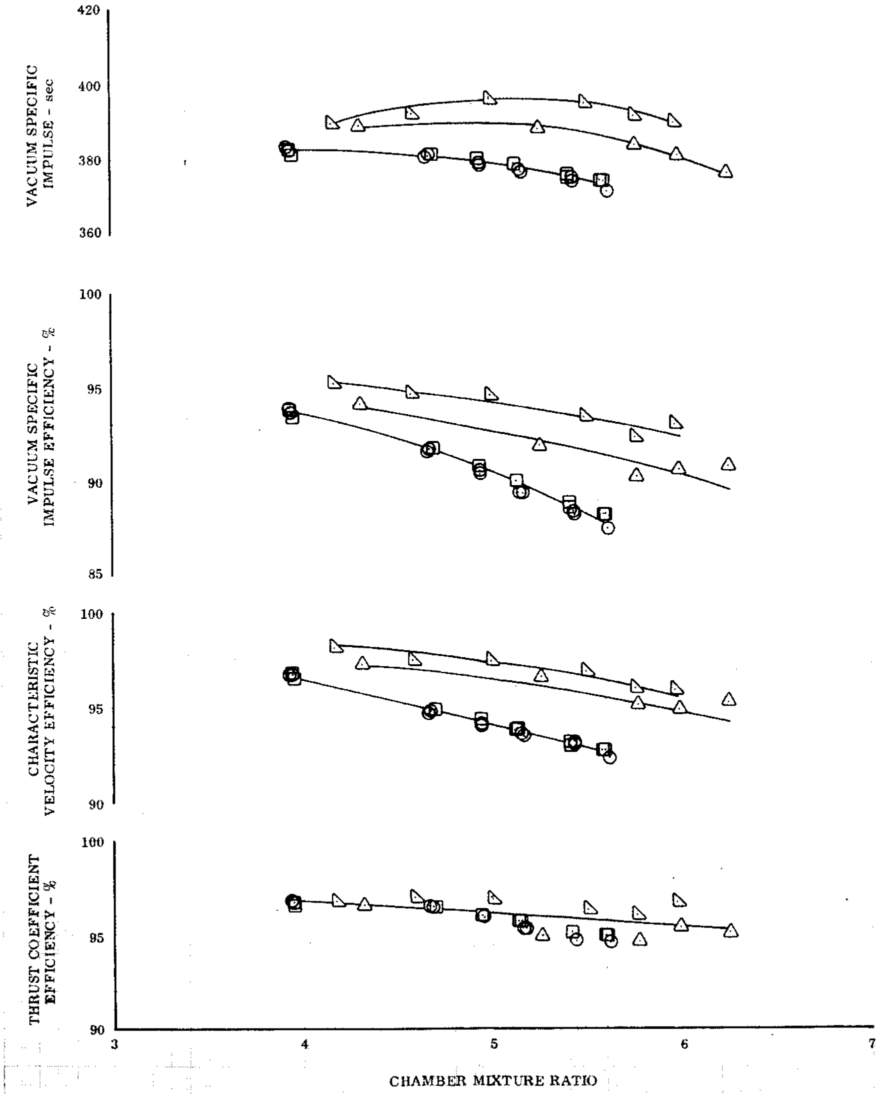

Figure 28. Altitude Test Performance Data for Converging Fuel Stream and Scarfed Element Injectors in the Water-Cooled Thrust Chamber

DF 84784

Table XI. F

TEST DESCRIPTION					TEST	CHAM		
Test No.	Test Type	Chamber L*	Mixture Ratio	Coolant Inlet Temp.	Parameter	Stave No. 1	Stave No. 2	Stave No. 3
9.01	Altitude	52	5.98	539	$\dot{w}$	1.001	1.027	1.013
					TB1	547	-	544
					TB2	-	-	-
					TBO	563	559	558
					TW1	-	-	-
					TW2	-	-	-
					Q	23.38	19.53	18.50
9.01	Altitude	52	6.24	539	$\dot{w}$	1.001	1.027	1.012
					TB1	546	-	545
					TB2	-	-	-
					TBO	559	558	557
					TW1	-	-	-
					TW2	-	-	-
					Q	19.87	19.02	17.70
10.01	Altitude	52	4.16	540	$\dot{w}$	0.999	1.025	1.010
					TB1	559	-	547
					TB2	-	-	-
					TBO	577	619	575
					TW1	-	-	-
					TW2	-	-	-
					Q	35.73	80.39	34.06
10.01	Altitude	52	4.59	540	$\dot{w}$	1.002	1.029	1.014
					TB1	561	-	546
					TB2	-	-	-
					TBO	587	627	573
					TW1	-	-	-
					TW2	-	-	-
					Q	45.95	88.67	32.21
10.01	Altitude	52	5.00	540	$\dot{w}$	1.000	1.027	1.012
					TB1	559	-	547
					TB2	-	-	-
					TBO	583	605	575
					TW1	-	-	-
					TW2	-	-	-
					Q	42.07	65.78	34.20
10.01	Altitude	52	5.49	540	$\dot{w}$	1.000	1.026	1.011
					TB1	558	-	547
					TB2	-	-	-
					TBO	587	604	580
					TW1	-	-	-
					TW2	-	-	-
					Q	45.89	64.57	39.94
10.01	Altitude	52	5.75	540	$\dot{w}$	1.002	1.028	1.013
					TB1	559	-	547
					TB2	-	-	-
					TBO	589	603	577
					TW1	-	-	-
					TW2	-	-	-
					Q	48.24	64.05	36.88
10.01	Altitude	52	5.96	540	$\dot{w}$	1.000	1.027	1.012
					TB1	560	-	547
					TB2	-	-	-
					TBO	597	602	578
					TW1	-	-	-
					TW2	-	-	-
					Q	56.47	62.67	37.16
11.01	Sea Level	52	3.97	540	$\dot{w}$	0.999	1.026	1.011
					TB1	574	-	566
					TB2	-	-	-
					TBO	630	576	588
					TW1	-	-	-
					TW2	-	720	-
					Q	89.06	36.16	47.77

Table XI. Fixed-Thrust Injector, Water-Cooled Thrust Chamber Heat Transfer Data

TEST DESCRIPTION					TEST	CHAMBER SECTION							SPOOLPIECE SECTION							THROAT SECTION							ALTITUDE NOZZLE SECTION						
Test No.	Test Type	Chamber L*	Mixture Ratio	Coolant Inlet Temp.	Parameter	Stave No. 1	Stave No. 2	Stave No. 3	Stave No. 4	Stave No. 5	Stave No. 6	Stave Avg.	Stave No. 1	Stave No. 2	Stave No. 3	Stave No. 4	Stave No. 5	Stave No. 6	Stave Avg.	Stave No. 1	Stave No. 2	Stave No. 3	Stave No. 4	Stave No. 5	Stave No. 6	Stave Avg.	Stave No. 1	Stave No. 2	Stave No. 3	Stave No. 4	Stave No. 5	Stave No. 6	Stave Avg.
1.01	Sea Level	30	4.01	539	$\dot{w}$	0.710	0.707	0.710	0.708	0.702	0.711	0.707								1.054	1.060	1.058	1.065	1.051	1.069	1.059							
					TB1*	553	565	480	561	623	593	563								610	659	630	624	631	700	642							
					TB2	-	-	-	-	-	-	-								-		-	-	-	-	-							
					TBO	602	598	628	612	624	598	610								644	643	656	653	660	645	650							
					TW1	622	644	652	615	-	-	633								-	-	-	-	-	841	841							
					TW2	-	-	-	-	-	-	-								788	849	940	830	970	822	867							
					Q	44.72	41.71	63.18	51.68	59.69	41.94	50.48								110.66	110.24	123.78	121.40	127.17	113.31	117.76							
3.01	Sea Level	30	4.07	540	$\dot{w}$	0.709	0.706	0.709	0.707	0.701	0.710	0.706								1.054	1.060	1.058	1.065	1.051	1.069	1.059							
					TB1	561	572	600	568	-	-	575								609	-	629	617	624	-	620							
					TB2	-	-	-	-	-	-	-								-	-	-	-	-	-	-							
					TBO	612	600	644	623	640	600	620								636	640	658	652	654	635	646							
					TW1	625	625	660	615	748	982	709								818	811	634	867	880	845	809							
					TW2	548	866	922	818	926	840	819								780	826	913	807	917	798	840							
					Q	50.64	41.62	73.11	58.18	69.60	42.11	55.88								100.08	105.03	124.34	118.53	118.65	100.43	111.18							
3.01	Sea Level	30	4.51	540	$\dot{w}$	0.711	0.708	0.711	0.709	0.703	0.712	0.708								1.056	1.062	1.060	1.067	1.053	1.071	1.061							
					TB1	561	567	594	565	-	-	572								620	-	634	616	633	-	625							
					TB2	-	-	-	-	-	-	-								-	-	-	-	-	-	-							
					TBO	614	598	638	617	638	598	617								649	646	664	653	662	646	653							
					TW1	621	617	645	613	672	992	693								842	809	623	864	892	864	816							
					TW2	554	810	916	756	942	809	798								793	841	937	812	960	834	863							
					Q	52.10	40.95	69.40	53.89	68.39	41.08	54.30								114.54	111.64	131.22	119.64	127.93	112.78	119.61							
3.01	Sea Level	30	5.00	540	$\dot{w}$	0.709	0.706	0.709	0.707	0.701	0.710	0.706								1.053	1.059	1.057	1.064	1.050	1.068	1.058							
					TB1	556	574	619	563	-	-	578								622	-	640	620	629	-	628							
					TB2	-	-	-	-	-	-	-								-	-	-	-	-	-	-							
					TBO	611	603	643	616	635	597	617								650	642	670	658	662	644	654							
					TW1	621	628	639	608	652	996	691								852	810	616	858	897	867	817							
					TW2	786	859	941	755	927	823	849								809	849	1075	817	941	811	884							
					Q	50.21	43.81	72.48	53.37	65.89	39.89	54.27								115.22	107.85	136.77	124.55	127.50	110.31	120.38							
7.02	Sea Level	30	4.13	54	$\dot{w}$	1.016	1.002	1.018	1.004	1.012	1.024	1.012								1.442	1.426	1.440	1.409	1.450	1.436	1.433							
					TB1	566	555	557	555	-	555	556								586	564	564	564	563	561	567							
					TB2	-	-	-	-	-	-	-								-	-	-	-	-	-	-							
					TBO	561	560	562	560	562	560	561								592	580	581	573	577	573	579							
					TW1	-	633	623	628	636	625	629								776	679	735	629	648	622	682							
					TW2	-	-	605	597	612	-	605								746	670	655	663	673	669	679							
					Q	17.27	16.03	18.32	16.06	18.21	16.38	17.04								69.21	51.33	53.27	40.86	47.84	41.64	50.69							
7.02	Sea Level	30	5.85	544	$\dot{w}$	1.012	0.998	1.014	0.999	1.008	1.019	1.008								1.436	1.419	1.434	1.402	1.443	1.429	1.427							
					TB1	554	552	555	552	-	552	553								596	566	568	565	571	567	572							
					TB2	-	-	-	-	-	-	-								-	-	-	-	-	-	-							
					TBO	559	558	558	557	559	557	558								599	580	585	576	585	580	584							
					TW1	-	589	605	596	591	586	587								800	779	744	639	674	675	719							
					TW2	-	-	583	604	613	-	600								823	695	708	654	695	692	711							
					Q	15.17	13.97	14.19	12.98	15.11	13.24	14.11								78.97	51.083	58.793	44.864	59.162	51.444	57.388							
9.01	Altitude	52	4.32	539	$\dot{w}$	1.002	1.028	1.013	1.017	1.003	1.012	1.012	1.016	1.002	1.018	1.003	1.012	1.023	1.012	1.442	1.425	1.440	1.408	1.449	1.435	1.433	1.182	1.140	1.140	1.155	1.141	1.155	1.152
					TB1	548	-	545	-	547	-	547	566	-	558	-	600	-	575	593	-	591	-	601	-	595	571	-	565	-	576	-	571
					TB2	-	-	-	-	-	-	-	-	-	-	-	-	-	-	-	-	-	-	-	-	-	600	-	593	-	602	-	598
					TBO	559	559	558	575	562	556	561	588	597	583	635	625	600	605	608	605	600	629	626	613	613	619	620	620	639	625	628	625
					TW1	-	-	-	630	-	-	630	-	-	-	-	526	-	526	-	-	-	-	907	-	907	-	-	642	-	713	-	678
					TW2	-	-	-	798	-	-	798	-	-	-	-	811	-	811	878	-	759	-	868	-	835	-	-	645	-	671	-	658
					Q	19.93	19.94	19.24	35.90	22.66	17.00	22.44	49.68	57.61	44.89	95.58	87.13	61.89	66.13	99.06	93.47	86.83	126.57	126.06	105.18	106.2	94.44	92.22	92.45	114.80	98.24	102.9	99.17
9.01	Altitude	52	5.25	539	$\dot{w}$	1.000	1.027	1.012	1.016	1.001	1.011	1.011	1.015	1.001	1.017	1.002	1.011	1.022	1.011	1.440	1.423	1.438	1.407	1.448	1.434	1.431	1.181	1.139	1.139	1.154	1.140	1.154	1.151
					TB1	547	-	545	-	547	-	546	572	-	555	-	602	-	576	590	-	589	-	606	-	595	574	-	561	-	576	-	571
					TB2	-	-	-	-	-	-	-	-	-	-	-	-	-	-	-	-	-	-	-	-	-	604	-	587	-	601	-	598
					TBO	560	558	556	567	562	555	560	553	595	584	624	625	600	597	613	612	603	628	629	620	617	621	620	613	639	626	629	626
					TW1	-	-	-	601	-	-	601	-	-	-	-	742	-	742	-	-	-	-	913	-	913	-	-	615	-	706	-	661
					TW2	-	-	-	736	-	-	736	-	-	-	-	816	-	816	875	-	745	-	907	-	842	-	-	642	-	670	-	656
					Q	20.78	18.95	17.30	28.32	22.77	15.49	20.60	14.10	55.57	45.90	84.60	86.96	61.97	58.19	106.6	103.6	91.02	124.6	129.3	115.3	111.7	96.99	92.41	89.82	115.0	98.95	103.3	99.42
9.01	Altitude	52	5.77	539	$\dot{w}$	1.001	1.027	1.013	1.016	1.002	1.011	1.011	1.015	1.001	1.017	1.003	1.011	1.023	1.011	1.441	1.424	1.439	1.407	1.448	1.434	1.432	1.181	1.140	1.139	1.155	1.141	1.155	1.151
					TB1	548	-	544	-	546	-	546	590	-	556	-	599	-	582	607	-	597	-	608	-	604	576	-	563	-	574	-	571
					TB2	-	-	-	-	-	-	-	-	-	-	-	-	-	-	-	-	-	-	-	-	-	605	-	586	-	599	-	597
					TBO	563	560	556	566	562	556	560	553	616	587	618	617	606	600	624	618	611	625	629	618	621	623	623	618	638	627	631	627
					TW1	-	-	-	598	-	-	598	-	-	-	-	709	-	709	-	-	-	-	893	-	893	-	-	635	-	686	-	661
					TW2	-	-	-	748	-	-	748	-	-	-	-	800	-	800	942	-	801	-	897	-	880	-	-	639	-	669	-	654
					Q	23.95	20.82	16.98	26.77	22.95	16.35	21.30	13.67	77.07	48.68	78.92	78.99	68.29	60.94	122.1	111.5	103.5	120.6	129.538	112.5	116.6	98.60	95.72	89.73	114.4	99.81	105.4	100.6

---

*Units are given in figure 29

Table XI. Fixed-Thrust Injector, Water-Cooled Thrust Chamber Heat Transfer Data (Continued)

TEST DESCRIPTION					TEST	CHAMBER SECTION							SPOOLPIECE SECTION							THROAT SECTION							ALTITUDE NOZZLE SECTION						
Test No.	Test Type	Chamber L*	Mixture Ratio	Coolant Inlet Temp.	Parameter	Stave No. 1	Stave No. 2	Stave No. 3	Stave No. 4	Stave No. 5	Stave No. 6	Stave Avg.	Stave No. 1	Stave No. 2	Stave No. 3	Stave No. 4	Stave No. 5	Stave No. 6	Stave Avg.	Stave No. 1	Stave No. 2	Stave No. 3	Stave No. 4	Stave No. 5	Stave No. 6	Stave Avg.	Stave No. 1	Stave No. 2	Stave No. 3	Stave No. 4	Stave No. 5	Stave No. 6	Stave Avg.
9.01	Altitude	52	5.98	539	$\dot{w}$	1.001	1.027	1.013	1.016	1.002	1.012	1.011	1.015	1.002	1.017	1.003	1.011	1.023	1.011	1.441	1.424	1.439	1.407	1.448	1.435	1.432	1.181	1.140	1.139	1.155	1.141	1.155	1.151
					TB1	547	-	544	-	547	-	546	587	-	558	-	612	-	586	615	-	595	-	605	-	605	576	-	561	-	574	-	570
					TB2	-	-	-	-	-	-	-	-	-	-	-	-	-	-	-	-	-	-	-	-	-	605	-	583	-	599	-	596
					TBO	563	559	558	566	561	555	560	554	610	589	619	624	600	599	628	620	611	626	626	619	622	622	624	617	637	626	630	626
					TW1	-	-	-	597	-	-	597	-	-	-	-	722	-	722	-	-	-	-	914	-	914	-	-	627	-	681	-	654
					TW2	-	-	-	768	-	-	768	-	-	-	-	819	-	819	992	-	776	-	909	-	892	-	-	633	-	669	-	671
					Q	23.38	19.53	18.50	27.03	21.71	15.81	20.99	14.68	70.56	50.49	79.55	85.06	61.84	60.36	127.5	114.0	103.5	121.42	124.9	114.1	117.5	97.79	96.63	88.22	112.6	98.68	104.0	99.67
9.01	Altitude	52	6.24	539	$\dot{w}$	1.001	1.027	1.012	1.016	1.002	1.011	1.011	1.015	1.001	1.017	1.002	1.011	1.022	1.011	1.441	1.424	1.439	1.407	1.448	1.434	1.432	1.181	1.139	1.139	1.154	1.140	1.158	1.151
					TB1	546	-	545	-	546	-	546	579	-	559	-	600	-	580	613	-	595	-	604	-	604	576	-	560	-	572	-	570
					TB2	-	-	-	-	-	-	-	-	-	-	-	-	-	-	-	-	-	-	-	-	-	606	-	582	-	597	-	595
					TBO	559	558	557	564	559	555	559	560	600	587	618	621	595	597	623	615	609	624	628	617	619	623	626	616	636	626	629	626
					TW1	-	-	-	592	-	-	592	-	-	-	-	765	-	765	-	-	-	-	924	-	924	-	-	626	-	671	-	648
					TW2	-	-	-	518	-	-	518	-	-	-	-	834	-	834	972	-	780	-	950	-	901	-	-	626	-	666	-	646
					Q	19.87	19.02	17.70	25.08	20.07	16.05	19.63	20.78	61.04	48.20	79.02	82.28	57.23	58.09	119.9	107.1	99.53	118.5	128.9	110.7	114.1	98.79	98.42	82.05	110.9	98.58	103.6	99.57
10.01	Altitude	52	4.16	540	$\dot{w}$	0.999	1.025	1.010	1.014	1.000	1.009	1.009	1.013	0.999	1.015	1.001	1.009	1.020	1.009	1.438	1.421	1.436	1.404	1.445	1.431	1.429	1.179	1.137	1.137	1.152	1.138	1.152	1.149
					TB1	559	-	547	-	552	-	553	593	-	591	-	592	-	592	615	-	612	-	610	-	612	580	-	575	-	581	-	579
					TB2	-	-	-	-	-	-	-	-	-	-	-	-	-	-	-	-	-	-	-	-	-	610	-	604	-	605	-	606
					TBO	577	619	575	573	576	572	582	630	675	649	649	628	620	642	637	635	631	629	624	629	631	630	641	633	635	625	640	634
					TW1	-	-	-	642	-	-	642	-	-	-	-	825	-	825	-	-	-	-	874	-	874	-	-	676	-	724	-	700
					TW2	-	-	-	678	-	-	678	-	-	-	-	879	-	879	911	-	823	-	923	-	886	-	-	652	-	672	-	662
					Q	35.73	80.39	34.06	32.07	35.13	31.87	41.54	90.08	133.9	109.3	108.4	87.42	80.35	101.5	138.2	133.1	129.0	123.1	120.3	126.0	128.3	104.7	113.3	104.2	108.4	95.18	114.5	106.7
10.01	Altitude	52	4.59	540	$\dot{w}$	1.002	1.029	1.014	1.018	1.003	1.013	1.013	1.017	1.003	1.018	1.004	1.012	1.024	1.012	1.443	1.426	1.441	1.409	1.450	1.436	1.434	1.183	1.141	1.141	1.156	1.142	1.156	1.153
					TB1	561	-	546	-	558	-	553	601	-	583	-	595	-	593	626	-	614	-	615	-	618	584	-	575	-	580	-	580
					TB2	-	-	-	-	-	-	-	-	-	-	-	-	-	-	-	-	-	-	-	-	-	615	-	604	-	604	-	607
					TBO	587	627	573	573	579	575	586	644	693	639	639	632	625	645	648	643	635	632	629	630	636	633	642	634	637	625	640	635
					TW1	-	-	-	654	-	-	654	-	-	-	-	839	-	839	-	-	-	-	925	-	925	-	-	668	-	721	-	695
					TW2	-	-	-	669	-	-	669	-	-	-	-	904	-	904	1080	-	832	-	945	-	952	-	-	652	-	670	-	661
					Q	45.95	88.67	32.21	32.90	38.59	34.48	45.47	105.2	152.4	99.72	97.90	92.9	86.19	105.7	155.0	145.5	135.0	127.9	127.3	127.8	136.4	108.8	115.1	106.5	110.9	95.71	115.1	108.7
10.01	Altitude	52	5.00	540	$\dot{w}$	1.000	1.027	1.012	1.016	1.001	1.011	1.011	1.015	1.001	1.017	1.002	1.011	1.022	1.011	1.440	1.423	1.438	1.406	1.447	1.434	1.431	1.181	1.139	1.138	1.154	1.140	1.154	1.150
					TB1	559	-	547	-	554	-	553	600	-	596	-	610	-	602	622	-	618	-	622	-	621	588	-	578	-	583	-	583
					TB2	-	-	-	-	-	-	-	-	-	-	-	-	-	-	-	-	-	-	-	-	-	621	-	607	-	608	-	612
					TBO	583	605	575	571	590	575	583	636	684	658	635	652	633	650	642	640	635	634	639	636	638	635	632	636	637	627	642	635
					TW1	-	-	-	673	-	-	673	-	-	-	-	928	-	928	-	-	-	-	942	-	942	-	-	674	-	734	-	704
					TW2	-	-	-	707	-	-	707	-	-	-	-	907	-	907	1076	-	848	-	1057	-	994	-	-	656	-	673	-	665
					Q	42.07	65.78	34.20	30.88	48.97	34.30	42.70	96.73	142.8	119.3	94.40	112.2	94.11	109.9	145.5	141.3	134.8	130.2	141.4	136.5	138.3	111.5	104.1	108.5	111.0	98.01	116.8	108.3
10.01	Altitude	52	5.49	540	$\dot{w}$	1.000	1.026	1.011	1.015	1.001	1.010	1.010	1.014	1.000	1.016	1.001	1.010	1.021	1.010	1.439	1.422	1.437	1.405	1.446	1.432	1.430	1.180	1.138	1.138	1.153	1.139	1.153	1.150
					TB1	558	-	547	-	575	-	560	602	-	604	-	608	-	605	616	-	622	-	613	-	617	590	-	580	-	587	-	586
					TB2	-	-	-	-	-	-	-	-	-	-	-	-	-	-	-	-	-	-	-	-	-	623	-	610	-	613	-	615
					TBO	587	604	580	576	594	575	586	640	678	648	629	648	629	645	640	643	640	632	637	636	638	638	624	638	636	630	640	634
					TW1	-	-	-	647	-	-	647	-	-	-	-	948	-	948	-	-	-	-	929	-	929	-	-	679	-	749	-	714
					TW2	-	-	-	759	-	-	759	-	-	-	-	911	-	911	1016	-	908	-	1024	-	983	-	-	660	-	679	-	670
					Q	45.89	64.57	39.94	35.97	52.84	34.05	45.54	100.2	136.7	109.2	88.17	108.2	90.49	105.5	142.1	144.6	142.7	127.9	138.6	135.8	138.6	114.1	95.06	110.5	109.3	101.3	114.6	107.5
10.01	Altitude	52	5.75	540	$\dot{w}$	1.002	1.028	1.013	1.017	1.003	1.012	1.012	1.016	1.002	1.018	1.003	1.012	1.023	1.012	1.442	1.425	1.440	1.408	1.449	1.435	1.433	1.182	1.140	1.140	1.155	1.141	1.155	1.152
					TB1	559	-	547	-	558	-	555	607	-	592	-	608	-	603	617	-	618	-	610	-	615	583	-	581	-	585	-	583
					TB2	-	-	-	-	-	-	-	-	-	-	-	-	-	-	-	-	-	-	-	-	-	615	-	611	-	612	-	612
					TBO	589	603	577	576	595	581	587	640	676	640	628	651	629	644	639	638	634	633	635	635	636	636	625	639	639	629	642	635
					TW1	-	-	-	664	-	-	664	-	-	-	-	925	-	925	-	-	-	-	918	-	918	-	-	681	-	738	-	709
					TW2	-	-	-	721	-	-	721	-	-	-	-	996	-	996	1022	-	846	-	966	-	945	-	-	659	-	680	-	669
					Q	48.24	64.05	36.88	36.03	54.37	40.95	46.75	101.2	135.7	100.7	87.62	111.4	90.35	104.5	141.6	138.41	134.5	130.3	135.8	135.5	136.0	112.6	95.97	111.5	112.9	100.3	116.9	108.4
10.01	Altitude	52	5.96	540	$\dot{w}$	1.000	1.027	1.012	1.016	1.001	1.011	1.011	1.015	1.001	1.017	1.002	1.011	1.022	1.011	1.440	1.423	1.438	1.407	1.448	1.434	1.431	1.181	1.139	1.139	1.154	1.140	1.154	1.151
					TB1	560	-	547	-	572	-	560	632	-	588	-	613	-	611	615	-	615	-	610	-	613	582	-	580	-	584	-	582
					TB2	-	-	-	-	-	-	-	-	-	-	-	-	-	-	-	-	-	-	-	-	-	613	-	610	-	611	-	611
					TBO	597	602	578	577	607	590	592	667	674	641	629	650	636	650	638	636	634	628	633	632	634	637	625	639	637	631	643	635
					TW1	-	-	-	603	-	-	603	-	-	-	-	990	-	990	-	-	-	-	929	-	929	-	-	680	-	737	-	708
					TW2	-	-	-	772	-	-	772	-	-	-	-	1025	-	1025	1012	-	909	-	1023	-	982	-	-	659	-	682	-	671
					Q	56.47	62.67	37.16	36.97	66.41	49.44	51.52	127.8	133.5	102.1	88.49	110.2	97.33	109.9	140.0	135.9	133.2	122.1	134.0	130.5	132.6	113.1	95.80	111.2	111.3	102.4	117.8	108.6
11.01	Sea Level	52	3.97	540	$\dot{w}$	0.999	1.026	1.011	1.015	1.000	1.010	1.010	1.014	1.000	1.015	1.001	1.009	1.021	1.009	1.439	1.422	1.437	1.405	1.446	1.425	1.428							
					TB1	574	-	566	-	561	-	567	609	-	609	-	591	-	603	608	-	616	-	-	-	612							
					TB2	-	-	-	-	-	-	-	-	-	-	-	-	-	-	-	-	-	-	-	-	-							
					TBO	630	576	588	567	582	581	587	662	615	648	599	626	622	629	633	610	622	611	634	-	622							
					TW1	-	-	-	643	-	-	643	-	-	-	-	799	-	799	-	-	-	-	905	-	905							
					TW2	-	720	-	678	-	-	699	-	-	-	-	863	-	863	906	-	830	-	964	-	900							
					Q	89.06	36.16	47.77	26.30	41.60	40.30	46.87	122.8	74.51	108.7	57.96	86.46	83.32	88.98	133.0	98.88	117.2	98.35	134.5	-	116.4							

Table XI. Fixed-Thrust Injector, Water-Cooled Thrust Chamber Heat Transfer Data (Continued)

TEST DESCRIPTION					TEST	CHAMBER SECTION							SPOOLPIECE SECTION						
Test No.	Test Type	Chamber L*	Mixture Ratio	Coolant Inlet Temp.	Parameter	Stave No. 1	Stave No. 2	Stave No. 3	Stave No. 4	Stave No. 5	Stave No. 6	Stave Avg.	Stave No. 1	Stave No. 2	Stave No. 3	Stave No. 4	Stave No. 5	Stave No. 6	Stave Avg.
11.01	Sea Level	52	4.77	540	ẇ	1.003	1.030	1.015	1.019	1.004	1.014	1.014	1.018	1.004	1.019	1.005	1.014	1.025	1.014
					TB1	579	-	587	-	591	-	585	609	-	606	-	620	-	611
					TB2	-	-	-	-	-	-	-	-	-	-	-	-	-	-
					TBO	633	902	589	577	611	605	653	671	597	626	608	647	640	632
					TW1	-	-	-	629	-	-	629	-	-	-	-	889	-	889
					TW2	-	685	-	663	-	-	674	-	-	-	-	948	-	948
					Q	92.06	372.3	48.60	37.08	70.77	64.62	114.2	132.6	56.26	86.63	67.14	107.5	101.9	92.02
11.01	Sea Level	52	5.27	541	ẇ	0.999	1.026	1.011	1.015	1.000	1.010	1.010	1.014	1.000	1.015	1.001	1.010	1.021	1.010
					TB1	573	-	574	-	589	-	579	607	-	627	-	646	-	627
					TB2	-	-	-	-	-	-	-	-	-	-	-	-	-	-
					TBO	632	634	610	576	636	583	612	663	609	657	614	690	613	641
					TW1	-	-	-	637	-	-	637	-	-	-	-	1022	-	1022
					TW2	-	735	-	658	-	-	696	-	-	-	-	1038	-	1038
					Q	90.42	95.02	69.70	35.32	95.38	41.93	71.30	123.1	68.22	117.4	73.06	150.2	73.92	101.0
11.01	Sea Level	52	5.42	541	ẇ	1.000	1.026	1.011	1.015	1.001	1.010	1.010	1.014	1.000	1.016	1.002	1.010	1.022	1.010
					TB1	556	-	576	-	569	-	567	602	-	618	-	656	-	625
					TB2	-	-	-	-	-	-	-	-	-	-	-	-	-	-
					TBO	637	639	608	592	621	594	615	680	637	650	638	668	610	647
					TW1	-	-	-	660	-	-	660	-	-	-	-	1004	-	1004
					TW2	-	678	-	708	-	-	693	-	-	-	-	1036	-	1036
					Q	95.55	100.4	67.54	52.02	79.83	53.84	74.87	140.6	95.72	110.6	92.10	128.4	70.29	107.1
11.01	Sea Level	52	5.72	540	ẇ	1.002	1.029	1.014	1.018	1.003	1.013	1.013	1.017	1.003	1.019	1.004	1.013	1.024	1.013
					TB1	556	-	577	-	565	-	566	626	-	627	-	643	-	632
					TB2	-	-	-	-	-	-	-	-	-	-	-	-	-	-
					TBO	640	551	607	586	605	589	596	689	660	665	626	647	601	648
					TW1	-	-	-	630	-	-	630	-	-	-	-	840	-	840
					TW2	-	704	-	747	-	-	725	-	-	-	-	879	-	879
					Q	99.31	10.12	67.07	45.62	64.15	48.58	55.81	150.4	119.2	126.8	85.29	107.1	61.40	108.3
14.01	Altitude	52	3.94	531	ẇ	1.440	1.399	1.418	1.380	1.391	1.423	1.408	1.547	1.454	1.445	1.454	1.445	1.454	1.465
					TBO	543	-	542	543	541	544	543	554	545	549	554	554	544	550
					TW2	-	-	-	-	-	-	-	-	-	-	-	-	-	-
					Q	17.25	-	15.40	16.19	13.31	18.93	16.19	34.62	19.94	25.59	32.80	33.22	18.98	27.48
14.01	Altitude	52	4.66	531	ẇ	1.440	1.399	1.418	1.380	1.391	1.424	1.408	1.547	1.454	1.445	1.454	1.446	1.454	1.465
					TBO	543	-	542	542	541	545	543	553	547	551	556	556	555	553
					TW2	-	-	-	-	-	-	-	-	-	-	-	-	-	-
					Q	17.32	-	15.09	15.04	12.85	19.01	15.84	32.73	23.33	27.89	35.91	35.65	34.93	31.76
14.01	Altitude	52	4.94	531	ẇ	1.439	1.398	1.418	1.379	1.390	1.423	1.407	1.546	1.453	1.445	1.453	1.445	1.453	1.465
					TBO	544	-	545	544	544	547	545	552	550	552	556	557	559	554
					TW2	-	-	-	-	-	-	-	-	-	-	-	-	-	-
					Q	17.41	-	18.40	17.39	17.20	21.99	18.45	30.93	27.49	30.09	36.28	36.35	39.53	33.49
14.01	Altitude	52	5.15	531	ẇ	1.440	1.399	1.418	1.380	1.391	1.424	1.408	1.547	1.454	1.446	1.454	1.446	1.454	1.465
					TBO	542	-	544	545	542	545	543	551	551	551	559	555	556	554
					TW2	-	-	-	-	-	-	-	-	-	-	-	-	-	-
					Q	15.23	-	17.20	18.17	14.30	19.36	16.84	30.94	28.39	28.70	39.54	33.73	35.87	32.90
14.01	Altitude	52	5.43	531	ẇ	1.440	1.399	1.418	1.379	1.390	1.423	1.407	1.546	1.453	1.445	1.453	1.445	1.453	1.465
					TBO	544	-	-	544	537	545	543	556	500	548	560	560	561	556
					TW2	-	-	-	-	-	-	-	-	-	-	-	-	-	-
					Q	18.20	-	-	17.05	7.92	18.95	15.50	38.27	26.71	23.28	40.82	41.31	42.48	35.47
14.01	Altitude	52	5.61	531	ẇ	1.439	1.398	1.417	1.379	1.390	1.423	1.407	1.546	1.453	1.445	1.453	1.445	1.453	1.465
					TBO	544	-	-	545	542	549	545	556	553	553	561	553	564	557
					TW2	-	-	-	-	-	-	-	-	-	-	-	-	-	-
					Q	17.45	-	-	18.67	14.25	25.16	18.87	37.21	30.45	31.53	42.65	31.14	46.49	36.59
17.02	Altitude	52	3.94	522	ẇ	1.440	1.399	1.419	1.380	1.391	1.424	1.408	1.547	1.454	1.446	1.454	1.446	1.454	1.465
					TBO	537	-	534	535	541	537	537	546	-	547	548	553	553	549
					TW2	-	-	-	-	-	-	-	-	-	-	-	-	-	-
					Q	21.79	-	17.38	18.07	26.39	21.64	21.04	36.42	-	35.79	37.13	45.42	45.38	40.03
17.02	Altitude	52	4.69	522	ẇ	1.440	1.399	1.418	1.380	1.391	1.423	1.408	1.547	1.453	1.445	1.453	1.445	1.453	1.465
					TBO	537	-	534	535	-	537	536	549	-	548	551	561	556	553
					TW2	-	-	-	-	-	-	-	-	-	-	-	-	-	-
					Q	21.97	-	17.32	18.03	-	20.51	19.36	41.47	-	37.33	41.57	56.52	48.54	45.09
17.02	Altitude	52	4.93	522	ẇ	1.440	1.399	1.419	1.380	1.391	1.424	1.408	1.547	1.454	1.446	1.454	1.446	1.454	1.466
					TBO	539	-	534	536	-	536	536	551	-	554	549	559	553	553
					TW2	-	-	-	-	-	-	-	-	-	-	-	-	-	-
					Q	23.52	-	16.93	18.46	-	19.30	19.45	45.06	-	46.56	39.50	52.56	45.01	45.71
17.02	Altitude	52	5.13	522	ẇ	1.441	1.399	1.419	1.380	1.391	1.424	1.408	1.547	1.454	1.446	1.454	1.446	1.454	1.466
					TBO	537	-	533	537	-	540	537	546	-	552	550	559	560	553
					TW2	-	-	-	-	-	-	-	-	-	-	-	-	-	-
					Q	20.86	-	16.19	20.09	-	24.93	20.42	36.47	-	43.06	41.00	52.89	55.44	45.84
17.02	Altitude	52	5.40	522	ẇ	1.440	1.399	1.418	1.380	1.391	1.424	1.408	1.547	1.454	1.445	1.454	1.445	1.454	1.465
					TBO	536	-	535	536	-	543	537	549	-	549	549	560	572	556
					TW2	-	-	-	-	-	-	-	-	-	-	-	-	-	-
					Q	19.82	-	17.69	19.41	-	30.06	21.63	41.84	-	38.81	39.49	54.41	72.42	49.43
17.02	Altitude	52	5.59	522	ẇ	1.440	1.399	1.418	1.380	1.391	1.424	1.408	1.547	1.454	1.446	1.454	1.446	1.454	1.466
					TBO	536	-	535	537	-	541	537	548	-	557	558	563	559	557
					TW2	-	-	-	-	-	-	-	-	-	-	-	-	-	-
					Q	19.55	-	18.29	20.72	-	26.97	21.28	39.51	-	50.16	52.24	59.73	54.35	51.29

TEST DESCRIPTION					TEST	THROAT SECTION							ALTITUDE NOZZLE SECTION						
Test No.	Test Type	Chamber L*	Mixture Ratio	Coolant Inlet Temp.	Parameter	Stave No. 1	Stave No. 2	Stave No. 3	Stave No. 4	Stave No. 5	Stave No. 6	Stave Avg.	Stave No. 1	Stave No. 2	Stave No. 3	Stave No. 4	Stave No. 5	Stave No. 6	Stave Avg.
11.01	Sea Level	52	4.77	540	ẇ	1.444	1.427	1.442	1.411	1.452	1.438	1.435							
					TB1	609	-	620	-	-	-	614							
					TB2	-	-	-	-	-	-	-							
					TBO	636	611	626	624	640	-	627							
					TW1	-	-	-	-	931	-	931							
					TW2	933	-	868	-	1022	-	941							
					Q	137.6	99.66	122.5	117.4	143.1	-	124.1							
11.01	Sea Level	52	5.27	541	ẇ	1.439	1.422	1.437	1.405	1.446	1.432	1.430							
					TB1	615	-	630	-	-	-	622							
					TB2	-	-	-	-	-	-	-							
					TBO	645	623	639	622	643	-	634							
					TW1	-	-	-	-	963	-	963							
					TW2	1002	-	952	-	1024	-	993							
					Q	149.9	116.7	140.0	114.0	147.7	-	133.7							
11.01	Sea Level	52	5.42	541	ẇ	1.439	1.422	1.437	1.406	1.447	1.433	1.430							
					TB1	618	-	624	-	-	-	624							
					TB2	-	-	-	-	-	-	-							
					TBO	642	632	640	625	624	-	633							
					TW1	-	-	-	-	935	-	935							
					TW2	971	-	866	-	1012	-	950							
					Q	144.8	128.8	142.8	117.3	120.5	-	130.9							
11.01	Sea Level	52	5.72	540	ẇ	1.443	1.426	1.441	1.409	1.450	1.437	1.434							
					TB1	610	-	623	-	-	-	616							
					TB2	-	-	-	-	-	-	-							
					TBO	641	630	638	627	623	-	632							
					TW1	-	-	-	-	925	-	925							
					TW2	1013	-	846	-	859	-	906							
					Q	144.9	126.2	139.1	120.7	119.0	-	130.0							
14.01	Altitude	52	3.94	531	ẇ	-	-	-	-	-	-	1.317	1.576	1.562	1.555	1.603	1.577	1.591	1.577
					TBO	-	-	-	-	-	-	581	-	-	-	-	-	-	605
					TW2	675	745	765	819	-	681	737	-	-	-	-	-	-	-
					Q	-	-	-	-	-	-	65.32	-	-	-	-	-	-	122.4
14.01	Altitude	52	4.66	531	ẇ	-	-	-	-	-	-	1.315	1.576	1.562	1.555	1.603	1.577	1.591	1.577
					TBO	-	-	-	-	-	-	585	-	-	-	-	-	-	612
					TW2	695	759	794	829	-	706	757	-	-	-	-	-	-	-
					Q	-	-	-	-	-	-	70.74	-	-	-	-	-	-	127.3
14.01	Altitude	52	4.94	531	ẇ	-	-	-	-	-	-	1.317	1.575	1.562	1.554	1.603	1.576	1.590	1.575
					TBO	-	-	-	-	-	-	586	-	-	-	-	-	-	612
					TW2	696	810	787	914	-	692	780	-	-	-	-	-	-	-
					Q	-	-	-	-	-	-	71.30	-	-	-	-	-	-	126.9
14.01	Altitude	52	5.15	531	ẇ	-	-	-	-	-	-	1.318	1.576	1.562	1.555	1.603	1.577	1.591	1.577
					TBO	-	-	-	-	-	-	592	-	-	-	-	-	-	607
					TW2	693	810	886	916	-	691	799	-	-	-	-	-	-	-
					Q	-	-	-	-	-	-	79.55	-	-	-	-	-	-	118.9
14.01	Altitude	52	5.43	531	ẇ	-	-	-	-	-	-	1.313	1.576	1.562	1.555	1.603	1.576	1.591	1.575
					TBO	-	-	-	-	-	-	595	-	-	-	-	-	-	605
					TW2	708	770	796	907	-	738	784	-	-	-	-	-	-	-
					Q	-	-	-	-	-	-	83.47	-	-	-	-	-	-	116.1
14.01	Altitude	52	5.61	531	ẇ	-	-	-	-	-	-	1.317	1.575	1.562	1.554	1.602	1.576	1.590	1.575
					TBO	-	-	-	-	-	-	596	-	-	-	-	-	-	602
					TW2	704	765	810	951	-	771	800	-	-	-	-	-	-	-
					Q	-	-	-	-	-	-	84.50	-	-	-	-	-	-	110.8
17.02	Altitude	52	3.94	522	ẇ	-	-	-	-	-	-	1.312	1.577	1.563	1.555	1.604	1.577	1.592	1.577
					TBO	-	-	-	-	-	-	-	-	-	-	-	-	-	-
					TW2	670	720	823	832	-	-	761	-	-	-	-	-	-	-
					Q	-	-	-	-	-	-	-	-	-	-	-	-	-	-
17.02	Altitude	52	4.69	522	ẇ	-	-	-	-	-	-	1.312	1.576	1.562	1.555	1.603	1.577	1.591	1.577
					TBO	-	-	-	-	-	-	-	-	-	-	-	-	-	-
					TW2	711	779	873	930	-	-	823	-	-	-	-	-	-	-
					Q	-	-	-	-	-	-	-	-	-	-	-	-	-	-
17.02	Altitude	52	4.93	522	ẇ	-	-	-	-	-	-	1.312	1.577	1.563	1.555	1.604	1.577	1.592	1.577
					TBO	-	-	-	-	-	-	-	-	-	-	-	-	-	-
					TW2	740	763	886	932	-	-	830	-	-	-	-	-	-	-
					Q	-	-	-	-	-	-	-	-	-	-	-	-	-	-
17.02	Altitude	52	5.13	522	ẇ	-	-	-	-	-	-	1.312	1.577	1.563	1.556	1.604	1.577	1.592	1.577
					TBO	-	-	-	-	-	-	-	-	-	-	-	-	-	-
					TW2	749	759	916	1091	-	-	879	-	-	-	-	-	-	-
					Q	-	-	-	-	-	-	-	-	-	-	-	-	-	-
17.02	Altitude	52	5.40	522	ẇ	-	-	-	-	-	-	1.312	1.576	1.562	1.555	1.603	1.577	1.531	1.577
					TBO	-	-	-	-	-	-	-	-	-	-	-	-	-	-
					TW2	751	761	874	867	-	-	813	-	-	-	-	-	-	-
					Q	-	-	-	-	-	-	-	-	-	-	-	-	-	-
17.02	Altitude	52	5.59	522	ẇ	-	-	-	-	-	-	1.312	1.576	1.563	1.555	1.604	1.577	1.591	1.577
					TBO	-	-	-	-	-	-	-	-	-	-	-	-	-	-
					TW2	726	815	848	870	-	-	815	-	-	-	-	-	-	-
					Q	-	-	-	-	-	-	-	-	-	-	-	-	-	-

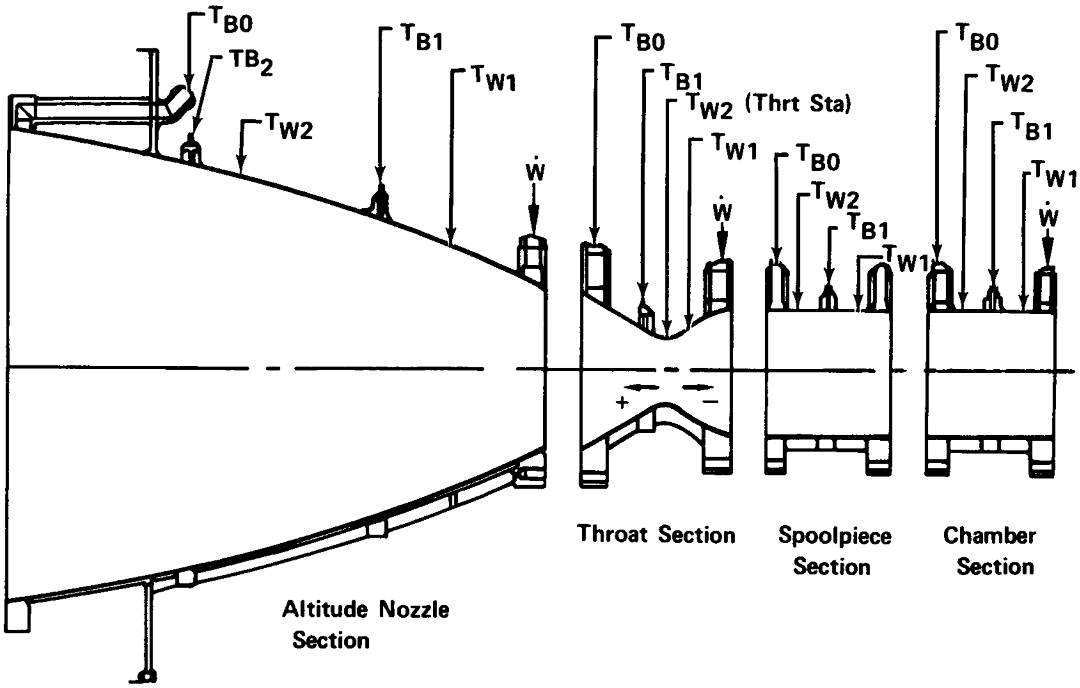

Parameter	Symbol	Units	Thermocouple Location - Surface Distance From Throat Station (in.)			
			Nozzle	Throat	Spoolpiece	Chamber
Coolant Flowrate	$\dot{W}$	lb$_m$/sec				
Coolant Intermediate Temperature No. 1	T_{B1}	°R	+12.045	+1.085	-5.238	-10.7
Coolant Intermediate Temperature No. 2	T_{B2}	°R	+20.395	–	–	–
Coolant Discharge Temperature	T_{B0}	°R	+28.190	+4.337	-2.340	-7.969
Upstream Wall Temperature	T_{W1}	°R	+ 8.768	-0.945	-6.562	-10.70
Downstream Wall Temperature	T_{W2}	°R	+18.233	0	-3.747	-9.376
Heat Transfer	Q	Btu/sec	–	–	–	–

Figure 29. Water-Cooled Chamber Heat Transfer Data Schematic FD45116A

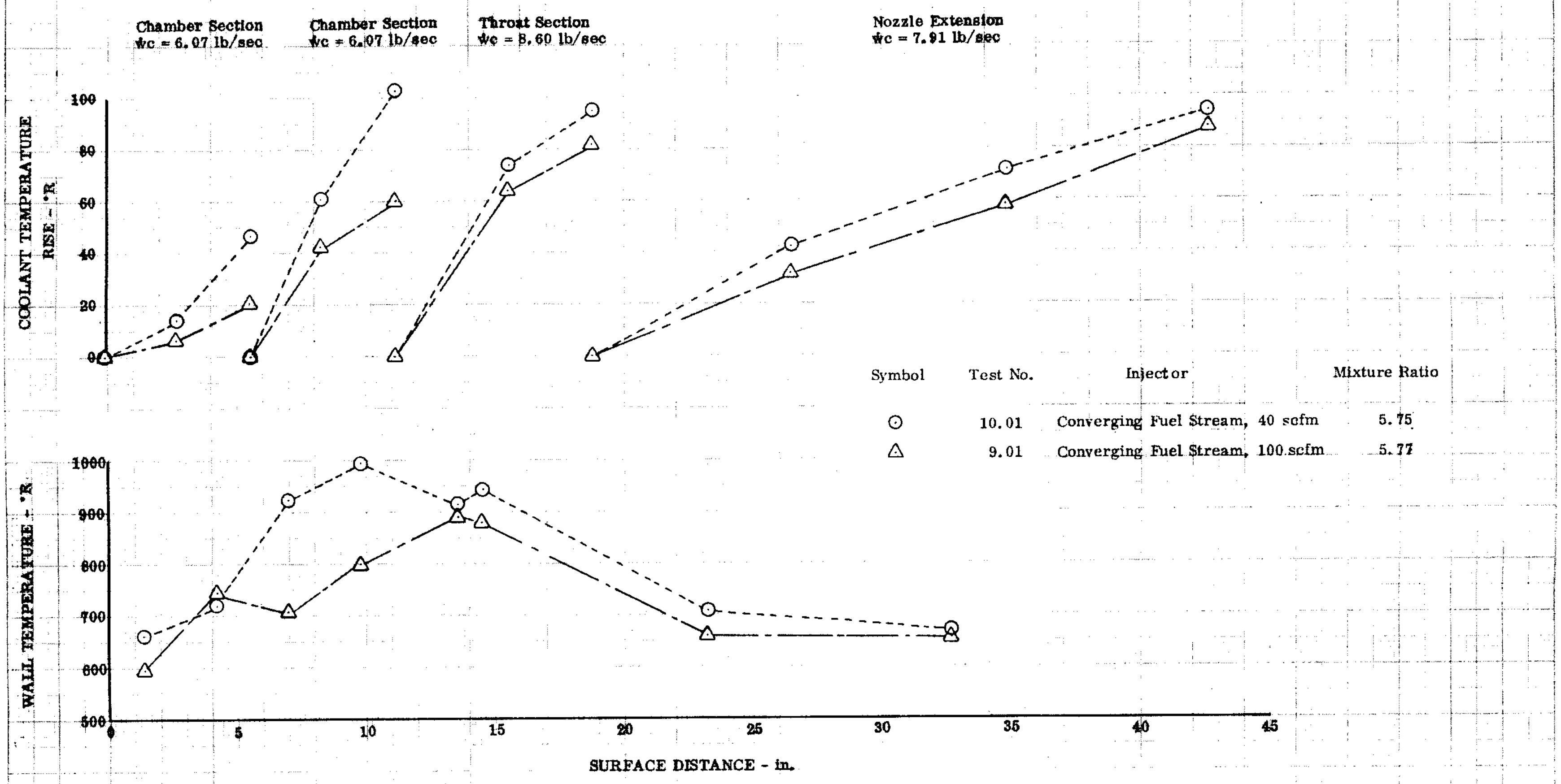

Figure 30. Axial Coolant and Wall Temperature Data

DF 83158A

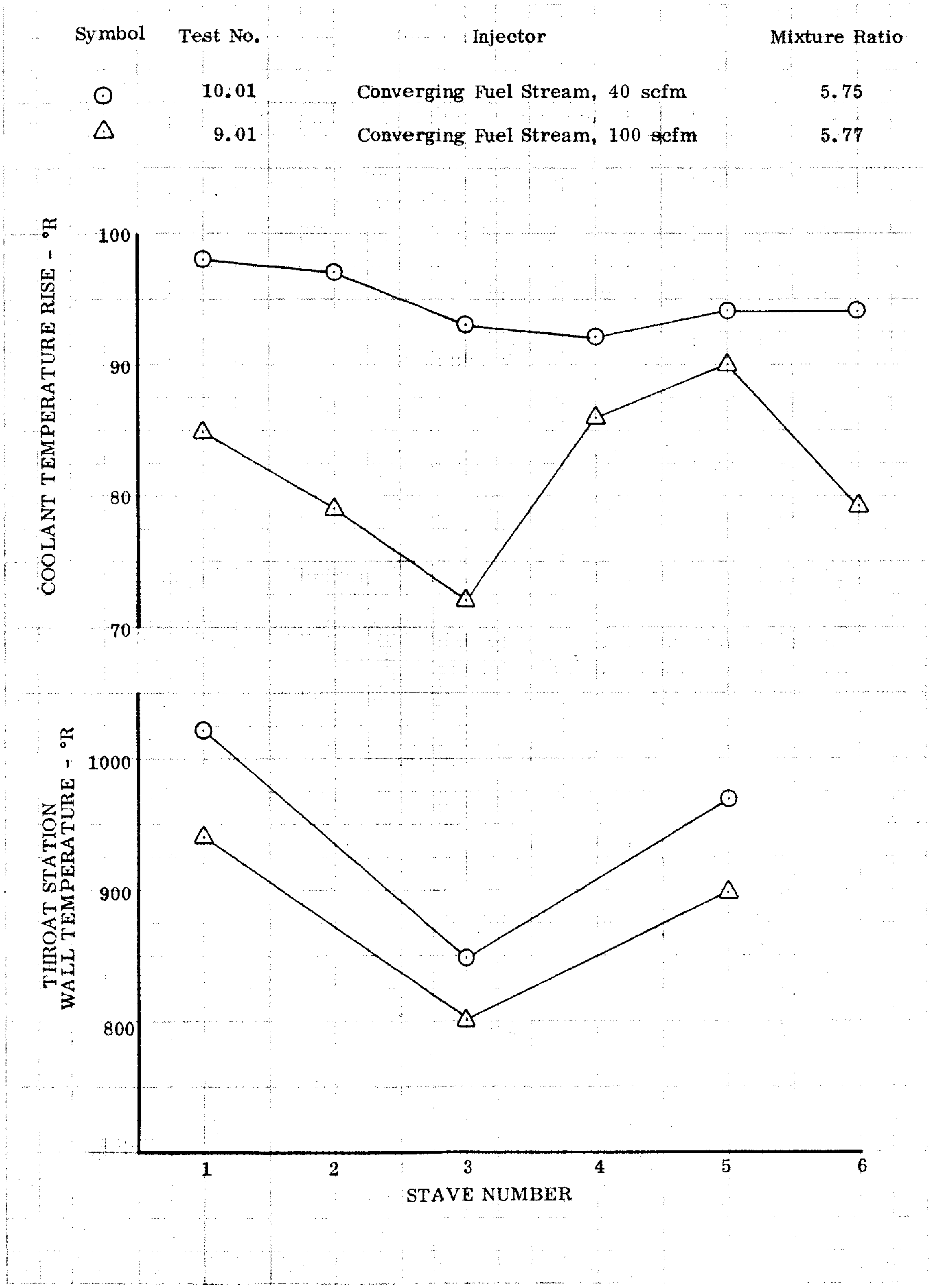

Figure 31. Representative Throat Section Circumferential Variations of Coolant and Wall Temperature

DF83156A

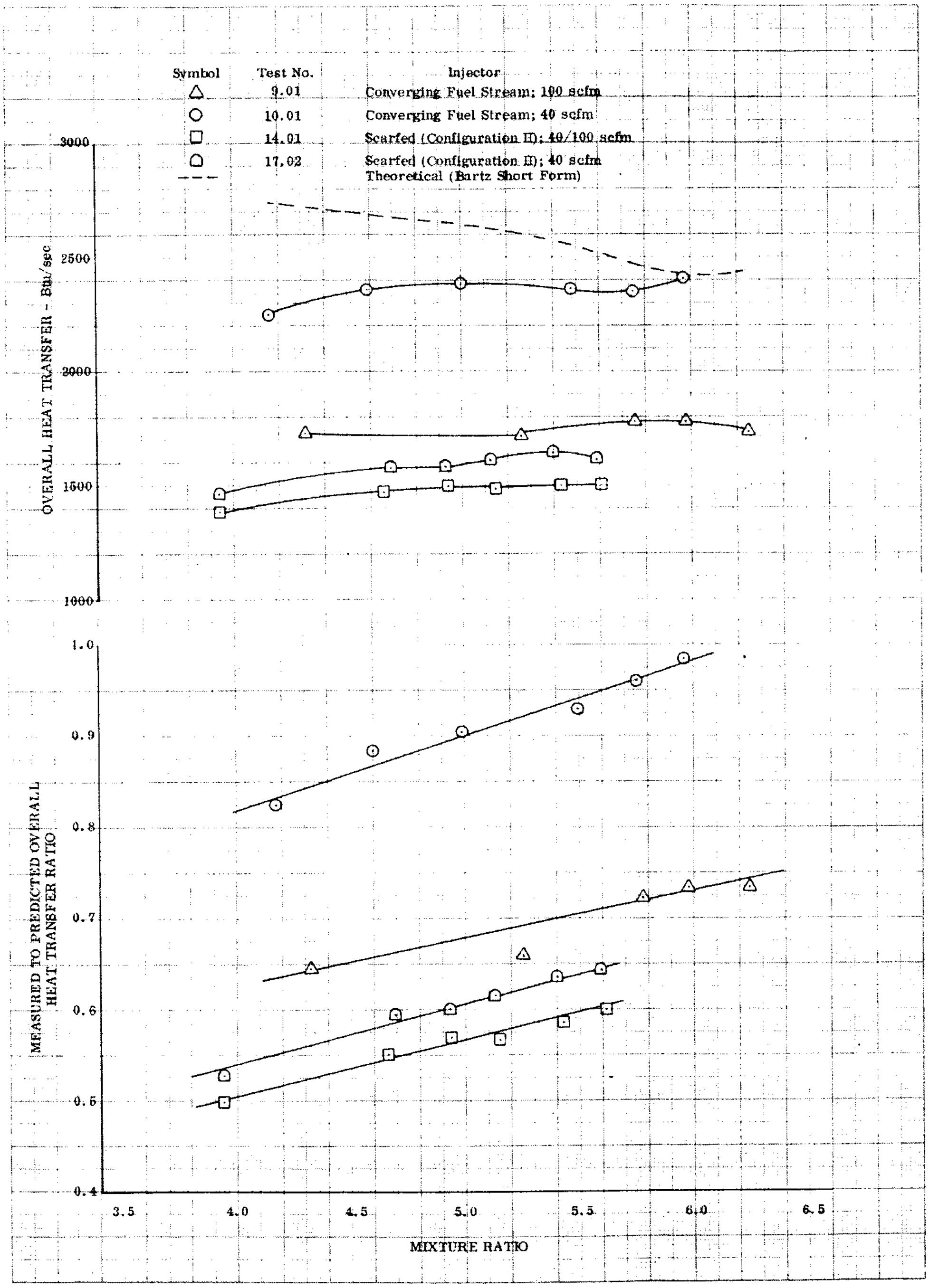

Figure 32. Overall Thrust Chamber Heat Transfer (Water-Cooled Chamber) DF 84785

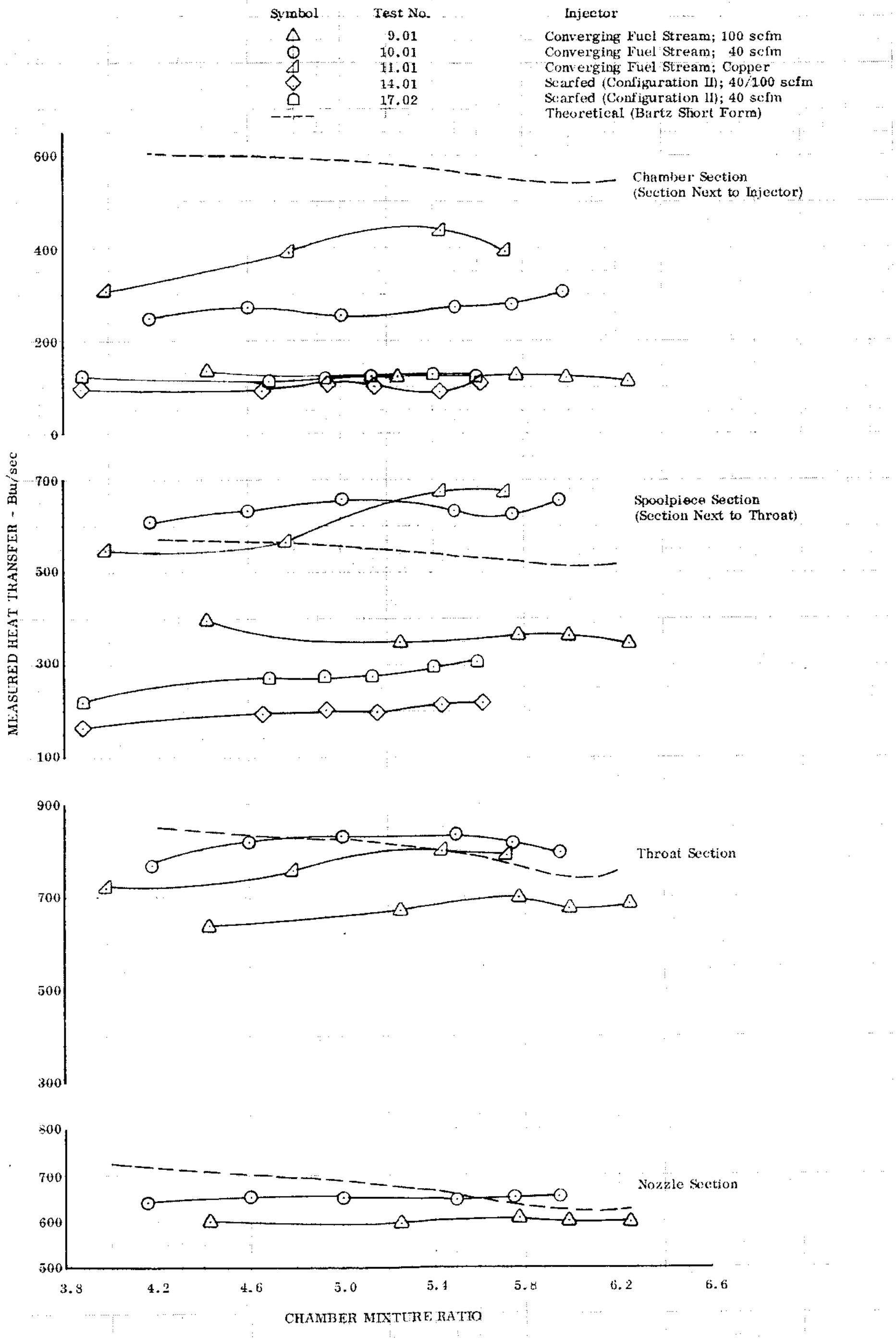

Figure 33. Thrust Chamber Component Heat Transfer Data (Water-Cooled Chamber) DF 84786

The equation for the combustion side heat transfer is:

$$h_g = \frac{1}{(T_{aw} - T_{wg})} \frac{dQ}{dA}$$

With this equation, local chamber heat transfer coefficients (h_g) can be determined from a knowledge of the adiabatic and combustion side wall temperatures and the local heat flux, dQ/dA. The adiabatic wall temperature (T_{aw}) was calculated using standard techniques. Combustion side wall temperature (T_{wg}) was determined using a curve through the measured data. (Because of the magnitude of the adiabatic wall temperature, in relation to the wall temperature, the combustion side coefficient is not a strong function of the latter temperature in this equation, so errors introduced by interpolating for wall temperatures between measurement locations are not significant.) To determine local heat flux values at several axial stations, the chamber heat transfer for each axial section was plotted as a function of thrust chamber surface area (figure 34). Local heat flux values can be determined graphically by measuring the slope at any station along the curve. This graphic method proved adequate where the curve was smooth through the measured data and had no inflection points, such as in the chamber and nozzle sections. However, because of the heat flux peak in the throat region there is an inflection point in the heat transfer versus surface area curve. In this section, the graphic method is not adequate and thus determination of the heat transfer coefficient requires an iterative solution involving the coolant side heat transfer, as well as the combustion side heat transfer equations. Briefly the solution used for the throat region was as follows:

1. A heat transfer vs surface area curve that fits the experimental data was assumed for the throat region. This permitted the determination of a first guess combustion side heat transfer coefficient curve for the region.

2. Coolant temperature and a coolant side coefficient were then calculated for the combustion side heat transfer coefficient determined in Step No. 1.

3. Using the computed coolant temperature and the coolant side heat transfer coefficient (from Step No. 2), and the measured wall temperature, the combustion side heat transfer coefficient could then be calculated parametrically using a two-dimensional analysis.

4. Using the new combustion side coefficient, a new heat-transfer-versus-surface-area curve was plotted and the steps repeated until the combustion side heat transfer coefficients determined in Steps No. 1 and 3 agreed.

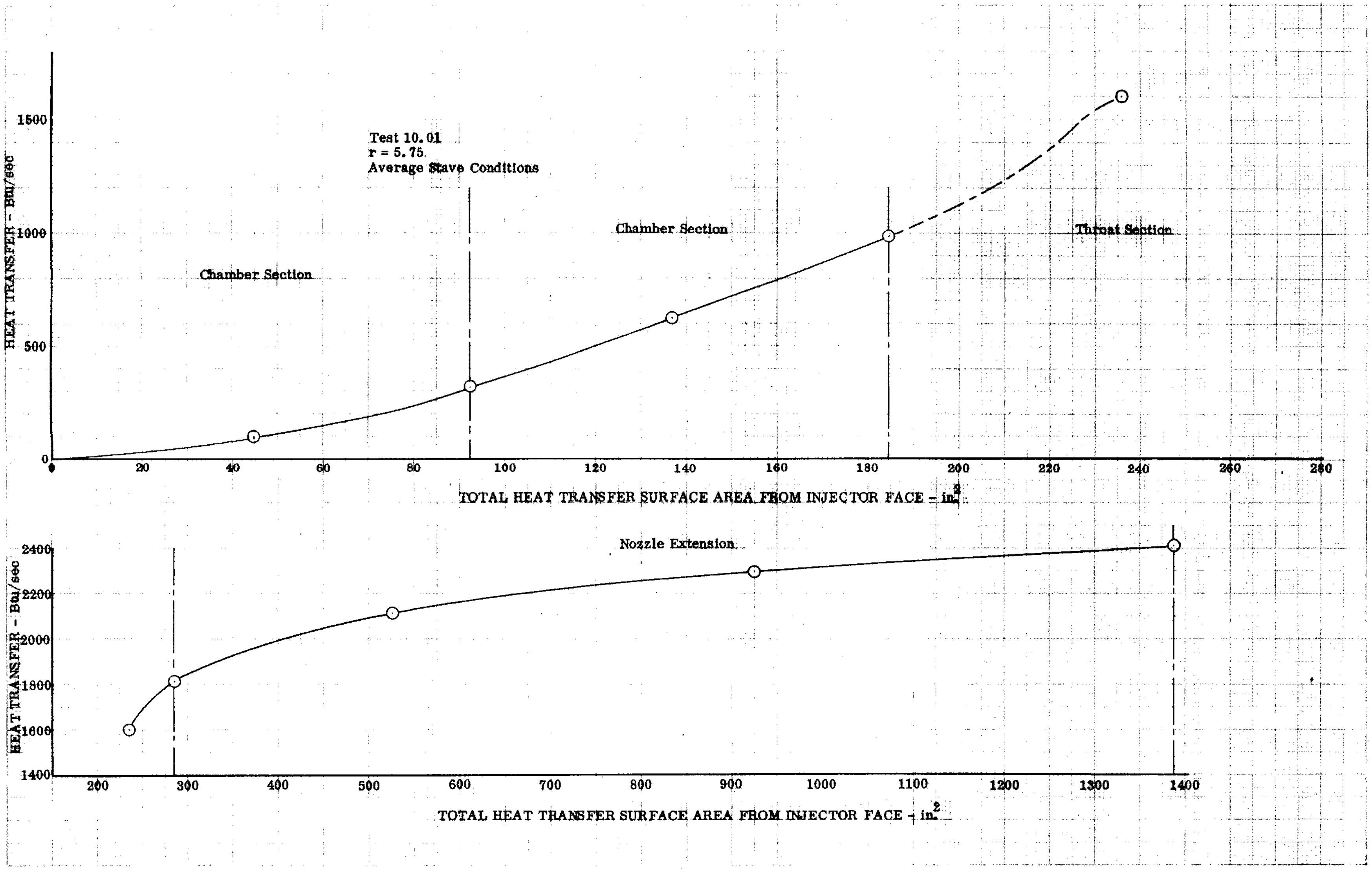

Figure 34. Overall Thrust Chamber Heat Transfer vs Surface Area

DF 83165A

Using the foregoing method, heat transfer coefficient profiles were determined for the converging fuel stream injector (the highest performing injector) for subsequent use in design of the regenerative chamber. Figures 35, 36, and 37 present heat transfer coefficient profiles determined for test conditions of interest. Figure 35 shows the average profile curves determined for the converging fuel stream injector with its 40-scfm and 100-scfm faceplates compared to the theoretical Bartz profile. The profile for the 40-scfm faceplate is lower than the Bartz profile in the combustion chamber near the injector, but demonstrates a much higher coefficient in the converging part of the chamber. In the throat and nozzle regions the profile with this faceplate is close to the Bartz curve. Figure 36 shows how the heat transfer coefficient profiles change with the mixture ratio for the 40-scfm faceplate. This figure indicates less severe heat transfer conditions for mixture ratios of 4.15 and 5.0 than for the optimum value (5.75). Figure 37 compares the maximum, minimum, and average profile curves obtained for the 40-scfm faceplate.

E. HARDWARE DURABILITY

1. Injectors

In tests with the concentric-tube injectors, good durability was demonstrated. Typical photographs of the injector faceplates after testing are shown in figures 38, 39, and 40. A uniform soot layer was present after each test. No overheating was noted in any of the tests, but the copper did warp sufficiently to adversely affect performance, and hence, the Rigimesh faceplates are preferred.

In the only test made with the pentad injector, severe injector face burning occurred (figure 41). Inspection of the injector indicated that recirculation of high-mixture-ratio combustion gases adjacent to the injector face between the fuel and oxidizer injection orifices, caused the burning.

2. Thrust Chamber

The durability of the water-cooled chamber hardware was generally acceptable for the purpose for which it was intended, although some difficulties were encountered. A chamber failure did occur in test No. 3.01; approximately 32 sec into the planned 60-sec duration of this test, burnouts occurred between adjacent staves in the throat and chamber sections; figure 42 shows the burned-through area in the throat section at a seam. This failure is attributed to the fact that coolant passages at the seams were farther apart than passages in the middle of the staves. As a result, the heat flux into these seam passages was sufficiently high to cause nucleate boiling, which by itself was not detrimental. However, with nucleate boiling in these seam passages and convective cooling occurring in the inside passages, a parallel heat exchanger effect resulted in which the coolant flowrate in the outer passages decreased in order to balance pressure drops with the non-boiling passages. This condition eventually bootstrapped to the point that film boiling and burnouts occurred. The chamber and throat sections (burned during test No. 3.01) were repaired by removing the damaged staves and welding in spares. Figure 43 shows the throat section with the two damaged staves removed.

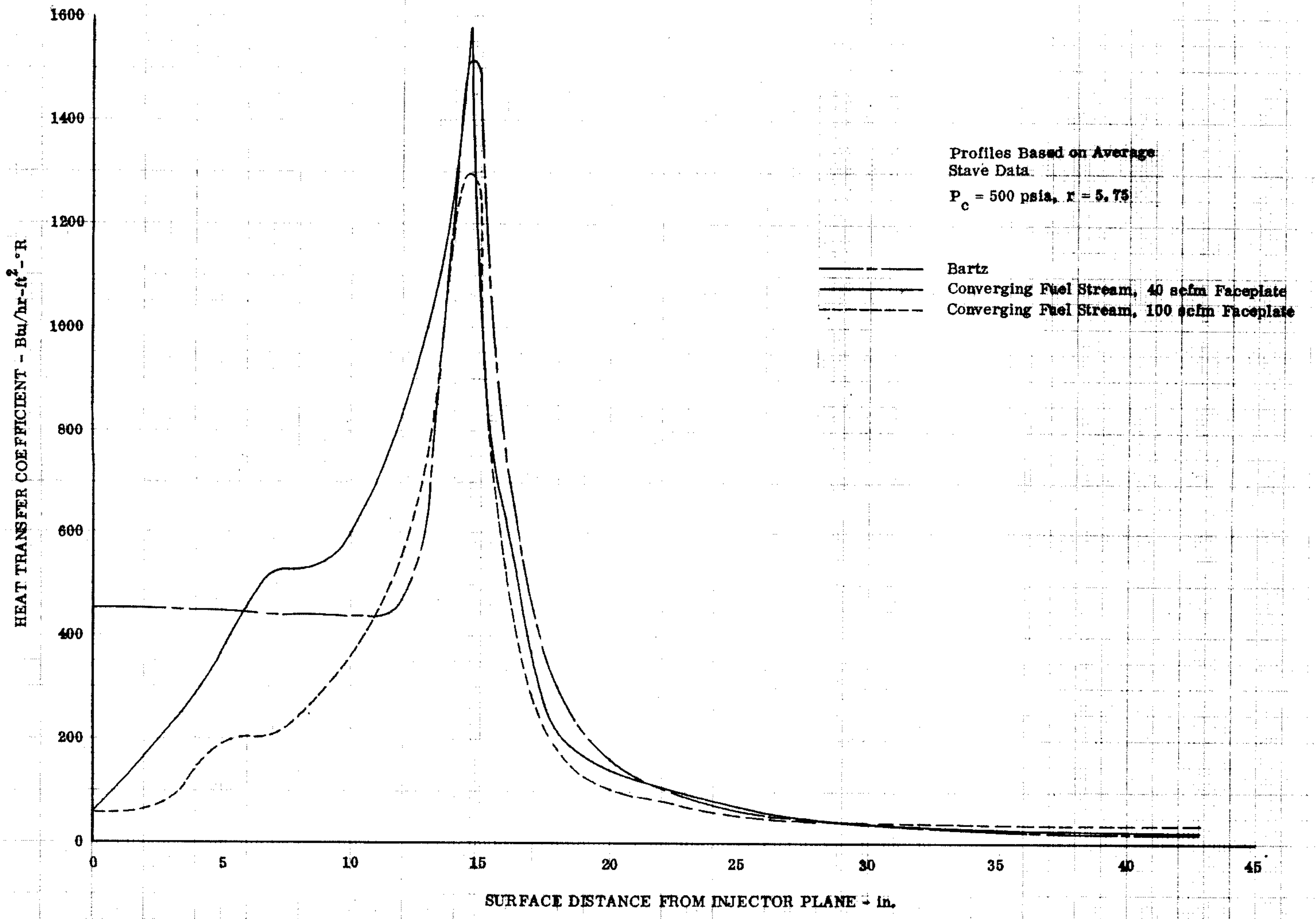

Figure 35. Theoretical and Experimental Combustion-Side Heat Transfer Coefficient Profiles

DF 83166A

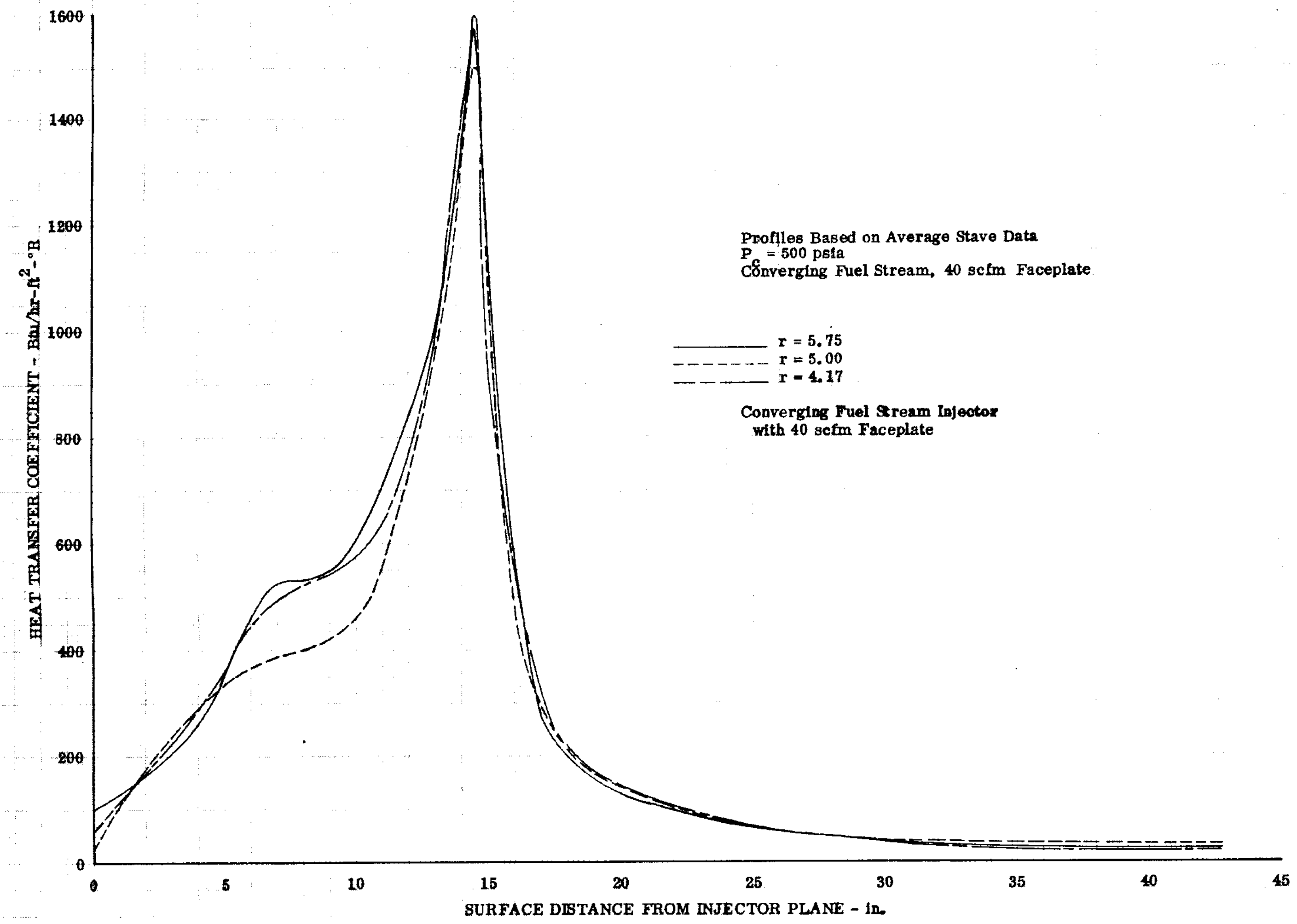

Figure 36. Combustion-Side Heat Transfer Coefficient Profiles for Different Mixture Ratios

DF 83164

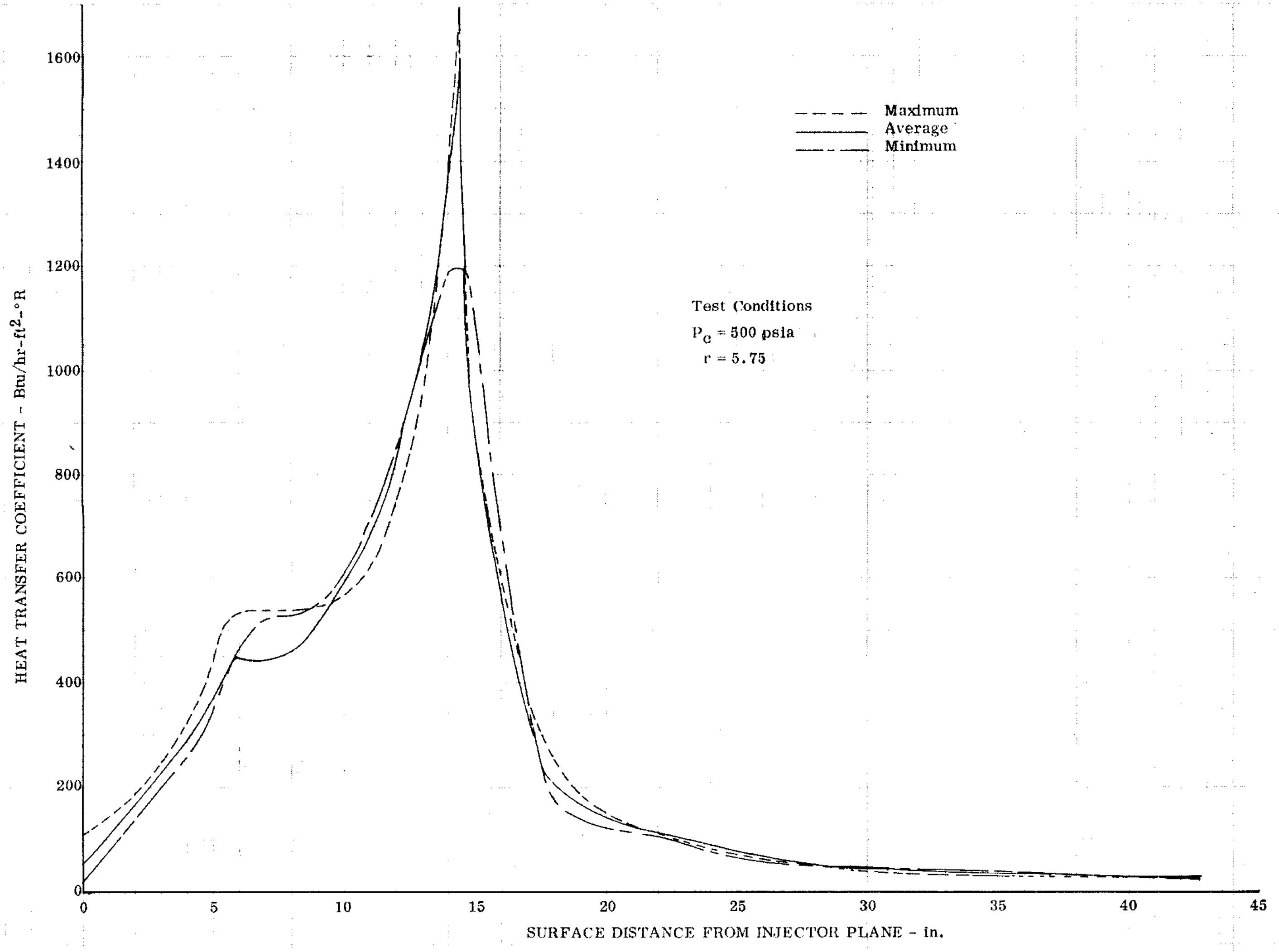

Figure 37. Experimental Combustion-Side Heat Transfer Coefficient Profiles for Converging Fuel Stream Injector with 40 scfm Faceplate

DF 84825

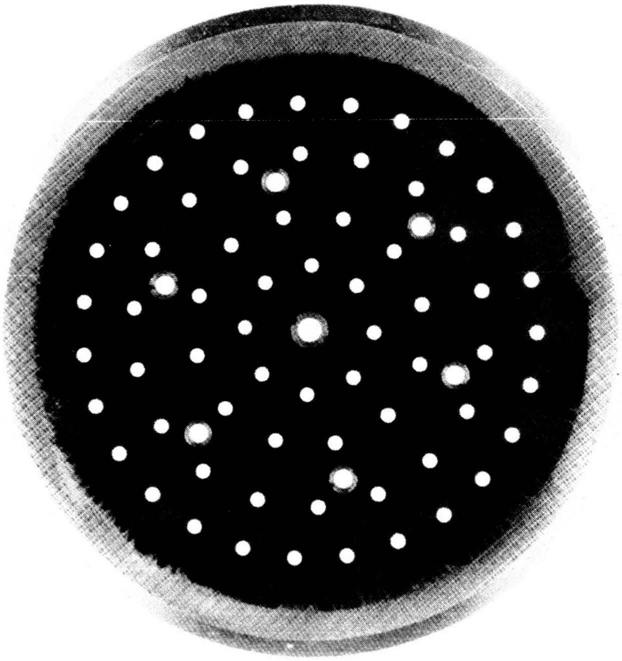

Figure 38. 100-scfm Rigimesh Faceplate for Converging Fuel Stream Injector after Testing FE 78475

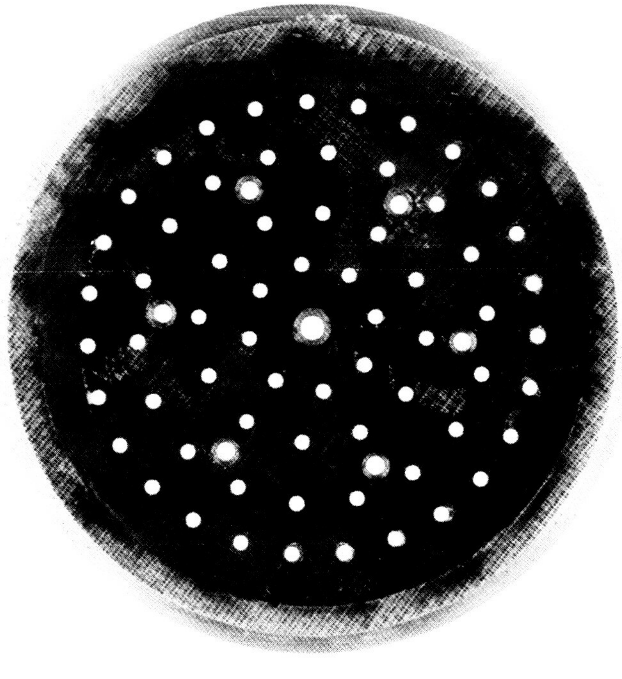

Figure 39. 40-scfm Rigimesh Faceplate for Converging Fuel Stream Injector after Testing FE 78474

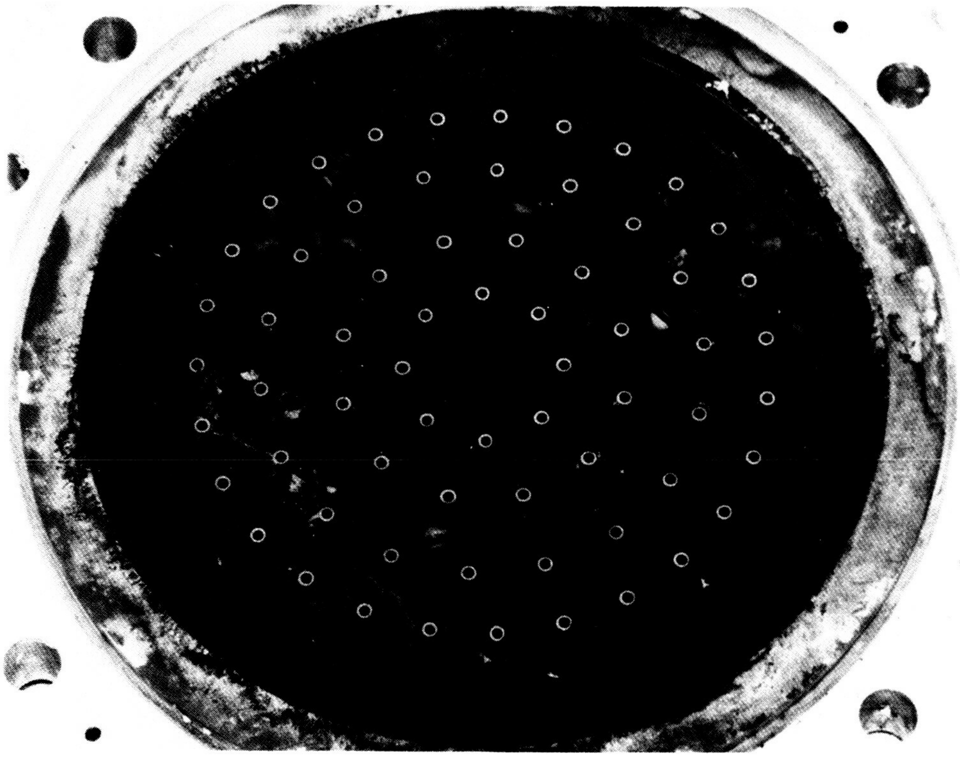

Figure 40. Converging Fuel Stream Injector with Copper Faceplate after Testing FE 78473

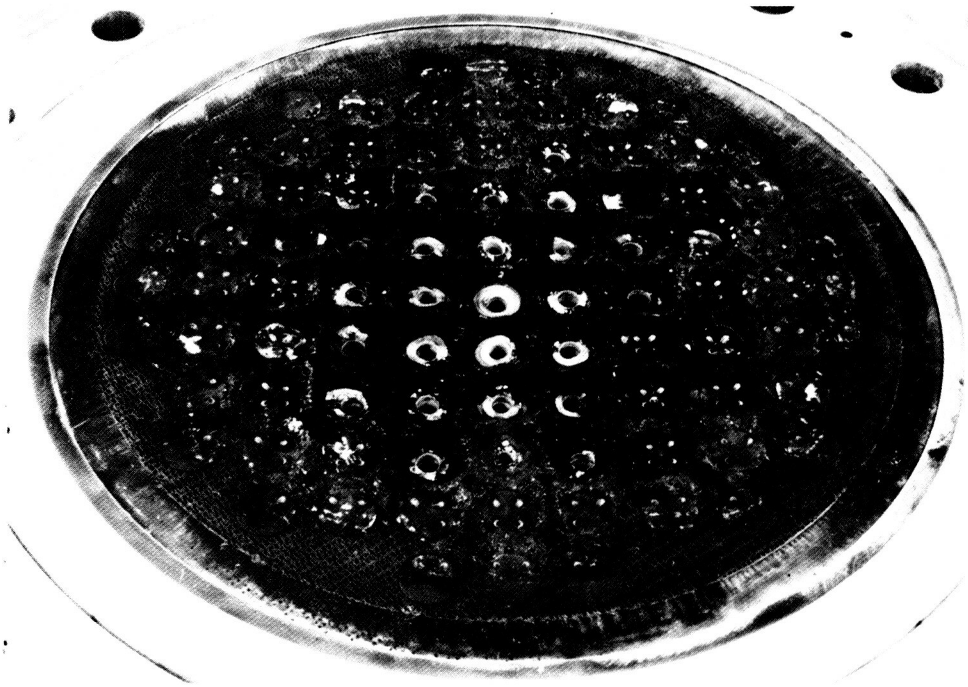

Figure 41. Pentad Injector after Testing FE 78036

Figure 42. Damaged Throat Section after Test No. 3.01 FE 77948

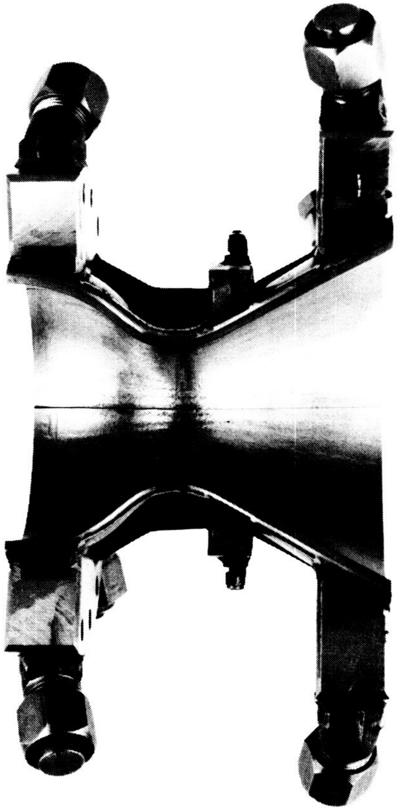

Figure 43. Throat Section with Damaged Staves Removed FE 78069

In subsequent tests, coolant water flow to each chamber section was increased to provide additional margin against boiling heat transfer. In tests 7.02 through 11.01, the hardware was tested for 194-sec firing time at 500-psia chamber pressure without major damage. Figures 44 and 45 are representative aftertest photographs of the chamber and throat section showing the characteristic soot layer. Three small water leaks were noted in the nozzle extension interior wall at the inlet flange location after test 10.01, due to slight erosion of a weld at this location. A water leak between two staves, caused by a burnthrough into the coolant passages (figure 46) also occurred during shutdown of test 11.01. The burnthrough, like that in test No. 3.01, was also attributed to boiling in the coolant passages caused by large seam land widths.

In tests 12.04, 14.01, and 17.02, the throat section of a 3-piece regenerative chamber was used. It was water-cooled successfully with no damage incurred. Discussion of the durability of this throat section operating in a water-cooled mode is given in Section X.

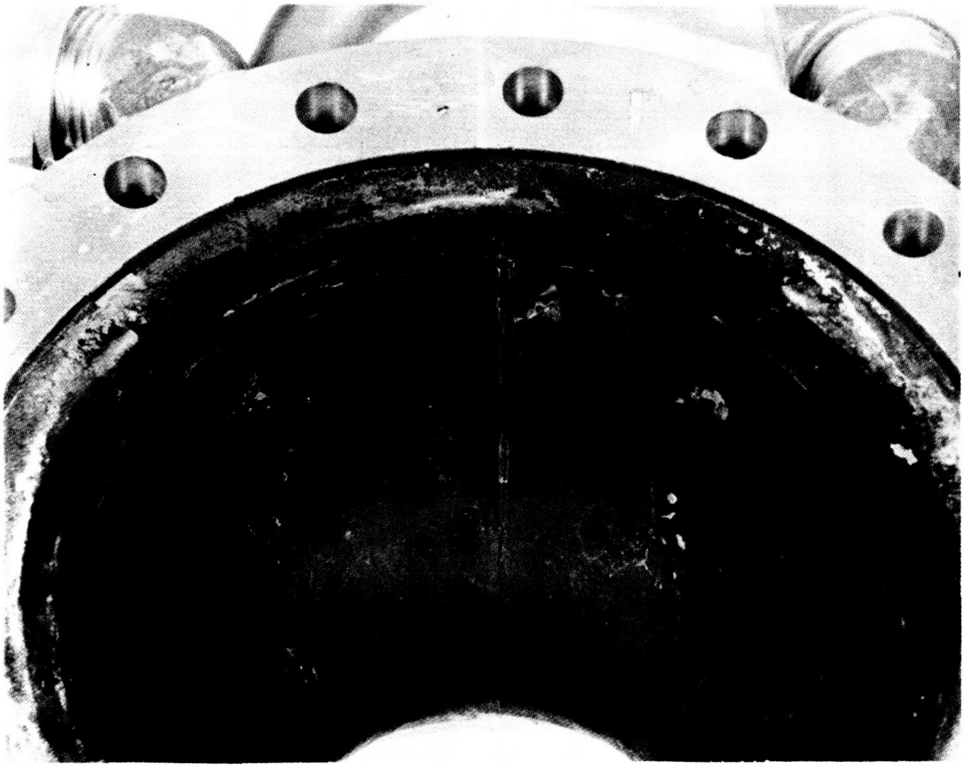

Figure 44. Throat Section after Testing FE 78487

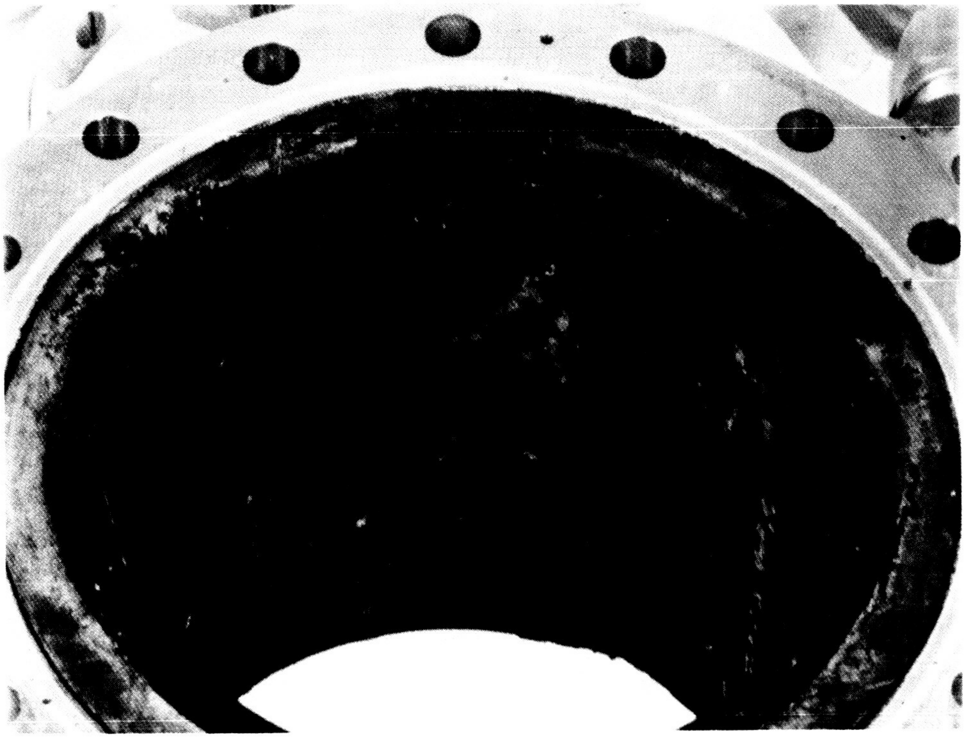

Figure 45. Chamber Section after Testing FE 78490

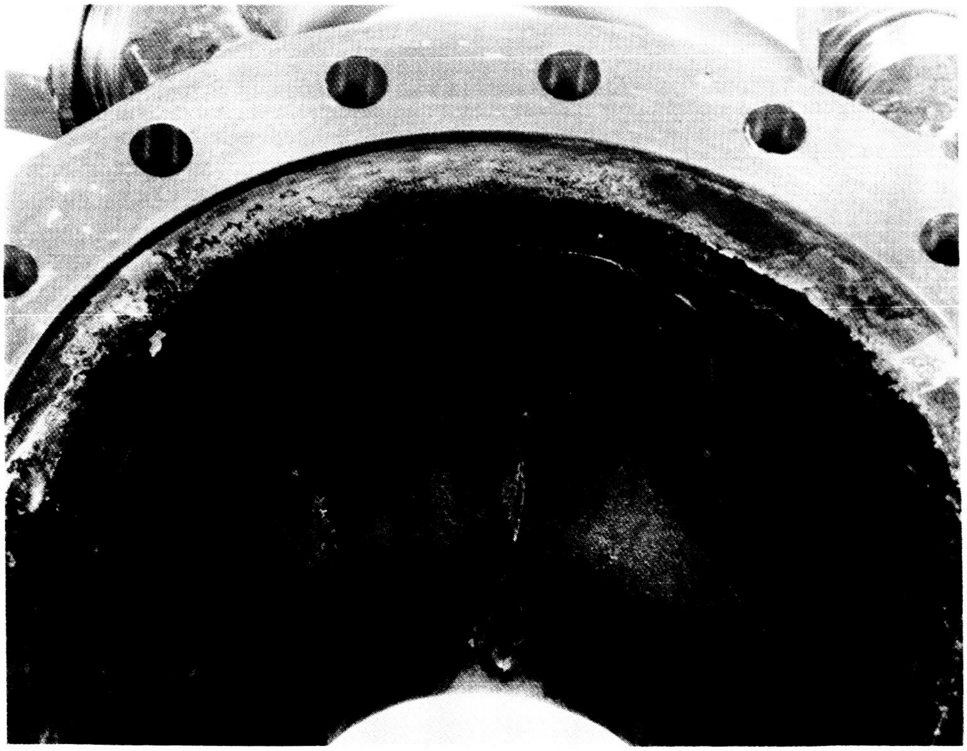

Figure 46. Throat Section Showing Burn Through after Test No. 11.01 FE 78488

SECTION VII
REGENERATIVE COOLED THRUST CHAMBER HARDWARE

A. GENERAL

Three regeneratively cooled THERMAL SKIN® thrust chambers were tested using Contract NAS3-11190 injectors. One chamber was fabricated under the contract; the other two were constructed independently using more advanced fabrication techniques for certain operations. Permission to use government-owned injectors in tests of the P&WA chambers was obtained with the understanding that results would be published in this report. Therefore, all three chambers are described herein.

The contract chamber and one of the independently built units were of one-piece construction like that shown in figure 47. The third chamber was a three section assembly. (See figure 48.) It was created as a repair of the second one-piece chamber after throat erosion was incurred during testing. The eroded throat was cut from the part and flanges were added to the severed combustion chamber and nozzle pieces to make them separate sections which could be mated to a new throat section. All three thrust chambers were of the same basic design with respect to cooling passage configuration and materials of construction. These common features are discussed in subsections B and C. The fabrication sequences for the chambers were also the same; however, there were differences in the fabrication methods used to bond the THERMAL SKIN plates into panels and in joining the staves at their edges. Table XII summarizes the methods employed; the reasons for these differences are discussed in paragraph D (note that for the 3-section chamber, the methods apply to the throat section only).

Table XII. Regenerative Thrust Chamber Fabrication Methods

Chamber	Plate Joining Method	Stave Joining Method
Contract One Piece	Silver Braze	TIG Weld
Independent One Piece	Silver Braze	EB Weld
Independent 3-Section	Diffusion Bond	EB Weld

B. DESCRIPTION

Important characteristics of the thrust chambers are given in table XIII. The design was sized for 5000-lb thrust at 500-psia chamber. At these conditions, the coolant passages were sized so that the chamber could operate at the highest mixture ratio (5.75) in the operating range. Structurally, the coolant passages and the hardware were designed for a maximum chamber pressure level of 1000 psia.

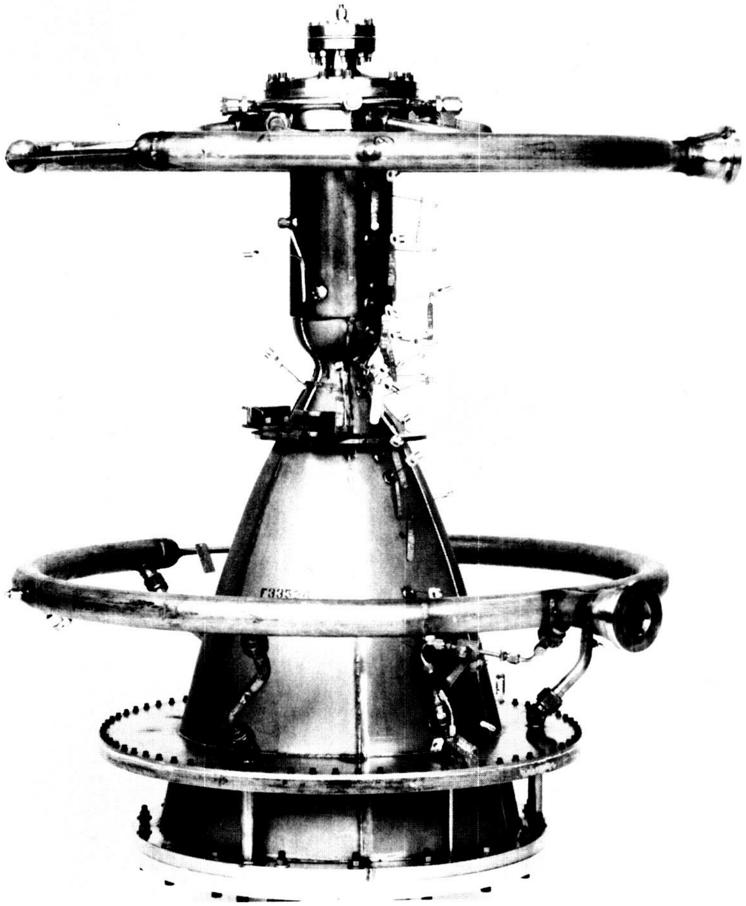

Figure 47. Full Length Regenerative Thrust Chamber FE 86786

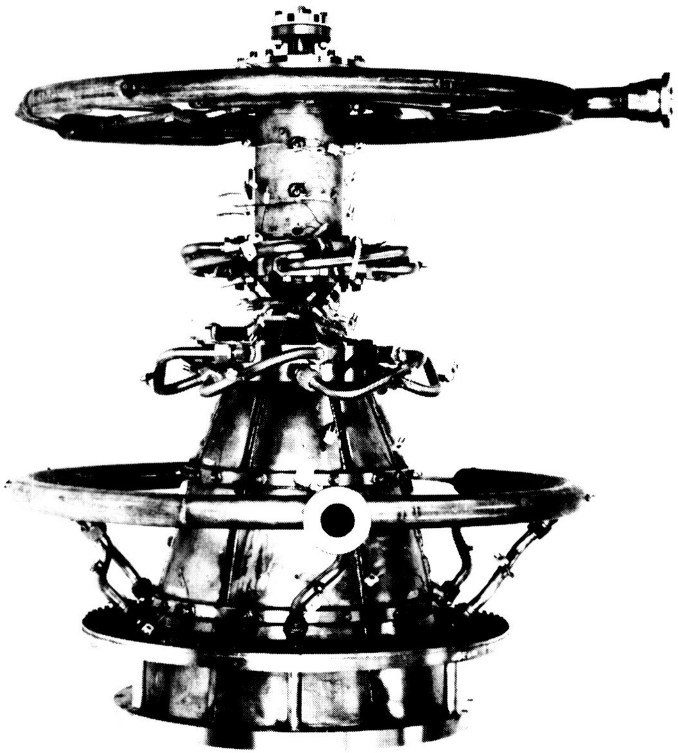

Figure 48. Three-Piece Regenerative Thrust Chamber FE 98735

Table XIII. Regenerative Thrust Chamber Characteristics and Design Conditions

Thrust, lb_f	5000 (Maximum 10,000)
Chamber Pressure, psia	500 (Maximum 1000)
Propellants	Flox/methane
Mixture Ratio	4 to 5.75
Expansion Ratio	60 to 1
Contraction Ratio	4 to 1
Chamber L*, in.	52
Coolant Direction	Counterflow

A chamber L* of 52 in. was selected because it provided a measurable performance increase at high mixture ratios over a 30-in. L* based on water-cooled chamber test results. The chamber contraction ratio (4 to 1), expansion ratio (60 to 1), and the chamber contour were the same as those used in the water-cooled chamber, so that the water-cooled chamber heat transfer results would be directly applicable to the regenerative thrust chamber design. The coolant flow direction was made counterflow based on Task I results to minimize coolant pressure drop.

THERMAL SKIN construction was selected for the chambers based on the Task I analytical studies which showed the necessity for nontubular construction. With THERMAL SKIN, the coolant passage size is readily tailored along the length of the chamber to permit close matching of the coolant heat transfer coefficient with local heat fluxes to minimize coolant pressure losses.

Each thrust chamber has six, 60-deg circumferential stave elements, each of which consists of a bonded nickel-Inconel sandwich with nickel used on the combustion side and Inconel 600 as the structural backplate.

Nickel was selected as the combustion side wall material based on Task I heat transfer studies that showed for the moderate heat flux levels (approximately 16 Btu/in.^{2}-sec), nickel permitted regenerative cooling with pressure drops less than those required with either stainless steel or super-alloys, such as the Haynes 25 material.

Inconel 600, a nickel alloy, was selected as the backplate material based on strength, etching, and fabrication considerations. The material is about twice as strong as nickel and hence its use results in a lighter weight chamber than if nickel were used for both plates. Also, Inconel 600 has etching characteristics similar to those of nickel, which permitted the use of the same etching methods for both the combustion side and backplate materials. Initially Inconel 625, a higher strength nickel alloy, was considered. However, attempts to etch this material were unsuccessful. Inconel 600 has a coefficient of thermal expansion (α) that is nearly equal to that of nickel. Matching α's of the plates is a requirement for a good braze or diffusion bond joint between the combustion side and backplate materials.

Inlet and exit manifolds were constructed of Inconel 625. The inlet manifold also served as the adapter flange for the injector. The exit flange had provisions for a blank-off plate so that the thrust chamber-injector assembly could be pressure checked. Other important mechanical parts seen in figures 47 and 48 are identified in figure 49. These parts, fabricated of Inconel 625, include: (1) a pressure shell in the combustion chamber region, (2) seam straps, (3) a support rod attachment ring, and (4) an altitude system adapter ring. The pressure shell backs up the THERMAL SKIN stave joints to provide additional hoop strength in the combustion chamber. Seam straps were used for the entire chamber length on the contract chamber; however, on the electron-beam welded P&WA chambers, they were used only in the throat region. The support rod and altitude system adapter rings were used to facilitate test stand mounting.

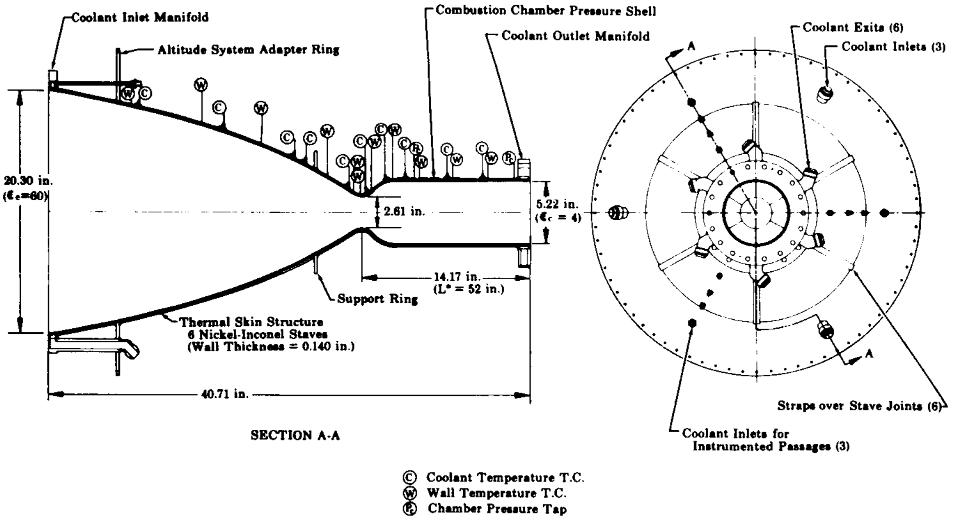

Figure 49. Regenerative Thrust Chamber Schematic

FD 25099

Chamber instrumentation provisions included chamber pressure taps and wall and coolant thermocouples located along the chamber. The locations of the thermocouples are indicated in figure 50. The thermocouple arrangement shown in this figure was used in three of the six staves. In addition, all six staves had wall temperature thermocouples at the throat (location W6) and in the combustion chamber at the predicted highest wall temperature point (location W3). In the one-piece thrust chambers the coolant thermocouples were located in three equally spaced coolant passages to which the coolant flow was separately supplied. Individual flow measurements in the instrumented coolant passages facilitated determination of chamber heat transfer. In the 3-section thrust chamber, coolant temperatures were measured at the same axial locations as in the one-piece assemblies, but the flows to the instrumented passages could not be conveniently measured.

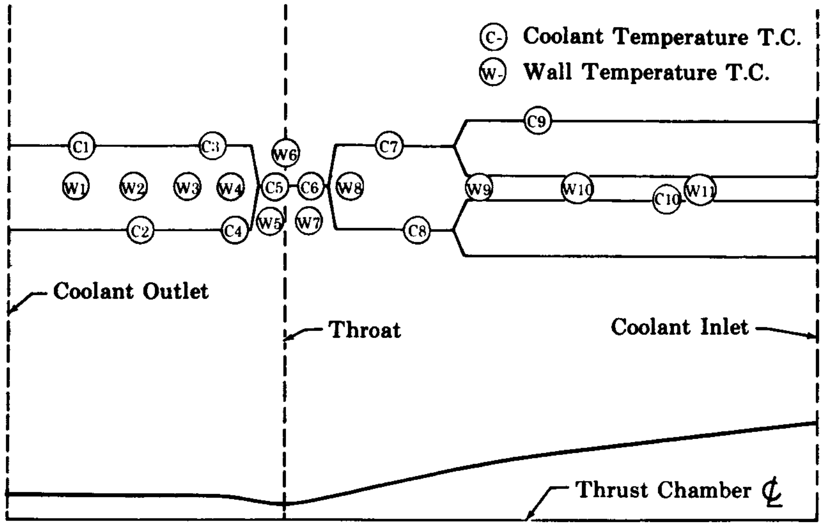

Figure 50. Coolant and Wall Temperature Locations (Regenerative Chamber) FD 25100

C. DESIGN

The coolant passages were sized using the heat transfer and stress analyses described in Appendix A. The passages were configured so that the chamber could operate at the highest mixture ratio (5:75) with the highest performing injector that was demonstrated in the water-cooled chamber tests: the converging fuel stream injector with the 40-scfm Rigimesh faceplate. The passages were designed to minimize coolant pressure drop while maintaining the wall temperatures at tolerable levels. The maximum allowable design wall temperature was 1700° F. This value corresponds to that specified by NASA for 347 stainless steel during the Task I heat transfer studies. This appeared to be a safe temperature limit for nickel when compared to the melting point, 2615° F, and the nickel reaction temperature with fluorine, 2100° F (as given in reference 15); however because erosion did occur at this temperature level (as will be discussed in Section VIII), it is apparently too high.

The coolant passage geometry is described in figure 51. Important features to note regarding the coolant passage dimensions are:

1. Three coolant passage depths were used. The multidepth design was achieved by etching both the nickel and the Inconel plates. The etched passage depth in the nickel plates was 0.033 in. throughout the chamber. The Inconel plates were not etched at the throat, but were etched to different depths in the lower-heat-flux regions of the combustion chamber and the nozzle to increase the coolant flow area, thus minimizing the coolant pressure drop.

2. At the inlet coolant manifold (i.e., at the nozzle exit in this counterflow design), there were 288 passages (48 passages/stave). The number of passages was reduced in steps as the thrust chamber radius decreased to maintain passage widths within practical limits. At the throat, 72 passages (12 passages/stave) were used.

3. The passage width varied from 0.150 to 0.053 in. along the chamber length. The maximum passage width was set by allowable stress considerations in the nickel wall, while the minimum passage width was set by etching limitations. For etched passages in one plate, the current depth-to-width limit is approximately 0.66.

4. Two other important dimensions not shown in figure 51 are the hot wall thickness and the seam land width. The hot wall thickness was 0.025 in. and the design seam land width was 0.050 in.

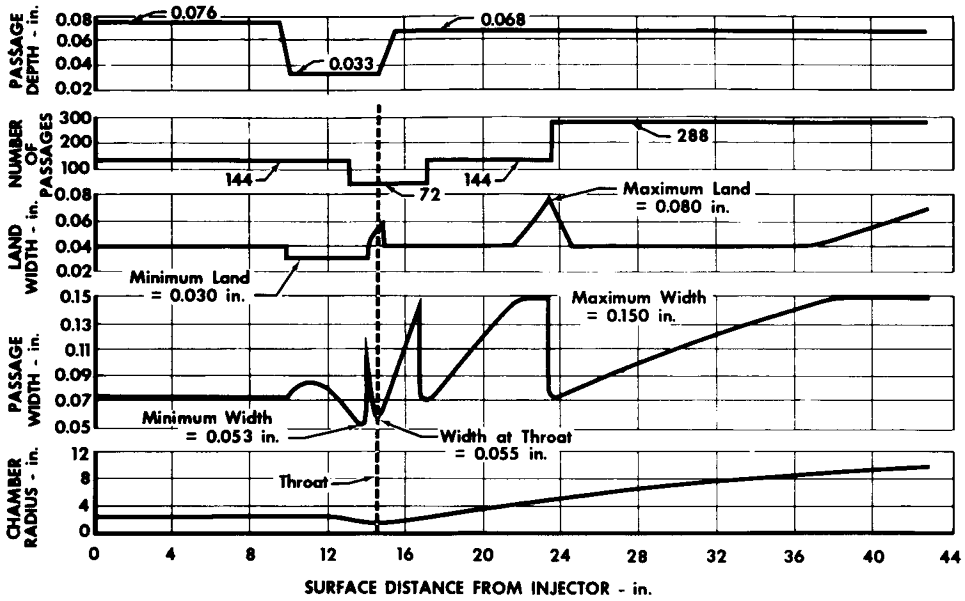

Figure 51. Regenerative Thrust Chamber Coolant Passage Dimensions GS 10989

Predicted variations in coolant pressure and temperature and combustion wall temperature at design conditions (i.e., for 500 psia chamber pressure, 5.75 mixture ratio, and for the heat flux levels measured for the converging fuel stream injector with a 40-scfm Rigimesh faceplate) are shown in figure 52. The calculated coolant pressure drop (most of which occurs at the throat) is 377 psi. The coolant chamber exit temperature is 1470° R. The combustion side wall temperature curve is for the passage crown. Wall temperature at the centers of the land are slightly higher, as indicated by the two-dimensional temperature profiles for the throat station given in figure 53.

Results of off-design calculations are presented in figures 54 and 55. Figure 54 shows that the coolant temperature and maximum wall temperature will decrease and coolant pressure drop will increase with decreasing mixture ratio (i.e., with increasing fuel flow). Figure 55 shows the trends of these chamber conditions for increasing chamber pressure.

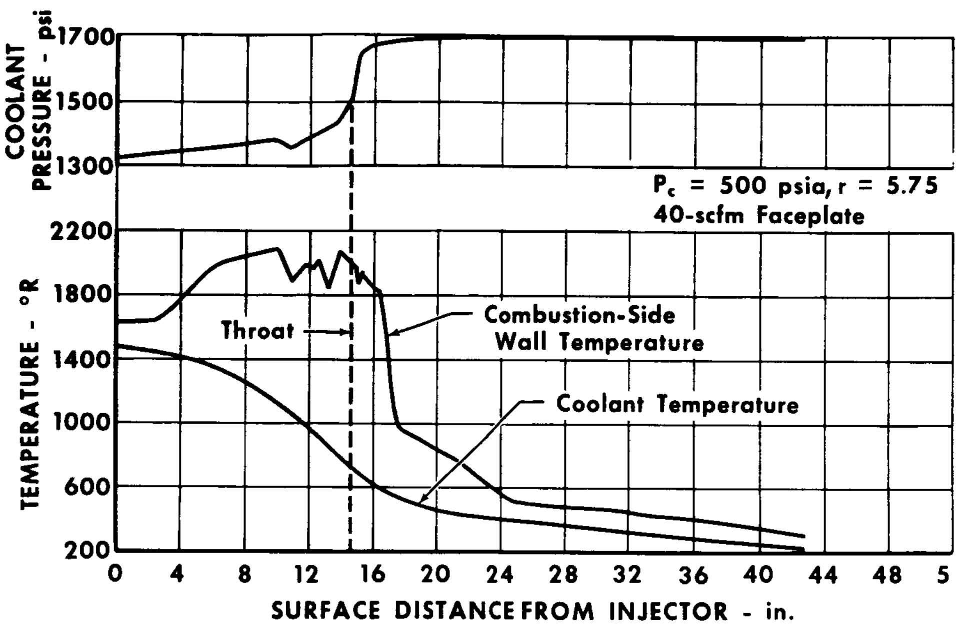

Figure 52. Predicted Regenerative Thrust Chamber Coolant Parameters GS 10080A

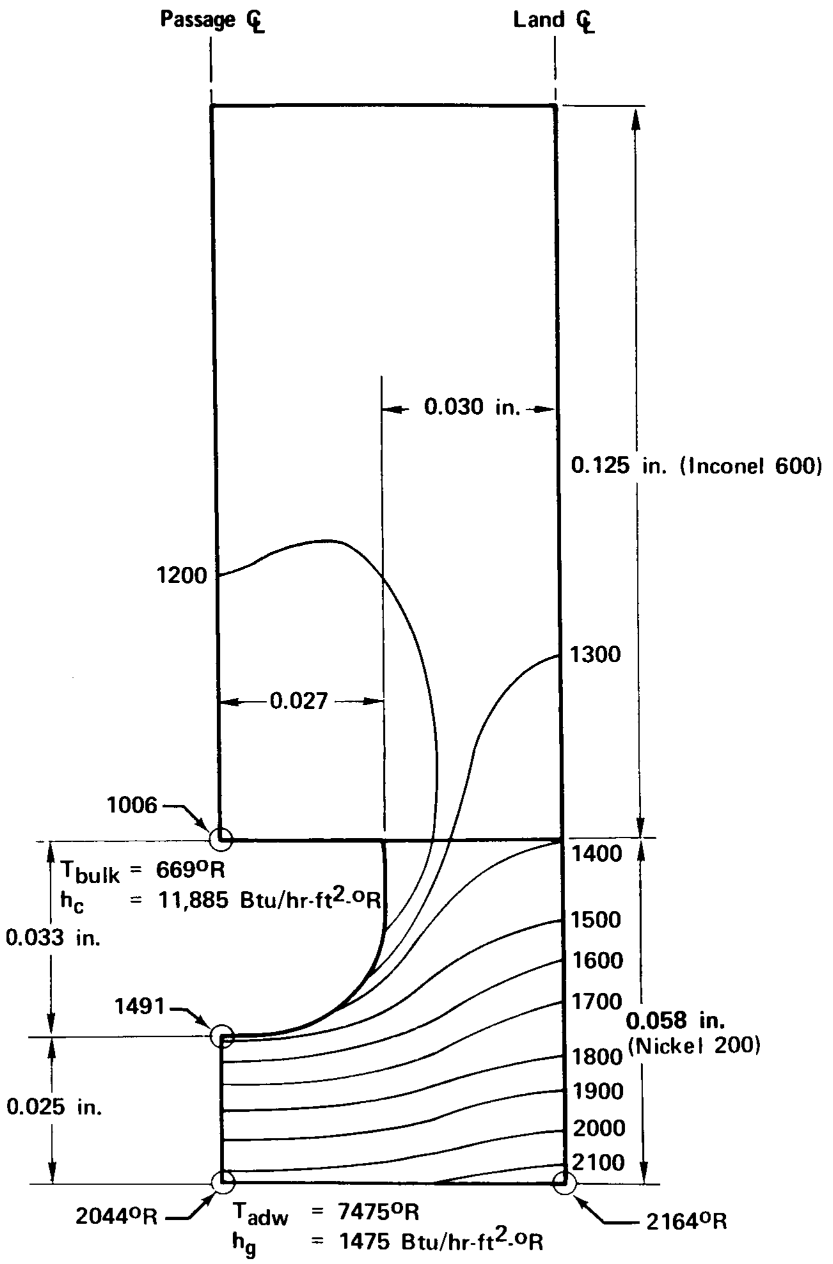

Figure 53. Predicted Two-Dimensional Temperature Profile for Cooling Passage at Throat Station of Regenerative Chamber

FD 45441

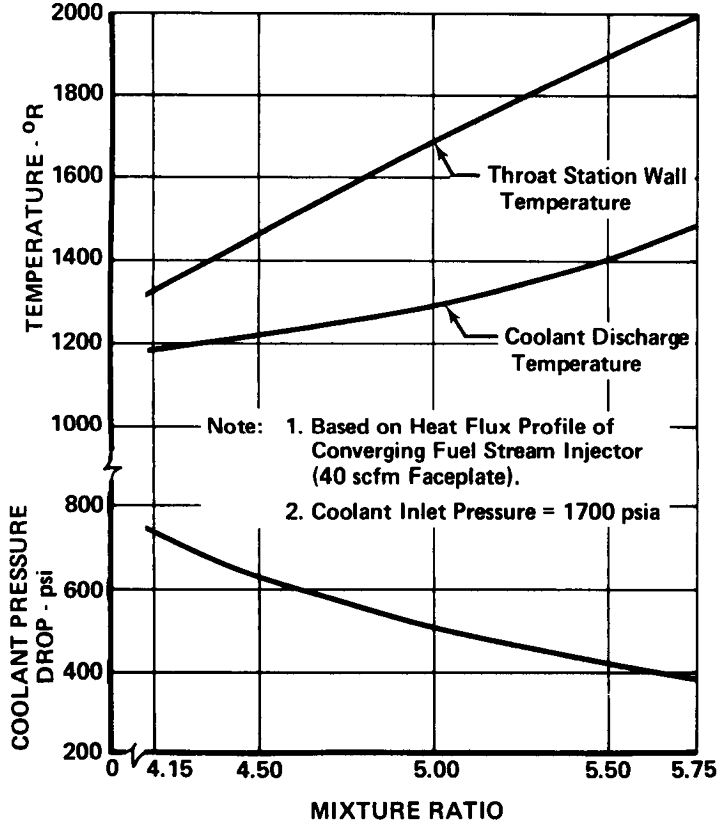

Figure 54. Variation of Regenerative Thrust Chamber Operating Conditions with Mixture Ratio

FD 45194A

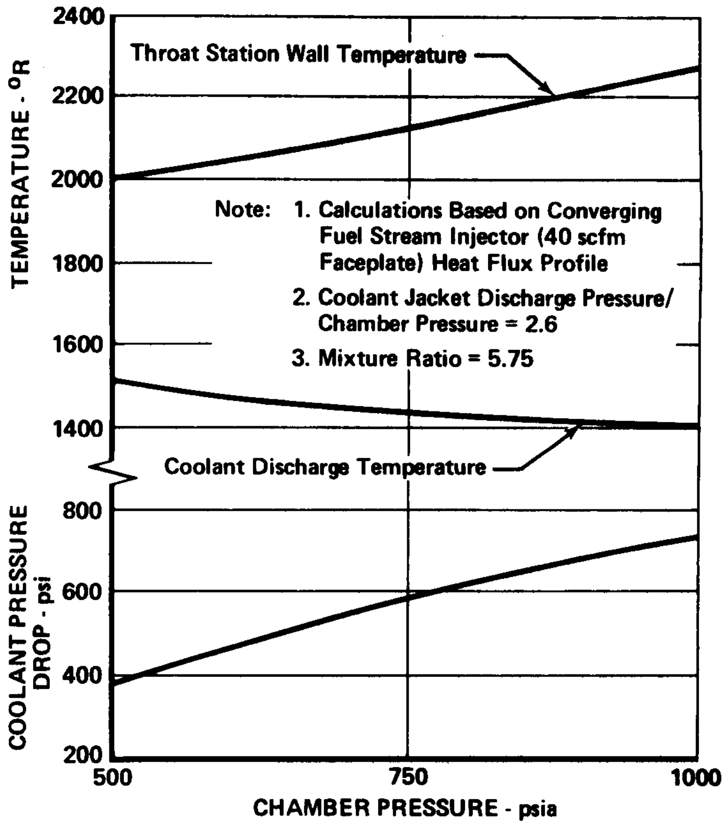

Figure 55. Variation of Regenerative Thrust Chamber Operating Conditions with Chamber Pressure

FD 45195A

D. FABRICATION

1. General

The regeneratively cooled thrust chambers were fabricated following the general procedure established in previous programs involving THERMAL SKIN chambers. The major steps include: (1) etching of the coolant passages, (2) bonding of the etched plates, (3) forming the brazed stave to the chamber contour, (4) trimming the staves to 60-deg segments, (5) joining the staves on their edges, (6) welding the flange manifolds and other support hardware to the liner assembly, and (7) final machining. These fabrication steps are discussed in detail in paragraph 2 below. Paragraph 3 describes the inspections performed on the chambers during fabrication and presents important inspection data.

2. Fabrication Steps

a. Passage Etching

Nickel and Inconel plates were supplied to the etching vendor by P&WA. Plate preparation at P&WA included cutting of the plates to approximate size and lapping of the surface to be etched to approximately 8 microinches rms finish. This smooth finish was specified primarily to assure good bonding of the plates after etching, but it also facilitated application of the maskant for photo-resist, used in the etching process.

The etching vendor developed etching masters using P&WA supplied X-Y coordinates, of a flat-plane layout of the cooling passages. The coordinates were transmitted in the form of IBM computer cards. The etching master was generated using a rectilinear coordinate Univac 418 computer, driving a Gerber 532 System Plotter outfitted with a high intensity light pen. The system is capable of plotting accuracies of 0.0005 in. The passage widths in the master were reduced by 0.008 in. to account for side etch. The amount of side etch compensation was determined by an iterative process involving etching and inspection of sample plates and subsequent correction of the etching master.

The etching master was positioned on the plates in a vacuum contact printer after the plate surfaces to be etched were coated with photo-resist, a photosensitive compound that is polymerized by a strong light source. After exposure to the light from a carbon arc lamp, the photo-resist that was unexposed, and therefore not polymerized, was removed with a solvent to "develop" the image. The plates were then ready for etching.

The plates were etched in a spray etcher. The equipment is illustrated schematically in figure 56. The etching solution was ferric chloride; the method employed is referred to as the "powder banking" process. In this process, the plates are etched until desired passage widths are obtained (this generally occurred at a passage depth of approximately 0.010 in.). At this point, the plates are removed from the etcher and then "banked" with a fusible resinous powder, which is applied so that it would adhere to the passage sidewalls. The powder is fused into a protective coating by heating the plate. Following banking, etching is resumed until the first resin deposit is undercut. Then another powder bank is applied and the process is repeated until the desired depth is achieved. Etched plates for the one-piece chamber are shown in figures 57 and 58.

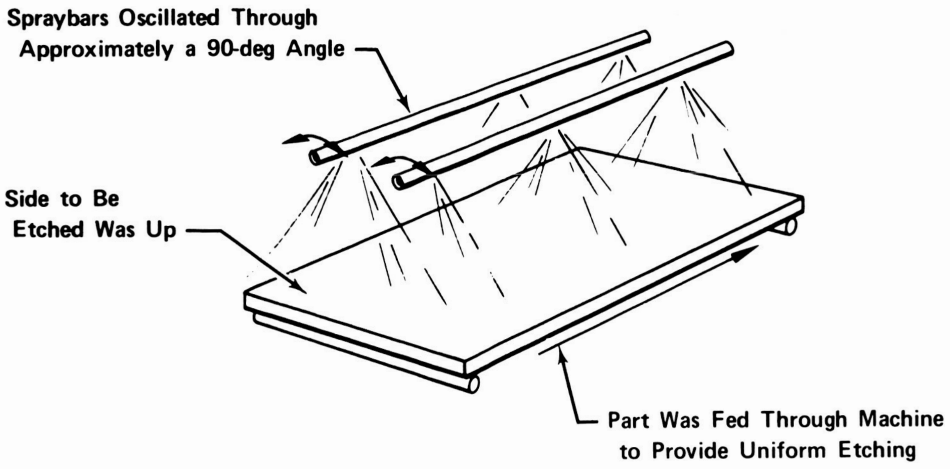

Figure 56. Spray Etcher Schematic FD 45504

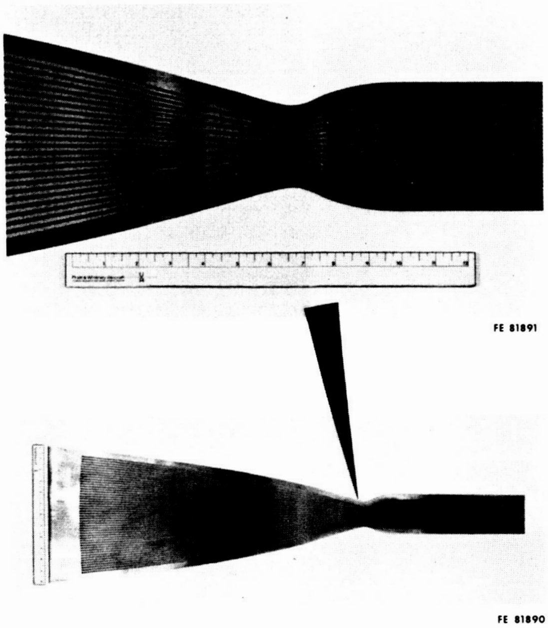

Figure 57. Etched Nickel Plate for Regenerative Thrust Chamber FD 27349

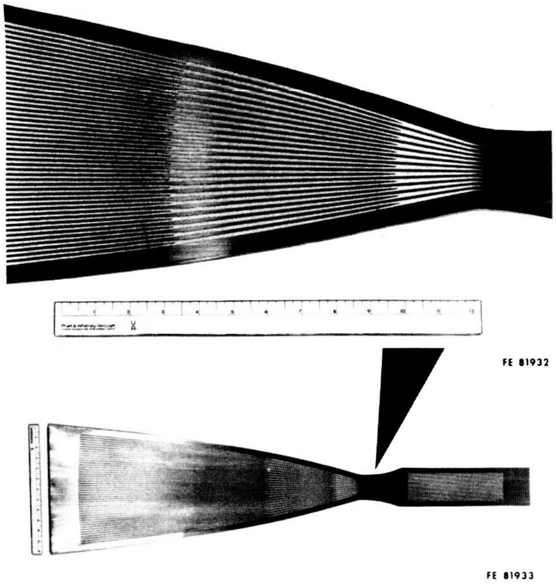

Figure 58. Etched Inconel Plate for Regenerative Thrust Chamber FD 27350

b. Etched Plate Bonding

As mentioned above, the etched nickel and Inconel plates were bonded together using two different methods. The plates for both one-piece chambers were silver brazed. The plates for the throat section of the 3-piece chamber were diffusion bonded so that undesirable features of the silver braze joint could be avoided. The silver braze provided a sufficiently strong bond; however, it was a relatively low temperature joint that was vulnerable to overheating during subsequent welding operations. Also, the silver filleted indiscriminately in the corners of the coolant passages and contributed to passage-to-passage flow variations. Because diffusion bonding provides a high temperature joint with bond strengths equal to that of the weaker of the two parent materials, and does not involve the melting of a filler material, it is the preferred process.

For brazing of THERMAL SKIN panels, the Inconel plates were plated with 0.0002 in. of silver. Then individual nickel and Inconel plates were assembled using dowel pins in accurately located holes in the plates for alignment. Individual nickel-Inconel staves were brazed in a retort with an inside depth equal to the stave thickness and a thin stainless steel cover sheet. The cover sheet was welded to the retort on its outer edges so that, after the retort was loaded and evacuated, it would act as a diaphragm to transmit atmospheric pressure to the stave to load it during the braze cycle. A hydrogen atmosphere of 100 to 400 microns of mercury was maintained in the retort following evacuation to provide a reducing atmosphere for brazing. The braze temperature of 1825° F was maintained for approximately 15 min.

Diffusion bonding of the etched plates was accomplished using a pressure-loading process. Gas pressure was applied to a sealed, etched plate assembly (evacuated internally) at elevated temperatures to effect a bond. The mated

Inconel and nickel plates were assembled, aligned, and then tack-welded together with a stainless steel cover sheet over the nickel plate to prevent collapsing of the nickel over the larger width portions of the etched passages. To prevent bonding of the nickel plate and the cover sheet, the latter was oxidized and coated with magnesium oxide, a bonding inhibitor. After the etched plates and the cover sheet were tack-welded together, the perimeter was sealed by electron beam welding while the assembly was in a vacuum of less than 10^{-5} torr. The assembly was subsequently leak checked by pressurizing externally to 200 psig with helium and then rapidly submerging it into an alcohol bath. Diffusion bonding was accomplished in an autoclave at 1000-psig pressure and 1700° F temperature. Dwell time at temperature was 3 hr. Staves were bonded both directly and using a 0.0005-in. copper plating applied to the nickel plate as a bonding aid. Subsequent inspections and pressure tests of the bonded staves indicated that direct bonded staves were feasible and hence a diffusion aid may not be required for bonding nickel to Inconel 600.

c. Stave Forming

The staves were formed in a one-step contouring operation using forming dies in a hydraulic press. The dies for the staves of the one-piece thrust chamber are shown in figure 59. These were constructed of Kirksite (a castable, zinc-base alloy with good machining characteristics) but had stainless steel throat inserts. The female die was bolted to the stationary bed of the press and the male die was attached to the ram. For forming, a stave was mounted and aligned to the female die by dowel pins; the passages of the bonded staves were filled with wax so that the coolant passages would not collapse.

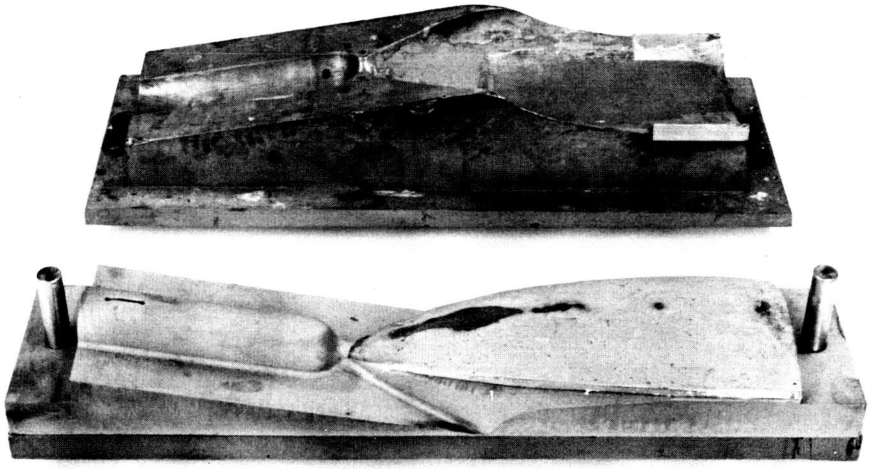

Figure 59. Forming Dies for Regenerative Chamber Stave FE 101935

d. Stave Trimming

The formed staves were trimmed to 60-deg circumferential segments in a special fixture using an end mill. Figure 60 shows the trim fixture used for the staves of the one-piece chambers. The procedure followed during the trimming operation was to (1) install the stave in the fixture for scribing the cutting planes, (2) remove the stave from the fixture, to check the distance between the outer passages and the cutting planes by X-ray, and (3) reinstall the stave into the fixture for milling the stave edges. A formed and trimmed stave is shown in figure 61.

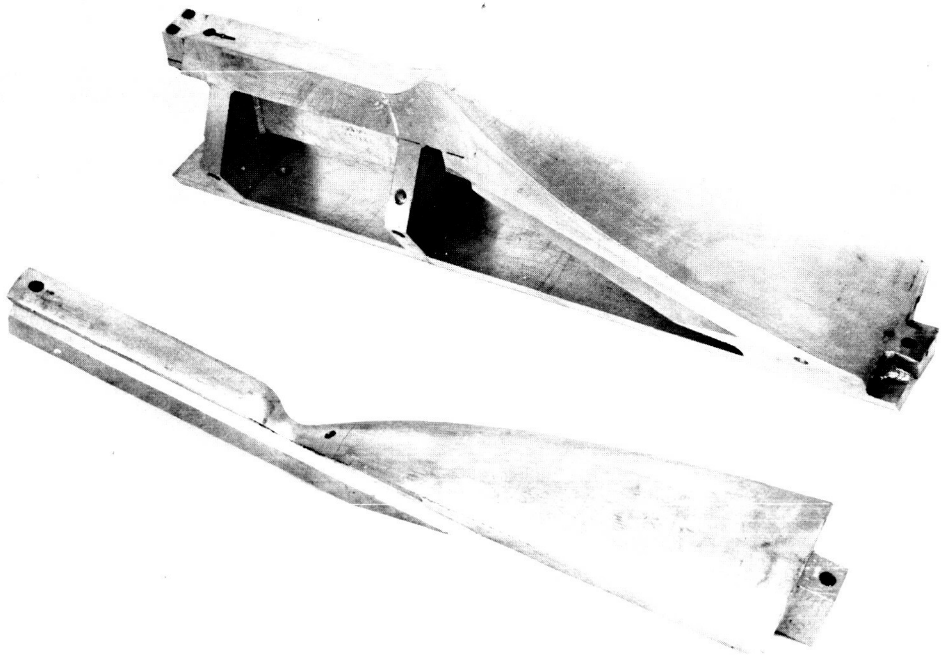

Figure 60. Trim Fixture for Regenerative Chamber Stave FE 101864

Figure 61. THERMAL SKIN® Stave for Regenerative Chamber GS 9888

e. Stave Joining

As mentioned earlier, staves were joined together at their edges using both tungsten inert gas (TIG) and electron-beam (EB) welding. For the first one-piece chamber, manual TIG welding, which had proved satisfactory in a 1,000-lb thrust (at 300-psia chamber pressure) hydrogen-fluorine thrust chamber constructed to demonstrate the feasibility of the concept, was used. The welding at the chamber OD was not difficult. However, because of the calculated high operating temperature, a pure nickel weld rod was selected for the ID weld. During the welding operation, the silver braze joint in two staves was overheated and the bond failed, making it necessary to remove the staves from the assembly. Two new staves were welded into position using lower temperature weld rods (silver-palladium and gold-nickel) for closing the seams at the ID. The welding was completed satisfactorily by this technique but the seam welds cracked during the first test. The first TIG-welded stave assembly is shown in figure 62.

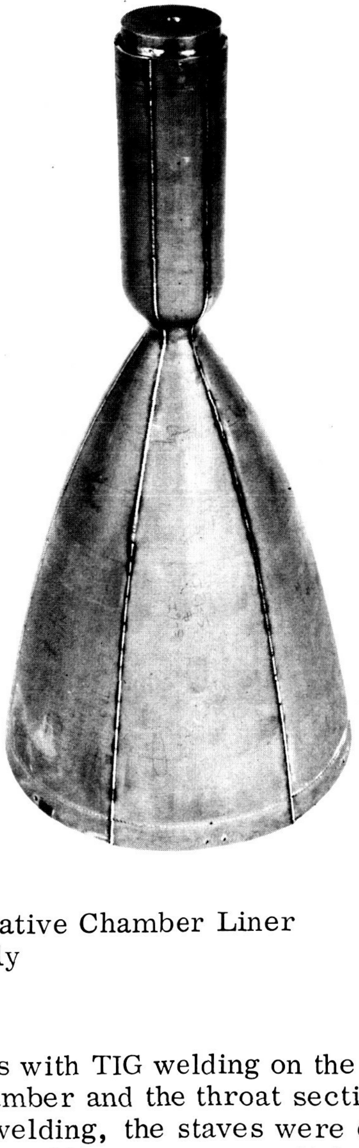

Figure 62. Regenerative Chamber Liner Assembly FE 84288

Because of difficulties with TIG welding on the first chamber, the seams of the second one-piece chamber and the throat section of the sectioned chamber were EB welded. For EB welding, the staves were clamped and tack-welded together on a mandrel. EB welding was accomplished using a Hamilton-Standard machine having a fixed gun and a translating table to which the part was attached. Four different setups (one for the nozzle region, one for the combustion chamber region, and two for the throat region) were required to weld each seam. Figure 63 shows the setups involved and indicates the welding sequence. For each setup the part was positioned 10 in. from the gun and cocked so that the length of seam to be welded was nearly perpendicular to the gun axis. Typical settings for the EB welder were a table speed of 35 in./min, a voltage of 140,000, and a current of 0.013 amps.

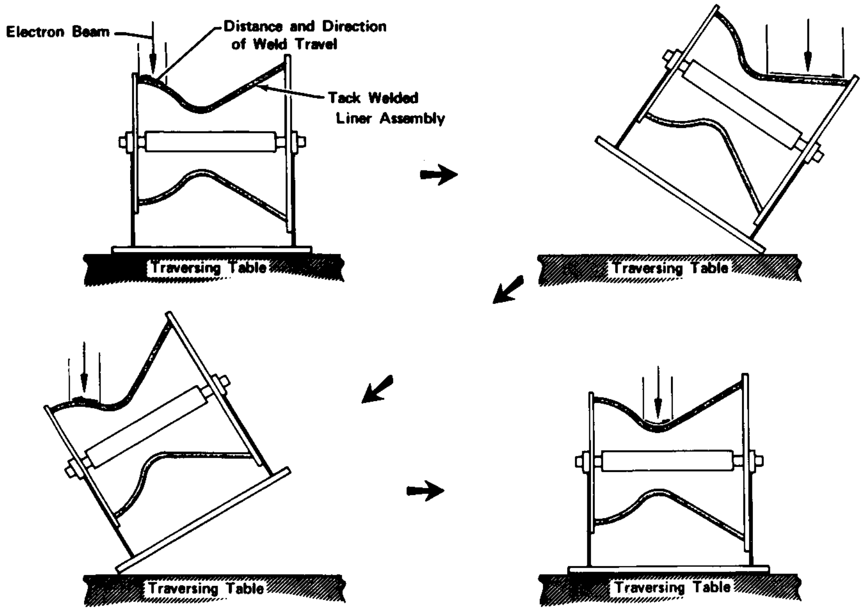

Figure 63. Sequence for Electron Beam Welding THERMAL SKIN® Throat Section

FD 45196

The EB welding operation proved to be much more satisfactory than manual TIG welding. It provided a full penetration weld (figure 64) and the heat input to the part did not damage the bond (either silver braze or diffusion bond) between the plates. However, in a few isolated instances (one passage in the one-piece chamber and three in the throat section) seam passages were partially blocked with weld splatter. In these cases, the blockage was eliminated by electrodischarge machining into the passages from the back side to clear them. After the passage geometry was restored, plugs were welded into position in the back plate and subsequently the passages were flow checked to verify that they were open. It was established that weld splatter occurred in locations where the EB welder was stopped and started. The problem can therefore be overcome by either (1) providing fixturing for beam stopping and starting, rather than relying on manual operation, or (2) using an EB welder with a tracking gun which eliminates the need for stopping and starting the welder along the seam.

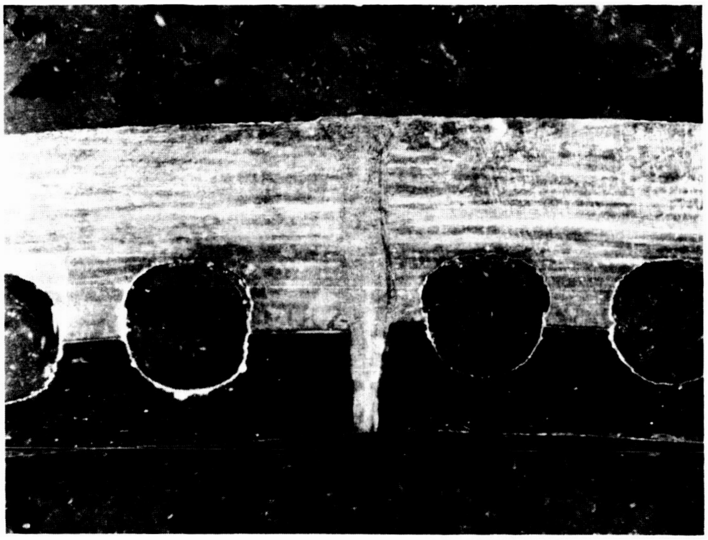

Figure 64. Cross Section of EB-Welded Seam of THERMAL SKIN® Staves FD 35280

f. Final Thrust Chamber Assembly

After the THERMAL SKIN liners were welded, they were surface-machined in a lathe in locations where the pressure shell, the inlet and exit manifolds, the support rod attachment ring, and the altitude system adapter ring were to be installed. These parts were subsequently assembled and welded to the liner. The final fabrication operation was the finish maching of the flanges.

3. Inspection and Structural Testing

a. General

Inspection and structural tests were accomplished during the fabrication process to assure quality and to demonstrate the structural adequacy of the completed thrust chambers for the subsequent combustion firing tests. These inspection and structural tests included the following:

1. Inspections of the coolant passages in the etched nickel and Inconel plates.
2. X-rays of the bonded staves prior to forming
3. Inspections of the formed stave contour using templates
4. Hydrostatic pressure checks of the formed staves to 4000 psig
5. Water flow tests of each passage in each stave
6. X-rays of the trimmed staves to determine final edge distances
7. X-ray and Zyglo inspections of the stave assembly seam welds

8. Helium leak checks of the coolant passages and manifolds of the completed thrust chamber

9. Liquid nitrogen cold-shock tests of the coolant passages and manifolds of the completed thrust chambers

10. Hydrostatic pressure checks of the coolant passages and manifolds of the completed thrust chamber to the maximum anticipated operating pressure

11. An inside-to-outside leak check of the completed thrust chambers.

The inspections of the coolant passage dimensions, the X-rays of the trimmed staves to determine final edge distances, and the water flow of the staves provided reportable information on thrust chamber hardware characteristics which is presented below.

b. Coolant Passage Tolerances

The coolant passages etched into the nickel and Inconel plates were inspected by direct measurements and by RTV rubber casting technique. Dimensional tolerances determined by direct measurements are plotted in figures 65 and 66 for the nickel and Inconel plates etched for the three thrust chamber assemblies. Using the values presented as an indication of current state-of-art tolerances for etched passages, they would be as follows:

Overall depth tolerance	±10%
Overall width tolerance	±10%
Throat station depth x width tolerance	±5%

Coolant passage shape was determined from sectioned staves and by using the RTV rubber casting technique. The RTV castings were sectioned and passage shape was subsequently determined from enlarged photographs of cross sections of the castings. Enlarged photographs of the sectioned staves were made directly. Results for the throat section removed from the second one-piece chamber are given in figure 67, which presents a curve of the shape factor parameter as a function of the width-to-depth ratio. The equation for the average curve has been determined as:

$$\frac{A}{W \times D} = 0.215 \frac{C}{D} + 0.785$$

where:

A = measured passage area,

C = straight cut wall depth,

D = centerline passage depth, and

W = passage width.

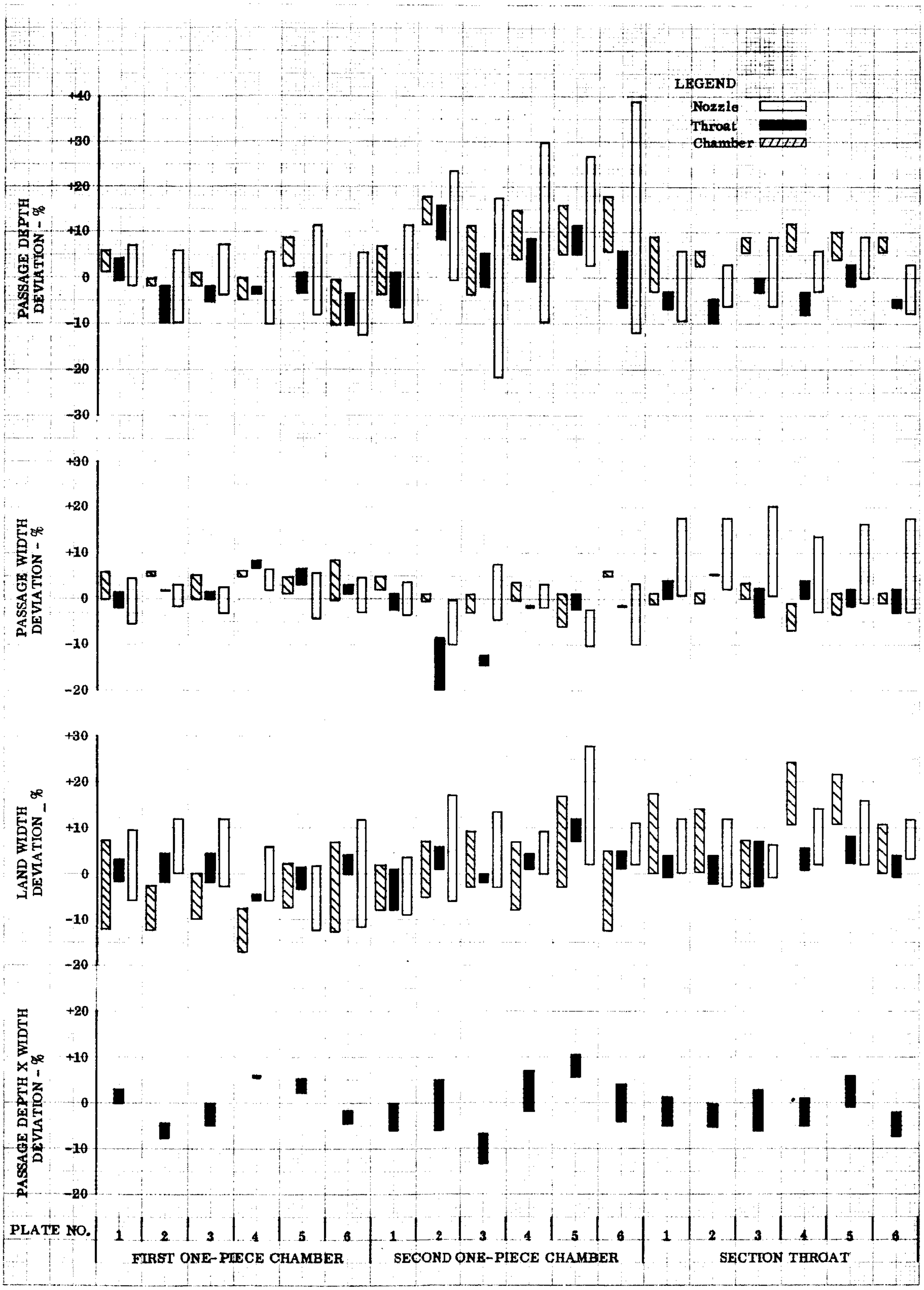

Figure 65. Summary of Nickel Plate Dimensional Variation for Regenerative Thrust Chambers

DF 83151

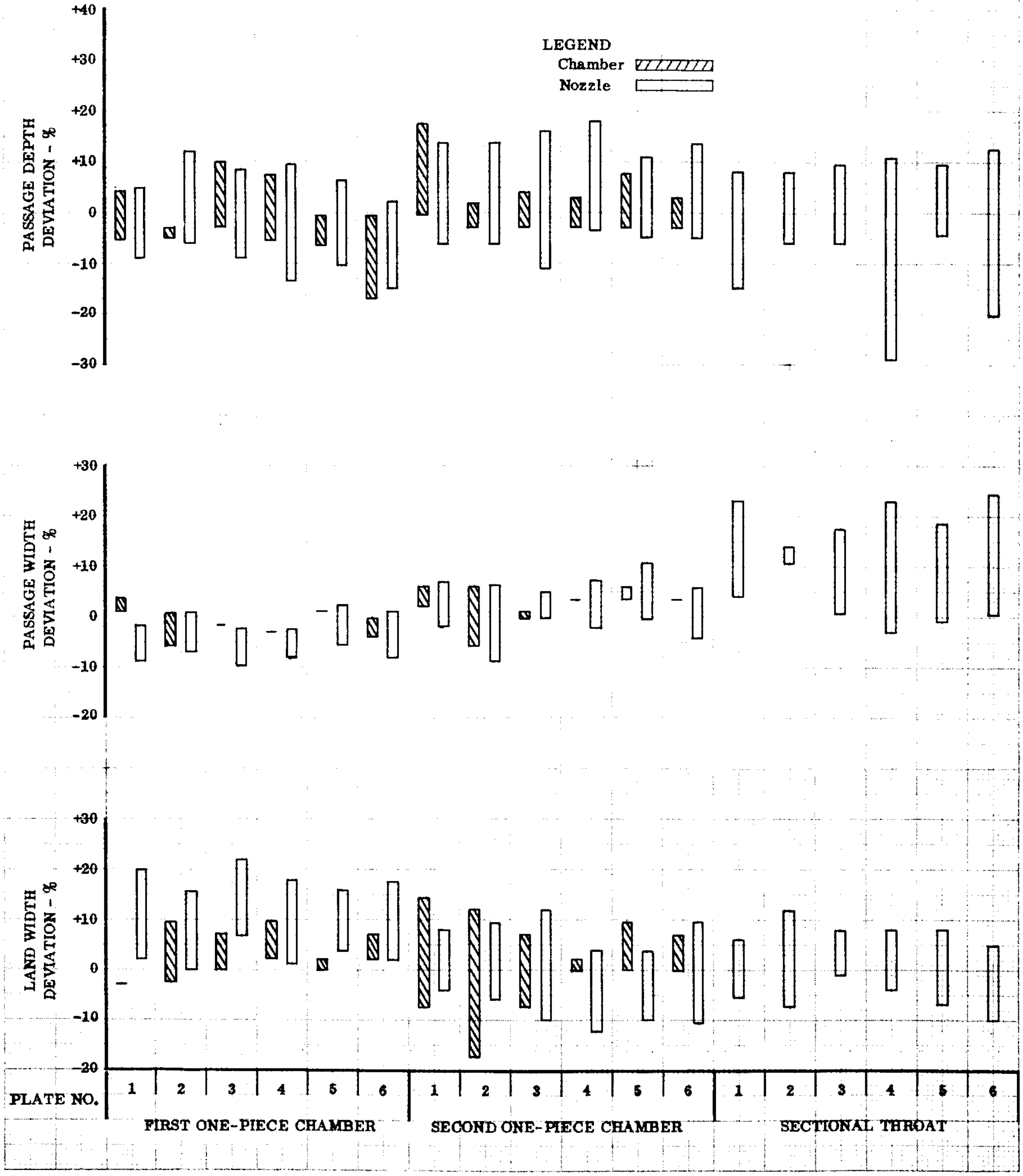

Figure 66. Summary of Inconel Plate Dimensional Variation for Regenerative Thrust Chambers DF 83152

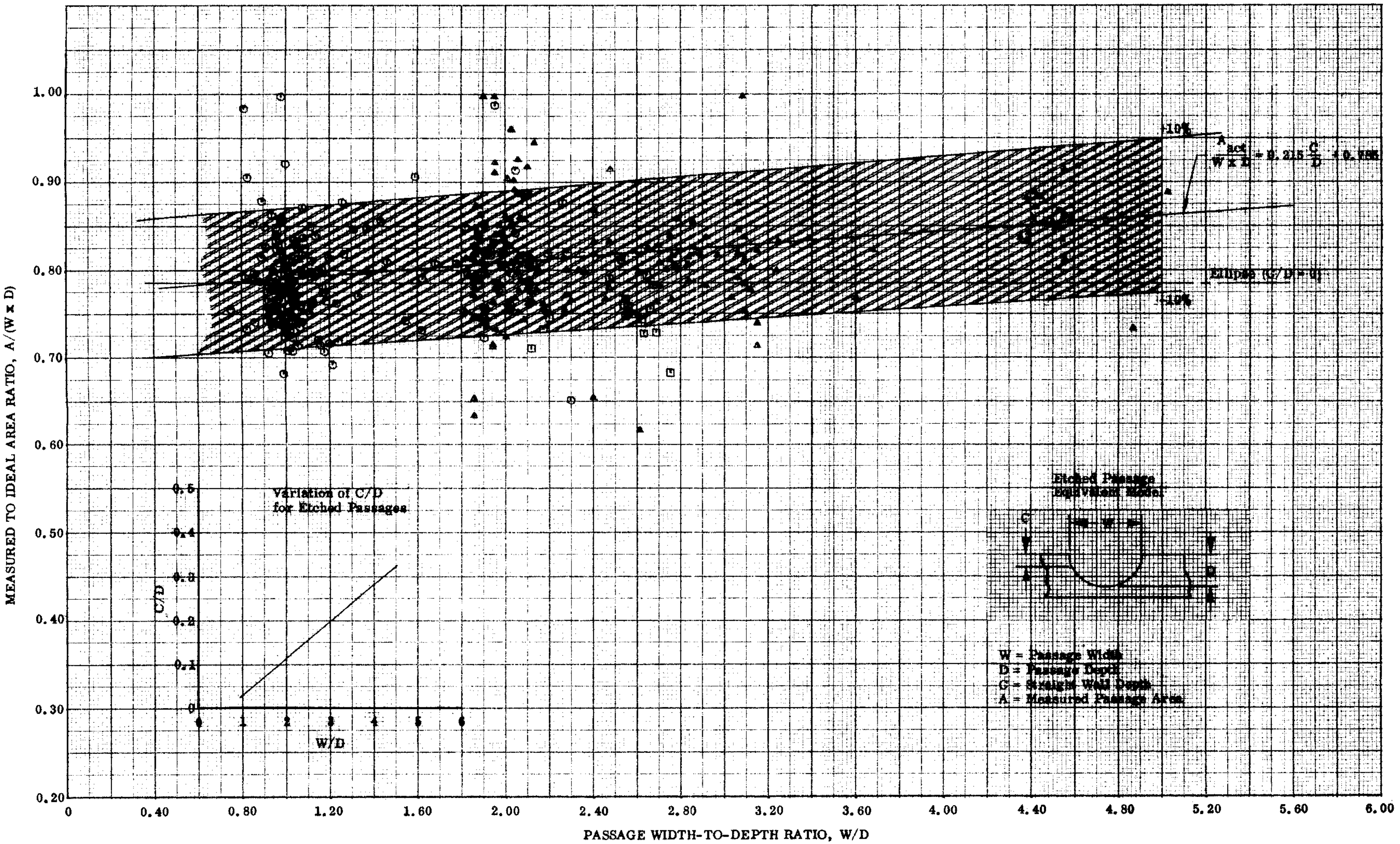

Figure 67. Etched Passage Flow Area Correlation for Regenerative Chamber

DF 83187

This equation was established by correlating the data with an equivalent passage model having an elliptical base and straight portions of the wall. (See insert of figure 67.) The straight wall portion increases with passage width-to-depth ratio. Use of this correlation enables prediction of the flow area, hydraulic diameter and heat flow path lengths in the region of the radiused corner. Most of the data falls within ±10% of the average values. An examination of the passage shapes for which the data points fell outside of the tolerance band revealed that the inconsistencies reflected undercut or inwardly-tapered passage walls. Shape factors for undercut passages fell above the upper 10% tolerance line, while those for passages with tapered walls fell below the lower 10% tolerance line. These abnormabilities occur during the etching process and can be eliminated by increased quality control.

Surface roughness is another parameter that is important in heat transfer calculations. Roughness values, measured with a profilometer, ranged in value from 90 to 190 microinches. The passages were sized for the weighted average roughness value obtained (150 microinches).

c. Passage Water Flow Data

The individual coolant passages in each stave of each thrust chamber assembly were water flow tested. Figures 68, 69, and 70 present the water flow data for the first and second one-piece chambers, and the throat section fabricated for the 3-piece thrust chamber respectively; the data were obtained with a pressure drop of 25 psid. The passage-to-passage flow deviations in the one-piece chambers were within ±25 (with the exception of one passage in the second chamber) of their respective average values. These deviations are attributed primarily to the passage-to-passage area variations resulting from the etching process and filleting of the silver braze. To protect against the seam damage that occurred on the first two chambers, the passages adjacent to the seams in the diffusion bonded throat section were increased in size in relation to the inside passages to provide more cooling in the seam areas. The passage-to-passage flow deviations in the non-seam passages of the throat section was reduced to ±15%, again with the exception of one passage. The flow deviations can be reduced in future chambers involving greater quantity runs by selective use of available staves.

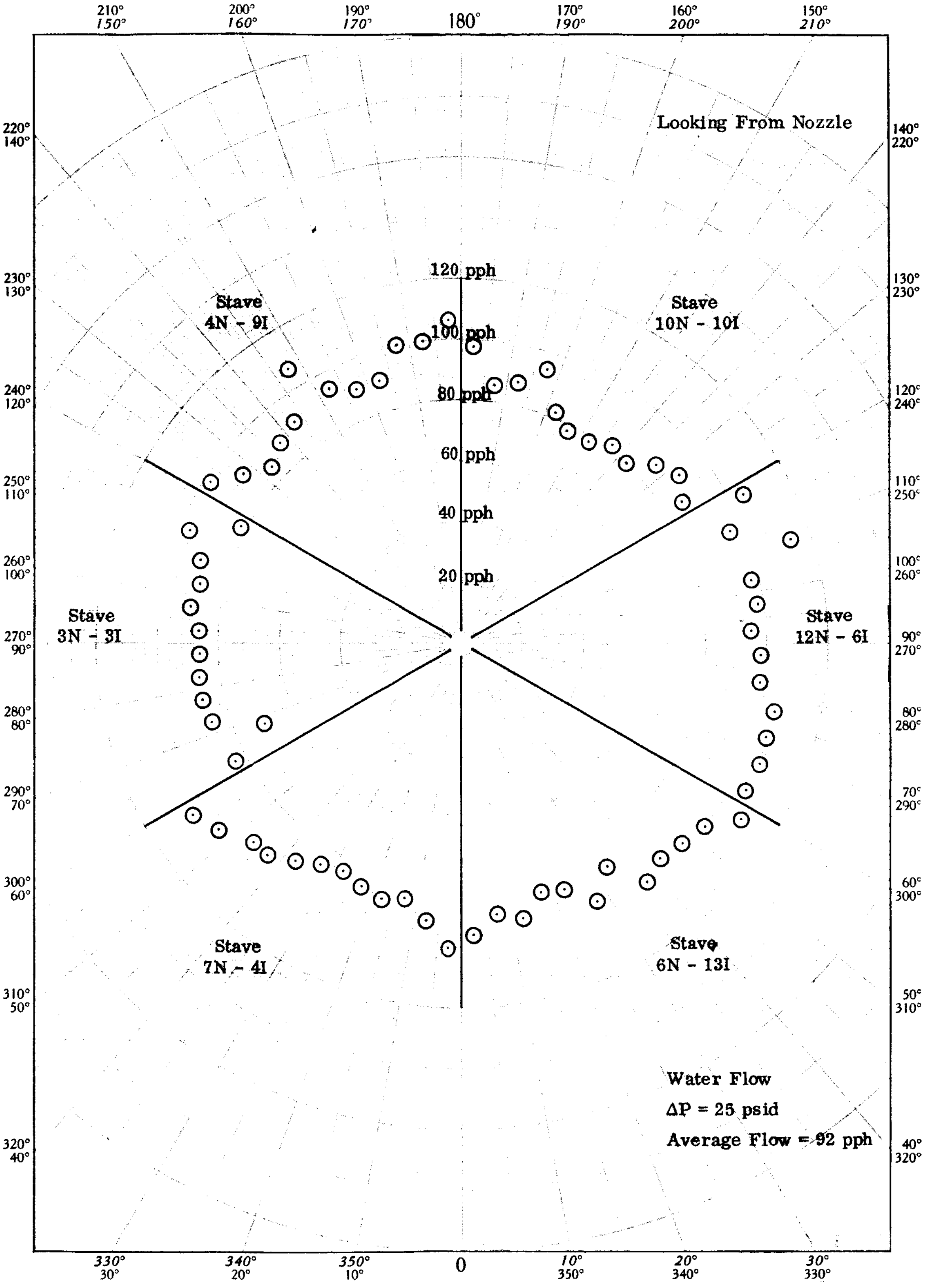

Figure 68. Coolant Passage Flow Data from First One-Piece Regenerative Chamber DF 83186A

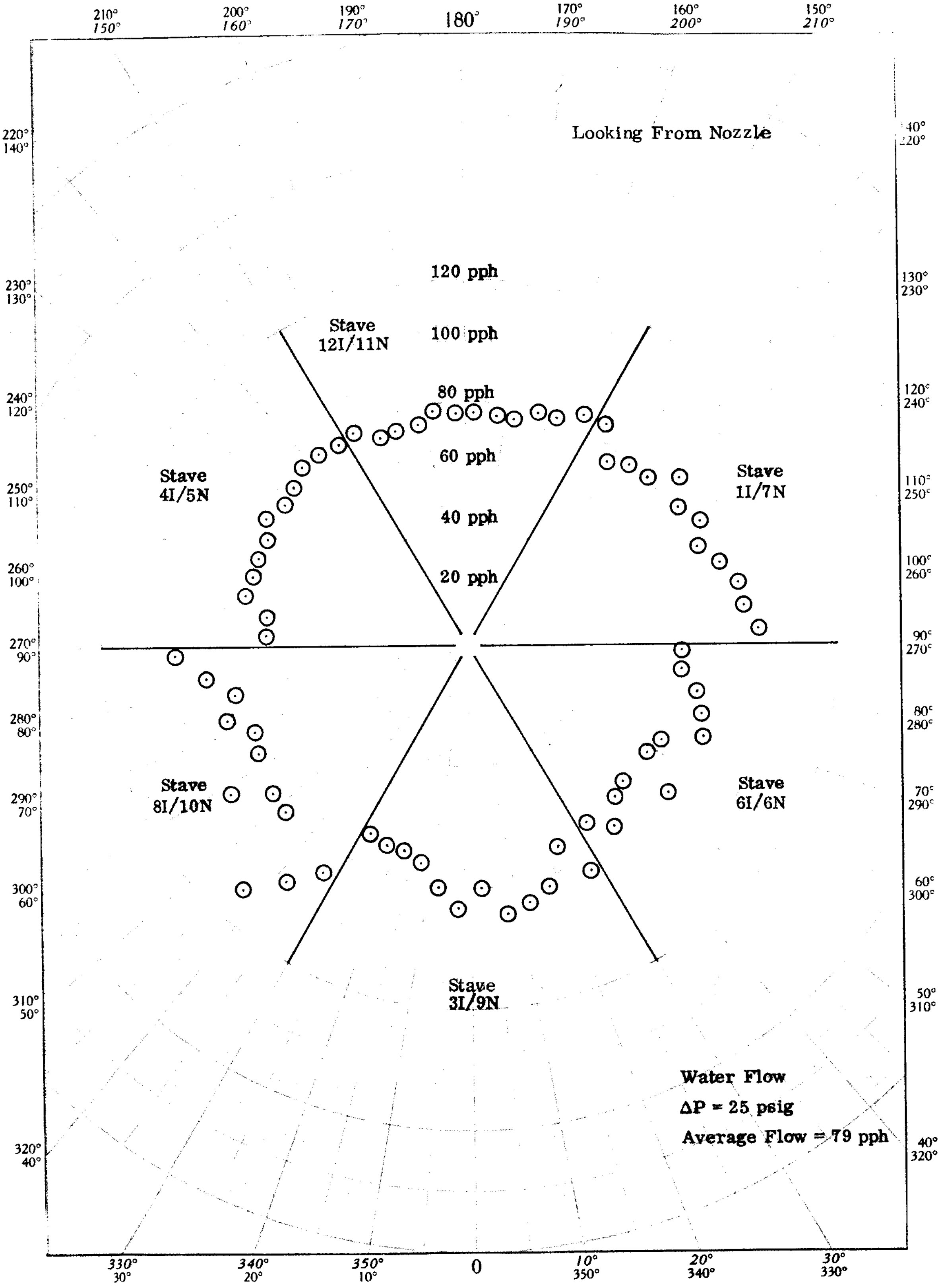

Water Flow
ΔP = 25 psig
Average Flow = 79 pph

Figure 69. Coolant Passage Flow Data for Second One-Piece Regenerative Chamber

DF 83185A

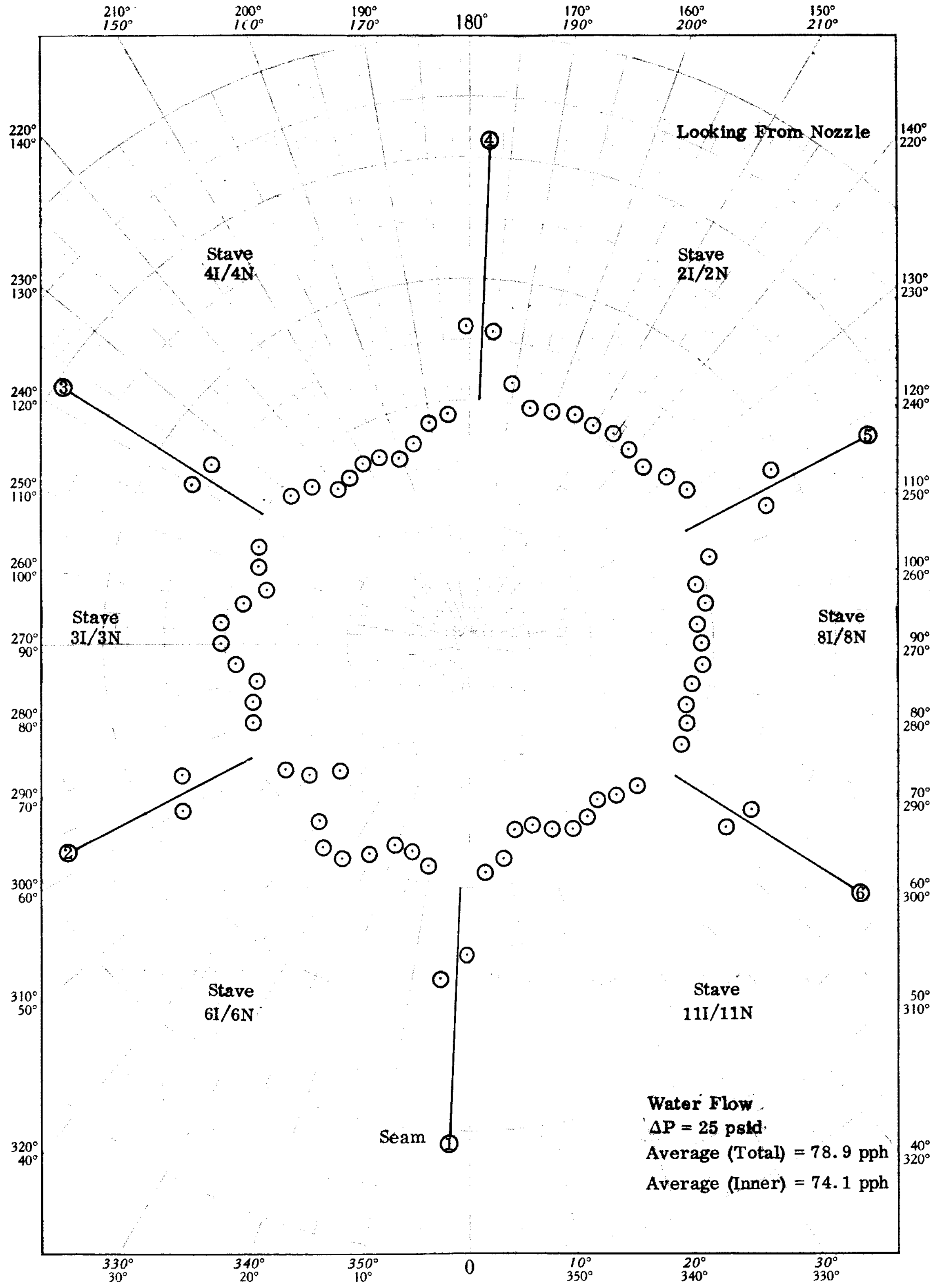

Figure 70. Coolant Passage Flow Data from Sectional Throat of Three-Piece Regenerative Chamber

DF 83184A

d. Seam Land Widths

X-rays of the trimmed staves provided a check on the accuracy of the etching master layout and specifically the ability to project the coolant passage geometry for a formed stave onto a flat surface. X-rays were taken after the staves were trimmed to 60-deg segments and after the staves had been welded together. Results are presented in figures 71, 72, and 73 for the three thrust chamber assemblies. The design seam land widths were 0.050 in. The seam lands for the two one-piece chambers are generally greater than this. (See figures 71 and 72.) The larger land widths in the seam result from the forming operations on the staves and the spacing of the passages. The forming operation elongated the staves, effecting a transverse deformation that resulted in a reduction in the arc length over which the coolant passages were spaced. Because the stave width is smallest at the throat station, most of the deformation occurred at this location. As a result, when the staves were trimmed to 60-deg circumferential segments, the seam land widths were greater than desired, primarily at the throat.

The passage spacing on the etching master for the throat section plates was revised to compensate for the stave stretching that was observed in the first two chambers. The masters were biased so that the throat station would have the minimum seam land widths (figure 73).

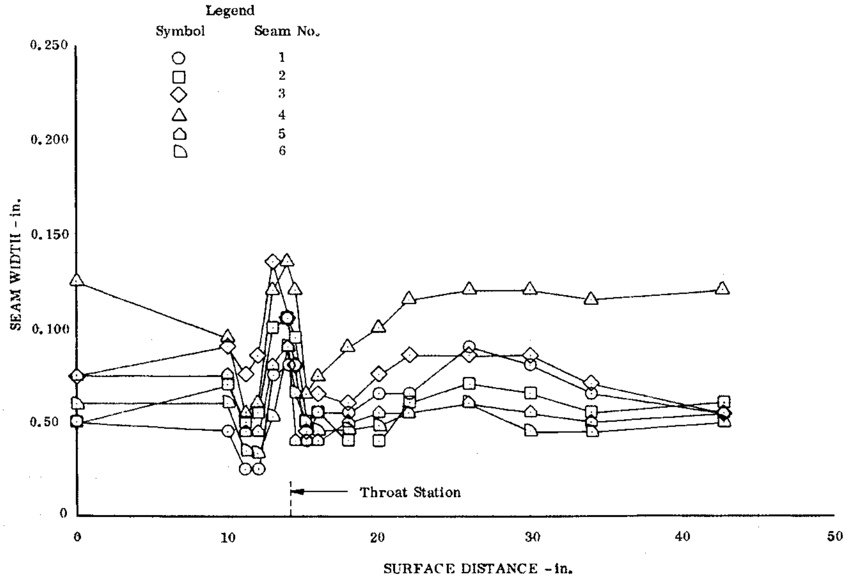

Figure 71. Seam Width Variation for First One-Piece Regenerative Chamber DF 83150

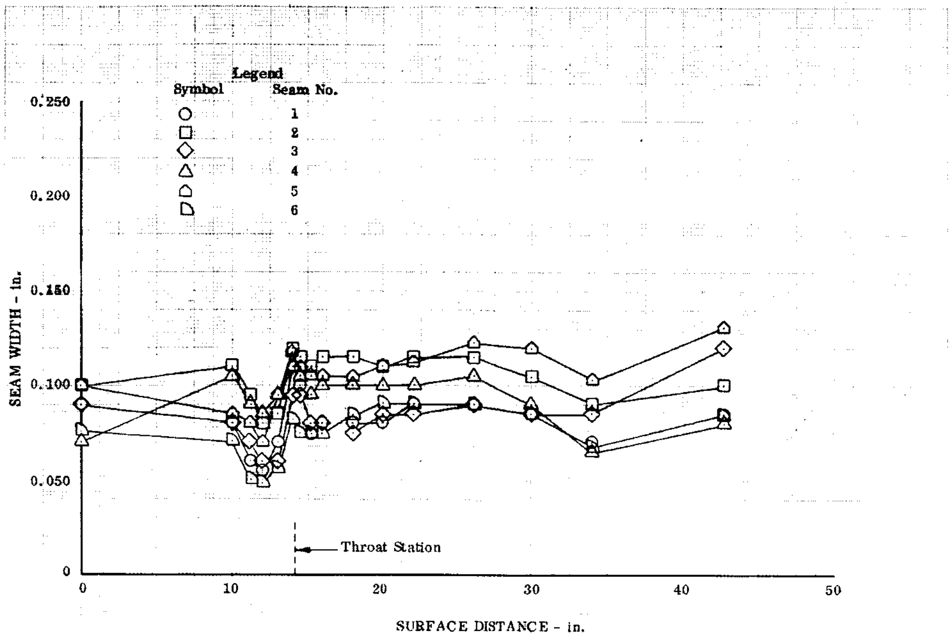

Figure 72. Seam Width Variation for Second One-Piece Regenerative Chamber DF 83149

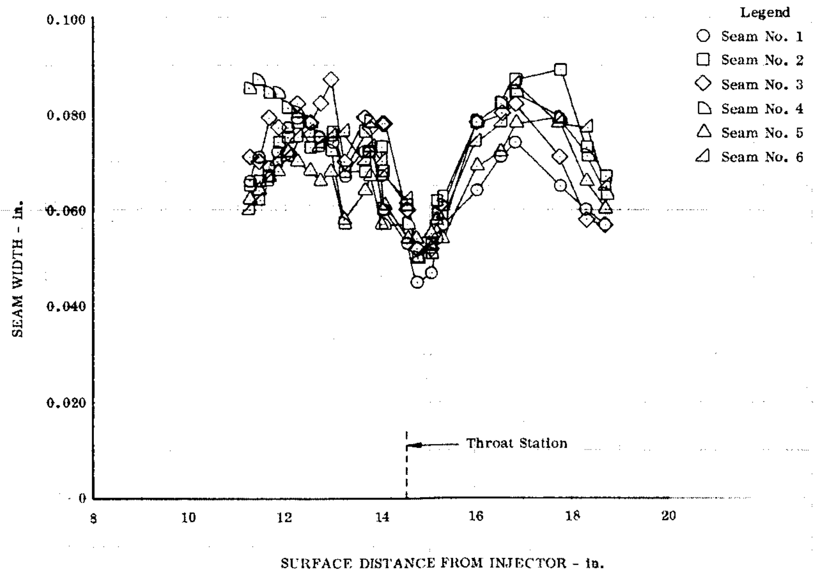

Figure 73. Seam Width Variation for Throat Section of Three-Piece Regenerative Chamber DF 80979

SECTION VIII
REGENERATIVE THRUST CHAMBER TESTS

A. GENERAL

A total of sixteen tests, in which 220 sec of firing time was accumulated, were made with regeneratively cooled chambers using flox/methane propellants. In five of the tests, the thrust chambers were separately supplied and overcooled with liquid methane while in the remaining eleven tests the thrust chambers were operated in a regenerative cooling mode. Performance and heat transfer results of the tests and hardware durability are discussed in this section.

In initial tests, durability problems were encountered primarily in the seam areas of the THERMAL SKIN® chambers. In later tests using the throat section in which the passage design was modified to improve cooling at the seams, good durability was demonstrated with an injector that provided relatively low thrust chamber heat fluxes. When higher performance injector configurations (which produced higher heat fluxes) were used, some chamber erosion did occur, but it was not concentrated in seam areas. Maximum measured wall temperatures were near the design value in the tests where erosion occurred, so the results indicate that a design wall temperature limit has been reached.

B. TEST SUMMARY

Table XIV summarizes the tests that were made with the regenerative chambers. Five of the tests were under the contract and the remaining 11 tests were made under an independent P&WA research program. All of the tests were made in the B-29 test stand of the Liquid Propellant Research Facility at FRDC. Appendix B describes this facility.

The thrust chamber test rigs used are shown in figures 74, 75, and 76. Figure 74 shows the first one-piece thrust chamber assembly used in test No. 1.02; the second one-piece thrust chamber used in test No. 1.03 was nearly identical in external appearance. The three-piece thrust chamber used in altitude tests No. 14.05 through 17.01 is shown in figure 75. A sea level chamber test rig, consisting of the chamber and throat sections only of the three-piece chamber, used in tests 3.01 through 13.01, is shown in figure 76.

Separately cooled and regeneratively cooled thrust chamber tests were made at both sea level and simulated altitude conditions. The test stand arrangements for the various modes are illustrated in figure 77. In all instances the flox and methane were pressure-fed to the test rig. The flox supply system was the same in all arrangements and identical to that used in water-cooled chamber tests. In the separately cooled chamber tests, gaseous methane heated to approximately 840°R was supplied directly to the injector; the thrust chamber was separately supplied and overcooled with liquid methane (figure 77a and 77b).

Table XIV. Regenerative Thrust Chamber Test Summary

P&WA Reference Test No.	Type	Flox Injector	Fuel Faceplate, scfm	Chamber	P_c, psia	r	Duration, sec	Comments
1.02 (F33524)	Altitude (overcooled)	Converging Fuel Stream	100	Full Length	500	4.0	5.5	Chamber weld seams cracked.
1.03*(F33536)	Altitude (overcooled)	Scarfed (Conf I)	100-40 Composite	Full Length	500	3.6 to 5.0	53.8	Three chambers seams eroded at the throat.
3.02 (F33536)	Sea Level (overcooled)	Scarfed (Conf I)	100	2-Section	500	3.73	10.2	Successful test.
5.01 (F33536)	Sea Level (overcooled)	Scarfed (Conf I)	100	2-Section	500	3.73, 4.98	15.4	Successful test.
6.01 (F33536)	Sea Level (overcooled)	Scarfed (Conf I)	100	2-Section	500	3.73, 4.15	11.3	Successful test.
7.03 (F33536)	Sea Level (Regen)	Scarfed (Conf I)	100	2-Section	500	4.18	9.9	Successful test.
8.03 (F33536)	Sea Level (Regen)	Scarfed (Conf I)	100	2-Section	500	4.56	10.2	Successful test.
9.01 (F33536)	Sea Level (Regen)	Scarfed (Conf I)	100	2-Section	500	4.57	10.6	Successful test.
10.04 (F33536)	Sea Level (Regen)	Scarfed (Conf I)	100	2-Section	500	5.14	10.2	Successful test.
11.01 (F33536)	Sea Level (Regen)	Scarfed (Conf I)	100	2-Section	500	5.18	10.3	Successful test.
12.01 (F33536)	Sea Level (Regen)	Scarfed (Conf I)	100	2-Section	500	5.19	10.0	Successful test.
13.01 (F33536)	Sea Level (Regen)	Scarfed (Conf I)	100	2-Section	500	5.5	10.2	Successful test.
14.05 (F33536)	Altitude (Regen)	Scarfed (Conf I)	100	3-Section	500	4.04, 4.99	15.3	Successful test.
15.01 (F33536)	Altitude (Regen)	Scarfed (Conf I)	40	3-Section	500	4.08, 5.0	13.6	Throat section eroded at two locations. Repaired by plating
16.01 (F33536)	Altitude (Regen)	Scarfed (Conf I)	100-40 Composite	3-Section	500	4.0, 5.25	12.0	Plating came off in repaired area. Replaced with weld deposited nickel.
17.01 (F33536)	Altitude (Regen)	Converging Fuel Stream	40	3-Section	500	4.0, 5.1	11.6	Throat eroded slightly in several locations.

*Test 1.03 through 13.01 were made under a separate Pratt & Whitney Research Program.

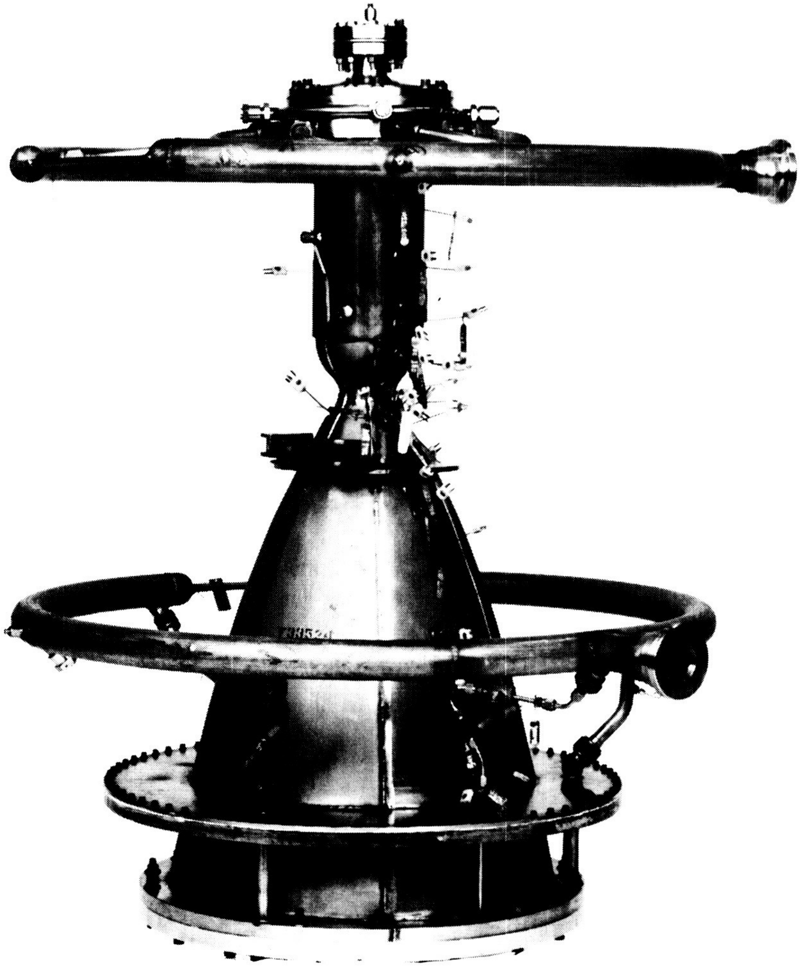

Figure 74. One-Piece Regenerative Thrust Chamber-Injector Assembly FE 86786

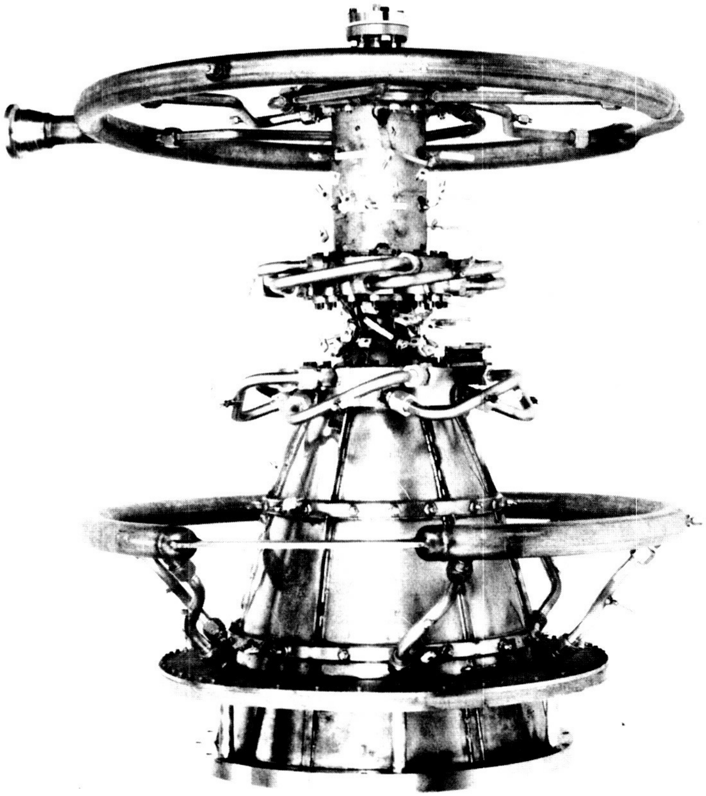

Figure 75. Three-Piece Regenerative Thrust Chamber-Injector Assembly FE 98734

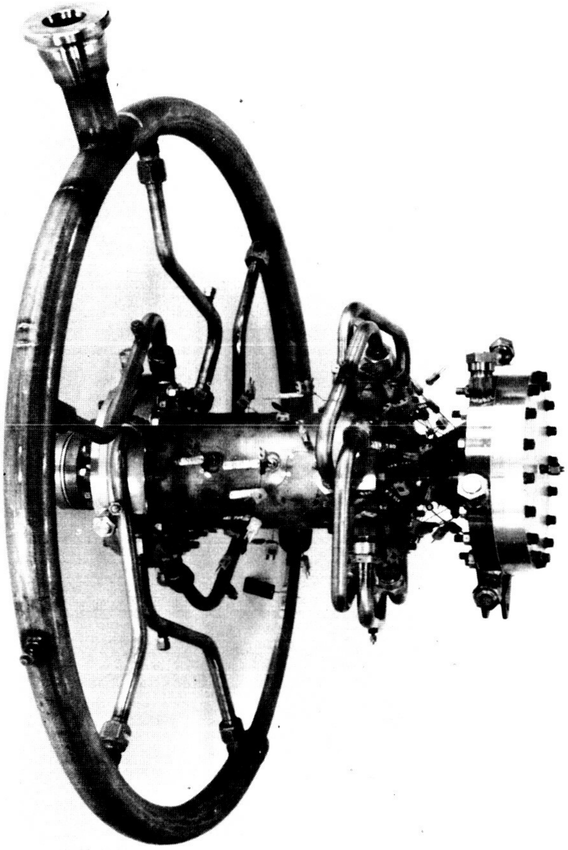

Figure 76. Two-Piece (Sea Level) Regenerative Thrust Chamber-Injector Assembly FE 97465

In regenerative tests of the full length thrust chambers, liquid methane was supplied to the thrust chamber (figure 77c). Sea level regenerative thrust chamber tests of the throat and combustion chamber sections only of the three-piece thrust chamber were conducted using an ambient-temperature methane gas supply (figure 77d). The sea level tests provided a valid evaluation of the throat and combustion chamber because the ambient-temperature gas closely approximated the temperature of the methane at the throat section in a full length thrust chamber.

Electrohydraulic valves were used to control test conditions. The test procedure for the separately cooled tests was similar to that used in the water-cooled chamber tests. The methane coolant flow was started prior to opening the propellant control valves; a coolant valve at the inlet of the thrust chamber controlled liquid methane flowrate while a discharge valve controlled chamber discharge pressure. The oxidizer valve was actuated through a feedback control loop sensing chamber pressure; the injector fuel valve control was based on mixture ratio. In the regenerative tests, the valve at the thrust chamber inlet regulated fuel flow, and therefore mixture ratio.

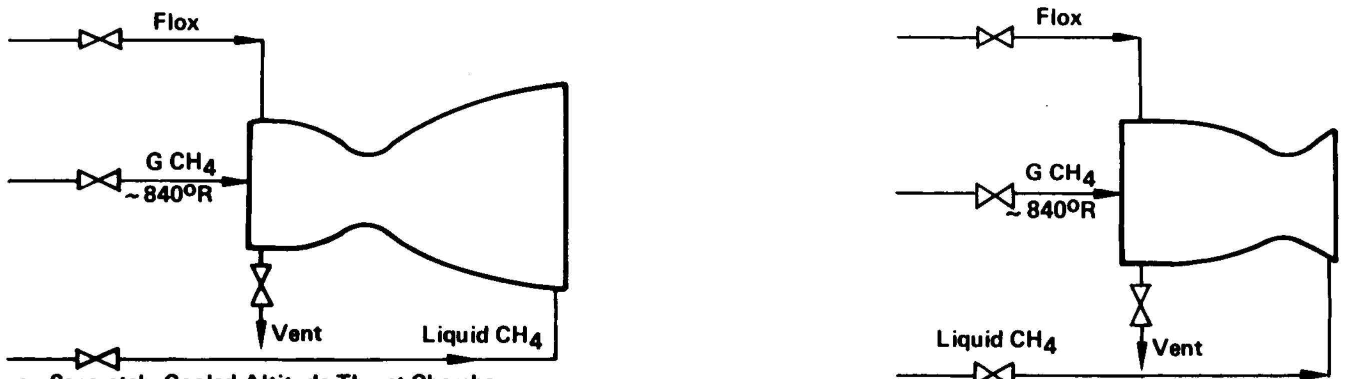

a. Separately Cooled Altitude Thrust Chamber Test Setup

b. Separately Cooled Sea Level Thrust Chamber Test Setup

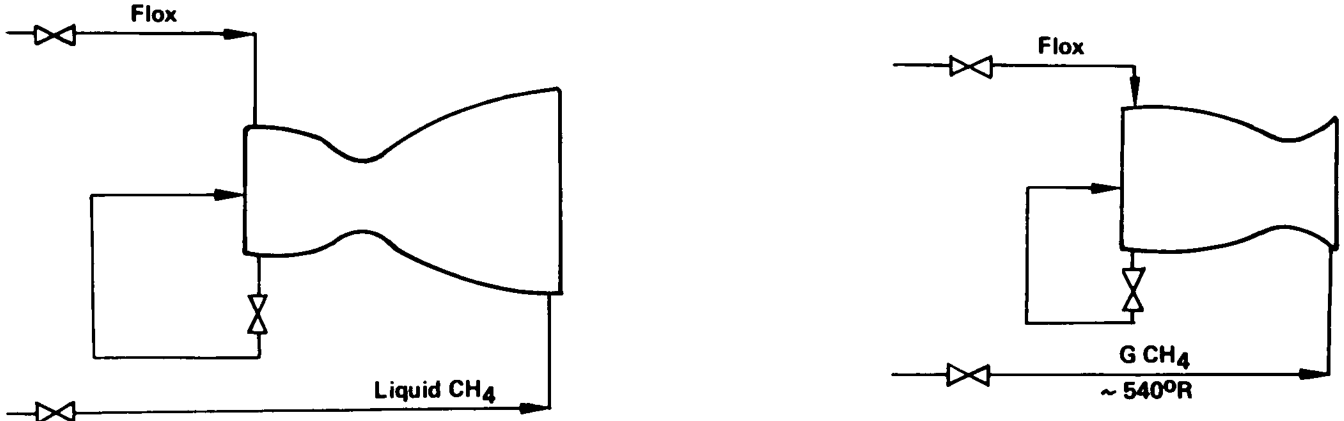

c. Regeneratively Cooled Altitude Thrust Chamber Test Setup

d. Regeneratively Cooled Sea Level Thrust Chamber Test Setup

Figure 77. Setups for Regenerative Chamber Tests

FD 45500A

Figure 78 presents plots of important test parameters versus time for the sea level regenerative thrust chamber tests. These tests were all approximately 10-sec duration. Chamber pressure was ramped up slowly (6 sec) so that the last 4 sec of the tests were at the design chamber pressure (500 psia) and a selected mixture ratio. Mixture ratio was progressively increased from 4.2 to 5.5 during the testing. As indicated by the coolant discharge temperature/time plots (figure 78), steady-state chamber conditions were established in the lower mixture ratio tests. However, the coolant exit temperature was still increasing but only slightly (20°R/sec) at shutdown in the higher mixture ratio firings. These results indicate that very short duration tests of 2 to 3 sec do not provide a valid evaluation of regenerative thrust chambers; steady-state chamber conditions were barely achieved after operating at the design chamber pressure and a given mixture ratio setpoint for 4 sec.

Traces for startup of regenerative tests with the full length three-section thrust chamber are presented in figure 79. Behavior was similar to that in the sea level tests. The initial test (test No. 14.05) was advanced to shutdown after obtaining test data at mixture ratios of approximately 4.0 and 5.0. The last three tests were advanced to shutdown prematurely when the throat station metal temperatures exceeded a predetermined safe value. Unfortunately, the coolant exit temperature did not reach steady-state values in these tests.

C. PERFORMANCE DATA

Tables XV and XVI present the measured and derived data obtained with the regenerative thrust chambers. Where possible, 2-sec data average periods were used in the tests. However, because steady-state conditions were not reached in the two final altitude tests with the full length chamber, shorter data average periods, as indicated in the tables, were used.

Performance parameters were calculated using equations similar to those used for the water-cooled chamber tests (see Appendix C). As in the water-cooled chamber tests, a throat discharge coefficient of 0.985 was used in calculating characteristic exhaust velocity $[c^*(P_c)]$ and the thrust coefficient $(C_{F\text{vac}})$. Throat total pressure was calculated using measurements made at an injector face tap. The measured values were reduced by a calculated momentum loss of 1.38%. A downstream chamber tap was available in the regenerative chamber; however, the tap had to be made so small in diameter (0.015 in.) because of the small land distances between coolant passages, the taps plugged with carbon and did not provide useful pressure measurements.

The momentum loss was verified in the water-cooled chamber tests. Further verification is provided in figure 80 where chamber-pressure-based-c* and thrust-based-c* data are compared. As in the water-cooled chamber tests, best agreement between the two sets of c* data is obtained at low mixture ratios where (as illustrated in the lower part of figure 80) there is close agreement between the experimentally-determined thrust coefficient efficiency data and the theoretical efficiency. Also as indicated in figure 80 the thrust coefficient efficiency data for the sea level regenerative chamber agrees with the curve established for the water-cooled sea level chamber (as it should because the two chambers are identical in the design features that affect nozzle efficiency).

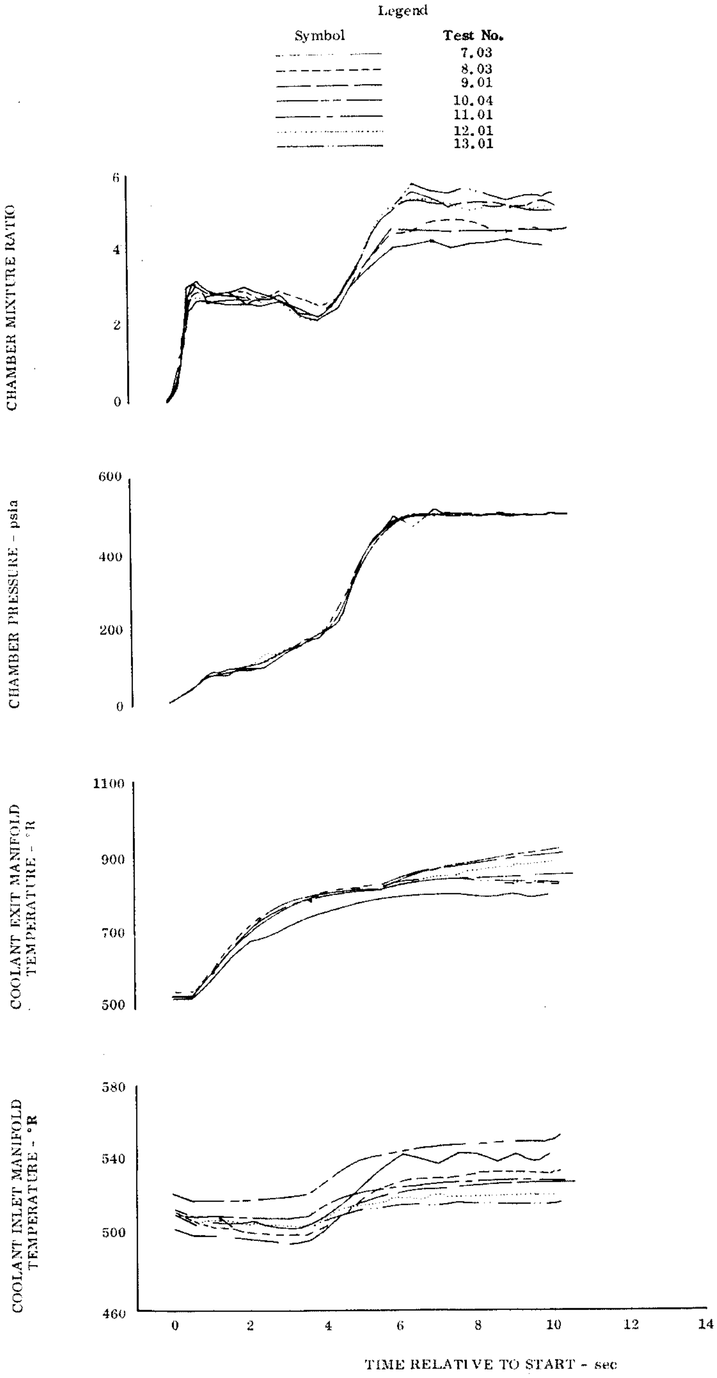

Figure 78. Sea Level Thrust Chamber Regenerative Test Parameters

DF 80741

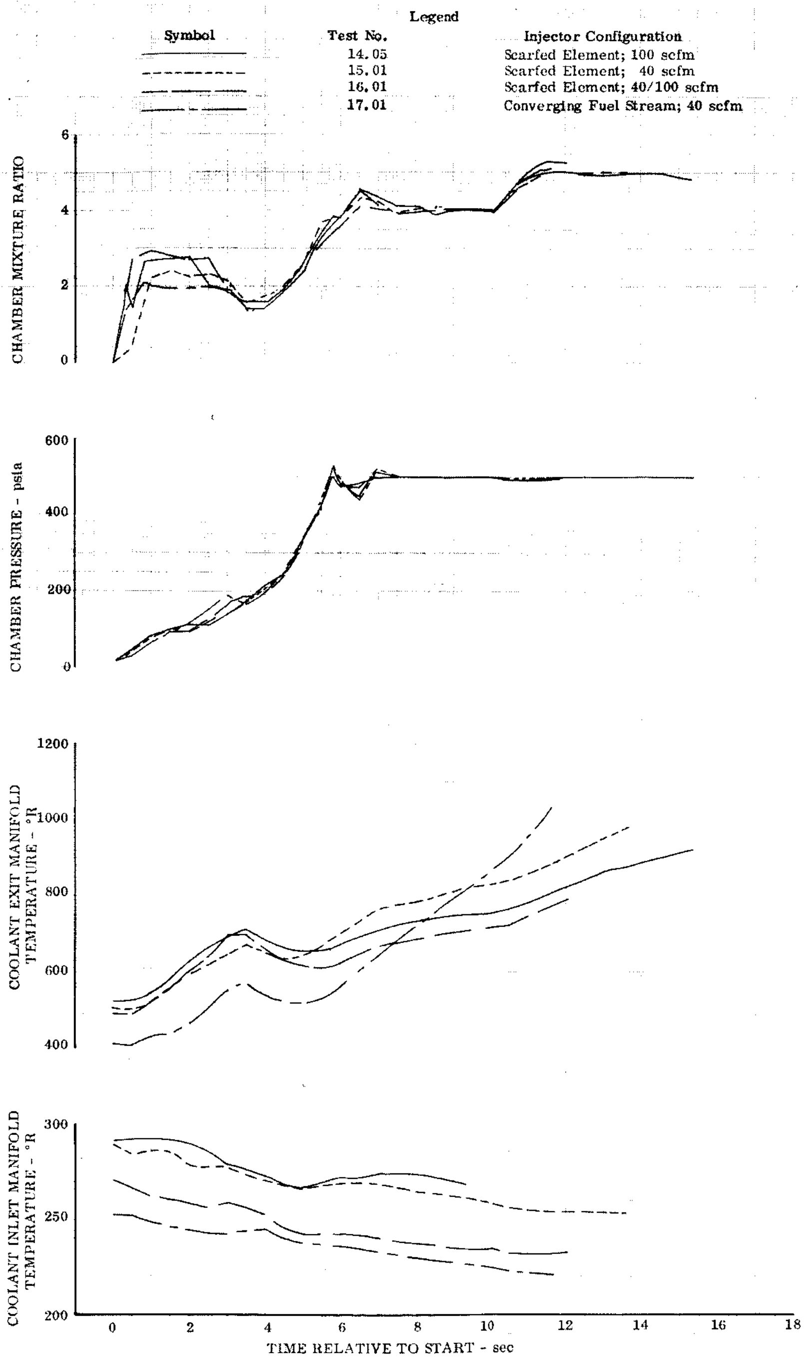

Figure 79. Altitude Thrust Chamber Regenerative Test Parameters

DF 80742

Table XV. Measured Data for Regenerative Thrust Chamber Tests

Test Description			Chamber							Oxidizer Injector		Fuel Injector	
P&WA Ref. Test No.	Injector	Test Type	Mixture Ratio	Chamber Press., Injector Face Static, psia	$\dot{W}_o$, lb_m/sec	$\dot{W}_f$, lb_m/sec	Thrust Net, lb	Ambient Press., psia	Diffuser Press., psia	Inlet Temp., °R	Inlet Press., psia	Inlet Temp., °R	Inlet Press., psia
1.03	Scarfed element (Conf.)/40-100 scfm faceplate	Altitude (Separately Cooled)	3.65	504.0	10.03	2.75	-3760	14.69	0.22	158.9	561.9	758.3	700.2
			4.13	505.2	10.13	2.45	-3777		0.25	156.0	564.6	777.7	666.7
			4.59	504.9	10.30	2.25	-3849		0.26	152.6	565.9	785.8	643.3
			4.58	504.7	10.29	2.25	-3848		0.26	152.5	565.9	787.8	643.3
			4.79	505.4	10.41	2.17	-3869		0.27	152.4	566.7	792.3	635.6
			4.80	505.2	10.41	2.17	-3860		0.27	152.4	566.3	792.6	635.4
			5.03	504.9	10.50	2.09	-3843		0.27	152.4	567.9	794.8	626.8
			5.02	504.9	10.46	2.08	-3877		0.27	152.5	567.2	796.7	626.2
3.02	Scarfed element (Conf. I)/100 scfm faceplate	Sea level (Separately Cooled)	3.75	503.9	10.38	2.77	3724	14.80	N/A	154.4	579.4	758.8	682.8
5.01	Scarfed element (Conf. I)/100 scfm faceplate	Sea level (Separately Cooled)	3.69	501.6	10.24	2.78	3707	14.75	N/A	156.8	576.6	719.3	674.9
			3.70	501.6	10.30	2.78	3702			157.9	576.2	723.9	676.6
			4.99	502.5	11.04	2.21	3696			157.7	586.0	733.3	623.1
			4.98	502.8	11.02	2.21	3697			156.5	585.8	735.3	623.4
6.01	Scarfed element (Conf. I)/100 scfm faceplate	Sea level (Separately Cooled)	3.74	499.7	10.18	2.72	3671	14.74	N/A	165.3	577.6	748.4	672.4
			4.16	498.8	10.42	2.50	3661			170.3	576.8	750.7	653.3
7.03	Scarfed element (Conf. I)/100 scfm faceplate	Sea level (Regen.)	4.21	502.6	10.47	2.48	3698	14.75	N/A	156.6	582.9	742.8	652.7
8.03	Scarfed element (Conf. I)/100 scfm faceplate	Sea level (Regen.)	4.59	507.6	10.76	2.35	3715	14.74	N/A	156.2	591.4	765.5	635.8
			4.59	506.8	10.73	2.34	3710			157.8	590.0	768.8	638.5
9.01	Scarfed element (Conf. I)/100 scfm faceplate	Sea level (Regen.)	4.61	503.7	10.68	2.32	3692	14.74	N/A	158.0	584.8	773.2	636.1
10.04	Scarfed element (Conf. I)/100 scfm faceplate	Sea level (Regen.)	5.19	502.6	10.91	2.10	3683	14.78	N/A	154.0	584.3	807.9	623.1
11.01	Scarfed element (Conf. I)/100 scfm faceplate	Sea level (Regen.)	5.25	505.0	11.02	2.10	3685	14.78	N/A	154.2	586.7	813.6	626.6
12.01	Scarfed element (Conf. I)/100 scfm faceplate	Sea level (Regen.)	5.26	505.3	10.98	2.09	3672	14.78	N/A	155.7	587.3	791.7	622.5
13.01	Scarfed element (Conf. I)/100 scfm faceplate	Sea level (Regen.)	5.56	504.5	11.37	2.04	3640	14.81	N/A	156.7	594.6	765.8	614.0
			5.55	504.8	11.34	2.04	3634			158.1	593.6	770.1	614.9
14.05	Scarfed element (Conf. I)/100 scfm faceplate	Altitude (Regen.)	4.04	501.3	10.43	2.58	-3609	14.79	0.41	157.4	574.5	696.0	643.0
			5.01	501.7	10.99	2.19	-3622		0.43	158.0	580.6	776.6	619.0
			4.98	502.1	10.97	2.20	-3621		0.43	157.1	580.5	804.6	622.4
15.01	Scarfed element (Conf. I)/40 scfm faceplate	Altitude (Regen.)	4.08	500.2	10.42	2.55	-3516	14.78	0.46	155.4	574.9	739.3	688.1
			4.92	499.8	10.64	2.16	-3592		0.47	156.5	575.3	807.9	656.6
			5.01	501.3	10.74	2.14	-3581		0.47	156.4	578.2	844.7	658.2
16.01	Scarfed element (Conf. I)/40 scfm faceplate	Altitude (Regen.)	4.01	501.6	10.41	2.60	-3600	14.76	0.38	152.9	571.2	652.1	656.5
			5.24	506.6	11.24	2.14	-3565		0.40	153.7	586.7	719.5	628.9
17.01	Converging fuel stream/40 scfm faceplate	Altitude (Regen.)	4.01	502.4	10.34	2.52	-3524	14.74	0.39	151.4	640.9	648.8	708.3
			3.99	501.9	10.39	2.61	-3514		0.39	152.9	642.8	708.9	724.7
			5.08	501.5	10.72	2.11	-3495		0.38	153.2	643.5	875.6	698.3

Table XVI. Derived Data for Regenerative Thrust Chamber Tests

P&WA Reference Test No.	Injector	Test Type	Mixture Ratio	Chamber Pressure, Throat Total, psia	Vacuum Thrust, lb.	I_{vac}, sec.	$c^*_{(P_c)}$, ft/sec	$C_{F_{vac}}$	$\eta_{I_{vac}}$ %	$\eta_{c^*(P_c)}$ %	$\eta_{c^*(F)}$ %	$\eta_{C_{F_{vac}}}$ %
1.03	Scarfed element (Conf. I)/40-100 scfm	Altitude (Separately Cooled)	3.65	497.0	4885	382.3	6536	1.89	94.20	95.56		98.67
			4.13	498.2	4860	386.4	6656	1.87	93.54	95.88		97.55
			4.59	497.9	4784	381.2	6669	1.84	91.34	94.81		96.34
			4.58	497.7	4784	381.5	6670	1.84	91.41	94.84		96.38
			4.79	498.4	4761	378.5	6660	1.83	90.22	94.22		95.76
			4.80	498.2	4771	379.3	6655	1.83	90.36	94.15		95.98
			5.03	497.9	4787	380.3	6648	1.84	90.01	93.65		96.11
			5.02	497.9	4753	378.8	6670	1.83	89.69	93.97		95.44
3.02	Scarfed element (Conf. I)/100 scfm	Sea level (Separately Cooled)	3.75	496.9	4236	322.0	6673	1.55	89.02	97.19	97.50	91.60
5.01	Scarfed element (Conf. I)/100 scfm	Sea level (Separately Cooled)	3.69	494.6	4217	324.0	6713	1.55	89.81	98.01	98.36	91.64
			3.70	494.6	4213	322.1	6679	1.55	89.25	97.45	97.75	91.59
			4.99	495.5	4206	317.3	6602	1.54	85.07	92.94	93.17	91.53
			4.98	495.8	4208	317.9	6617	1.54	85.26	93.17	93.38	91.51
6.01	Scarfed element (Conf. I)/100 scfm	Sea level (Separately Cooled)	3.74	492.8	4182	324.1	6745	1.54	89.61	98.27	98.14	91.19
			4.16	491.9	4171	322.9	6725	1.54	88.21	96.65	96.61	91.27
7.03	Scarfed element (Conf. I)/100 scfm	Sea level (Regen.)	4.21	495.6	4208	325.0	6796	1.53	88.37	97.11	96.79	91.00
8.03	Scarfed element (Conf. I)/100 scfm	Sea level (Regen.)	4.59	500.5	4226	322.4	6785	1.53	86.80	95.89	95.07	90.52
			4.59	499.8	4220	322.8	6792	1.53	86.91	96.01	95.19	90.53
9.01	Scarfed element (Conf. I)/100 scfm	Sea level (Regen.)	4.61	496.7	4202	323.4	6791	1.53	87.03	95.93	95.32	90.72
10.04	Scarfed element (Conf. I)/100 scfm	Sea level (Regen.)	5.19	495.6	4195	322.3	6771	1.53	85.68	94.53	93.84	90.64
11.01	Scarfed element (Conf. I)/100 scfm	Sea level (Regen.)	5.25	498.0	4197	319.8	6746	1.52	84.95	94.10	93.04	90.27
12.01	Scarfed element (Conf. I)/100 scfm	Sea level (Regen.)	5.26	498.3	4184	320.2	6777	1.52	85.03	94.54	93.13	89.94
13.01	Scarfed element (Conf. I)/100 scfm	Sea level (Regen.)	5.56	497.5	4152	309.6	6588	1.51	82.10	91.85	88.92	89.39
			5.55	497.8	4147	309.8	6604	1.51	82.12	92.06	89.94	89.20
14.05	Scarfed element (Conf. I)/100 scfm	Altitude (Regen.)	4.04	494.3	5044	387.8	6748	1.85	94.37	96.95		97.34
			5.01	494.7	5027	381.5	6674	1.84	90.29	93.43		96.64
			4.98	495.1	5028	381.7	6681	1.84	90.40	93.55		96.64
15.01	Scarfed element (Conf. I)/40 scfm	Altitude (Regen.)	4.08	493.3	5120	394.7	6760	1.88	95.94	96.98		98.93
			4.92	492.9	5039	393.6	6850	1.85	93.36	96.07		97.19
			5.01	494.3	5051	392.2	6831	1.85	92.82	95.61		97.08
16.01	Scarfed element (Conf. I)/40-100 scfm	Altitude (Regen.)	4.01	494.6	5046	388.0	6746	1.85	94.59	97.11		97.40
			5.24	499.6	5101	381.2	6631	1.85	89.78	92.55		97.01
17.01	Converging fuel stream/40 scfm	Altitude (Regen.)	4.01	495.4	5103	395.1	6818	1.86	96.34	98.12		98.19
			3.99	494.9	5113	393.4	6767	1.87	96.00	97.39		98.57
			5.08	494.5	5135	400.3	6864	1.88	94.63	95.89		98.69

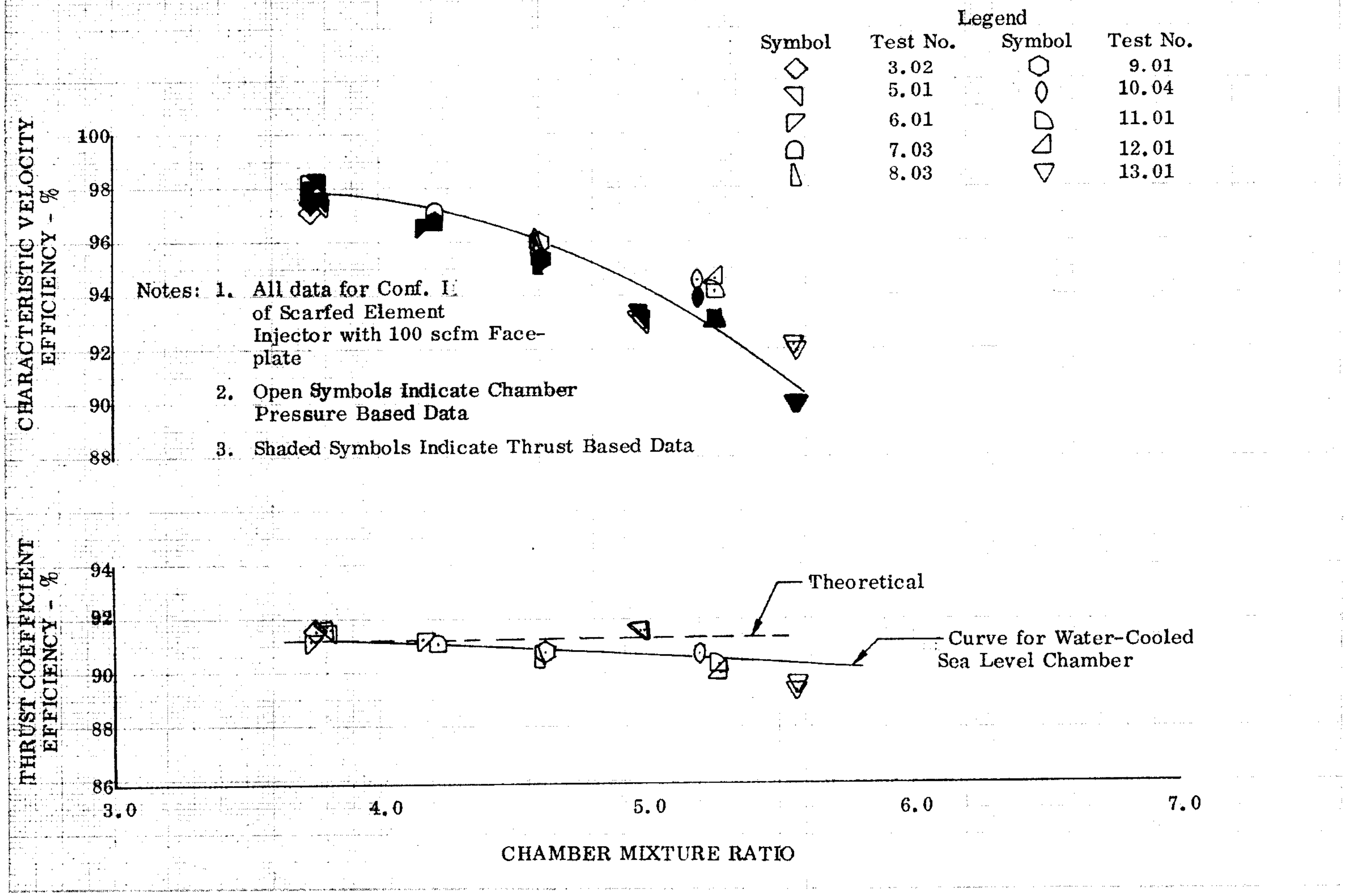

Notes: 1. All data for Conf. I of Scarfed Element Injector with 100 scfm Face-plate

2. Open Symbols Indicate Chamber Pressure Based Data

3. Shaded Symbols Indicate Thrust Based Data

Figure 80. Regenerative Chamber Sea Level Performance Parameters

Performance data obtained in tests with the regenerative thrust chamber are plotted in figures 81 and 82 as a function of mixture ratio. Figure 81 displays the c* efficiency data obtained with the scarfed element injector using different faceplates, and figure 82 presents altitude performance information.

The scarfed element injector used in the regenerative chamber tests corresponds to configuration I of the injector; the spuds in its fourth (or outer) and third rows were scarfed to angles of 45 and 22.5 deg respectively. Configuration II of the injector, which had spuds on the fourth rows scarfed to 22.5 deg and those on the third rows flush (i.e., unscarfed), was tested in a water-cooled chamber, and a mean c* curve for this unit is included in figure 81. The data obtained with configuration I of the injector in the regenerative tests straddles the curve obtained in the water-cooled chamber with configuration II; therefore, it appears that changes to the scarf angle of the outer row spuds had no significant effect on performance.

Figure 82 presents the performance data obtained in the altitude tests of the regenerative thrust chamber superimposed on data obtained in water-cooled chamber tests of configuration II of the scarfed element injector and of the converging fuel element injector. The regenerative chamber data agree with corresponding data obtained in water-cooled chamber tests with two exceptions: the data obtained in regenerative tests 15.01 and 17.01. Test 15.01 was made with configuration I of the scarfed element injector using a 40-scfm faceplate. Based upon the comparable performance levels of all configurations of the scarfed element injector in all other regenerative and water cooled tests, the impulse, impulse efficiency and c* efficiency data obtained in test 15.01 are higher than one would expect them to be. However, there is no apparent reason to discredit the data from that test.

For test 17.01 of the converging fuel stream injector with a 40-scfm faceplate, the c* efficiency appears to be too low and the thrust coefficient efficiency data too high; these apparent data abnormalities can be attributed, as will be discussed below, to the transient conditions that prevailed in that regenerative test and to a thrust measurement problem.

It was shown earlier that coolant temperatures did not reach steady-state levels in the regenerative tests and transient conditions prevailed. As a result, the remotely located test stand flowmeter used for fuel flow measurement did not necessarily indicate correctly time-phased flowrates. To assess the effect of the transient flow data on performance parameter levels, fuel flows were also calculated from injector characteristics. A comparison of the turbine meter and injector-based fuel flow data is shown in figure 83. Data for test 15.01 is also shown, and there is close agreement between the two sets of data in that instance. However, for test 17.01 the injector based flow was below the turbine meter flow. Thus, if injector fuel flowrates were used instead of the turbine meter values on this test, mixture ratio would increase appreciably but performance parameters only slightly. As a result, the c* efficiency point for test 17.01 would move to the right in figure 82 resulting in closer agreement with it and that obtained in the water-cooled chamber tests.

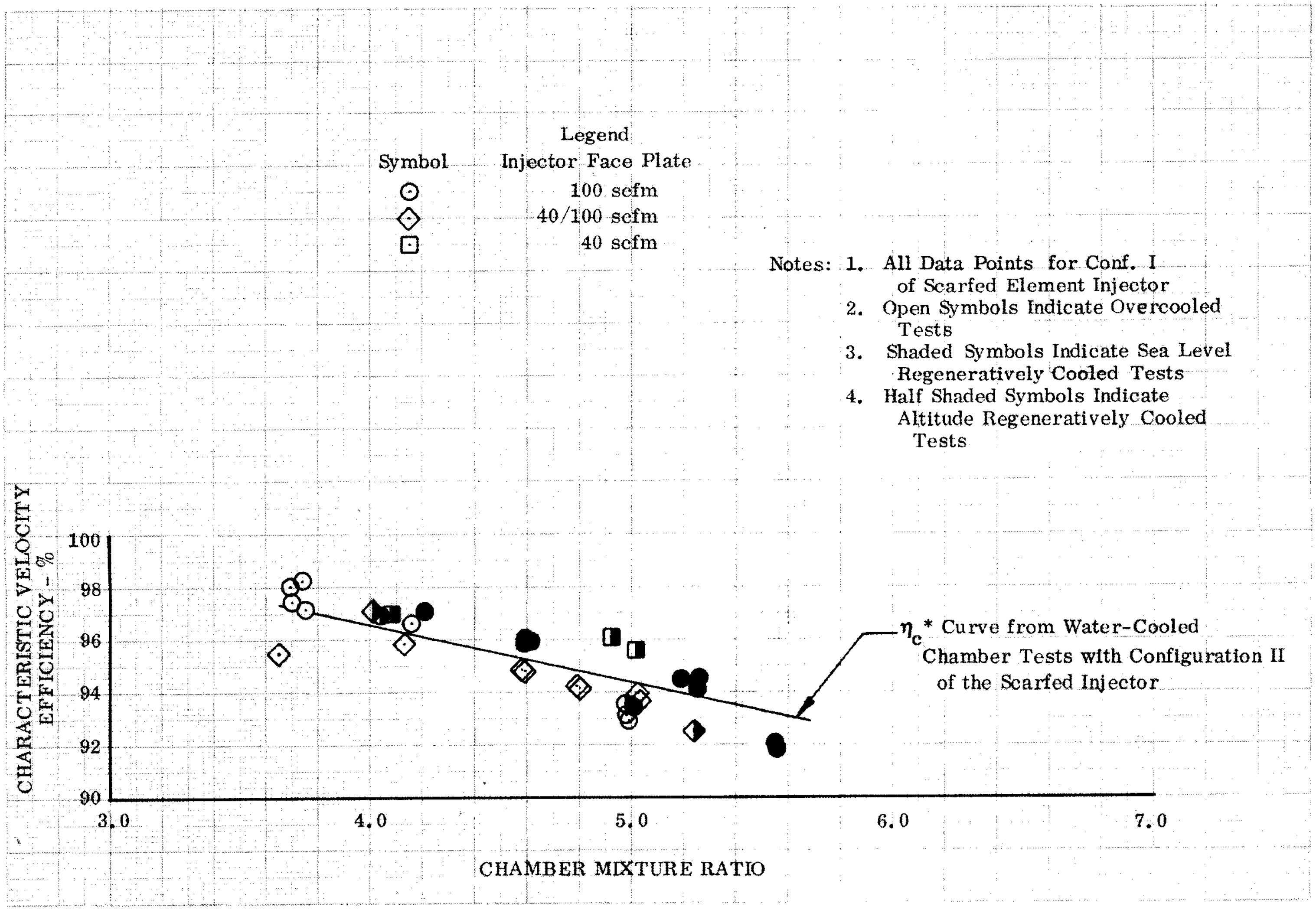

Figure 81. c* Efficiency Data for Configuration II of the Scarfed Element Injector

DF 84801

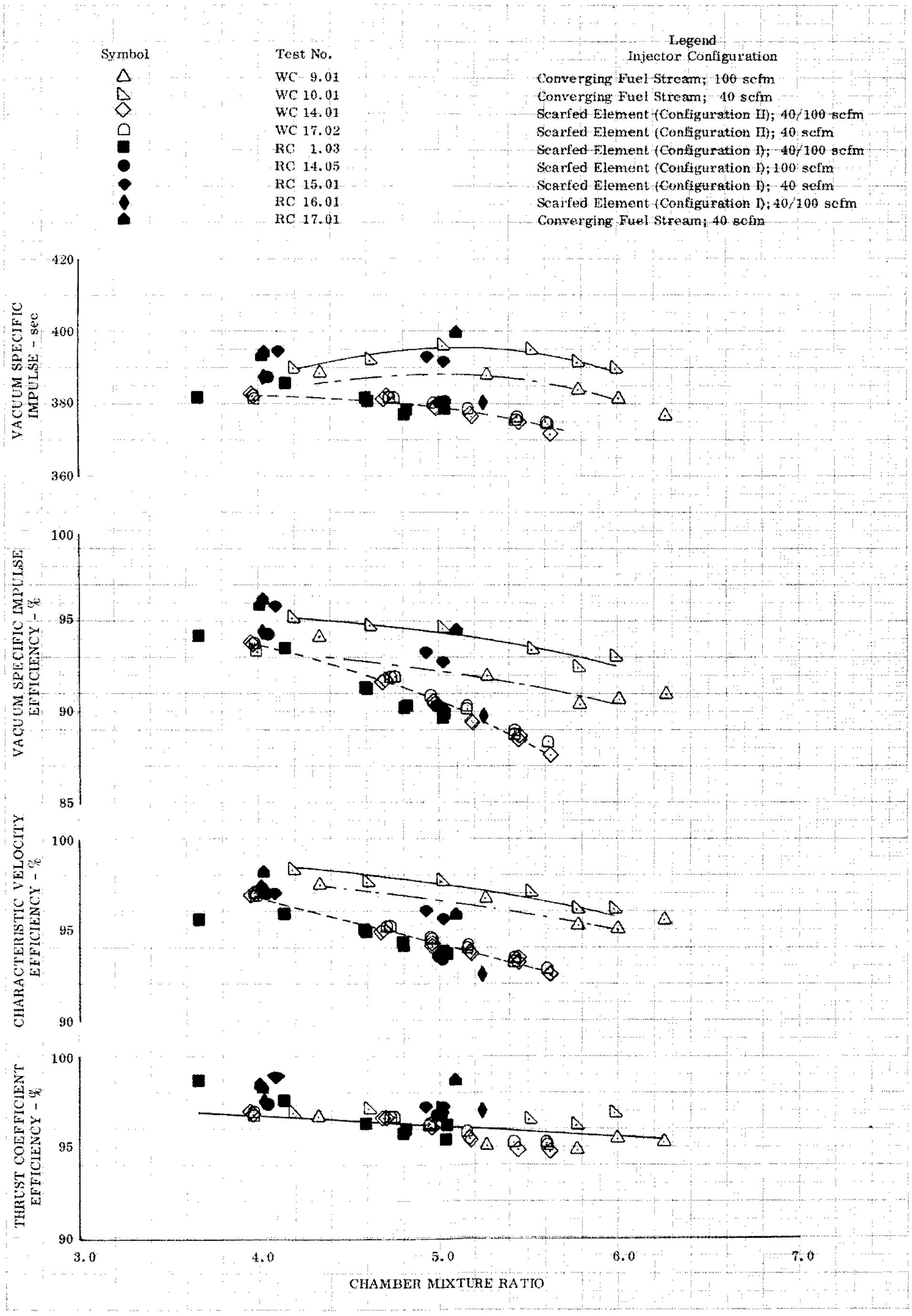

Figure 82. Comparison of Regenerative Chamber and Water-Cooled Chamber Altitude Performance Data DF 84802

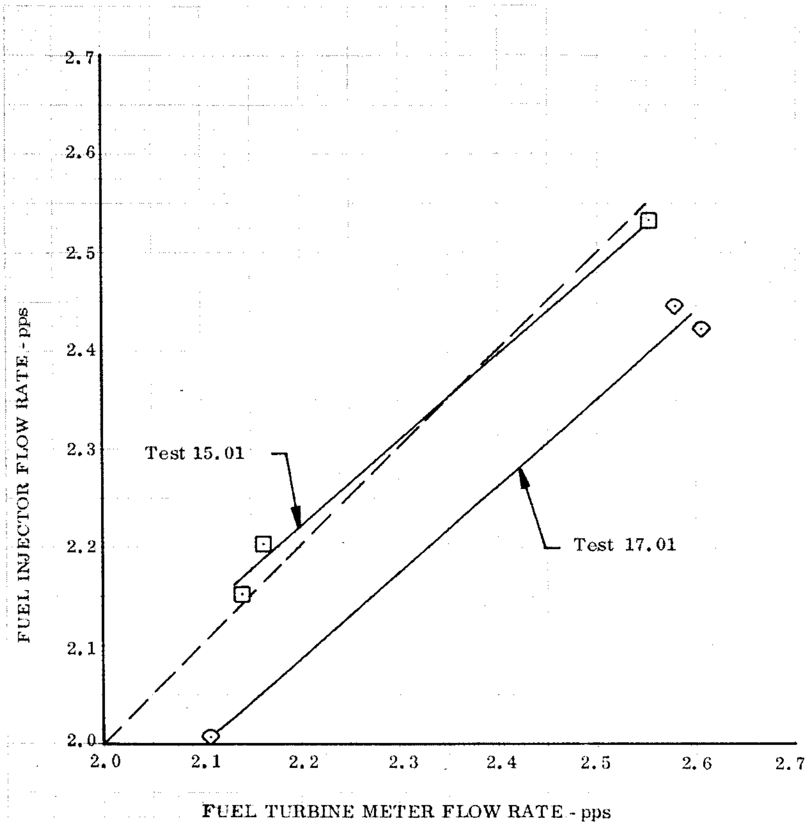

Figure 83. Comparison of Injector and Turbine-Meter Flowrates for Regenerative Tests 15.01 and 17.01 DF 84803

In both the water-cooled and regeneratively cooled chamber tests, thrust system tare was measured prior to test initiation (i.e., just before starting propellant flows) with the propellant piping pressurized and at operating temperatures. Although a post-test tare value was also taken, it was used only as a check on the thrust system repeatability. In the regenerative tests there was good repeatability between the pre- and post-test tare values; the maximum difference was 27 lb_f, which corresponds to only about 0.5% of the nominal thrust level (5000 lb_f). However, in the water-cooled chamber tests and in the separately cooled methane chamber tests larger differences, as much as 130 lb_f, were observed. In these cases the pre-test tare value was always greater than the post-test value, and therefore if the post-test tare were used, higher impulse values would have been calculated. The reason for the tare differences was eventually traced to the line that supplied heated methane gas to the injector. The support for this line was too rigid and, as a result, when the line wall reached operating temperature during a test, the expansion of the line caused a tare shift. The support was revised during the dual orifice injector test program so that the expansion could be tolerated, but for tests of the fixed-thrust injectors in which a heated methane supply was employed, there was a measurable tare shift. To assess the effect of this shift on performance, and specifically on the differences in performance observed in regenerative and water-cooled chamber tests, thrust coefficient efficiencies were computed using a tare level corresponding to the average of the pre- and post-test values. The results are presented in figure 84. On this basis, there is better agreement between the regenerative chamber test data and water-cooled chamber test data. Furthermore, the delivered impulse of the converging fuel stream injector with the 40-scfm faceplate (in the water-cooled chamber) would be slightly above 400 sec over a mixture ratio range from 4.7 to 5.5 as illustrated in figure 85, which substantiates the measured level obtained with this injector in the regenerative chamber.

Referring once again to figure 84, it can be seen that the representative thrust coefficient efficiency versus mixture ratio curve established using average tare values would be approximately 1% higher than that previously established using pre-test tares; furthermore, it agrees with the theoretical nozzle efficiency, calculated considering divergence, frictional and transonic losses but not chemical kinetics at low mixture ratios. Thus, it appears, based on the regenerative chamber test data and the tare-averaged, water-cooled chamber test data, that nozzle kinetic losses are negligible at mixture ratios of 5 and below.

D. CHAMBER HEAT TRANSFER

Table XVII presents a tabulation of the heat transfer data obtained in the regenerative chamber tests. Figure 86 illustrates the location of the coolant and wall temperature measurement stations referred to in the table. There are some differences in the data that was recorded in the tests. For example, the full length chamber used in test 1.03 had three separately supplied coolant passages in which individual coolant flowrates were measured to facilitate determination of axial and circumferential heat transfer profiles. Separately supplied passages were not retained as a feature in the three-section thrust chamber due to the interruption of the coolant flowpath caused by the section attachment flanges. Other differences which can be noted are in the number and location of wall and bulk temperature thermocouples recorded. In general, because of the data system recording limitations, the selection of temperatures to be monitored in a given test were made with emphasis on the throat and chamber regions of the thrust chamber.

In subsection B preceding, it was pointed out that the coolant exit temperature did not reach steady-state conditions at the higher mixture ratios in the last series of regenerative tests (tests 14.05 through 17.01). For these tests, transient plots of the average wall and coolant temperature data for selected stations in the nozzle, throat, and combustion chamber are shown in figures 87 and 88. By inspection of the slope of these curves at test termination, the degree of steadiness of the data can be judged. Regarding the coolant temperatures, with the exception of test 14.05, it appears that the coolant temperatures on the combustion chamber side of the throat, as well as in the coolant exit manifold, did not reach steady-state values. However, the wall temperatures had either reached steady-state (as in test 14.05) or were approaching steady-state (as in tests 15.01 through 17.01). The exception to this appears to be the combustion chamber wall temperature in test 17.01, which was apparently being affected by the increasing coolant bulk temperature in that test.

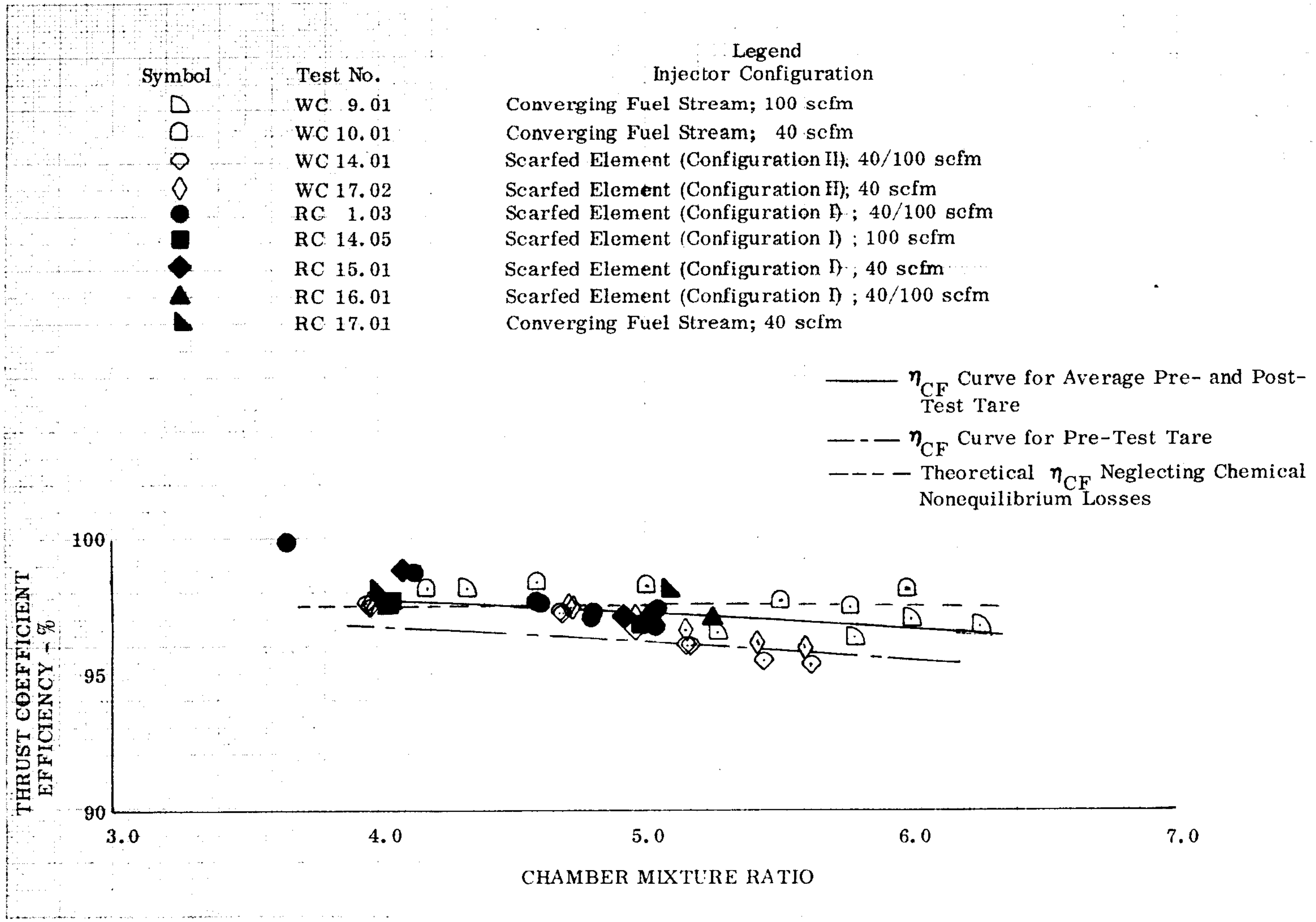

Figure 84. Altitude Thrust Chamber Coefficient Efficiency Data Based on Average of Pre- and Post-Test Tare Values

DF 84804

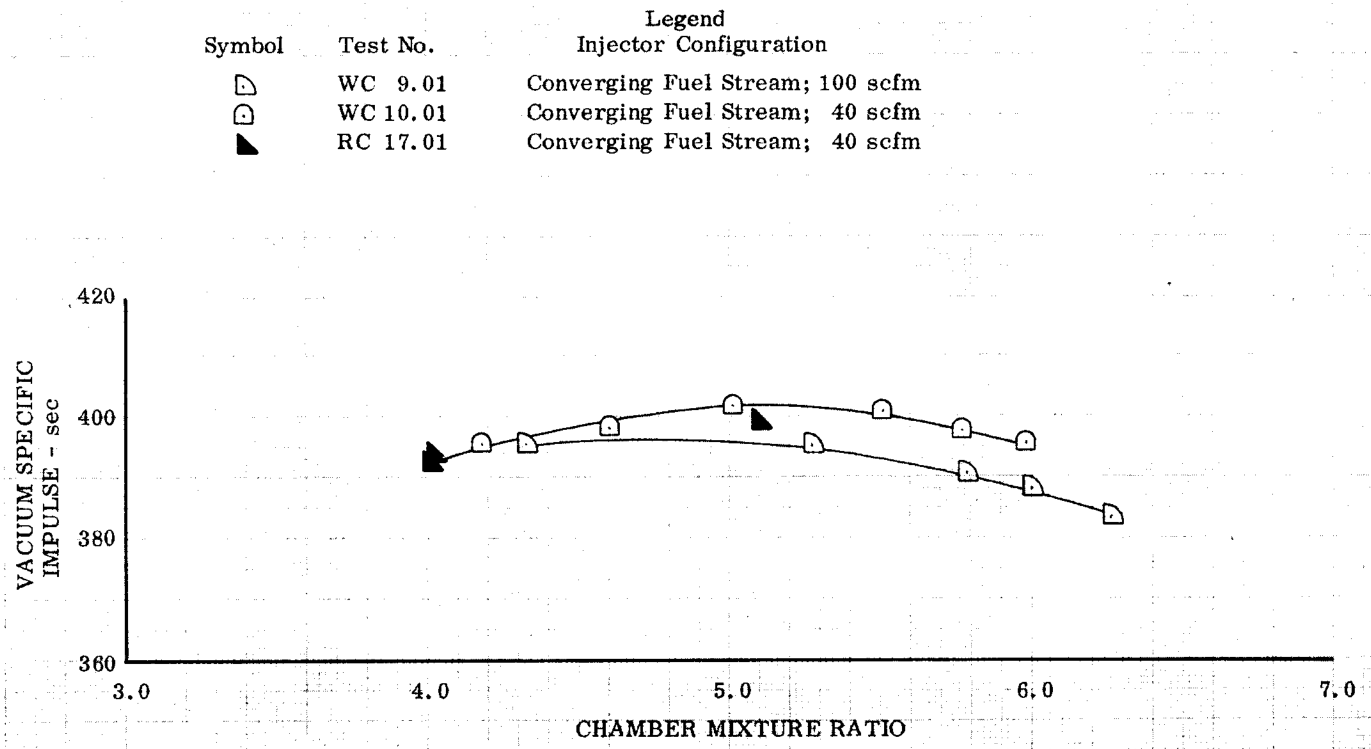

Figure 85. Vacuum Specific Impulse Performance for Converging Fuel Stream Injector Based on Average of Pre- and Post-Test Tare Values

DF 84805

Table XVII. Regenerative Thrust Chamber Heat Transfer Data

				Coolant Inlet Conditions			Coolant Discharge Conditions			Instrumented Passage Data																					Sectional Chamber Data						
											Coolant Conditions in Instrumented Passages												Wall Temperatures Along Instrumented Passages									Altitude Nozzle Coolant Discharge Conditions			Throat Section Coolant Discharge Conditions		
Run No.	Cooling Scheme	Test Type	Mixture Ratio	Coolant Flowrate (lbm/sec)	Coolant Inlet Temperature (°R)	Coolant Inlet Pressure (psia)	Coolant Temperature (°R)	Coolant Pressure (psia)	Heat Transfer (Btu/sec)	Stave No.	ẇ (lb_m/sec)	TB1 (°R)	TB2 (°R)	TB3 (°R)	TB4 (°R)	TB5 (°R)	TB6 (°R)	TB7 (°R)	TB8 (°R)	TB9 (°R)	TB10 (°R)	TB11 (°R)	TW1 (°R)	TW2 (°R)	TW3 (°R)	TW4 (°R)	TW5 (°R)	TW6 (°R)	TW7 (°R)	TW8 (°R)	Stave No.	Coolant Temperature (°R)	Coolant Pressure (psia)	Heat Transfer (Btu/sec)	Coolant Temperature (°R)	Coolant Pressure (psia)	Heat Transfer (Btu/sec)
1.03	Separate	Altitude	3.65	2.69	270	1969	638	839	1038	1	-	-	-	-	-	-	-	-	-	-	-	-	-	-	637	-	-	763	-	-	1						
										2	.044	284	359	387	437	435	464	491	525	539	565	562	655	640	609	-	-	700	629	543	2						
										3	-	-	-	-	-	-	-	-	-	-	-	-	-	-	-	-	-	1048	-	-	3						
										4	.034	312	-	-	-	-	508	552	-	-	-	645	-	744	717	702	726	804	-	-	4						
										5	-	-	-	-	-	-	-	-	-	-	-	-	-	-	-	-	-	1017	-	-	5						
										6	.028	319	-	-	502	-	549	647	-	722	699	721	-	823	782	910	954	1014	770	-	6						
																															AVG						
1.03	Separate	Altitude	4.13	2.47	244	1931	817	838	1250	1	-	-	-	-	-	-	-	-	-	-	-	-	-	-	747	-	-	967	-	-	1						
										2	.045	253	335	368	422	416	452	527	551	566	632	609	677	713	684	-	-	835	784	570	2						
										3	-	-	-	-	-	-	-	-	-	-	-	-	-	-	-	-	-	1178	-	-	3						
										4	.034	276	-	-	-	-	508	558	-	-	-	708	-	768	815	768	759	846	-	-	4						
										5	-	-	-	-	-	-	-	-	-	-	-	-	-	-	-	-	-	1152	-	-	5						
										6	.028	276	-	-	501	-	543	672	-	787	817	848	-	904	928	999	951	1049	802	-	6						
																															AVG						
1.03	Separate	Altitude	4.59	2.47	237	1906	832	838	1285	1	-	-	-	-	-	-	-	-	-	-	-	-	-	-	685	-	-	939	-	-	1						
										2	.059	243	315	341	385	379	406	419	434	433	499	476	504	510	507	-	-	671	618	485	2						
										3	-	-	-	-	-	-	-	-	-	-	-	-	-	-	-	-	-	1186	-	-	3						
										4	.034	262	-	-	-	-	507	559	-	-	-	711	-	745	745	736	759	877	-	-	4						
										5	-	-	-	-	-	-	-	-	-	-	-	-	-	-	-	-	-	1300	-	-	5						
										6	.028	262	-	-	480	-	529	697	-	798	828	868	-	1109	925	968	983	1159	860	-	6						
																															AVG						
1.03	Separate	Altitude	4.80	2.54	233	1875	815	836	1310	1	-	-	-	-	-	-	-	-	-	-	-	-	-	-	616	-	-	756	-	-	1						
										2	.064	-	300	327	363	360	384	397	403	403	448	433	483	469	467	-	-	655	601	454	2						
										3	-	-	-	-	-	-	-	-	-	-	-	-	-	-	-	-	-	1196	-	-	3						
										4	.032	-	-	-	-	-	511	600	-	-	-	792	-	846	939	848	782	960	-	-	4						
										5	-	-	-	-	-	-	-	-	-	-	-	-	-	-	-	-	-	1159	-	-	5						
										6	.030	-	-	-	448	-	491	582	-	725	761	812	-	954	857	914	861	883	764	-	6						
																															AVG						
1.03	Separate	Altitude	5.02	2.50	230	1850	821	836	1315	1	-	-	-	-	-	-	-	-	-	-	-	-	-	-	660	-	-	623	-	-	1						
										2	.056	274	299	335	367	368	394	428	425	443	476	475	541	524	570	-	-	849	655	510	2						
										3	-	-	-	-	-	-	-	-	-	-	-	-	-	-	-	-	-	1056	-	-	3						
										4	.038	303	-	-	-	-	450	481	-	-	-	614	-	622	792	624	669	843	-	-	4						
										5	-	-	-	-	-	-	-	-	-	-	-	-	-	-	-	-	-	1226	-	-	5						
										6	.028	304	-	-	467	-	526	692	-	802	826	884	-	985	927	953	913	1216	822	-	6						
																															AVG						
3.02	Separate	Sea level	3.75	4.68	249	2104	388	1499	796	1							-	-			-	-	-	-	370		-	413	-		1				-	1562	
										2							276	308			351	357	395	363	357		559	377	296		2				333	1562	
										3							-	-			-	-	-	-	400		-	510	-		3				-	1562	
										4							281	320			367	371	407	391	387		-	528	384		4				358	1562	
										5							-	-			-	-	-	-	392		-	547	-		5				-	1562	
										6							285	316			356	362	380	404	371		436	459	386		6				344	1562	
																															AVG				345	1562	492
5.01	Separate	Sea level	3.70	5.06	233	2065	371	1395	820	1							-	-			-	-	-	-	344		-	407	-		1				-	1466	
										2							261	296			337	344	383	357	346		521	369	280		2				320	1466	
										3							-	-			-	-	-	-	380		-	444	-		3				-	1466	
										4							264	303			355	359	384	384	383		-	532	353		4				343	1466	
										5							-	-			-	-	-	-	388		-	530	-		5				-	1466	
										6							269	301			339	345	360	376	349		453	445	364		6				329	1466	
																															AVG				331	1466	530
5.01	Separate	Sea level	4.98	5.05	225	2073	373	1394	877	1							-	-			-	-	-	-	361		-	454	-		1				-	1469	
										2							252	297			343	348	395	350	347		550	383	279		2				330	1469	
										3							-	-			-	-	-	-	373		-	517	-		3				-	1469	
										4							256	313			362	369	408	400	416		-	655	423		4				350	1469	
										5							-	-			-	-	-	-	426		-	616	-		5				-	1469	
										6							257	300			343	348	355	374	360		471	490	384		6				334	1469	
																															AVG				338	1469	614
6.01	Separate	Sea level	3.73	5.09	235	2093	373	1399	832	1							-	-			-	-	-	-	349		-	414	-		1				-	1474	
										2							263	296			-	344	387	347	344		513	365	283		2				330	1474	
										3							-	-			-	-	-	-	370		-	460	-		3				-	1474	
										4							266	303			360	366	382	373	448		-	502	352		4				348	1474	
										5							-	-			-	-	-	-	404		-	603	-		5				-	1474	
										6							271	300			346	351	371	394	353		439	437	354		6				334	1474	
																															AVG				337	1474	561
7.03	Regen.	Sea level	4.20	2.50	542	2267	798	810	504	1							-	-			-	-	-	-	851		-	933	-		1				-	1008	
										2							572	648			745	776	823	798	779		1002	793	642		2				702	1008	
										3							-	-			-	-	-	-	825		-	987	-		3				-	1008	
										4							585	700			756	774	850	831	827		-	1090	906		4				744	1008	
										5							-	-			-	-	-	-	852		-	1067	-		5				-	1008	
										6							579	668			764	795	856	879	835		897	992	846		6				758	1008	
																															AVG				735	1008	394
8.03	Regen.	Sea level	4.55	2.35	533	2213	830	1114	531	1							-	-			-	-	-	-	891		-	977	-		1				-	1263	
										2							569	663			767	806	919	817	804		967	787	654		2				719	1263	
										3							-	-			-	-	-	-	875		-	1162	-		3				-	1263	
										4							582	727			783	806	850	847	857		-	1158	969		4				764	1263	
										5							-	-			-	-	-	-	864		-	975	-		5				-	1263	
										6							585	738			797	848	907	991	864		974	1224	959		6				774	1263	
																															AVG				752	1263	403
9.01	Regen.	Sea level	4.60	2.34	527	2142	846	1023	563	1							-	-			-	-	-	-	913		-	959	-		1				-	1173	
										2							560	652			765	815	917	857	803		928	800	642		2				710	1173	
										3							-	-			-	-	-	-	943		-	1121	-		3				-	1173	
										4							573	710			803	831	916	868	885		-	1111	939		4				787	1173	
										5							-	-			-	-	-	-	945		-	1054	-		5				-	1173	
										6							574	725			797	842	912	970	898		932	1086	994		6				782	1173	
																															AVG				760	1173	423

Table XVII. Regenerative Thrust Chamber Heat Transfer Data (Continued)

				Coolant Inlet Conditions			Coolant Discharge Conditions		
Run No.	Cooling Scheme	Test Type	Mixture Ratio	Coolant Flowrate (lbm/sec)	Coolant Inlet Temperature (°R)	Coolant Inlet Pressure (psia)	Coolant Temperature (°R)	Coolant Pressure (psia)	Heat Transfer (btu/sec)
10.04	Regen.	Sea level	5.20	2.12	549	2024	895	783	545
11.01	Regen.	Sea level	5.18	2.12	529	1986	896	786	579
12.01	Regen.	Sea level	5.23	2.11	521	1959	884	795	553
13.01	Regen.	Sea level	5.50	2.06	517	1897	835	768	488
14.05	Regen.	Altitude	4.03	2.58	272	2263	757	849	1144
14.05	Regen.	Altitude	5.00	2.20	262	2164	913	861	1230
15.01	Regen.	Altitude	4.07	2.55	264	2264	830	840	1277
15.01	Regen.	Altitude	5.03	2.14	255	2129	990	855	1332
16.01	Regen.	Altitude	3.99	2.60	237	2157	714	863	1169
16.01	Regen.	Altitude	5.21	2.14	233	2020	795	897	1079
17.01	Regen.	Altitude	3.99	2.61	228	2266	870	875	1478
17.01	Regen.	Altitude	5.09	2.11	222	2128	1038	833	1459

	Instrumented Passage Data																				
		Coolant Conditions in Instrumented Passages												Wall Temperatures Along Instrumented Passages							
Run No.	Stave No.	ẇ (lbm/sec)	TB1 (°R)	TB2 (°R)	TB3 (°R)	TB4 (°R)	TB5 (°R)	TB6 (°R)	TB7 (°R)	TB8 (°R)	TB9 (°R)	TB10 (°R)	TB11 (°R)	TW1 (°R)	TW2 (°R)	TW3 (°R)	TW4 (°R)	TW5 (°R)	TW6 (°R)	TW7 (°R)	TW8 (°R)
10.04	1							-	-			-	-	-	-	1009		-	1063	-	
	2							589	706			799	853	958	871	853		1011	860	1042	
	3							-	-			-	-	-	-	1004		-	1113	-	
	4							609	781			869	914	1031	1019	1009		-	1202	1063	
	5							-	-			-	-	-	-	1026		-	1145	-	
	6							603	782			859	906	991	1127	969		1061	1160	1030	
11.01	1							-	-			-	-	-	-	972		-	1067	-	
	2							571	679			788	836	946	856	839		989	825	1042	
	3							-	-			-	-	-	-	1050		-	1186	-	
	4							588	763			865	906	1029	965	1018		-	1234	1003	
	5							-	-			-	-	-	-	1061		-	1188	-	
	6							592	774			873	926	991	1180	1043		1062	1155	1062	
12.01	1							-	-			-	-	-	-	971		-	1074	-	
	2							563	674			774	823	948	832	824		998	816	1045	
	3							-	-			-	-	-	-	977		-	1164	-	
	4							583	738			856	906	1028	976	999		-	1126	978	
	5							-	-			-	-	-	-	1012		-	1149	-	
	6							585	800			822	863	928	1068	937		1064	1225	1069	
13.01	1							-	-			-	-	-	-	847		-	1040	-	
	2							559	621			762	798	882	803	794		893	739	961	
	3							-	-			-	-	-	-	878		-	918	-	
	4							579	739			808	828	880	860	877		-	1121	1006	
	5							-	-			-	-	-	-	935		-	1109	-	
	6							568	649			761	789	840	835	795		861	910	855	
14.05	1							-	-			-	-	-	-	878		-	742	-	
	2							571	617			741	775	831	789	783		829	680	786	
	3							-	-			-	-	-	-	834		-	969	-	
	4							593	698			397	716	779	780	750		-	966	926	
	5							-	-			-	-	-	-	721		-	958	-	
	6							534	647			655	732	785	844	780		887	888	913	
14.05	1							-	-			-	-	-	-	1067		-	972	-	
	2							651	763			862	904	977	928	915		1077	868	928	
	3							-	-			-	-	-	-	1007		-	1311	-	
	4							651	807			409	878	1038	933	949		-	1123	1050	
	5							-	-			-	-	-	-	904		-	1175	-	
	6							590	821			725	939	1001	1121	1025		1196	1262	1157	
15.01	1							-	-			-	-	-	-	871		-	748	-	
	2							562	657			789	847	969	872	856		989	760	737	
	3							-	-			-	-	-	-	858		-	959	-	
	4							593	731			392	762	857	831	870		-	1073	953	
	5							-	-			-	-	-	-	849		-	1067	-	
	6							529	624			619	799	858	966	879		852	885	857	
15.01	1							-	-			-	-	-	-	1067		-	1020	-	
	2							625	795			928	995	1064	1022	1007		1151	902	987	
	3							-	-			-	-	-	-	1027		-	1243	-	
	4							646	889			399	928	1033	1015	1075		-	1417	1153	
	5							-	-			-	-	-	-	1067		-	1424	-	
	6							577	737			663	956	1043	1158	1053		1079	1021	1057	
16.01	1							-	-			-	-	-	-	753		-	627	-	
	2							527	578			715	745	835	762	755		816	996	624	
	3							-	-			-	-	-	-	727		-	928	-	
	4							555	653			367	691	935	796	595		-	776	831	
	5							-	-			-	-	-	-	653		-	1179	-	
	6							500	537			606	642	669	621	662		706	683	574	
16.01	1							-	-			-	-	-	-	863		-	754	-	
	2							578	734			819	869	948	879	877		1008	1170	743	
	3							-	-			-	-	-	-	855		-	1172	-	
	4							578	735			-	784	1135	895	894		-	900	869	
	5							-	-			-	-	-	-	786		-	1519	-	
	6							522	649			679	734	755	716	775		926	920	680	
17.01	1							-	-			-	-	-	-	1060		-	869	-	
	2							522	658			768	820	896	828	834		948	-	875	
	3							-	-			-	-	-	-	885		-	1261	-	
	4							564	835			-	835	1134	944	599		-	1167	797	
	5							-	-			-	-	-	-	945		-	1380	-	
	6							502	616			582	724	739	829	785		874	942	609	
17.01	1							-	-			-	-	-	-	1408		-	1160	-	
	2							595	882			938	1009	1085	924	1032		1188	-	755	
	3							-	-			-	-	-	-	1207		-	1527	-	
	4							630	997			-	1103	1281	1386	601		-	1691	1322	
	5							-	-			-	-	-	-	1274		-	1689	-	
	6							523	748			606	902	924	1053	1001		1094	1179	755	

	Sectional Chamber Data						
		Altitude Nozzle Coolant Discharge Conditions			Throat Section Coolant Discharge Conditions		
Run No.	Stave No.	Coolant Temperature (°R)	Coolant Pressure (psia)	Heat Transfer (Btu/sec)	Coolant Temperature (°R)	Coolant Pressure (psia)	Heat Transfer (Btu/sec)
10.04	1				-	946	
	2				742	946	
	3				-	946	
	4				852	946	
	5				-	946	
	6				848	946	
	AVG				814	946	424
11.01	1				-	942	
	2				729	942	
	3				-	942	
	4				838	942	
	5				-	942	
	6				837	942	
	AVG				801	942	437
12.01	1				-	942	
	2				718	942	
	3				-	942	
	4				836	942	
	5				-	942	
	6				814	942	
	AVG				789	942	431
13.01	1				-	918	
	2				725	918	
	3				-	918	
	4				768	918	
	5				-	918	
	6				758	918	
	AVG				750	918	367
14.05	1	454	2195		-	1038	
	2	572	2195		725	1038	
	3	566	2195		-	1038	
	4	608	2195		725	1038	
	5	547	2195		-	1038	
	6	557	2195		706	1038	
	AVG	551	2195	716	719	1038	356
14.05	1	475	2105		-	1034	
	2	640	2105		847	1034	
	3	619	2105		-	1034	
	4	657	2105		915	1034	
	5	590	2105		-	1034	
	6	611	2105		885	1034	
	AVG	599	2105	716	882	1034	462
15.01	1	450	2197		-	1047	
	2	554	2197		760	1047	
	3	560	2197		-	1047	
	4	613	2197		785	1047	
	5	542	2197		-	1047	
	6	552	2197		730	1047	
	AVG	545	2197	715	758	1047	429
15.01	1	460	2072		-	1036	
	2	606	2072		902	1036	
	3	602	2072		-	1036	
	4	670	2072		985	1036	
	5	575	2072		-	1036	
	6	603	2072		851	1036	
	AVG	569	2072	663	913	1036	544
16.01	1	419	2099		-	1036	
	2	525	2099		709	1036	
	3	544	2099		-	1036	
	4	594	2099		672	1036	
	5	502	2099		-	1036	
	6	524	2099		547	1036	
	AVG	518	2099	744	643	1036	296
16.01	1	435	1977		-	1040	
	2	567	1977		810	1040	
	3	581	1977		-	1040	
	4	655	1977		822	1040	
	5	530	1977		-	1040	
	6	560	1977		660	1040	
	AVG	555	1977	689	764	1040	342
17.01	1	417	2220		-	1072	
	2	517	2220		773	1072	
	3	519	2220		-	1072	
	4	563	2220		882	1072	
	5	500	2220		-	1072	
	6	514	2220		772	1072	
	AVG	505	2220	732	809	1072	615
17.01	1	434	2091		-	1019	
	2	572	2091		930	1019	
	3	571	2091		-	1019	
	4	631	2091		1049	1019	
	5	529	2091		-	1019	
	6	568	2091		979	1019	
	AVG	551	2091	689	986	1019	677

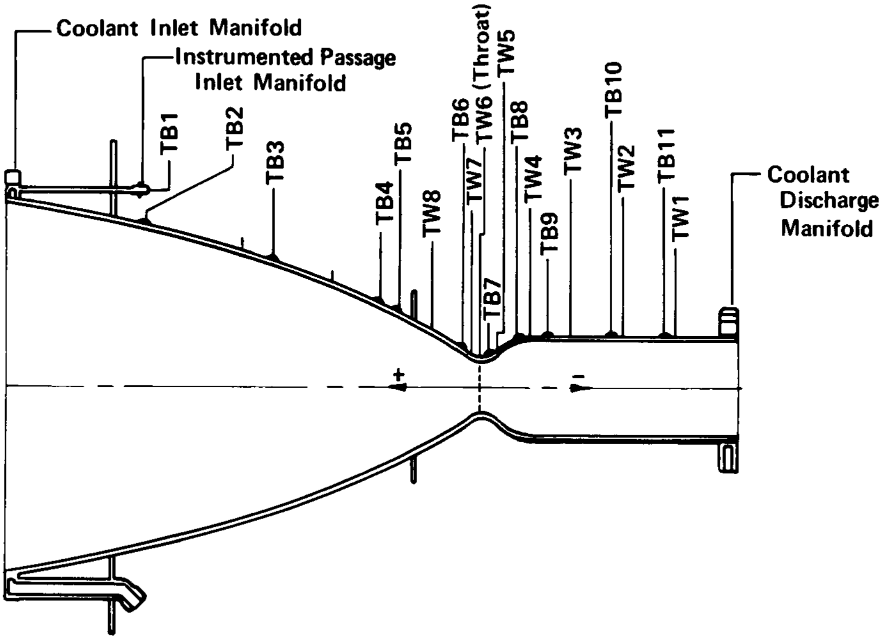

Parameter	Symbol	Units	Thermocouple Location Surface Distance From Throat Station, in.
Instrumented Passage Flowrate	$\dot{w}$	$\mathrm{lb_m}$/sec	- - -
Instrumented Passage Coolant Inlet Temperature	TB1	°R	28.16
Instrumented Passage Bulk Temperature	TB2	°R	20.37
Instrumented Passage Bulk Temperature	TB3	°R	13.26
Instrumented Passage Bulk Temperature	TB4	°R	6.80
Instrumented Passage Bulk Temperature	TB5	°R	5.51
Instrumented Passage Bulk Temperature	TB6	°R	0.58
Instrumented Passage Bulk Temperature	TB7	°R	-0.54
Instrumented Passage Bulk Temperature	TB8	°R	-2.47
Instrumented Passage Bulk Temperature	TB9	°R	-4.04
Instrumented Passage Bulk Temperature	TB10	°R	-7.54
Instrumented Passage Bulk Temperature	TB11	°R	-10.54
Wall Temperature	TW1	°R	-10.94
Wall Temperature	TW2	°R	-7.94
Wall Temperature	TW3	°R	-5.04
Wall Temperature	TW4	°R	-2.87
Wall Temperature	TW5	°R	-0.75
Wall Temperature (Throat)	TW6	°R	- - -
Wall Temperature	TW7	°R	+1.02
Wall Temperature	TW8	°R	+3.25

Figure 86. Heat Transfer Schematic (Regenerative Chamber)

FD 49502

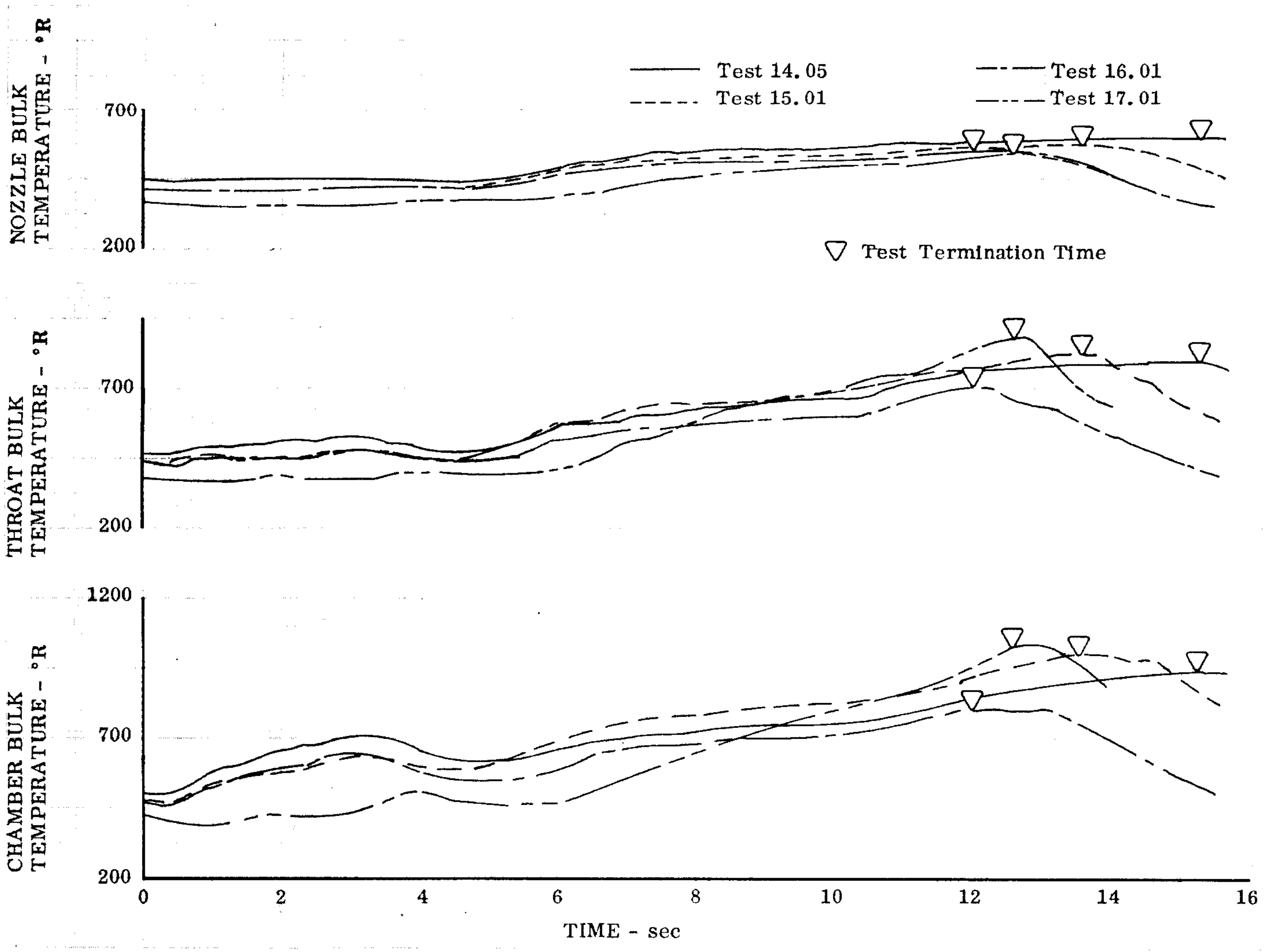

Figure 87. Bulk Temperature vs Time Plots for Regenerative Chamber Tests

DF 84806

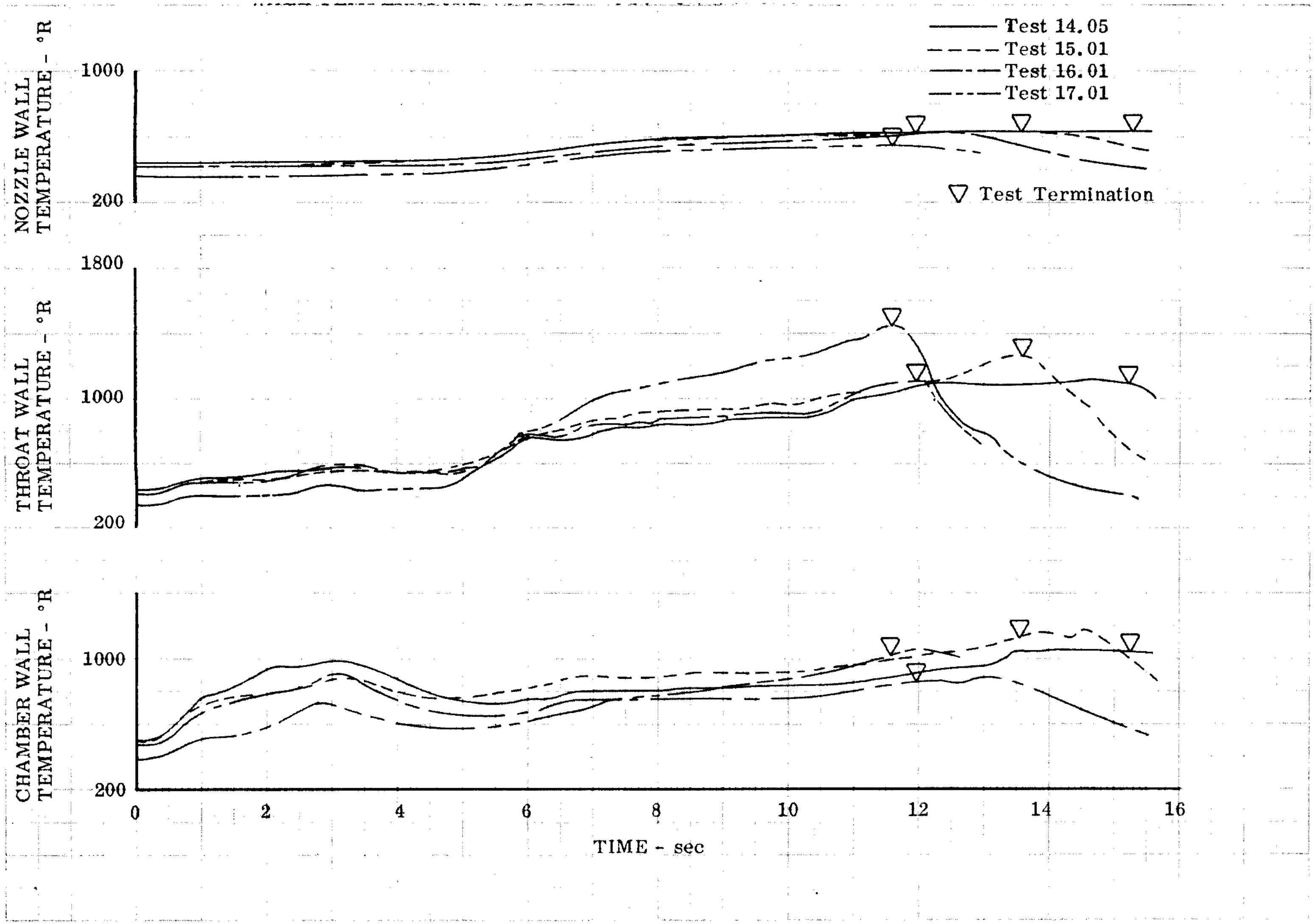

Figure 88. Wall Temperature vs Time Plots for Regenerative Chamber Tests

DF 84807

Additional typical plots of the coolant and wall temperature data obtained in the regenerative tests are presented and discussed below. Data from tests 14.05 and 17.01 were selected for these plots since they represent respectively the minimum and maximum levels of heat transfer observed in the regenerative tests. As pointed out above, the wall temperatures were approaching a steady-state condition in the throat region, but coolant temperatures were still increasing when test 17.01 was terminated. Therefore, the somewhat transient conditions must be recognized in the following discussion.

Coolant temperature profiles are shown in figure 89. The design profile, established for the heat transfer levels measured in water-cooled chamber tests of the converging fuel stream injector with a 40-scfm faceplate is also shown for comparison. The rather flat temperature profile shown for test 17.01 in the combustion chamber region is attributed to the transient nature of the data as previously mentioned. Had steady-state coolant conditions been achieved, the bulk outlet temperature should have been very close to the predicted level of 1400°R.

Because the steady-state, local heat flux in a regeneratively cooled thrust chamber is proportional to the slope of the coolant bulk temperature curve at a particular location, some insight as to the significant effect that injector design has on the throat region heat flux can be gained by inspecting the temperature rise between the two thermocouples that bracket the throat station. The relative change in throat region heat flux between the two tests is approximately proportional to the ratio of the slopes of the coolant temperature lines between these measured values. The computed ratio of these slopes indicates an average throat region heat flux for the converging fuel stream injector approximately 1.8 times that obtained with the scarfed element/100-scfm faceplate injector combination.

Wall temperature data are presented in figures 90 and 91. Figure 90 presents the measured surface wall axial temperature profiles based on an average of thermocouple readings at each axial location. Circumferential variations in wall temperature are shown in figure 91 for the throat station. Wall temperature thermocouples were installed 0.025 in. from the combustion-side surface; therefore, estimates of the corresponding combustion surface temperatures are also shown in the figures. The circumferential variation in wall temperatures shown in figure 91 are attributed primarily to (1) variations in passage-to-passage coolant flow and surface area, and (2) nonuniformities in the combustion side heat transfer caused by the injectors.

Measured heat transfer data obtained with the regenerative chamber are compared in figure 92 with similar data obtained in the water-cooled chamber tests. This figure includes only that test data obtained where steady-state conditions were achieved. Thus, for the regenerative chamber test 17.01, none of the data was used. Also, the higher mixture ratio points from tests 15.01 and 16.01 with the regenerative chamber were excluded.

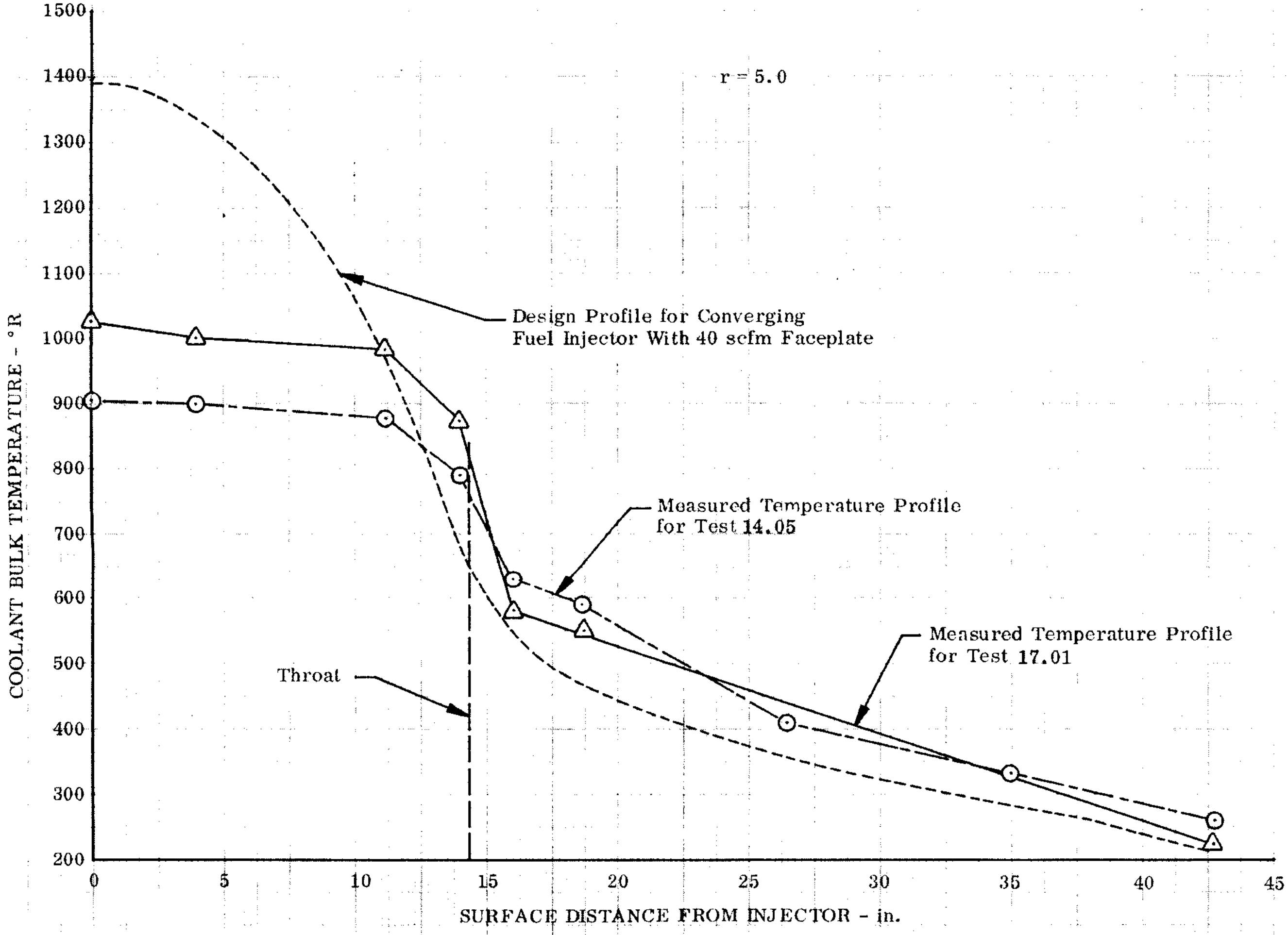

Figure 89. Coolant Bulk Temperature Profiles (Regenerative Chamber Tests)

DF 84808

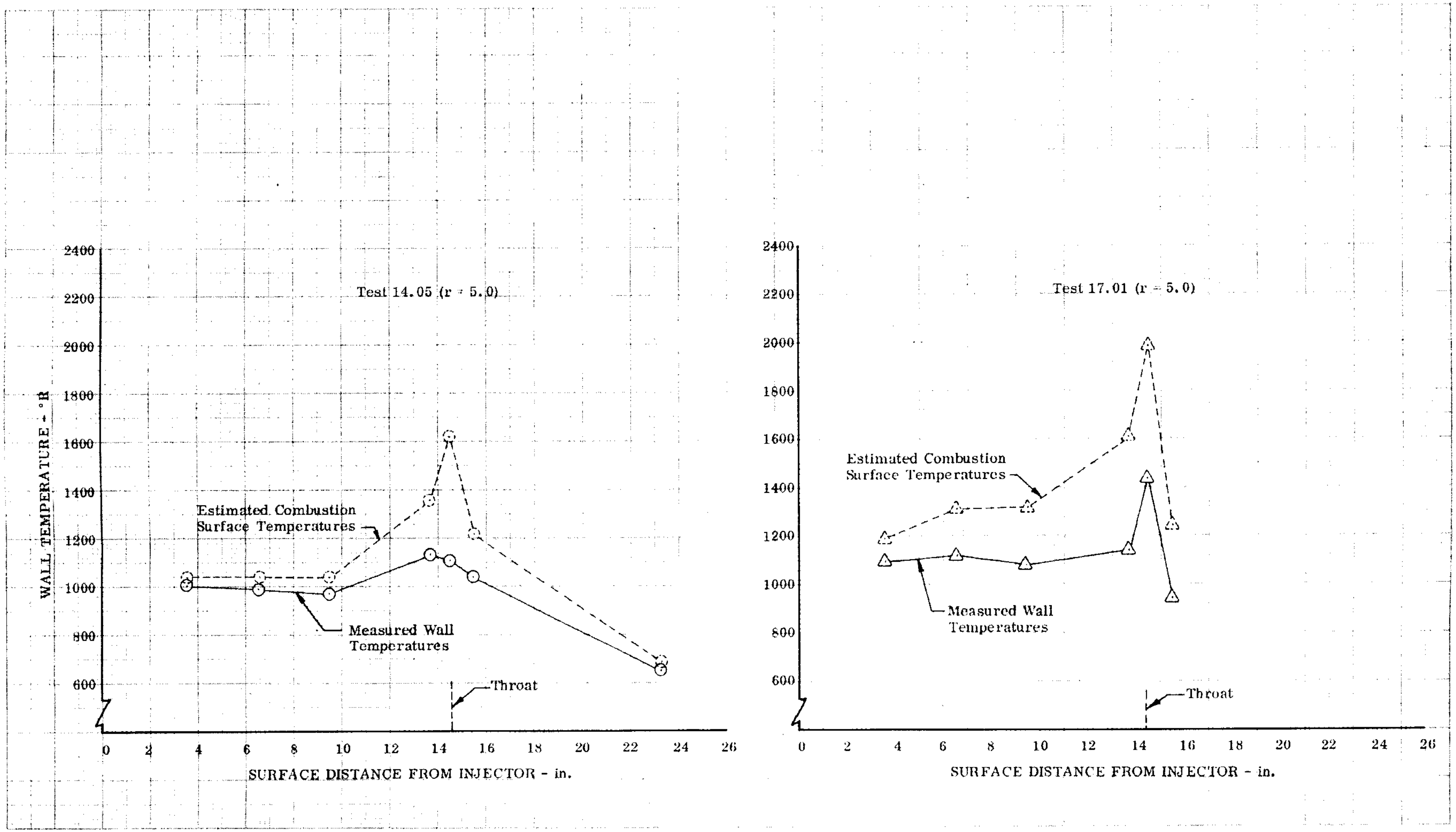

Figure 90. Axial Wall Temperature Profiles (Regenerative Chamber Tests)

DF 84809

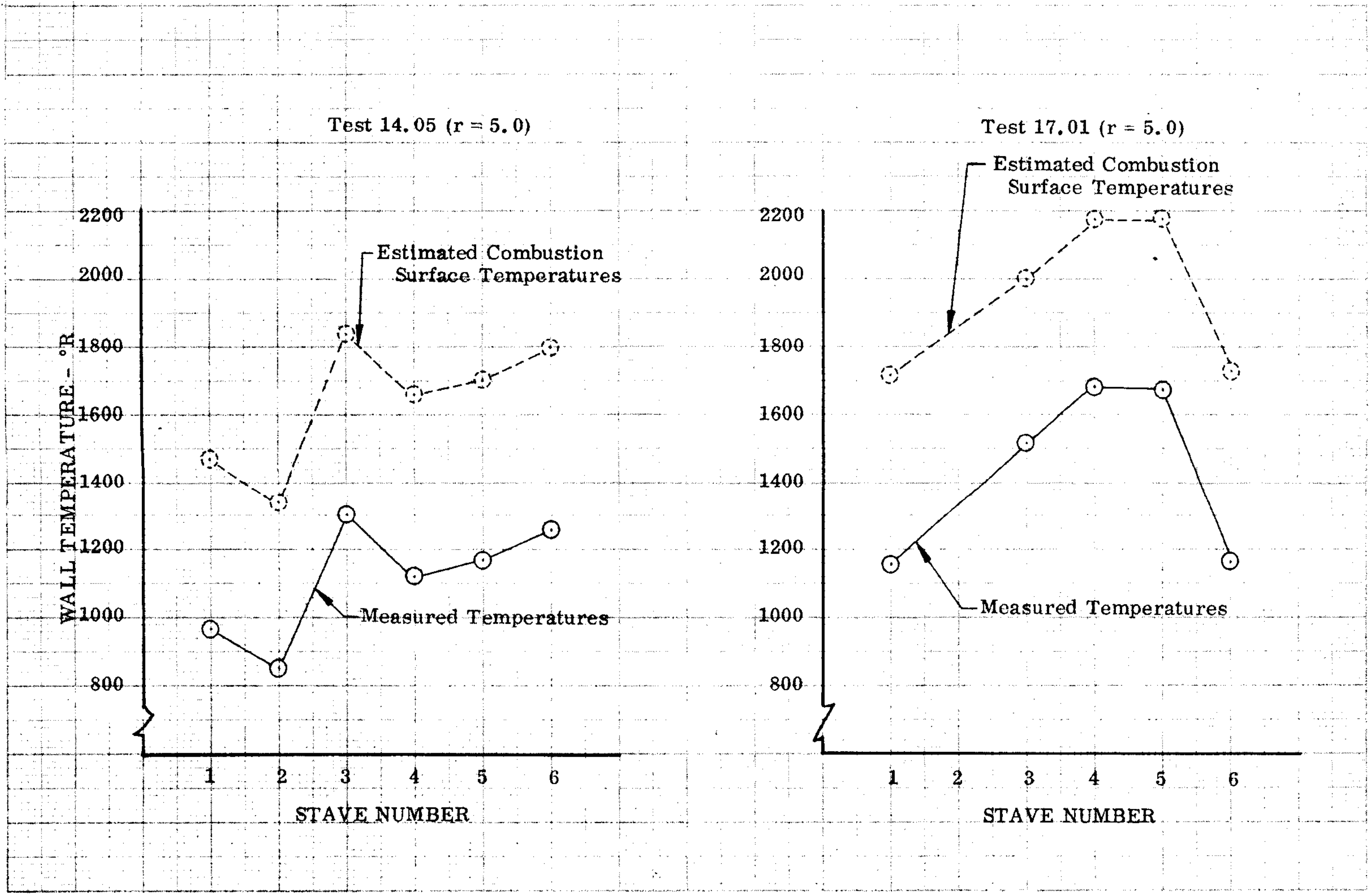

Figure 91. Throat Section Circumferential Wall Temperature Profiles (Regenerative Chamber Tests) DF 84810

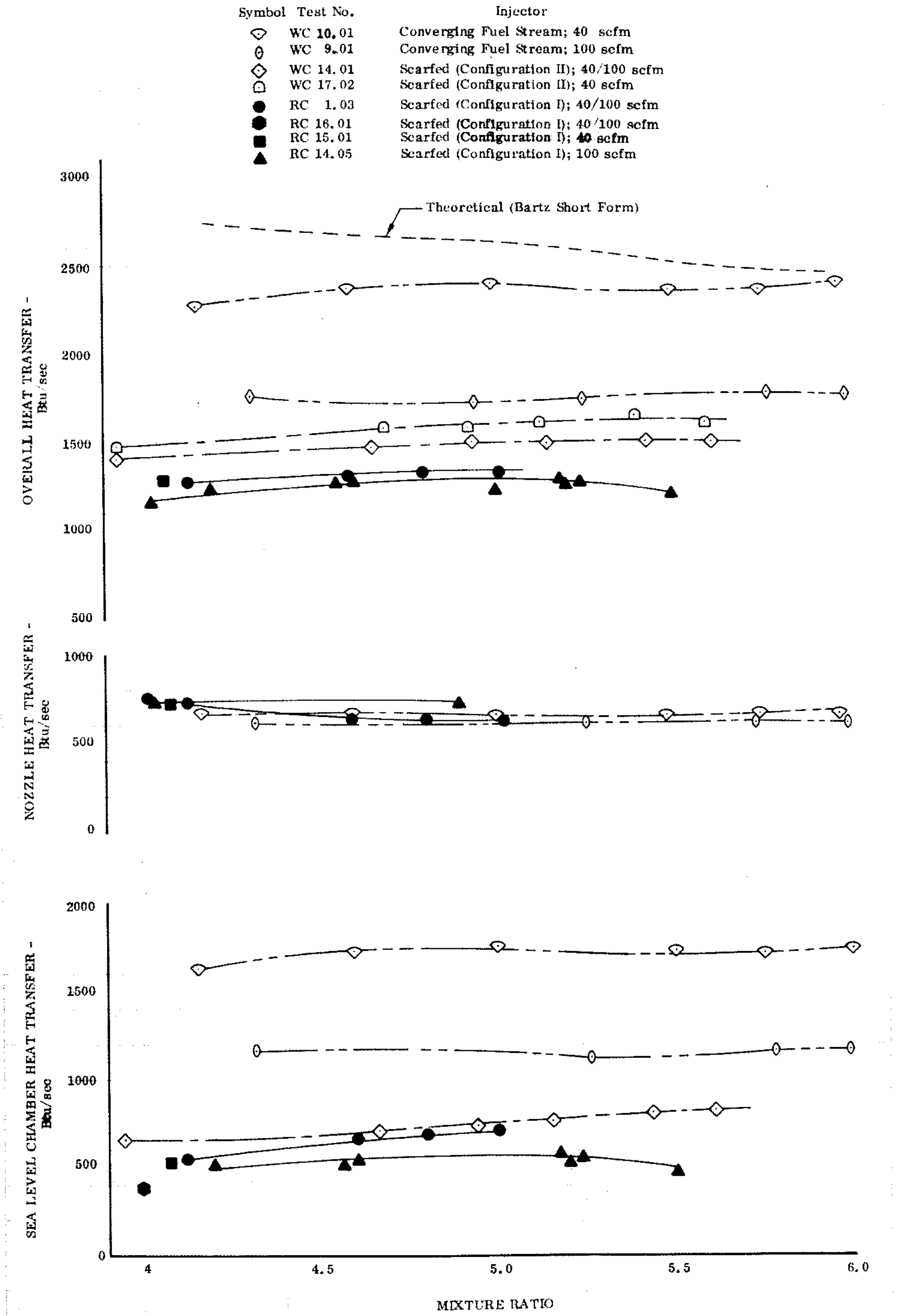

Figure 92. Thrust Chamber Heat Transfer (Regenerative Chamber Tests) DF 84811

Heat transfer rates for the altitude thrust chamber assembly, the sea level thrust chamber, and the nozzle extension are presented in figure 92. Most of the data presented for configuration I of the scarfed element injector, using a 100-scfm faceplate in the altitude thrust chamber plot, were obtained in the sea level regenerative tests. To obtain values for an altitude chamber, the nozzle heat transfer measured in regenerative test 14.05 with the same injector was added to the sea level chamber values.

Injector configuration has a significant effect on combustion chamber and throat heat transfer as reflected by the large differences demonstrated in heat transfer rates in the altitude and sea level chambers. The converging fuel stream injector with a 40-scfm faceplate had the highest heat transfer rates. The lowest rates were obtained with configuration I of the scarfed element injector, which had scarf angles of 45 and 22.5 deg on its fourth (outer) and third spud rows respectively. Intermediate heat transfer rates were obtained for configuration II of the scarfed element injector; this injector utilized spuds scarfed to 22.5 deg on its fourth row and unscarfed spuds on the three inside rows.

Nozzle extension heat transfer is not greatly dependent on injector configuration. Hence in design of a counterflow regeneratively-cooled thrust chamber the coolant conditions at the throat location can be predicted independent of the type of injector to be used.

E. THRUST CHAMBER COOLANT PRESSURE LOSSES

Pressure losses in the regenerative chambers were considerably higher than design values because coolant passage areas at the throat station were smaller than intended. Cooling passage flow areas were estimated from water flow data and these estimates were later verified by direct measurements from enlarged photographs of the first one-piece chamber which was sectioned after testing. Table XVIII compares measured and design values.

Table XVIII. Regenerative Thrust Chamber Coolant Passage Area Comparison

Surface Distance from Injector, in.	Single Passage Design Area, $in.^2$	Single Passage Measured Area, $in.^2$
12.86	0.00118	0.000931
13.06	0.00247	0.002295
14.54 (throat)	0.0013	0.000954

This comparison shows that in the combustion chamber region there was generally good agreement between the measured and design values, but the measured value at the throat is 36% lower than the design value. The passage area reduction at the throat is attributed to the elongation during the forming process described in Section VII. The elongation caused a "necking down" in the throat region with a consequent reduction of coolant passage widths that had not been compensated for in the design phase. The effect of the reduced coolant passage area was to raise coolant pressure losses.

The majority of the regenerative testing was accomplished with the coolant exit manifold pressure set at approximately 800 psia, which produced choked coolant flow conditions at the throat location. Measured coolant inlet pressures for the test are compared with those based on the design throat area in figure 93. There is a significant difference between the measured data and design curve; however, by using the measured passage flow areas, the actual pressure losses can be accurately predicted as indicated by the agreement between the upper curve in figure 93 and the test data.

During two of the sea level regenerative tests (tests No. 8.03 and 9.01), the back pressure was raised to approximately 1000 psia, which permitted unchoked coolant flow. The data from these tests allow a comparison of measured pressure losses obtained during the firings and design values. In figure 94, measured pressure values at the throat inlet, and the chamber inlet and exit manifolds are compared with (1) a predicted curve using passage flow areas estimated from water flow data and (2) the design curve. The discontinuities in the predicted curve correspond to the calculated losses for manifolds of the sectioned chamber. The large measured coolant pressure loss is attributed to the coolant passage area reduction at the throat station. Had the desired flow area of 0.0013 in.^{2} been achieved, the pressure drop for this test would have been close to the design value.

F. HARDWARE DURABILITY

1. Injectors

The converging fuel stream and scarfed element injectors proved to be very durable in the regenerative tests. As in the water-cooled thrust chamber tests, no oxidizer spud burning was encountered. The only damage to the oxidizer side of an injector occurred in Test No. 1.02 when the control system malfunctioned at test shutdown. This permitted backflow through the oxidizer side of the converging fuel side injector, which damaged the swirler caps (figure 95). The swirler caps were subsequently drilled out and replaced with spare caps; the repaired injector was reused in Test No. 17.01.

Only minor damage to the fuel faceplates was sustained. The worst occurred to the 40-100 scfm Rigimesh faceplate of the scarfed element injector in Test No. 1.03. There was slight erosion of the faceplate in two areas and some erosion of the heads of the screws that support the faceplate (figure 96). The faceplate erosion has been attributed to the fact that the fuel gap spacers around spuds that encircled the faceplate attaching screws were not installed because of mechanical interference. As a result, the spuds did not remain centered in their faceplate orifices at operating temperature. The erosion to the screws was attributed to the fact that the porosity on the surface of the countersink holes in the faceplates had not been restored after the holes were machined. For subsequent tests, the spacers were reworked so that they could be used around all the spuds and the surfaces of the countersink holes were eloxed (electro-discharge machined) to restore porosity. These changes appeared to have solved the problem because no additional erosion was encountered in a later test (test 16.01) with the faceplate (figure 97).

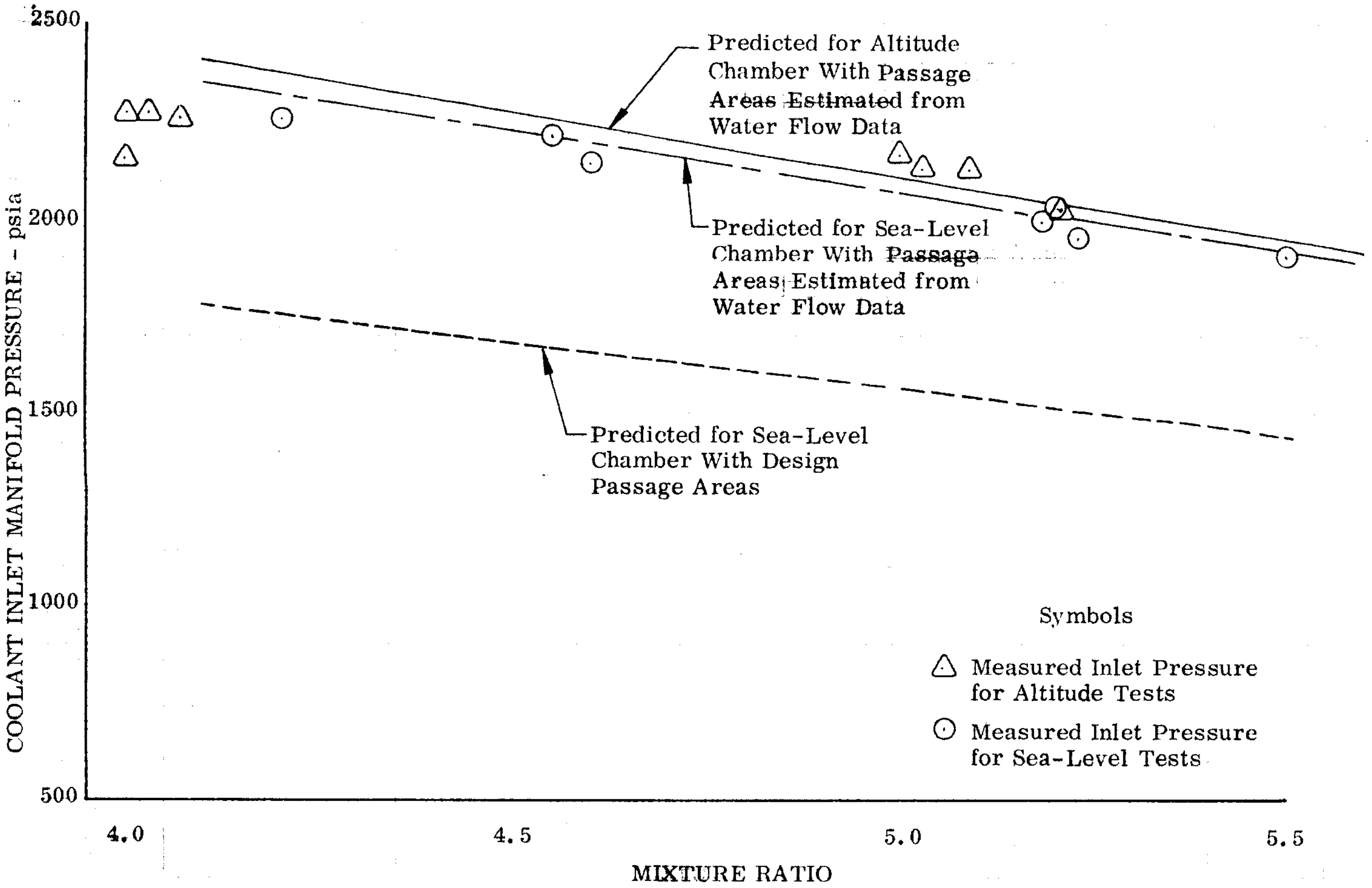

Figure 93. Coolant Inlet Pressures for Regenerative Chamber Tests

DF 84870

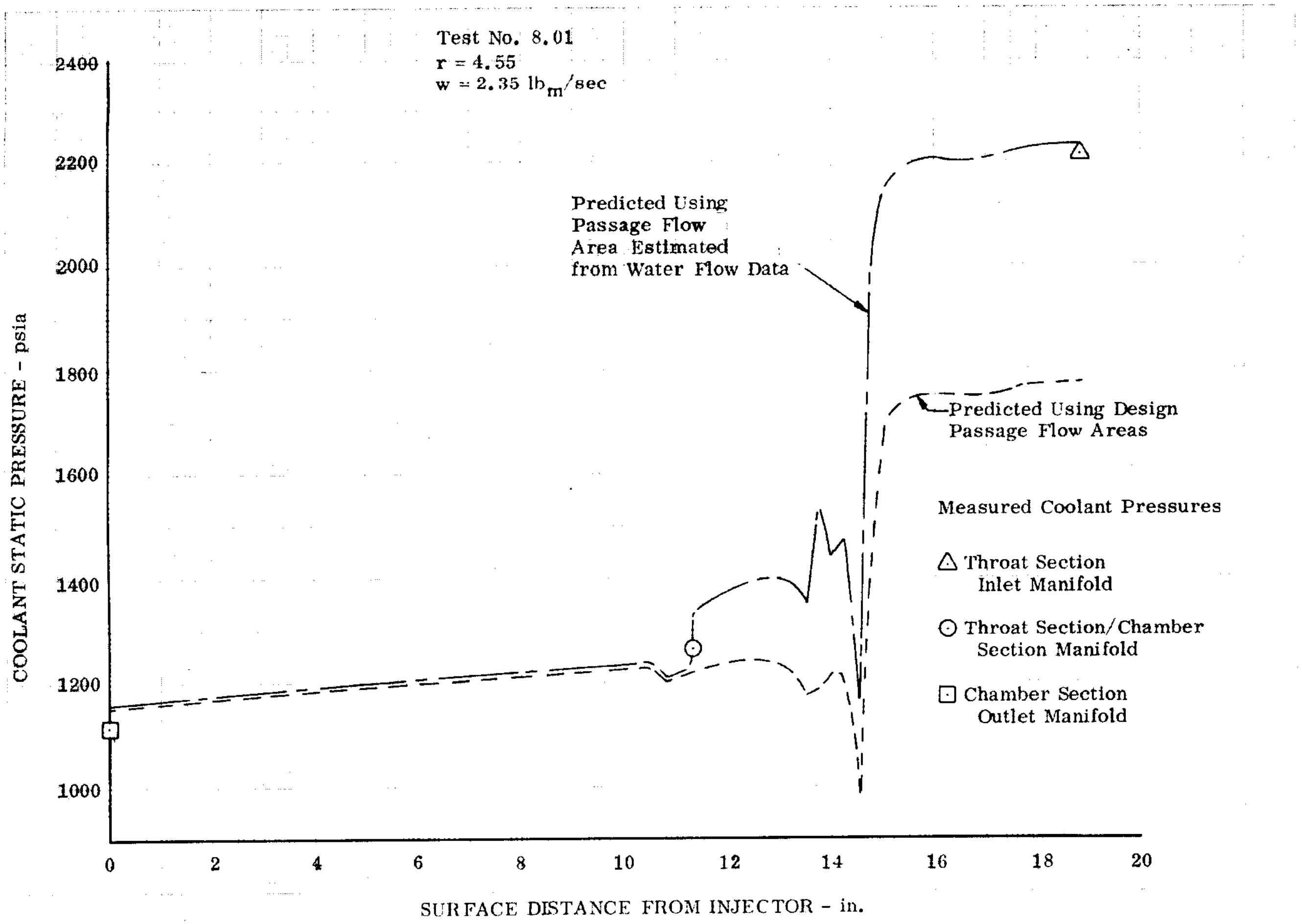

Figure 94. Comparison of Predicted and Measured Coolant Pressure Profiles in Sea Level Regenerative Chamber

DF 84871

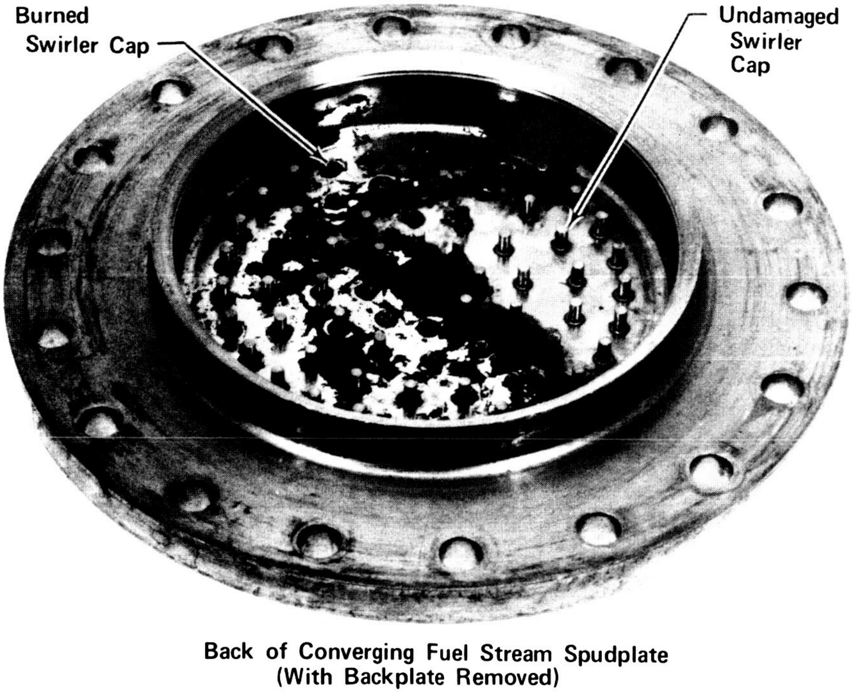

Figure 95. Damaged Injector Swirler Caps FD 33408A

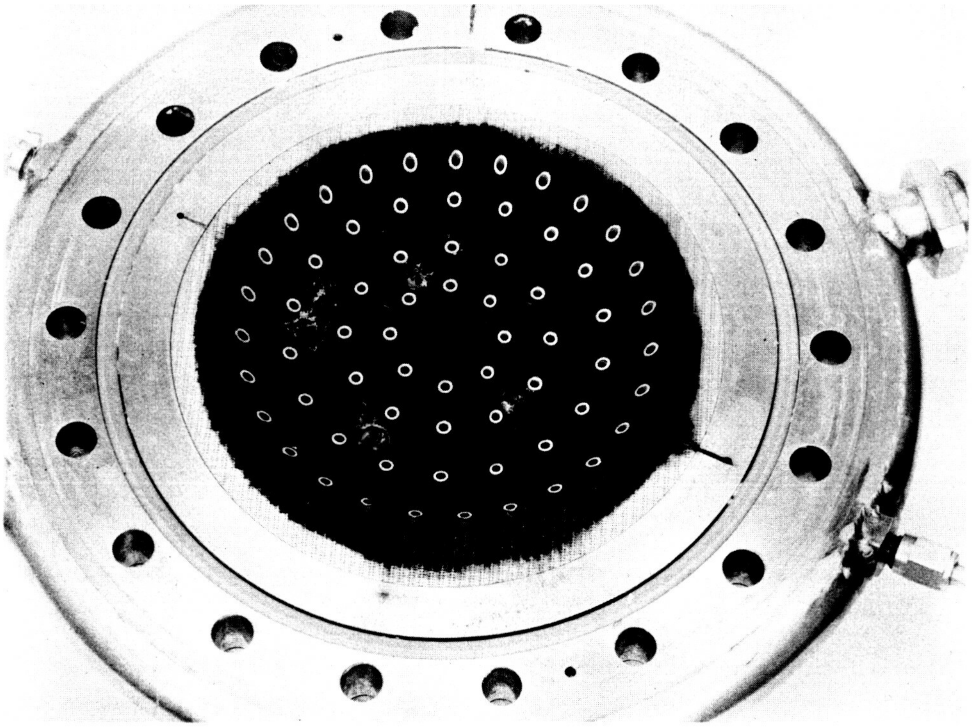

Figure 96. Scarfed Element Injector (Configuration I) after Regenerative Test No. 1.03 FE 89686

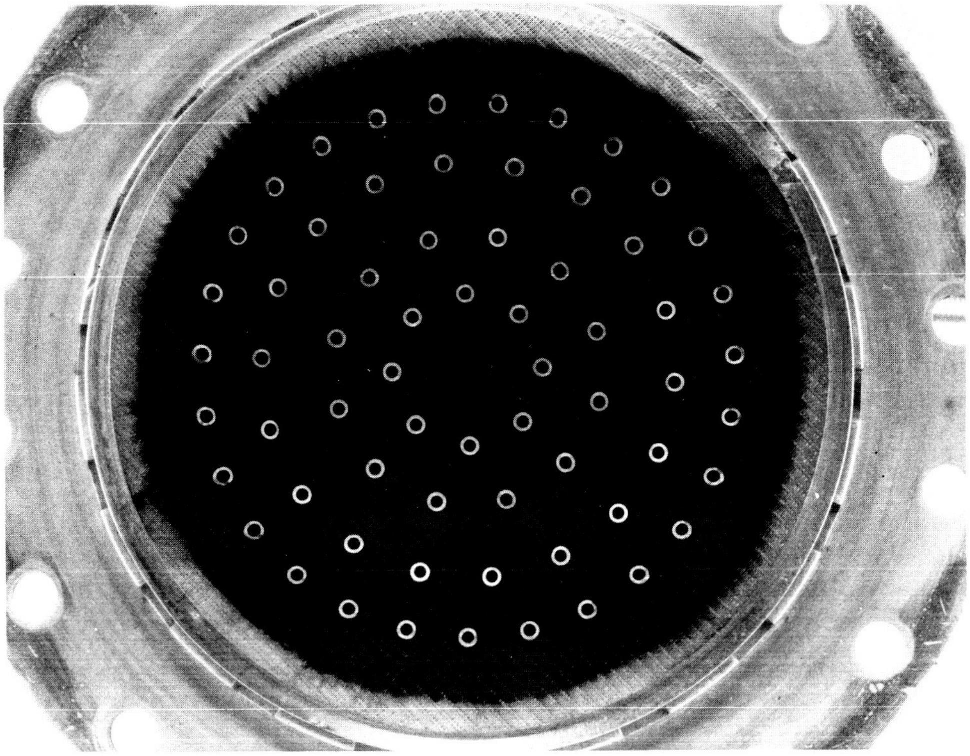

Figure 97. Scarfed Element Injector (Configuration I) after Regenerative Test No. 16.01

FE 98443

2. Thrust Chamber

In the tests with the one-piece chambers, seam durability problems were encountered. Three seams of the first chamber were cracked (figure 98) in its initial test (Test No. 1.02), after only 6 sec of firing time. As reported in Section VII, this chamber was constructed of staves that were manually TIG welded together on their edges. The cracks that occurred were in the seams that were TIG welded with silver-palladium and gold-nickel weld rods. These are moderate temperature welding rods, selected to facilitate welding without damaging the silver braze between the etched plates. Three seams did remain intact in the tests. These seams were made using a pure nickel rod; although the nickel rod did provide a higher temperature weld joint, the seams could not be reliably welded without damaging the silver braze joint between the etched plates. Therefore, none of the welds rods used proved to be acceptable and TIG welding was subsequently dropped in favor of electron beam welding for making the seam welds.

Three seams were eroded in the throat region of the second one-piece thrust chamber during an initial test (Test No. 1.03). The test duration, however, was 54 sec and data were obtained at several mixture ratio points. The test was terminated when a hole (figure 99) was burned through the chamber wall. A post-test inspection of the chamber revealed that in addition to the hole there were two separate burned areas in the throat. (See figure 100.) Severity of the burns varied from the hole through the wall (approximately 1/16 in. wide by 1/2 in. long) to a small pit in the combustion side wall. All three of the burns occurred in the weld seams between the THERMAL SKIN® staves.

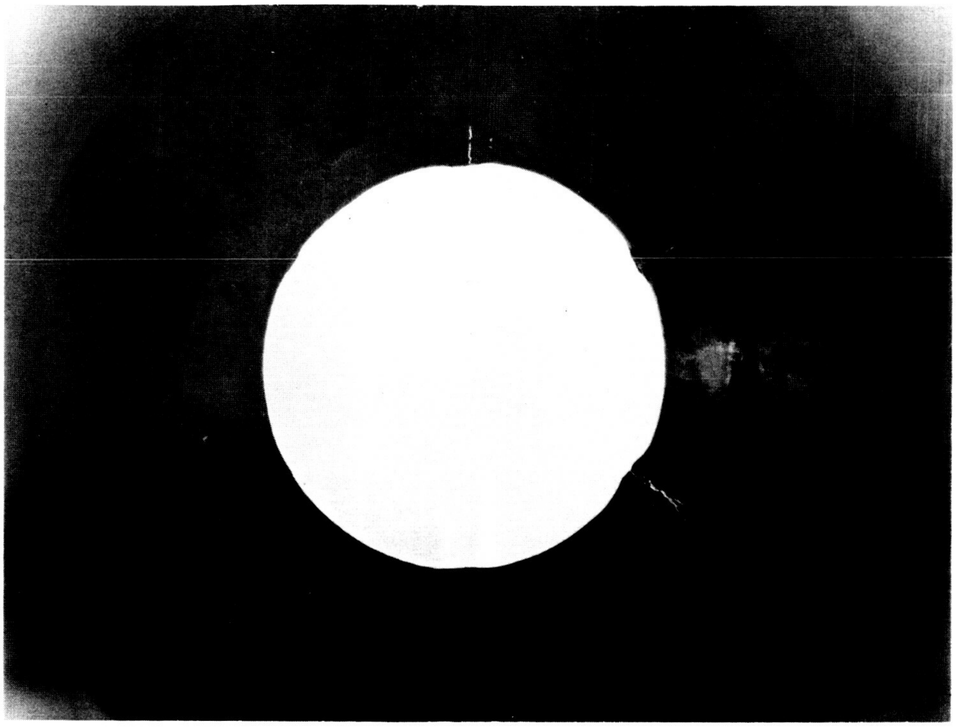

Figure 98. First One-Piece Regenerative Chamber after Test 1.02 Showing Cracked Seams FE 88122

These seam failures have been attributed to the combined effect of larger distances between adjacent passages in seam locations (as compared to the middle of the staves) and low coolant flows in the passages adjacent to the seams. At the throat, the seam land widths (distance between passages) were as large as 0.120 in., which compares to 0.065-in. lands in the middle of the staves. As discussed previously, the larger land widths in the seams resulted from forming operations on the staves and the spacing of the passages. The forming operation elongated the staves, effecting a transverse deformation that resulted in a reduction in the arc length over which the coolant passages were spaced. Because the stave width is smallest at the throat station, most of the deformation occurred there. As a result, when the staves were trimmed to 60-deg circumferential segments, the seam land widths here were greater than desired. Results of water flow tests, conducted after the staves were formed, indicated that there were passage-to-passage flow variations in the chamber. The passages adjacent to the burned seams had flowrates as much as 17% below the average passage flowrate.

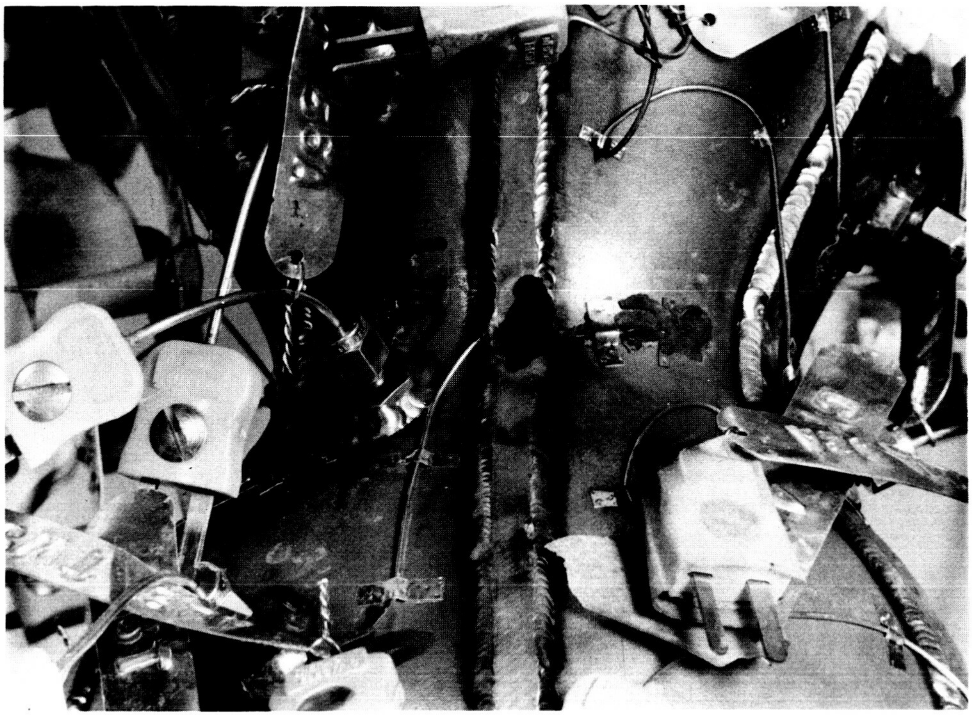

Figure 99. Second One-Piece Regenerative Chamber after Test 1.03 Showing Burn-through FE 89690

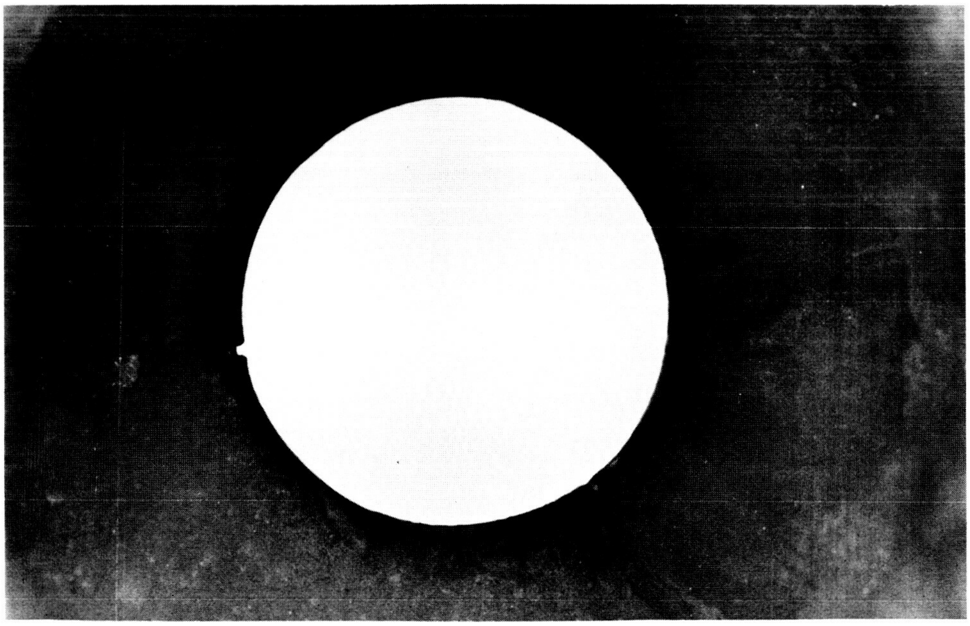

Figure 100. Second One-Piece Regenerative Chamber after Test 1.03 Showing Eroded Seams FE 89691

After the failure in the throat region of the second one-piece chamber, the assembly was cut into three separate sections: a combustion chamber section, a throat section, and a nozzle extension. Two design changes made to the throat section to provide added cooling in the seams (revising the etching master to account for the deformation cause by the forming operation, and increasing seam passage widths to provide more coolant flow in these passages) solved the seam erosion problem. Fourteen total tests were made with this chamber. The first 11 of these tests (Test No. 3.02 to 14.05) were made using the scarfed element injector with a 100-scfm faceplate. In these tests, there was no erosion or damage of any type to the chamber hardware.

In the last three tests (Tests No. 15.01, 16.01, and 17.01) of the three-piece chamber, some throat erosion occurred. Post-test inspection of the chamber after the second altitude test (Test No. 15.01) revealed some erosion to the throat section shown in figure 101. Note that although there was erosion in a seam, there was also erosion in a non-seam area. This erosion is attributed to local blockage of the 40-scfm Rigimesh faceplate of the scarfed element injector (figure 102). The blocked area of the Rigimesh faceplate was suspect because of its appearance after machining, and an acid etch was used to restore porosity in the affected area prior to testing. However, this was apparently not completely effective because the erosion in the throat section stave was aligned with the damaged Rigimesh area.

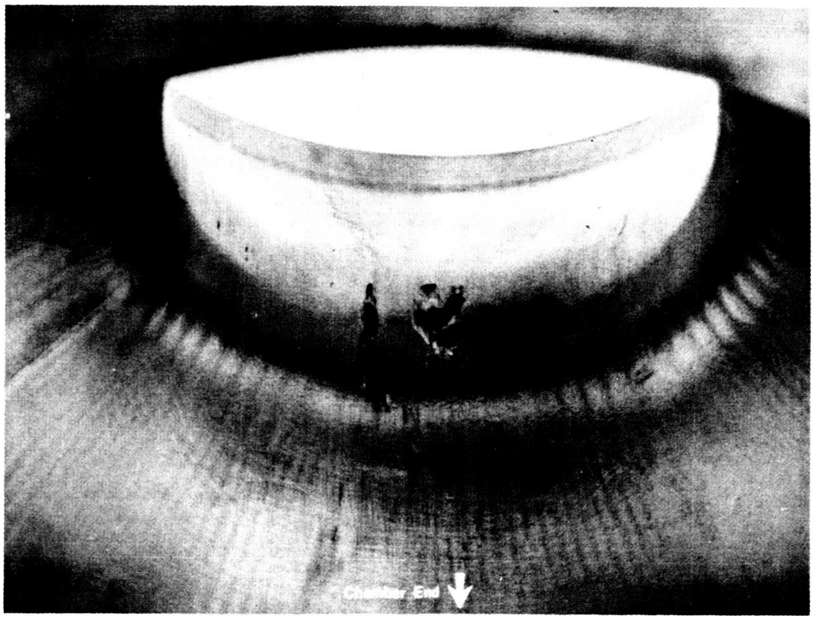

Figure 101. Regenerative Throat Section Erosion after Test 15.01 FD 41287

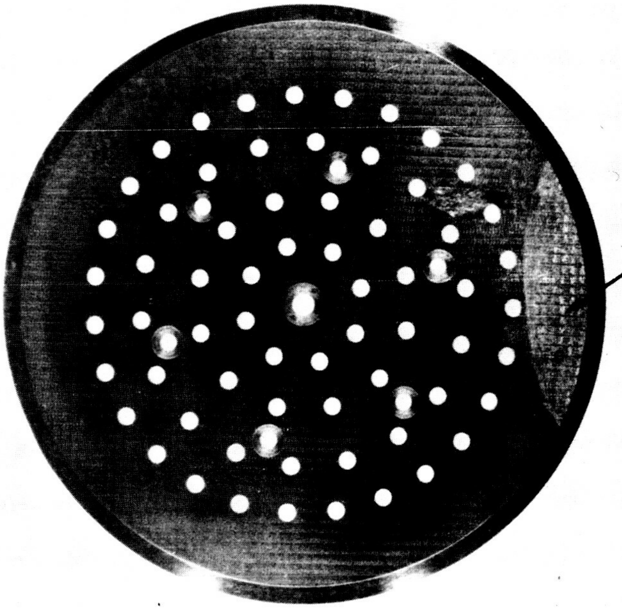

Figure 102. 40-scfm Faceplate for Scarfed Element Injector Showing Blocked Area FD 49747

To permit continuation of testing, the areas of the throat section eroded in Test No. 15.01 were repaired by electroplating nickel to fill the voids. Unfortunately, the plating came off during the third altitude test (Test No. 16.01), as shown in figure 103. The remainder of the nickel plate was subsequently removed and the eroded areas were filled by weld depositing nickel. In the last altitude test with the converging fuel stream/40-scfm faceplate injector configuration, some of the weld in the damaged area in the middle of the stave came off (figure 104), but that in the seam remained intact. Erosion was also observed in other areas of the throat after Test No. 17.01. The most severe was in the same stave previously damaged in Test No. 15.01. (See figure 104.) In other staves, the erosion was very slight and it could more correctly be described as areas where the surface was roughened. Attempts to correlate the eroded regions with coolant passage flowrates and coolant bulk temperature were unsuccessful as indicated in figure 105. The eroded areas generally align with the outer injection elements. However, a post-test inspection of the injector revealed that all of the injector swirler caps were intact and therefore gross injector streaking was not the problem.

The highest measured wall temperature (0.025 in. from the combustion-side) was 1689°R, which should correspond to a combustion side wall temperature of 2189°R (very close to the design value of 2160°R, or 1700°F). From this comparison, it appears that the design wall temperature for the chamber was too high for the flox/methane combustion environment. In Tests No. 3.02 to 14.05, where no chamber erosion occurred, the maximum indicated combustion side wall temperature was approximately 1400°F. Therefore, a design wall temperature for a nickel THERMAL SKIN® chamber that would provide good hardware durability can at least be bracketed. Specifically, it would appear that the design wall temperature could be above 1400°F, but less than 1700°F.

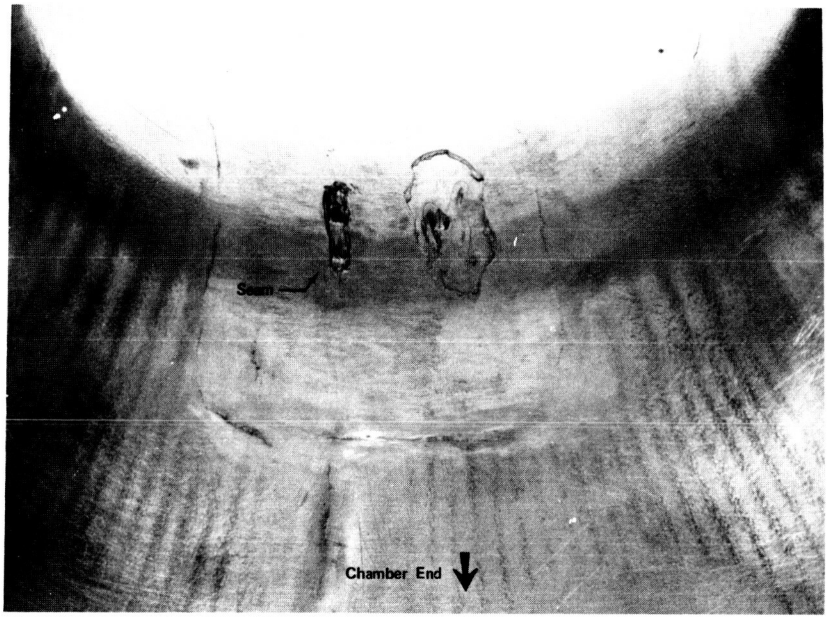

Figure 103. Regenerative Throat Section after Test No. 16.01 Showing Erosion of Plating Repair FD 41289

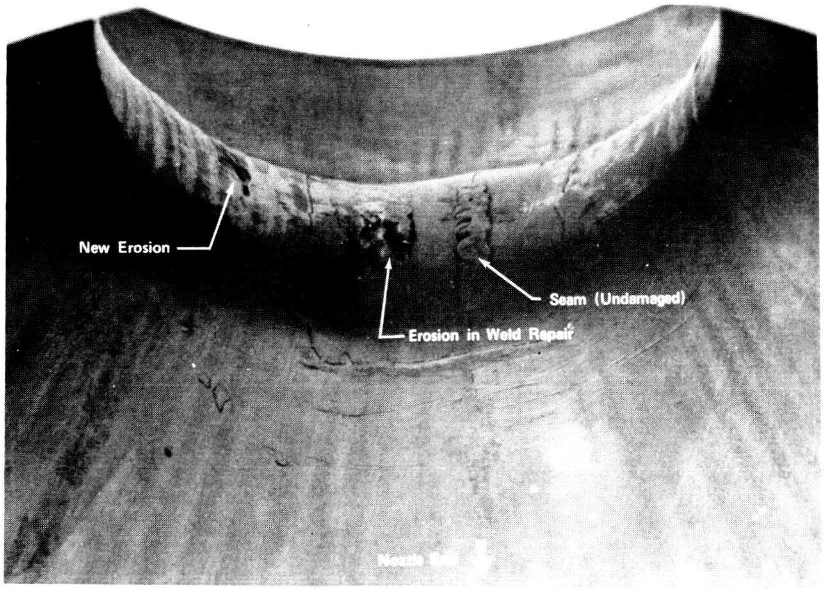

Figure 104. Regenerative Throat Section after Test No. 17.01 FD 41290

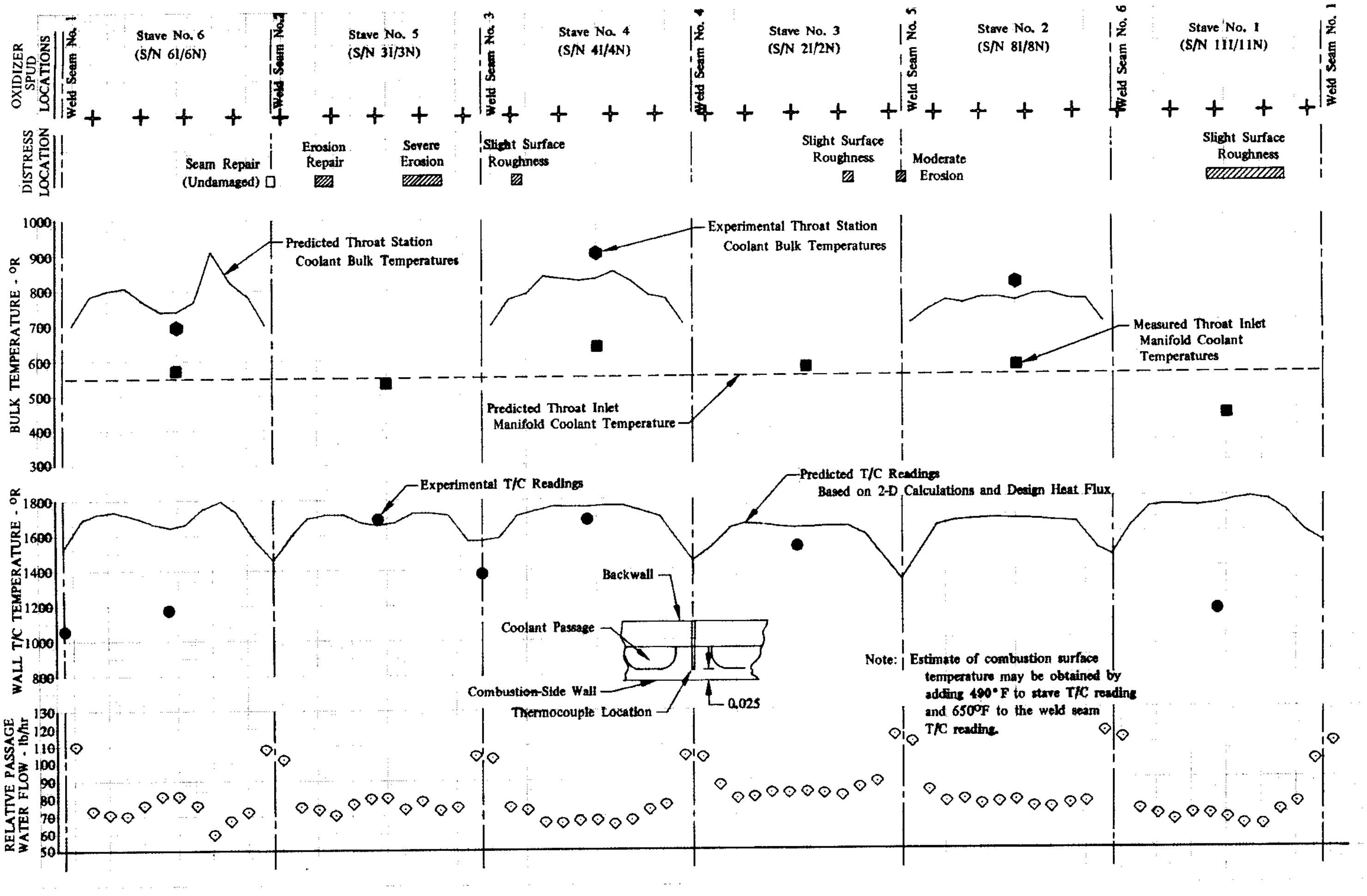

Note: Estimate of combustion surface temperature may be obtained by adding 490°F to stave T/C reading and 650°F to the weld seam T/C reading.

Figure 105. Correlation of Regenerative Throat Erosion with Operating Parameters (Test 17.01)

DF 80837

SECTION IX
THROTTLING INJECTOR HARDWARE

A. GENERAL

In addition to the fixed-thrust injectors described in Section IV, a dual orifice throttling injector was designed, fabricated and tested under the contract. The dual orifice injector was sized for a maximum thrust level of 5,000 lb at 500 psia chamber pressure and for a throttling range of 10 to 1 using flox/methane propellants. In this section of the report, the dual orifice injection principle and P&WA's experience with this type injector are given. The injector hardware and results of injector cold flow tests are discussed.

B. DUAL ORIFICE INJECTION PRINCIPLE AND P&WA EXPERIENCE

To provide a throttling capability with liquid propellants, an injector must have characteristics that maintain relatively high injection velocities and pressure drops as the thrust level (and therefore flowrate) is decreased. In the engine application of interest in this program, where the fuel is used to regeneratively cool the thrust chamber and thus reaches the injector in a gaseous state, the injector requirements for achieving throttling are simplified because the density of the methane fuel will increase as the thrust level (and hence chamber pressure) is decreased. Hence a conventional fixed-area injector can be used on the fuel side. With it, the injection velocity will remain essentially constant, and the pressure drop will not decrease as rapidly as with a liquid propellant.

Dual orifice injection elements were used in the oxidizer injector for throttling the liquid oxidizer, flox. The dual orifice injector principle can be explained by use of the single element flow schematic presented in figure 106. In dual orifice injectors, individual injection elements consist of two concentric orifices that are fed from two separate flow circuits. The inner (primary) orifice is sized to provide high pressure drops and high injection velocities at low-thrust flowrates, and the outer (secondary) orifice is sized for maximum-thrust flowrates.

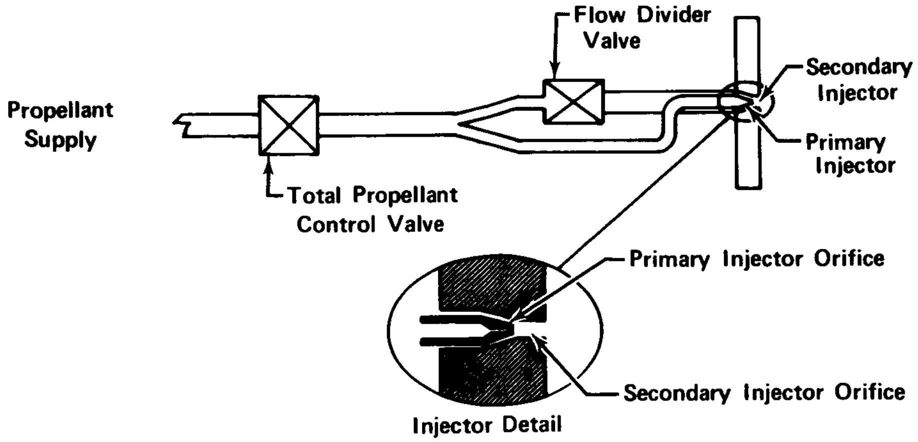

Figure 106. Dual Orifice Injector Flow System Schematic

FD 48023

A close-coupled flow divider valve in combination with the dual orifice injector provides the throttling capability. As the thrust level is decreased and the secondary injector pressure drop decreases, the flow divider valve is closed down to maintain a high pressure drop across the primary injector. The resulting high velocity flow emitted from the primary orifice energizes the flow from the secondary orifice by a momentum exchange between the concentric flow streams. Thus, even though the secondary injector pressure drop decreases as thrust level is decreased, the injection velocity is maintained at a high level.

Dual orifice injection systems have been used successfully for years for fuel injection in turbojet engines. Swirl-type dual orifice orifices are used in the turbojet to promote high combustion performance over a wide thrust range. The applicability of dual orifice injectors was extended to rocket engines in Air Force research contracts. In an initial contract dual orifice injectors having triplet and quadruplet impinging elements were demonstrated with the earth-storable propellants, N_2O_4/50% UDMH-50% N_2H_4. In two later contracts dual orifice injectors having concentric-tube elements were demonstrated with fluorine/hydrogen propellants. Injectors of 1000-lb and 8500-lb_f thrust ratings were tested. Both injectors were designed for injection of the hydrogen fuel as a gas.

High performance was obtained over a wide thrust range with both the earth-storable and fluorine/hydrogen propellant combinations. Results of the contract efforts are reported in references 7, 8, and 16.

At the conclusion of the Air Force contracts, the 8500-lb_f maximum thrust injector was evaluated with flox/methane propellants under an independent research program. Tests were made at chamber pressures of 250, 500 and 750 psia. The c* performance data obtained with this injector are presented in figure 107. At 500- and 750-psia chamber pressure where it was not possible to vary primary-to-secondary injector flow split appreciably (because of injector structural and geometry limitations), the c* efficiency level was about the same as that obtained with fixed-thrust concentric-tube RL10 injectors tested with the same propellants. At 250 psia chamber pressure, flow split could be varied over a wider range and hence it was possible to obtain much higher performance. For example, at mixture ratio of 5.75, c* efficiency with the 8500-lb_f thrust dual orifice injector was 96%.

Outstanding dual orifice injector durability was demonstrated with flox/methane as well as with the earth-storable and fluorine/hydrogen propellants. With these three propellant combinations a total of 5364 sec of firing time was accumulated with dual orifice injectors in 140 tests.

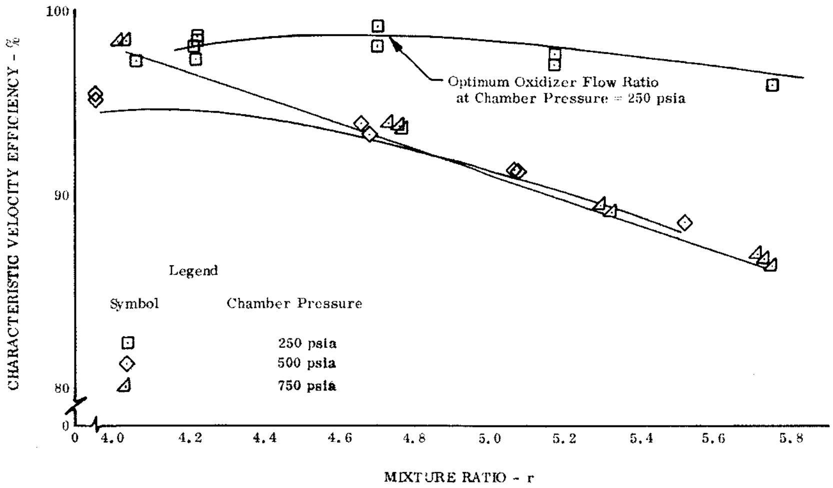

Figure 107. 8500-lb$_f$ Thrust Dual Orifice Injector Performance DF 84000

C. DESCRIPTION

The dual orifice injector evaluated in the program is illustrated in figure 108. It is a concentric-tube injector that has features and materials of construction that were demonstrated with the fixed-thrust injectors. These include: (1) a flange-type attachment for thrust chamber mounting, (2) bolt-on fuel injector parts that permit easy removal from the oxidizer injector so that the latter can be separately cleaned and passivated, (3) fuel gap spacers to keep the oxidizer spuds centered in the orifices of the faceplates, and (4) nickel and Inconel material for the oxidizer injector parts. Also as in the fixed-thrust injectors, a welded and brazed oxidizer assembly is used. The backplate is welded to the primary and secondary injector spud plates by circumferential welds. The primary spuds were brazed into the primary spud plate using gold-nickel braze material.

The two injector faceplates illustrated in figure 108 were fabricated for the dual orifice injector. One was of a conventional design in which the oxidizer spud tips were flush with the combustion-side surface of the faceplate. The other design had the spud tips recessed 0.100 in. behind the faceplate*. With both faceplates, the fuel was injected axially. Also, both faceplates were composite designs, having high permeability (100-scfm) Rigimesh material in a 0.250-in. wide annular ring near the combustion chamber wall to reduce heat transfer near the wall. The center portion of the flush-spud faceplate was constructed of 40-scfm Rigimesh material, while copper was used for the center of the recessed-spud faceplate.

---

*This spud recessment length was selected based on single element tests presented in subsection E.

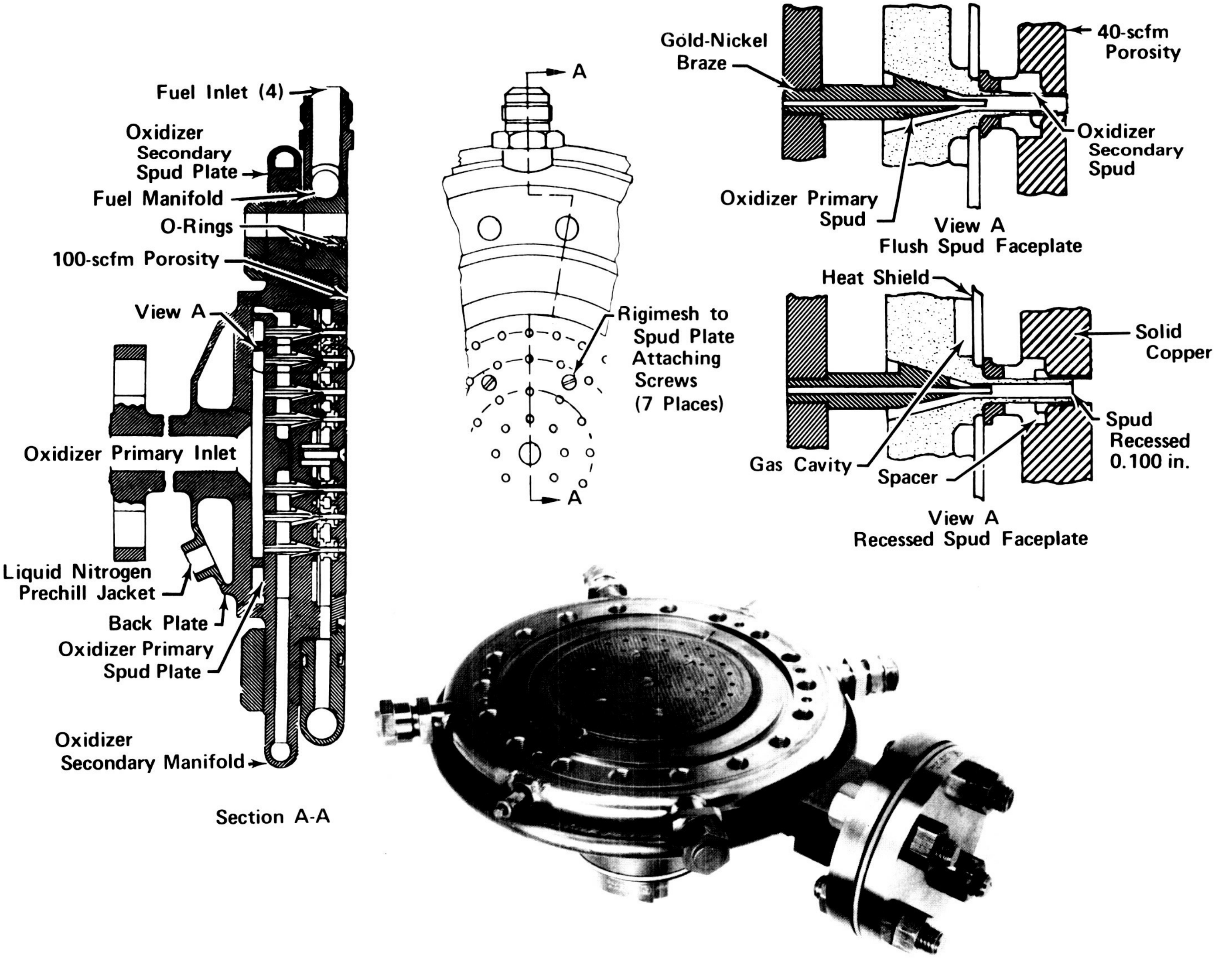

Figure 108. Dual Orifice Injector

FD 49664

The heat shield and the liquid nitrogen jacket shown in figure 108 are two features not previously used on the fixed-thrust injectors and hence they deserve explanation. The heat shield was used to reduce heat transfer between the gaseous methane fuel and the flox at throttled conditions. It is held in place on machined steps at the base of the oxidizer spuds by the fuel gap spacers to form a stagnant gas cavity between itself and the oxidizer spud plate. With the gas cavity, the heat shield was calculated to be four times more effective than using an insulating shield alone. The liquid nitrogen jacket is provided on the back of the injector for cooling during pretest periods to maximize the steady-state period of the low thrust level tests.

From a performance standpoint, the dual orifice injector was designed based on the experience cited in subsection B above, and using the guidelines established for the fixed-thrust injectors, given in Section IV. It has the same number of elements (65) and element spacing used for the fixed-thrust injectors. Table XIX presents injector element characteristic dimensions and important injector operating conditions. The injector orifices were sized to achieve a high fuel-to-oxidizer momentum ratio and to provide injector pressure drops (that would be consistent with those for the 5K flox/methane pump-fed engine designed under Contract NAS3-12010 (reference 17). At maximum thrust (5,000-lb_f thrust and 500-psia chamber pressure) and a mixture ratio of 5.25, the approximate fuel and oxidizer secondary pressure drops are 170 and 70 psi respectively. The corresponding injection fuel-to-oxidizer momentum ratio is 3.5. The primary injector was sized so that at the 10% thrust level, with a flow split of 50% the approximate pressure drop would be 25 psi. Structurally the injector was designed to operate with primary-to-secondary pressure drops up to 400 psi. This pressure capability was provided so that adjustments could be made to the test stand flow divider valve during firing tests to vary and optimize the flow split at any thrust level and mixture ratio. Figure 109 illustrates the range of flow splits over which the injector can be operated as a function of thrust level. The injector was also designed for uniform mass and mixture ratio profiles. To achieve these features, the oxidizer orifices and the fuel gaps on the outer spud row had to be made larger than those on the three inside spud rows.

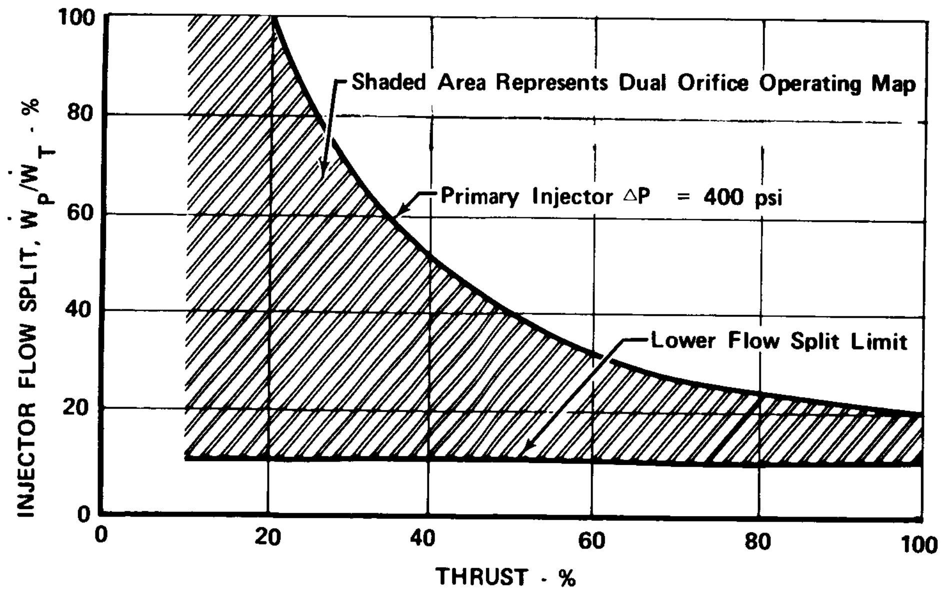

Figure 109. Dual Orifice Injector Oxidizer Flow Split Map FD 48030

Table XIX. Dual Orifice Injector Characteristic Dimensions And Operating Conditions

Oxidizer secondary orifice diameter, in.	
Inner row	0.069
Outer row	0.075
Oxidizer primary orifice diameter, in.	
Inner row	0.0175
Outer row	0.0192
Fuel injector gap size	
Inner row	0.009
Outer row	0.012
Design oxidizer secondary injector ΔP^*, psi	70
Oxidizer primary injector ΔP^*, psi	70 to 400
Design fuel injector ΔP^*, psi	170
Design fuel-to-oxidizer momentum ratio*	3.5

*Chamber pressure = 500 psia; Mixture ratio = 5.25

D. INJECTOR COLD FLOW TESTS

As with the fixed-thrust injectors, cold flow tests were made with the dual orifice injector to obtain spray pattern photographs, calibration data, and mass and mixture ratio injection profiles. Figures 110 through 114 show the photographs of the injector spray patterns. Spray patterns for approximately maximum-thrust flowrates are shown in figure 110. The first photograph in this figure was taken with water flowing through the oxidizer side of the injector; the two remaining photographs show the added effect of nitrogen gas injected through the faceplates. Figure 110b was taken with the flush-spud 40-100 scfm faceplate and figure 110c with the recessed-spud, copper-100 scfm faceplate. Note that the spray plume is wider with the recessed spud faceplate, thus indicating better atomization and mixing. Figures 111, 112, 113, and 114 show spray patterns obtained at 100%, 50%, 20%, and 10% thrust levels with the recessed-spud copper-100 scfm faceplate. In each photograph the progressive effect of increasing primary injector flow and gas injection is shown. At all thrust levels atomization improves with increasing primary flow and with gas injection.

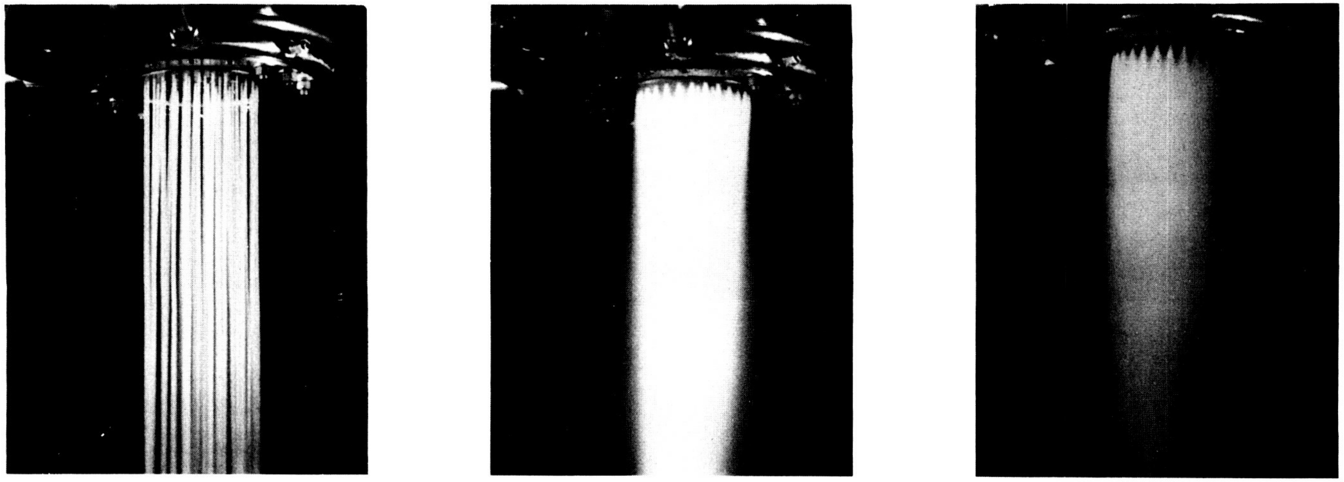

FE 101779

FE 102120

FE 102527

a. ΔP_s = 52 psid, ΔP_p = 55 psid
W_p/W_t = 10%, ΔP_f = 0

b. 40-100 scfm Faceplate (Flush Spud)
ΔP_s = 52 psid, ΔP_p = 55 psid
W_p/W_t = 10%, ΔP_f = 150 psid

c. Copper-100 scfm Face (Recessed Spud)
ΔP_s = 66 psid, ΔP_p = 66
W_p/W_t = 10%, ΔP_f = 150 psid

Figure 110. Comparison of Spray Patterns Obtained with Flush and Recessed Spud Faceplates

FD 48024

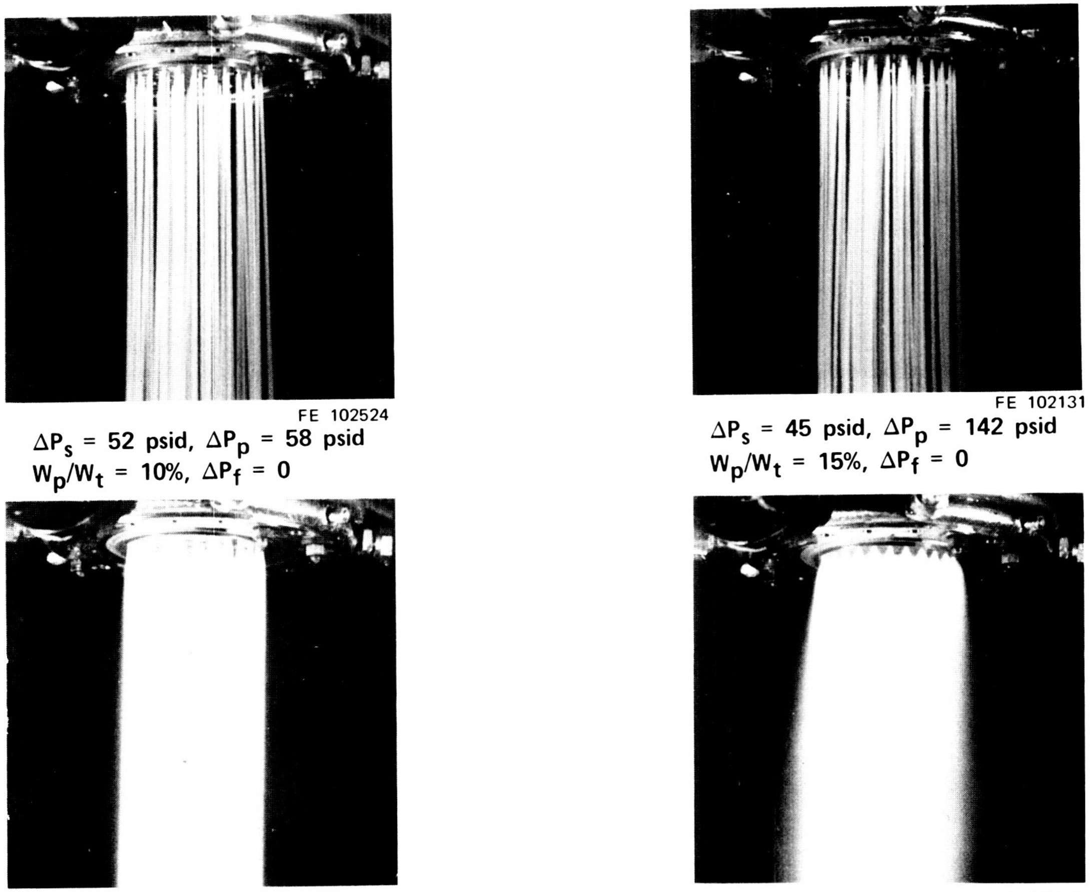

FE 102524

ΔP_s = 52 psid, ΔP_p = 58 psid
W_p/W_t = 10%, ΔP_f = 0

FE 102131

ΔP_s = 45 psid, ΔP_p = 142 psid
W_p/W_t = 15%, ΔP_f = 0

FE 102781

ΔP_s = 38 psid, ΔP_p = 298 psid
W_p/W_t = 20%, ΔP_f = 0

FE 102782

ΔP_s = 48 psid, ΔP_p = 295 psid
W_p/W_t = 20%, ΔP_f = 150 psid

Figure 111. Dual Orifice Injector Spray Patterns (100% Thrust)

FD 48025

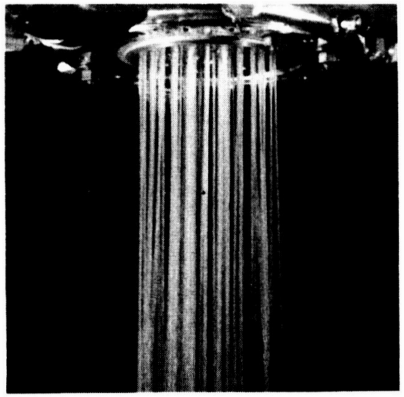

FE 102132

ΔP_s = 14 psid, ΔP_p = 14 psid
W_p/W_t = 10%, ΔP_f = 0

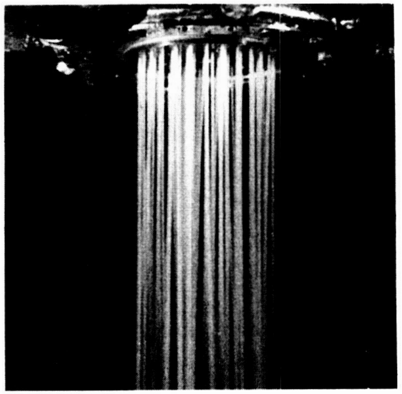

FE 102134

ΔP_s = 10 psid, ΔP_p = 61 psid
W_p/W_t = 20%, ΔP_f = 0

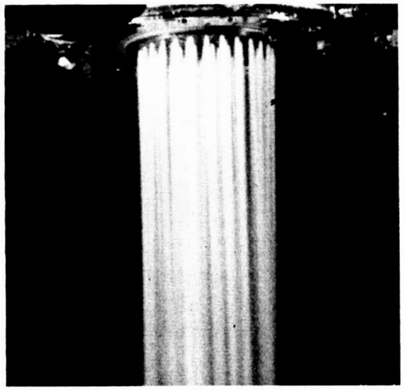

FE 102765

ΔP_s = 4 psid, ΔP_p = 146 psid
W_p/W_f = 30%, ΔP_f = 0

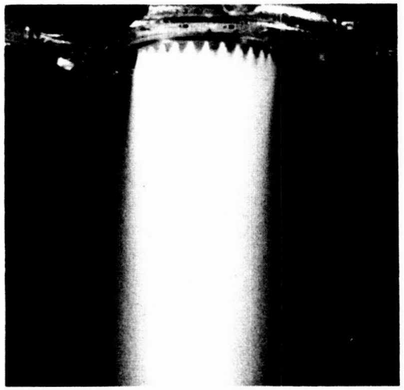

FE 102766

ΔP_s = 5 psid, ΔP_p = 147 psid
W_p/W_f = 30%, ΔP_f = 75 psid

Figure 112. Dual Orifice Injector Spray Patterns (50% Thrust)

FD 48026

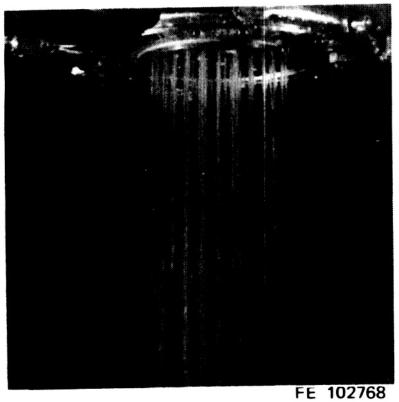

FE 102768

ΔP_s = 2.5 psid, ΔP_p = 1 psid
W_p/W_t = 10%, ΔP_f = 0

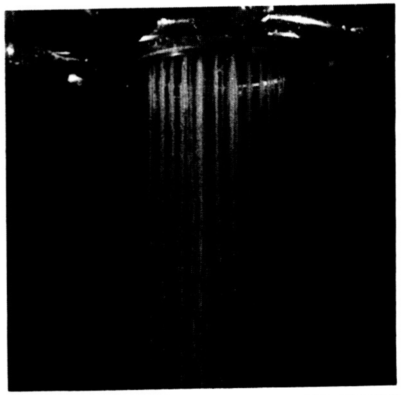

FE 102770

ΔP_s = 1.7 psid, ΔP_p = 10 psid
W_p/W_t = 20%, ΔP_f = 0

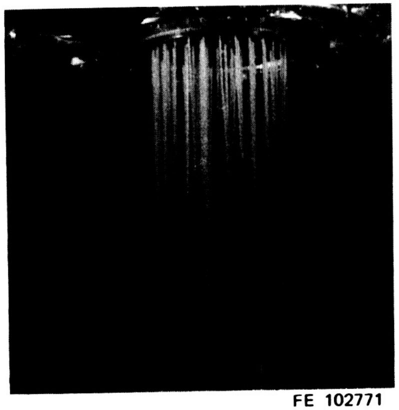

FE 102771

ΔP_s = 0.5 psid, ΔP_p = 40 psid
W_p/W_t = 40%, ΔP_f = 0

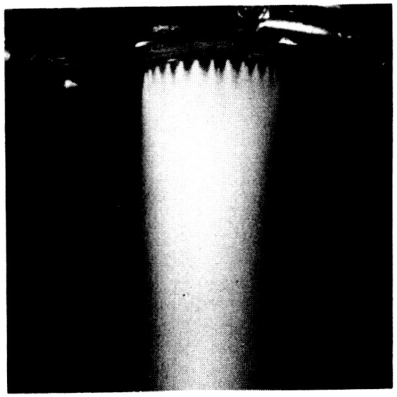

FE 102784

ΔP_s = 0.5 psid, ΔP_p = 40 psid
W_p/W_t = 40%, ΔP_f = 30 psid

Figure 113. Dual Orifice Injector Spray Patterns (20% Thrust)

FD 48027

FE 102773

$\Delta P_s = 0.7$ psid, $\Delta P_s = 0.1$ psid
$W_p/W_t = 10\%$, $\Delta P_f = 0$

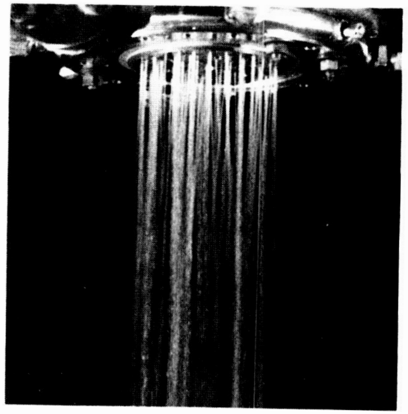

FE 102776

$\Delta P_s = 0.2$ psid, $\Delta P_p = 17$ psid
$W_p/W_t = 50\%$, $\Delta P_f = 0$

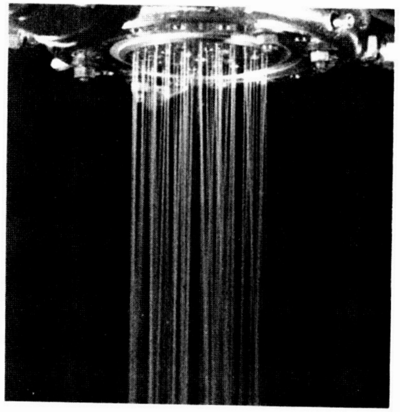

FE 102779

$\Delta P_s = 0$, $\Delta P_p = 66$ psid
$W_p/W_t = 100\%$, $\Delta P_f = 0$

FE 102780

$\Delta P_s = 0$, $\Delta P_p = 65$ psid
$W_p/W_t = 100\%$, $\Delta P_f = 15$ psid

Figure 114. Dual Orifice Injector Spray Patterns (10% Thrust)

FD 48028

The injector was calibrated to determine the effective flow areas of (1) the oxidizer primary injector, (2) the oxidizer secondary injector, (3) the fuel injector, and (4) the Rigimesh of the faceplates. The oxidizer injector calibration was accomplished using water; gaseous nitrogen was used to calibrate the fuel injector and the Rigimesh. In Rigimesh calibrations, the fuel injector orifices were plugged. The effective flow areas determined during the calibration tests are given in table XX.

Table XX. Dual Orifice Injector Effective Flow Areas

Oxidizer primary injector AC_D - in.^{2}	0.016	[0.0153]*
Oxidizer secondary injector AC_D - in.^{2}	0.167	[0.1797]
40–100 scfm Rigimesh faceplate		
Overall AC_D - in.^{2}	0.212	[0.274]
Rigimesh AC_D - in.^{2}	0.0705	[0.0388]
Rigimesh flow - %	33.3	[14.2]
Copper - 100 scfm Rigimesh faceplate		
Overall AC_D - in.^{2}	0.200	[0.246]
Rigimesh AC_D - in.^{2}	0.0104	[0.0108]
Rigimesh flow - %	5.2	[4.4]

*Bracketed terms are design values.

The patternator described in Section IV was used in the cold flow tests to determine mass and mixture ratio profiles. Mass flow profiles were obtained by injecting water through the oxidizer and fuel sides of the injector in separate tests. A mixture ratio profile was calculated from the measured mass flux data. It is shown together with the mass flux profiles in figure 115.

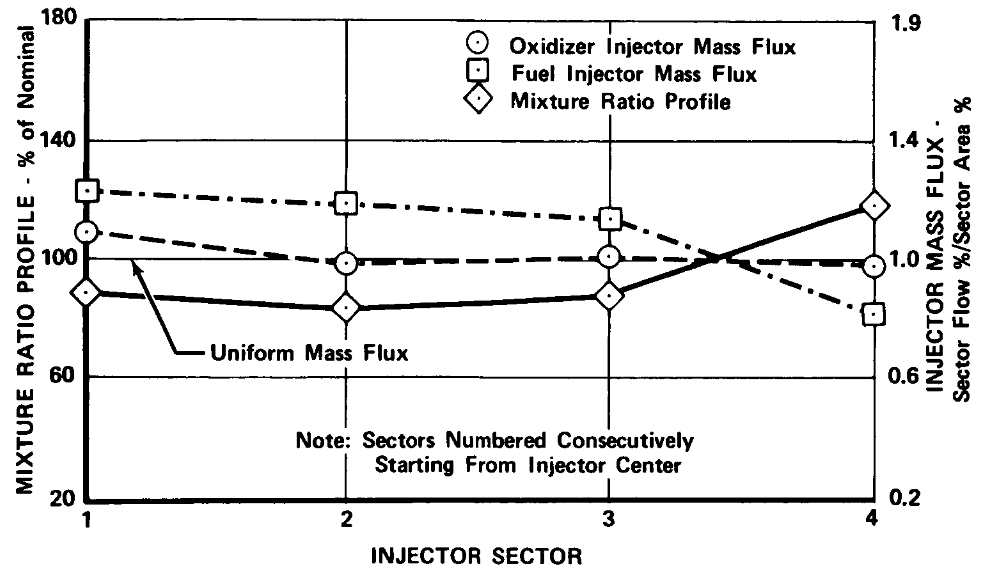

Figure 115. Dual Orifice Injector Mass Flux and Mixture Ratio Profiles FD 48029

E. SINGLE INJECTOR ELEMENT, RECESSED SPUD COLD FLOW TESTS

Single-injector element cold flow tests were made to evaluate the effect of spud recessment on atomization and thereby establish the recessment length to be used with the copper-100 scfm faceplate for the dual orifice injector. The spud configuration evaluated in the tests is shown in figure 116. Spud recessments from flush to 0.200 in. were evaluated with water injected through the oxidizer spud and gaseous nitrogen through the fuel gap. Photographs of the spray pattern shown in figure 116, were obtained with an open shutter camera and a short (0.8 μsec) flash duration. Improvement in mixing and atomization was indicated as the spud recess length was increased.

In the flow tests, it was noted that as the gaseous nitrogen flow through the fuel gap was increased, corresponding increases had to be made in the oxidizer spud pressure drop in order to maintain a constant water flowrate. Figure 117 shows the spud pressure drops that were required to maintain a water flowrate of 0.14 lb/sec as a function of the fuel injector inlet pressure and spud recess dimension. The required increase in spud pressure drop increased with increases in both fuel injector inlet pressure and spud recess length. Furthermore, with spud recessment length of greater than 0.125 in., variations in the recessment of only 0.010 in can cause a significant spud pressure drop change. Thus in an injector where the spuds have a common manifold, small deviations in spud recessment length could cause oxidizer spud-to-spud flow variations. This effect, together with a concern for faceplate durability, led to the selection of a recessment of 0.100 in for the copper-100 scfm faceplate. From an atomization standpoint alone a recess of up to 0.200 in. would be preferred; however, with a 0.100 in. length, small changes in spud recessment due to manufacturing tolerances and/or faceplate warpage during test should cause less oxidizer spud-to-spud flow deviations, and hence less mixture ratio variations in the chamber than if the spud recessment were larger.

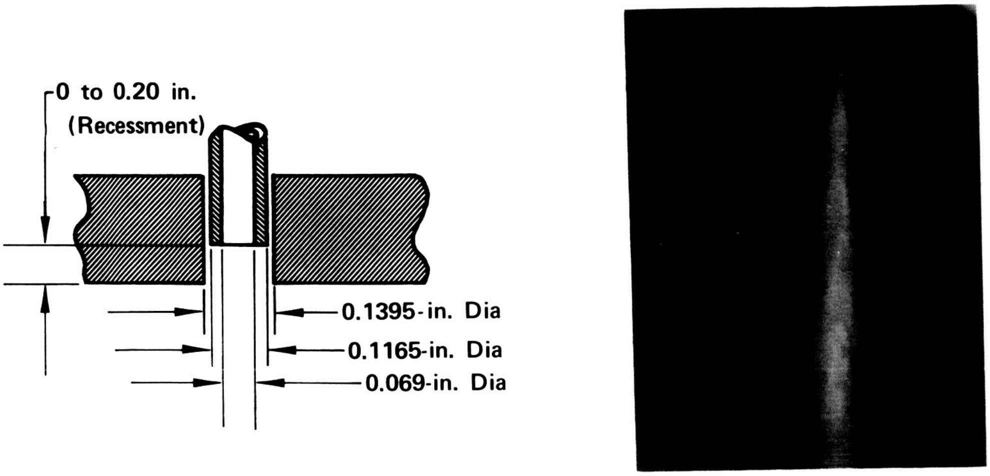

FE 96287

a. Schematic

b. Spray Pattern With
Recessment = 0
(Flush)

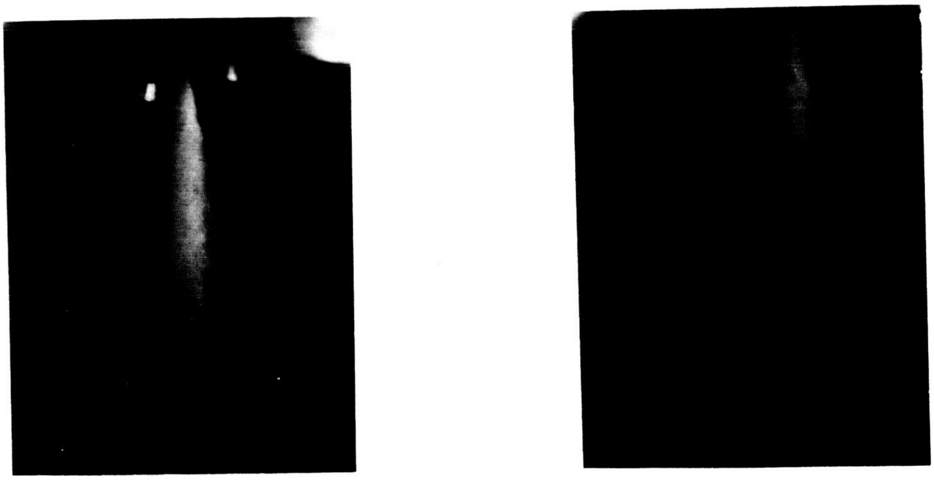

FE 95887

FE 95371

c. Spray Pattern With
Recessment =
0.075 in.

d. Spray Pattern With
Recessment =
0.200 in.

Figure 116. Single Element Recessed Spud Schematic and Spray Patterns

FD 48177

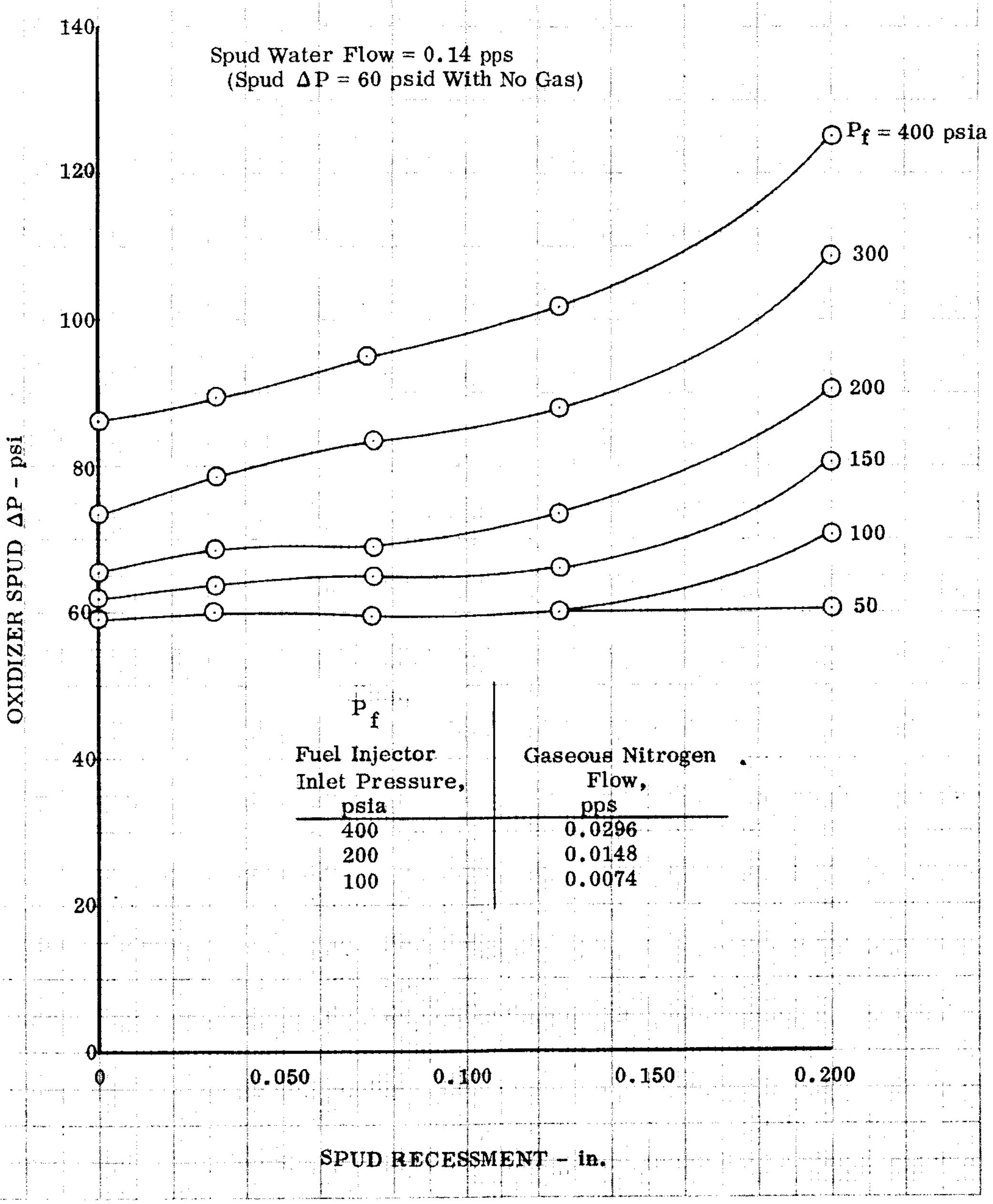

Figure 117. Recessed Spud Cold Flow Test Results

DF 85027

SECTION X
THROTTLING INJECTOR TESTS

A. GENERAL

Four dual orifice injector tests were conducted in the program; all were of long duration and were made with a water-cooled thrust chamber. The total firing time accumulated was 295 sec. Separate tests were made at chamber pressures of 500, 250, and 100 psia. At each chamber pressure level, the effect of mixture ratio and dual orifice injector primary-to-secondary injector flow split on performance was evaluated. Results of the tests are presented in this section.

B. TEST SUMMARY

Table XXI summarizes dual orifice injector testing. Only the flush-spud 40-100 scfm Rigimesh faceplate was used. A full-length water-cooled thrust chamber assembly, consisting of the throat section from the 3-piece regenerative chamber assembly and the water-cooled combustion chamber sections and altitude nozzle extension (described in Section V), was expanded to simulated-altitude exhaust conditions. The characteristic combustion chamber length was 52 in. and the thrust chamber expansion area ratio was 60 to 1. Tests were accomplished in the B-29 test stand of the Liquid Propellant Research Center at P&WA's Florida Research and Development Center, which is described in Appendix B. As in fixed-thrust injector tests, the methane gas supplied to the injector was heated to approximately 840°R in a steam heat exchanger. Data were obtained at chamber pressure levels of 500, 250 and 100 psia; at each chamber pressure level, excursions of oxidizer injector flow split and mixture ratio were made.

C. PERFORMANCE DATA

1. General

Tables XXII and XXIII present the measured and derived data obtained in the dual orifice injector tests. All of the measured data for tests 18.01, 19.01 and 21.01, represent average values for 2-sec steady-state periods. Reduced time periods for data averaging had to be used in test 20.02 because of the chugging-type combustion instability encountered in that test. The instability, which was eliminated in the following test, is discussed in Subsection D.

The equations used to determine performance parameters of table XXII are described in detail in Appendix C. As in the water-cooled chamber tests, a throat discharge coefficient of 0.985 was used to calculate c* and thrust coefficient data. The throat total pressure was determined from injector face tap measurements; the measured values were reduced to account for a momentum loss of 1.38% which had been verified in sea level thrust chamber tests described in Sections VI and VIII.

Table XXI. Dual Orifice Injector Test Summary

P&WA Ref. Test No.	Date	Type	Flox Injector	Fuel Faceplate	P_c, psia	r	Duration, sec.	Comment
18.01 (F35114)	12/03/70	Altitude (Water-Cooled)	Dual Orifice	100-40 scfm Composite	500	4 to 5.75	100.0	Successful test.
19.01 (F35114)	12/04/70	Altitude (Water-Cooled)	Dual Orifice	100-40 scfm Composite	250	4 to 5.75	98.2	Successful test. Test was advanced 2 sec. prematurely because of steam depletion.
20.02 (F35114)	12/08/70	Altitude (Water-Cooled)	Dual Orifice	100-40 scfm Composite	100	4 to 5.75	24.5	Planned 100 sec. test prematurely advanced when chugging instability occurred at a low primary-to-secondary injector flow split and caused burnouts in P_c transducer connector tubes.
21.01 (F35114)	12/08/70	Altitude (Water-Cooled)	Dual Orifice	100-40 scfm Composite	100	4 to 5.75	72.4	Successful test. Combustion stability achieved by increasing primary-to-secondary injector flow split.

Table XXII. Measured Data for Dual Orifice Injector Tests

Test Description				Chamber									Injector					
													Oxidizer Injector				Fuel Injector	
P&WA Reference Test No.	Beginning Data Sample Time	Injector	Test Type	Mixture Ratio	Chamber Pressure psia	$\dot{W}_o$ lb_m/sec	$\dot{W}_p$ (Oxidizer Primary Flow Rate) lb_m/sec	$\dot{W}_f$ lb_m/sec	Thrust Net, lb(f)	Ambient Press., psia	Diffuser Press., psia	Primary Inlet Temp, °R	Secondary Inlet Temp, °R	Primary Inlet Press, psia	Secondary Inlet Press, psia	Inlet Temp, °R	Inlet Press, psia
18.01	380	Dual Orifice/ 40-100 scfm Faceplate	Altitude	3.96	504.2	10.28	0.866	2.60	-3722.	14.83	0.385	208.7	156.8	576.6	574.6	780.8	714.5
	389			4.69	505.9	10.68	0.931	2.28	-3709.	14.83	0.387	172.1	153.1	581.0	577.8	800.8	673.8
	390			4.69	505.6	10.72	0.929	2.29	-3713.	14.83	0.388	172.0	153.0	580.3	577.1	802.2	675.3
	394			5.20	505.6	10.96	0.953	2.11	-3706.	14.83	0.391	169.8	151.5	585.1	581.3	805.5	651.5
	399			5.20	505.7	10.94	0.954	2.10	-3710.	14.83	0.389	165.9	149.3	584.5	580.7	808.3	651.7
	400			5.20	505.8	10.93	0.955	2.10	-3711.	14.83	0.390	165.4	149.2	584.5	580.8	808.7	651.7
	409			5.66	505.6	11.16	0.979	1.97	-3716.	14.83	0.389	162.0	148.8	588.7	584.5	810.3	634.5
	410			5.66	505.6	11.18	0.979	1.97	-3716.	14.83	0.389	161.8	148.7	588.8	584.5	810.5	635.0
	418			5.65	506.0	11.18	1.418	1.98	-3709.	14.83	0.387	160.1	148.8	691.1	574.5	811.0	636.6
	419			5.64	505.6	11.17	1.418	1.98	-3712.	14.83	0.387	159.7	148.9	690.6	574.2	811.0	636.2
	420			5.65	505.8	11.17	1.418	1.98	-3711.	14.83	0.389	159.5	148.8	690.6	574.4	811.0	636.3
	426			5.18	506.2	10.90	1.385	2.11	-3711.	14.83	0.386	158.9	148.8	680.9	570.9	811.7	653.6
	429			5.17	506.2	10.91	1.386	2.11	-3711.	14.83	0.386	158.6	148.8	681.0	570.9	812.3	654.0
	430			5.17	506.2	10.89	1.388	2.10	-3709.	14.83	0.385	158.0	148.8	681.3	570.9	812.5	653.3
	439			4.70	506.4	10.70	1.357	2.28	-3721.	14.83	0.382	158.1	148.7	672.2	566.8	814.3	679.5
	440			4.70	506.2	10.71	1.356	2.28	-3722.	14.83	0.380	158.1	148.7	671.9	566.6	814.4	679.6
	449			4.68	505.4	10.69	1.481	2.28	-3738.	14.83	0.372	157.7	148.8	704.7	564.0	815.3	679.0
	450			4.69	505.5	10.68	1.482	2.28	-3737.	14.83	0.371	157.2	148.8	705.0	564.2	815.4	678.7
	457			5.17	505.5	10.90	1.519	2.11	-3725.	14.83	0.373	157.2	148.8	717.0	568.4	815.2	654.1
	459			5.18	505.4	10.92	1.521	2.11	-3730.	14.83	0.372	157.2	148.8	717.1	568.3	815.4	654.5
	460			5.18	505.3	10.91	1.522	2.11	-3729.	14.83	0.373	157.3	148.9	717.6	568.5	815.4	654.4
	466			5.64	505.2	11.17	1.567	1.98	-3724.	14.83	0.373	157.0	148.7	731.2	572.5	815.3	637.1
	469			5.64	505.2	11.19	1.568	1.98	-3730.	14.83	0.370	157.2	148.8	731.7	572.7	815.4	637.6
	470			5.64	505.2	11.17	1.570	1.98	-3728.	14.83	0.370	157.2	148.8	732.4	572.8	815.4	637.3
19.01	343	Dual Orifice/ 40-100 scfm Faceplate	Altitude	4.09	255.0	5.37	0.443	1.31	-6158.	14.77	0.354	212.1	170.8	272.1	273.2	759.1	363.5
	344			4.05	255.1	5.33	0.440	1.32	-6165.	14.77	0.352	210.4	168.4	271.7	273.0	763.1	365.0
	352			4.62	253.9	5.38	0.460	1.17	-6187.	14.77	0.348	195.2	163.1	271.7	272.8	781.4	343.7
	353			4.65	253.2	5.41	0.464	1.16	-6195.	14.77	0.349	191.7	162.5	270.8	271.9	783.1	343.0
	362			5.09	253.8	5.54	0.479	1.09	-6192.	14.77	0.353	177.5	158.0	272.0	273.3	793.2	333.7
	363			5.11	255.5	5.57	0.483	1.09	-6181.	14.77	0.352	177.3	157.7	273.7	275.5	794.2	335.3
	372			5.60	254.7	5.71	0.495	1.02	-6190.	14.77	0.366	172.4	155.5	274.5	276.1	799.3	325.7
	373			5.59	255.0	5.72	0.497	1.02	-6190.	14.77	0.366	172.1	155.5	275.0	276.6	799.8	326.5
	374			5.56	255.1	5.69	0.499	1.02	-6191.	14.77	0.367	172.0	155.2	275.2	275.9	800.3	326.2
	382			5.54	253.6	5.58	0.971	1.01	-6212.	14.77	0.357	165.3	153.5	342.1	270.0	803.3	323.5
	383			5.58	253.9	5.61	0.976	1.01	-6210.	14.77	0.357	164.4	153.3	343.0	270.6	803.6	323.6
	390			5.06	254.6	5.49	0.963	1.09	-6199.	14.77	0.354	161.4	152.7	340.1	269.3	806.0	335.3
	392			5.09	254.2	5.52	0.959	1.09	-6204.	14.77	0.358	160.8	152.8	338.7	269.0	806.4	335.1
	393			5.07	254.6	5.52	0.961	1.09	-6202.	14.77	0.354	160.6	152.7	339.6	269.6	806.7	335.9
	402			4.64	253.9	5.40	0.942	1.16	-6221.	14.77	0.342	159.5	152.5	334.6	267.4	808.7	347.1
	403			4.65	254.5	5.42	0.946	1.17	-6214.	14.77	0.341	159.4	152.4	335.8	268.2	808.9	347.6
	412			4.64	254.4	5.40	1.271	1.16	-6119.	14.77	0.711	158.5	151.9	405.4	262.5	810.0	347.5
	413			4.63	254.3	5.40	1.270	1.16	-6073.	14.77	0.884	158.3	151.8	405.0	262.4	810.1	347.8
	414			4.62	254.3	5.39	1.269	1.17	-6043.	14.77	1.024	158.7	151.7	404.8	262.5	810.3	347.8
	422			5.08	253.9	5.48	1.298	1.08	-5858.	14.77	1.753	157.1	151.5	411.6	262.8	810.3	334.5
	423			5.09	254.3	5.49	1.301	1.08	-5824.	14.77	1.859	157.0	151.5	412.4	263.2	810.3	334.9
	424			5.09	254.3	5.51	1.303	1.08	-5794.	14.77	1.959	157.3	151.5	412.7	263.2	810.3	335.4
	428			5.56	253.3	5.62	1.329	1.01	-5709.	14.77	2.288	157.3	151.3	418.9	262.9	810.2	324.4
	432			5.54	254.1	5.60	1.337	1.01	-5551.	14.77	2.749	157.0	151.2	421.5	263.8	810.1	325.2
20.02	423	Dual Orifice/ 40-100 scfm Faceplate	Altitude	4.50	113.5	2.62	.517	0.58	-7644.	14.84	0.498	190.2	168.7	141.6	123.4	713.4	160.9
	424			4.51	116.3	2.62	.506	0.58	-7559.	14.84	0.471	192.3	167.5	143.8	125.8	716.0	162.4
	435			5.08	103.3	2.56	.455	0.50	-7714.	14.84	0.495	180.3	163.3	124.6	111.2	734.8	144.4
21.01	388	Dual Orifice/ 40-100 scfm Faceplate	Altitude	4.46	109.8	2.57	0.644	0.58	-7651.	14.84	0.393	198.5	165.4	154.2	117.4	705.5	156.7
	389			4.46	109.7	2.57	0.642	0.58	-7652.	14.84	0.397	191.3	164.2	153.0	116.3	708.6	157.0
	397			4.96	107.6	2.57	0.622	0.52	-7665.	14.84	0.386	176.1	163.8	146.7	111.5	723.9	148.3
	399			4.97	106.3	2.56	0.607	0.51	-7695.	14.84	0.408	175.6	164.4	145.4	111.4	727.0	146.5
	403			4.98	105.6	2.55	.612	0.51	-7680.	14.84	0.401	175.5	163.2	143.2	110.7	733.0	146.4
	412			5.58	104.5	2.55	0.608	0.46	-7720.	14.84	0.389	165.4	161.7	141.1	111.0	740.0	138.3
	413			5.58	103.0	2.56	0.605	0.46	-7724.	14.84	0.410	165.0	161.2	139.3	110.8	741.0	137.9
	419			5.57	99.8	2.50	0.758	0.45	-7167.	14.84	1.778	161.2	160.3	155.6	103.1	745.8	134.0
	420			5.57	100.3	2.51	0.757	0.45	-7046.	14.84	2.019	160.7	159.9	155.9	103.5	746.7	134.7
	421			5.57	102.3	2.53	0.758	0.45	-6948.	14.84	2.186	160.6	159.4	157.0	106.3	747.9	136.7
	431			5.01	105.1	2.51	0.763	0.50	-6401.	14.84	3.226	158.3	157.9	160.7	107.9	757.4	145.7
	433			5.01	105.5	2.51	0.760	0.50	-6312.	14.84	3.390	157.9	157.6	160.9	107.9	758.6	145.9
	438			4.50	107.7	2.50	0.738	0.56	-6098.	14.84	3.790	159.9	157.0	160.0	109.6	763.1	156.8
	442			4.50	107.1	2.51	0.731	0.56	-5984.	14.84	4.023	160.8	156.5	158.6	108.6	765.5	156.6
	443			4.50	106.7	2.49	0.729	0.55	-5957.	14.84	4.087	160.6	156.4	158.1	108.2	766.1	155.8
	446			4.51	106.2	2.47	0.729	0.55	-5832.	14.84	4.330	160.4	156.0	157.4	107.8	767.5	155.0

Table XXIII. Derived Data for Dual Orifice Injector

P&WA Reference Test No.	Injector	Test Type	L*, in.	Mixture Ratio	Chamber Pressure Throat Total, psia	Vacuum Thrust lb	Oxidizer Flow Split (Primary to Total)	I_{vac}, sec	c* ft/sec	$C_{F_{vac}}$	$\eta_{I_{vac}}$ %	$\eta_{c^*(Pc)}$ %	$\eta_{C_{F_{vac}}}$ %
18.01	Dual Orifice/ 40-100 scfm Faceplate	Water-Cooled Altitude Thrust Chamber	52	3.96	497.2	4964.	8.4	385.3	6775.	1.83	94.46	98.38	96.01
				4.69	498.8	4977.	8.7	384.3	6762.	1.83	92.74	96.38	96.22
				4.69	498.5	4973.	8.7	382.3	6730.	1.83	92.27	95.92	96.18
				5.20	498.5	4979.	8.7	381.1	6700.	1.83	91.00	94.69	96.09
				5.20	498.6	4975.	8.7	381.5	6713.	1.83	91.08	94.88	95.99
				5.20	498.8	4973.	8.7	381.5	6718.	1.83	91.11	94.95	95.95
				5.66	498.5	4969.	8.8	378.4	6665.	1.83	89.90	93.90	95.73
				5.66	498.6	4969.	8.8	377.9	6657.	1.83	89.77	93.77	95.72
				5.65	499.0	4976.	12.7	378.1	6657.	1.83	89.82	93.77	95.78
				5.64	498.6	4974.	12.7	378.4	6660.	1.83	89.90	93.81	95.83
				5.65	498.7	4974.	12.7	378.3	6659.	1.83	89.86	93.80	95.79
				5.18	499.1	4975.	12.7	382.4	6736.	1.83	91.35	95.24	95.91
				5.17	499.2	4974.	12.7	382.2	6734.	1.83	91.28	95.20	95.88
				5.17	499.2	4977.	12.8	383.1	6746.	1.83	91.51	95.38	95.94
				4.70	499.4	4966.	12.7	382.6	6755.	1.82	92.32	96.27	95.89
				4.70	499.1	4965.	12.7	382.2	6745.	1.82	92.22	96.13	95.93
				4.68	498.3	4952.	13.9	381.9	6747.	1.82	92.18	96.19	95.82
				4.69	498.4	4952.	13.9	382.3	6755.	1.82	92.26	96.30	95.80
				5.17	498.5	4964.	13.9	381.7	6730.	1.82	91.18	95.15	95.83
				5.18	498.4	4960.	13.9	380.9	6719.	1.82	90.96	94.98	95.76
				5.18	498.3	4960.	14.0	381.1	6721.	1.82	91.02	95.02	95.78
				5.64	498.2	4965.	14.0	377.5	6650.	1.83	89.68	93.68	95.72
				5.64	498.2	4960.	14.0	376.5	6639.	1.82	89.44	93.52	95.63
				5.64	498.2	4962.	14.1	377.3	6651.	1.83	89.64	93.69	95.68
19.01	Dual Orifice/ 40-100 scfm Faceplate	Water-Cooled Altitude Thrust Chamber	52	4.09	251.5	2503.	8.2	374.8	6610.	1.82	92.38	96.41	95.81
				4.05	251.5	2497.	8.2	375.5	6641.	1.82	92.67	96.97	95.57
				4.62	250.3	2476.	8.5	378.1	6712.	1.81	92.11	96.72	95.23
				4.65	249.7	2467.	8.6	375.3	6670.	1.81	91.35	96.04	95.11
				5.09	250.3	2470.	8.7	372.8	6633.	1.81	89.88	94.80	94.80
				5.11	251.9	2481.	8.7	372.4	6639.	1.80	89.73	94.86	94.59
				5.60	251.2	2468.	8.7	366.8	6554.	1.80	87.90	93.31	94.20
				5.59	251.5	2468.	8.7	366.1	6548.	1.80	87.74	93.23	94.10
				5.56	251.6	2466.	8.8	367.6	6584.	1.80	88.13	93.74	94.02
				5.54	250.1	2449.	17.4	371.8	6667.	1.79	89.19	94.94	93.94
				5.58	250.3	2451.	17.4	370.5	6645.	1.79	88.85	94.62	93.90
				5.06	251.1	2462.	17.5	374.5	6706.	1.80	90.36	95.88	94.24
				5.09	250.7	2456.	17.4	371.7	6659.	1.80	89.62	95.18	94.16
				5.07	251.1	2459.	17.4	372.3	6673.	1.79	89.8	[illegible]	94.12
				4.64	250.3	2443.	17.4	372.1	6693.	1.79	90.5	[illegible]	93.96
				4.65	250.9	2451.	17.5	372.5	6695.	1.79	90.	[illegible]	94.02
				4.64	250.8	2446.	23.5	373.0	6714.	1.79	90.80	96.70	93.89
				4.63	250.8	2446.	23.5	372.7	6709.	1.79	90.76	96.66	93.89
				4.62	250.8	2439.	23.5	372.2	6720.	1.78	90.67	96.84	93.63
				5.08	250.4	2429.	23.7	370.4	6704.	1.78	89.35	95.84	93.23
				5.09	250.7	2434.	23.7	370.4	6699.	1.78	89.32	95.75	93.28
				5.09	250.7	2437.	23.7	369.9	6683.	1.78	89.20	95.52	93.38
				5.56	249.8	2434.	23.7	367.4	6618.	1.79	88.10	94.24	93.48
				5.54	250.6	(1)	23.9	(1)	6653.	(1)	(1)	94.75	(1)
20.02	Dual Orifice/ 40-100 scfm Faceplate	Water-Cooled Altitude Thrust Chamber	52	4.50	111.9	1019.	20.3	318.4	6137.	1.67	78.05	89.69	87.02
				4.51	114.7	1112.	20.1	347.6	6292.	1.78	85.17	91.92	92.65
				5.08	101.9	950.	17.9	310.1	5836.	1.71	75.21	84.45	89.05
21.01	Dual Orifice/ 40-100 scfm Faceplate	Water-Cooled Altitude Thrust Chamber	52	4.46	108.3	1041.	25.1	330.8	6040.	1.76	81.22	88.39	91.88
				4.46	108.2	1038.	25.0	330.4	6044.	1.76	81.15	88.47	91.73
				4.96	106.1	1028.	24.2	332.4	6025.	1.78	80.79	87.32	92.52
				4.97	104.8	992.	23.7	322.8	5987.	1.73	78.45	86.76	90.42
				4.98	104.1	1010.	24.0	330.0	5974.	1.78	80.21	86.57	92.65
				5.58	103.1	972.	23.9	323.8	6027.	1.73	78.16	86.97	89.86
				5.58	101.5	963.	23.7	319.4	5913.	1.74	77.09	85.33	90.34
				5.57	98.4	(1)	30.3	(1)	5855.	(1)	(1)	84.51	(1)
				5.57	98.9	(1)	30.1	(1)	5858.	(1)	(1)	84.54	(1)
				5.57	100.9	(1)	30.0	(1)	5936.	(1)	(1)	85.67	(1)
				5.01	103.6	(1)	30.4	(1)	6046.	(1)	(1)	87.58	(1)
				5.01	104.0	(1)	30.3	(1)	6070.	(1)	(1)	87.92	(1)
				4.50	106.2	(1)	29.5	(1)	6097.	(1)	(1)	89.13	(1)
				4.50	105.6	(1)	29.2	(1)	6054.	(1)	(1)	88.48	(1)
				4.50	105.2	(1)	29.2	(1)	6064.	(1)	(1)	88.63	(1)
				4.51	104.7	(1)	29.5	(1)	6095.	(1)	(1)	89.07	(1)

1) Data Not Applicable Due To Nozzle Separation.

The oxidizer injector flow split, defined as the ratio of the primary injector flow to the total oxidizer flow, is included in the derived data table. The primary flow rate used to calculate this parameter was computed using the primary injector pressure drop measured in the tests and the effective flow area for the primary injector determined in water flow calibrations. Curves of the oxidizer primary flow rate and injector flow split are given in figure 118 as functions of primary injector pressure drop.

Impulse data could not be derived for some data points in tests 19.01 and 21.01 because the steam accumulators, which supply the ejectors of the test stand altitude system, were depleted during these tests and as a result, adequately low nozzle exit pressures could not be maintained. (This is not a normal occurrence; tests 19.01 and 21.01 were started with an abnormally low steam accumulator pressure level to expedite testing.)

In all of the dual orifice tests, as in the fixed-thrust injector tests, thrust system tare was established at pre-test conditions (i.e., with the propellant and coolant supply lines pressurized and at operating temperature). It was theorized that the differences between pre- and post-test tares observed in fixed-thrust tests were caused by expansion of the heated methane supply line; therefore, thermocouples were installed to monitor the line metal temperatures prior to the dual orifice injector tests. Also the test procedure was modified to allow for longer duration heated methane ventings to raise the line temperature before each test. This modified test procedure was not completely effective because, as shown in figure 119, the line metal temperature increased during the tests, and, more importantly, in first two tests (18.01 and 19.01), differences in pre- and post-test tare values as large as 51 lb_f were obtained. As a result, the support for the heated methane supply line was changed before the final two tests from a ground-type to a hanging-type, with which large pipe expansions (or contractions) could be tolerated. This apparently solved the thrust tare problem because the pre- and post-test tare values for the last two tests agreed within 9 lb_f.

2. Performance Comparisons

Performance data were obtained in the dual orifice injector tests over the 100- to 500-psia chamber pressure range, at mixture ratios from 4.0 to 5.7 and with oxidizer injector flow splits from 8 to 30%. Figures 120, 121 and 122 show the effect of flow split on c* efficiency at the three chamber pressure levels (500, 250 and 100 psia) evaluated.

At 500-psia chamber pressure, c* efficiency was practically unaffected by changes in flow split. This result is attributed to the fact that at this chamber pressure level the contribution of the primary injector is small, even with high pressure drops. In the 500-psia chamber pressure test, primary injector pressure drop was increased from 87 to 240 psid without affecting performance. At the lower chamber pressures (250 and 100 psia) the effect of oxidizer injector flow is more pronounced. At the higher mixture ratios for 250-psia chamber pressure and at all mixture ratios at 100 psia chamber pressure, c* efficiency increased with increasing primary injector flow. At 250-psia chamber pressure and for mixture ratios above 5.0, performance was increased by about 1% by increasing flow split from 8.5 to 25%. At 100-psia chamber pressure, although all the c* data are low (less than 90%), significant performance improvements were obtained by increasing flow split; at a mixture ratio of 5.0, c* efficiency increased about 4% as the flow split was increased from approximately 18 to 30%. At this mixture ratio, as well as 4.5, it appears that further performance increases could be achieved with higher flow splits. Additional testing would be required to evaluate higher flow splits at this chamber pressure.

From the tests that have been made with the dual orifice injector, a curve showing how flow split should vary with chamber pressure to achieve highest performance can at least be approximated. Figure 123 presents such a curve; it indicates that as chamber pressure is decreased, higher flow splits are required for highest performance.

Altitude performance information obtained with the dual orifice injector at flow splits near optimum values is presented in figure 124. Also shown in this figure are the performance curves for the converging fuel stream injector, the highest performing fixed-thrust injector tested in the program. All of the data for the dual orifice injector falls below that for the converging fuel stream injector. The impulse and impulse efficiency reflect reduced values obtained for the more basic performance parameters, c* efficiency and thrust coefficient efficiency. The c* efficiencies are less with the dual orifice injector, apparently because of poorer atomization and mixing achieved by this injector. The 40-100 scfm faceplate, which provides a conventional flush oxidizer spud configuration, was used on the dual orifice injector in all tests. Because the water flow tests made with the recessed-spud, copper-100 scfm faceplate indicate better atomization and mixing (Section IX), that faceplate should provide higher performance. Recessing the oxidizer spuds of concentric-tube injectors has raised performance with oxygen-hydrogen propellants (reference 18) and probably will be beneficial with flox/methane as well.

The thrust coefficient efficiencies obtained with dual orifice injector agree with the curve established for the converging fuel stream injector at 500-psia chamber pressure but are lower at lower chamber pressures. Although these reduced thrust coefficient efficiencies could be attributed to increased chemical non-equilibrium losses at the lower chamber pressures, and possibly (at 100 psia chamber pressure) to the effect of abnormally low c* efficiencies, additional tests would have to be made to substantiate either effect.

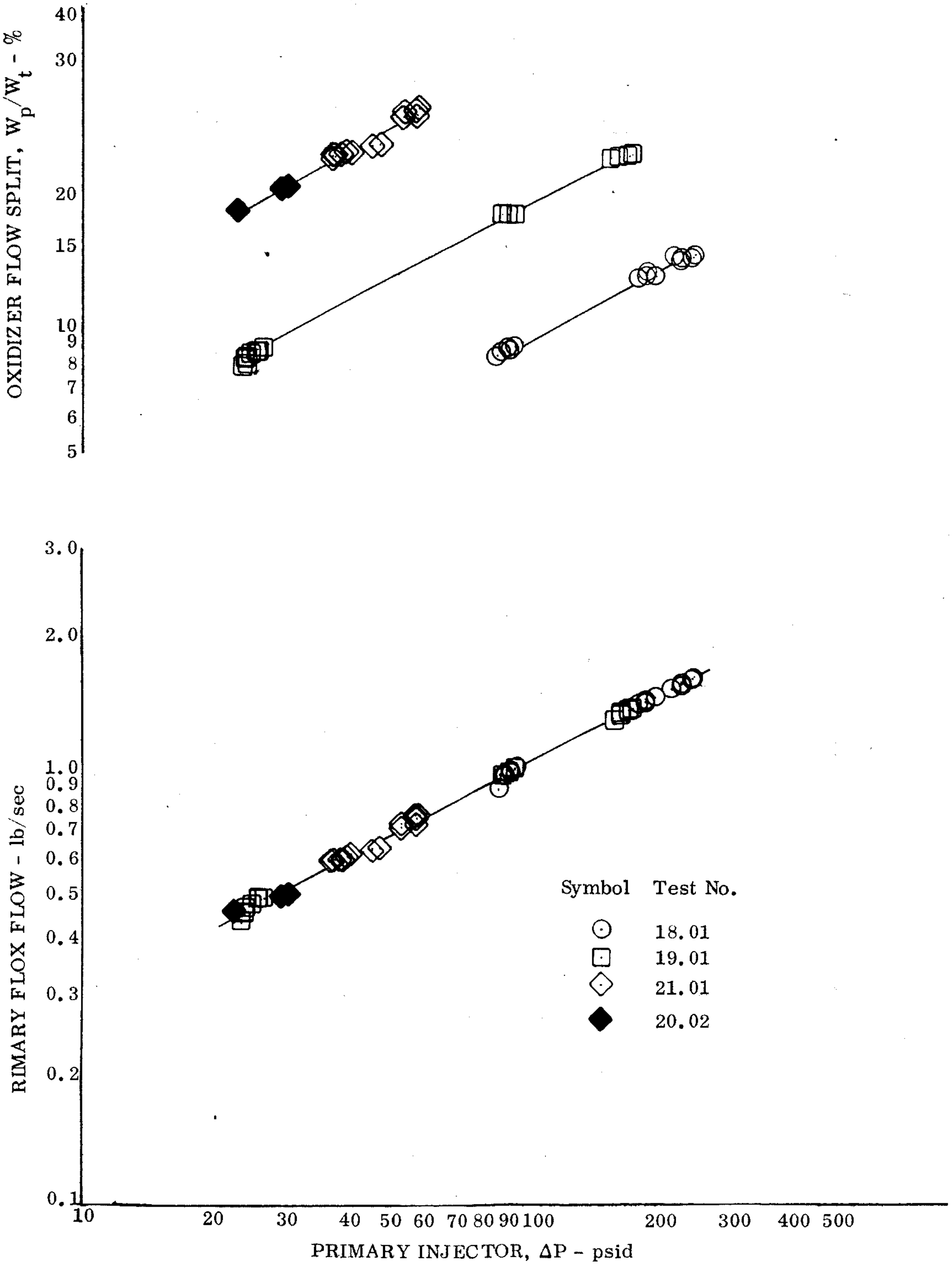

Figure 118. Variation of Oxidizer Primary Injector Flow and Flow Split with Injector Pressure Drop

DF 84977

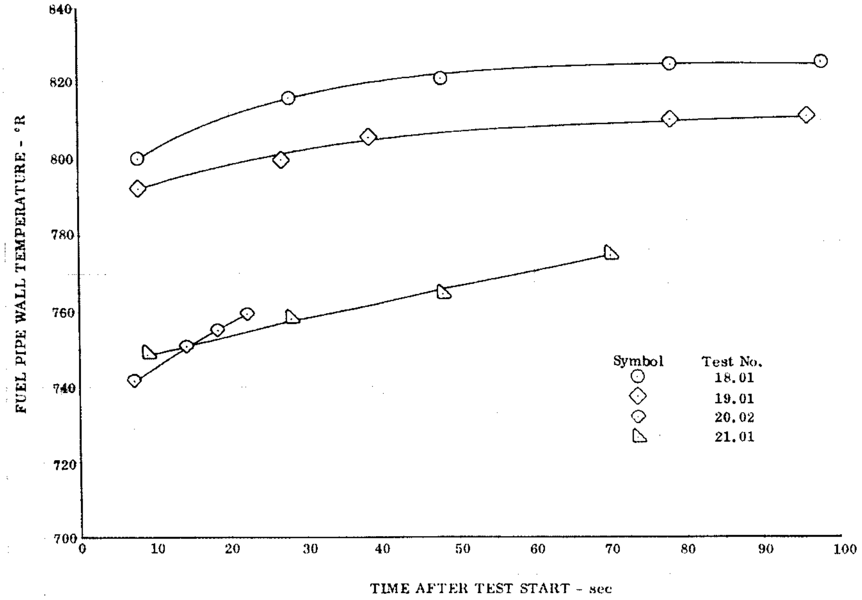

Figure 119. Fuel Line Wall Temperature Variation with Time DF 84976

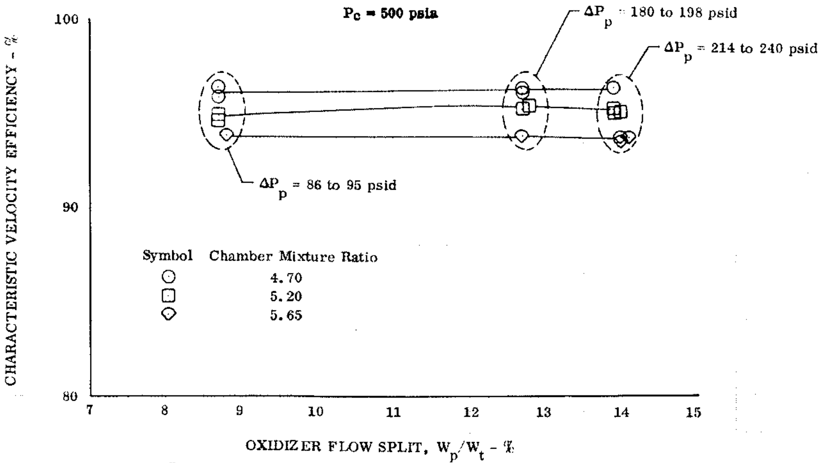

Figure 120. c* Efficiency Variation with Dual Orifice Injector Flow Split (Chamber Pressure = 500 psia, Test No. 18.01) DF 84975

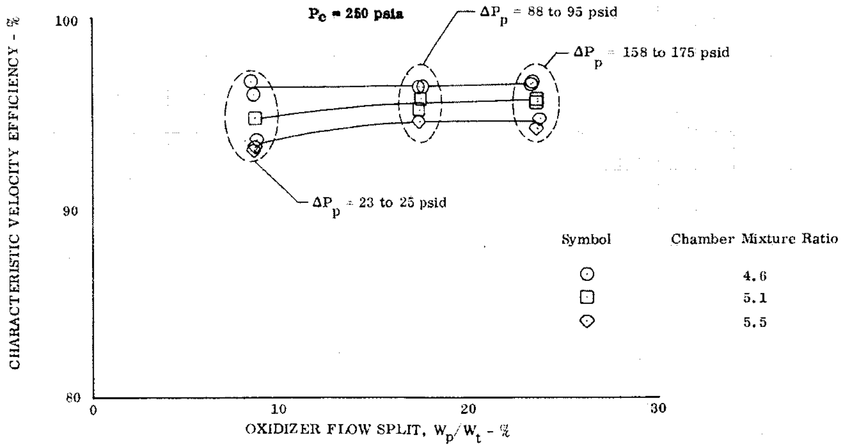

Figure 121. c* Efficiency Variation with Dual Orifice Injector Flow Split (Chamber Pressure = 250 psia, Test No. 19.01) DF 84974

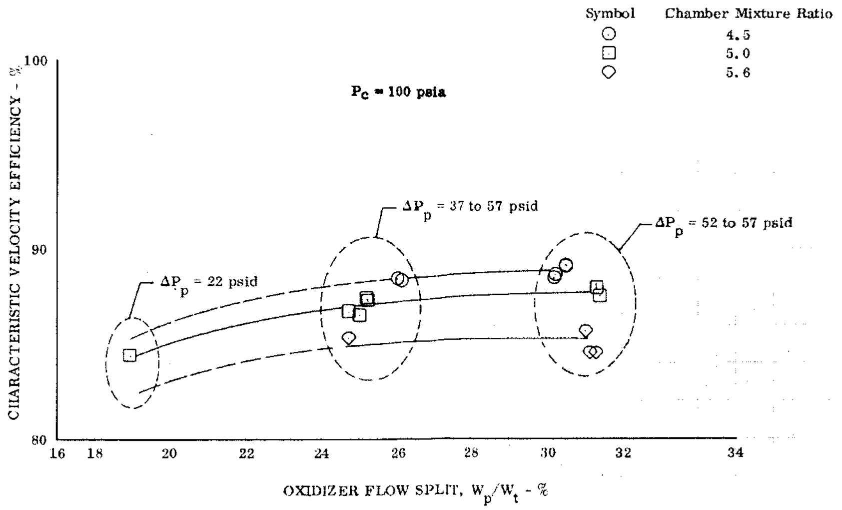

Figure 122. c* Efficiency Variation with Dual Orifice Injector Flow Split (Chamber Pressure = 100 psia, Tests No. 20.02 and 21.01) DF 84973

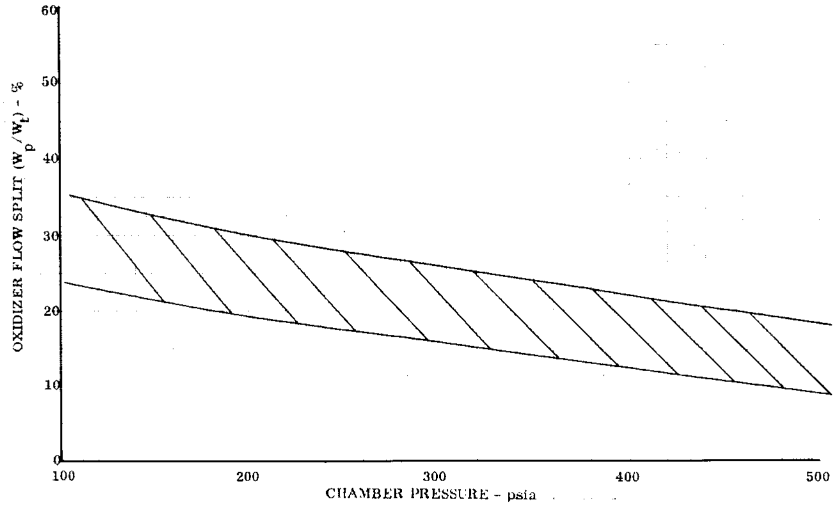

Figure 123. Optimum Dual Orifice Injector Flow Split Variation with Chamber Pressure DF 84972

D. STABILITY

The dual orifice injector provided stable combustion at all chamber pressure levels. No high frequency instability was noted. However, low frequency (1 to 3 cps) chugging-type instability was encountered at the 100-psia chamber pressure level with low oxidizer injector flow splits in test 20.02. Figure 125 shows an oscillograph trace for this test, illustrating the instability that was encountered; the flow split was 18%. Stable combustion was achieved at this chamber pressure level with higher flow splits in test 21.01; figure 126 illustrates the stability obtained with a 30% flow split. The peak-to-peak amplitudes of the most unstable test parameter, oxidizer secondary injector pressure drop are correlated with injector flow split in figure 127. As indicated by the decay of the peak-to-peak amplitudes, stability increased with increasing dual orifice flow split.

E. CHAMBER HEAT TRANSFER DATA

The water-cooled chamber hardware described in Section V, together with the throat section of the three piece regenerative chamber, was used in the dual orifice tests. The heat transfer data obtained are presented in table XXIV; parameters included in this table are defined in figure 29 of Section VI.

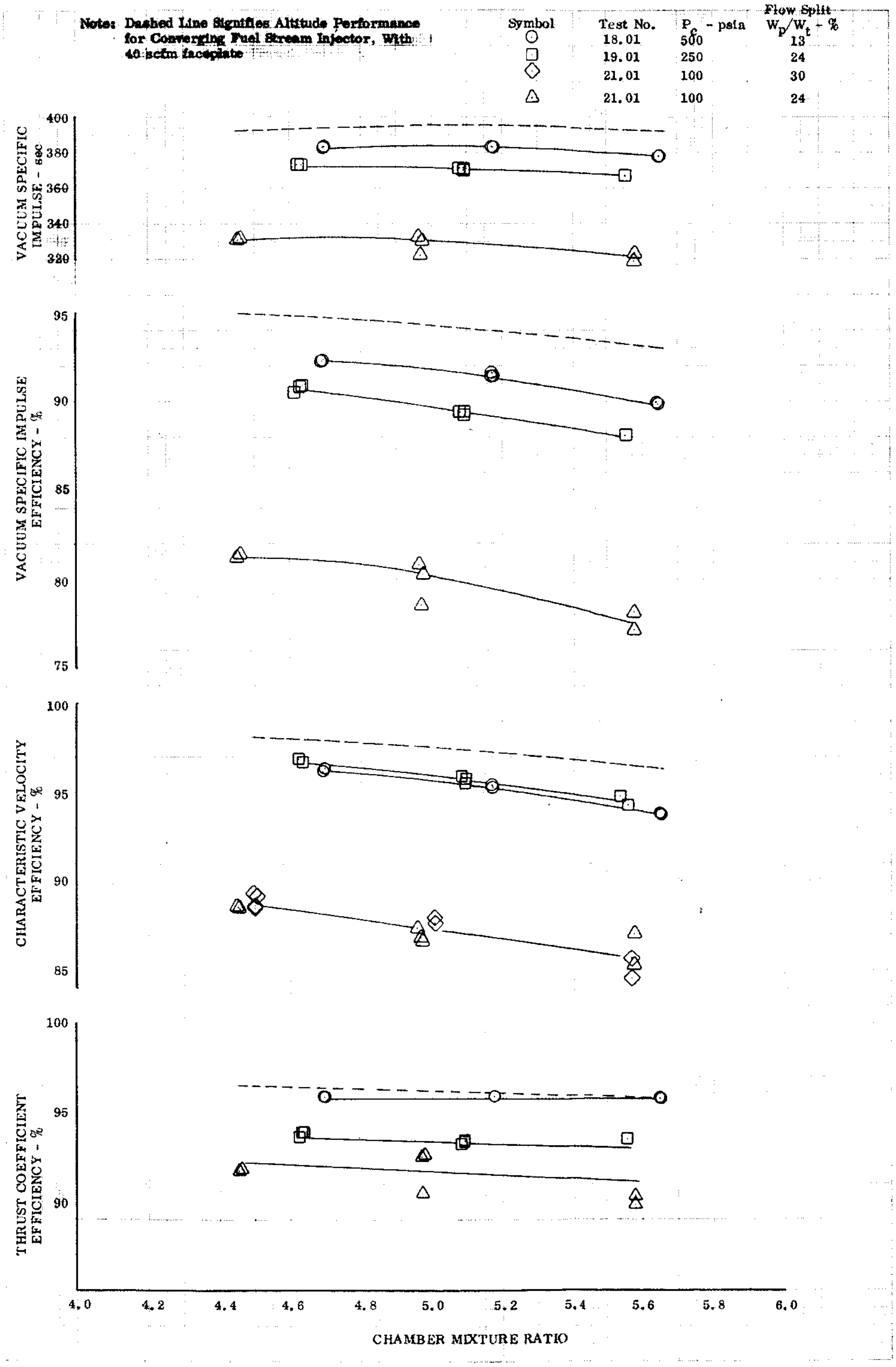

Figure 124. Altitude Test Performance Data for Dual Orifice Throttling Injector and Water-Cooled Thrust Chamber

DF 84981

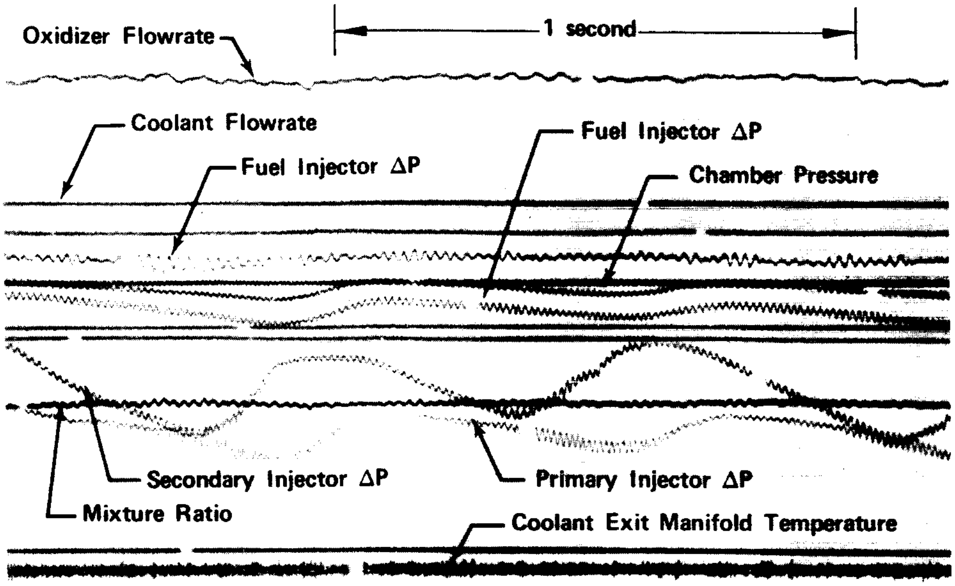

Figure 125. Oscillograph Trace for Dual Orifice Injector Test No. 20.02, P_c = 100 psia, r = 5.08 $(W_p/W_t)_{ox}$ = 18% FD 48054

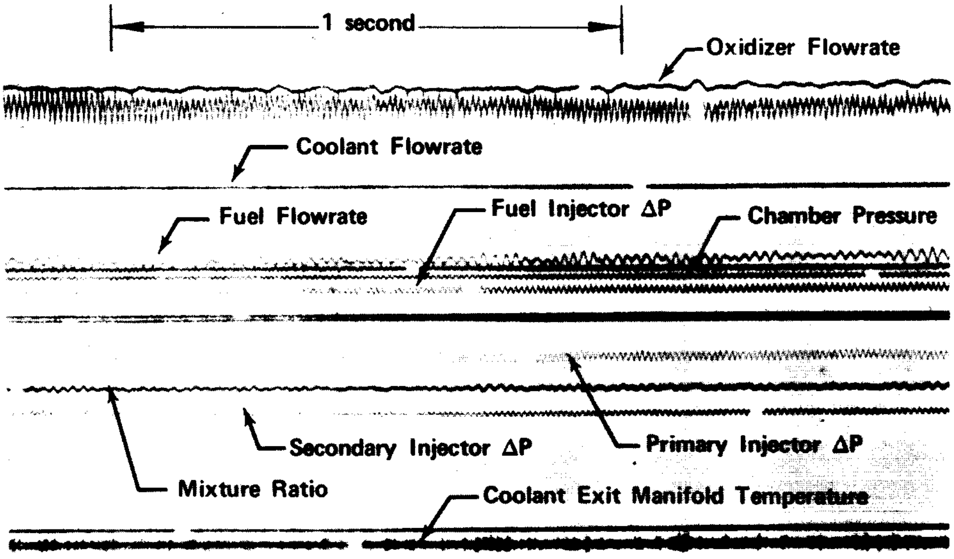

Figure 126. Oscillograph Trace for Dual Orifice Injector Test No. 21.01, P_c = 100 psia, r = 5.01 $(W_p/W_t)_{ox}$ = 30% FD 48053

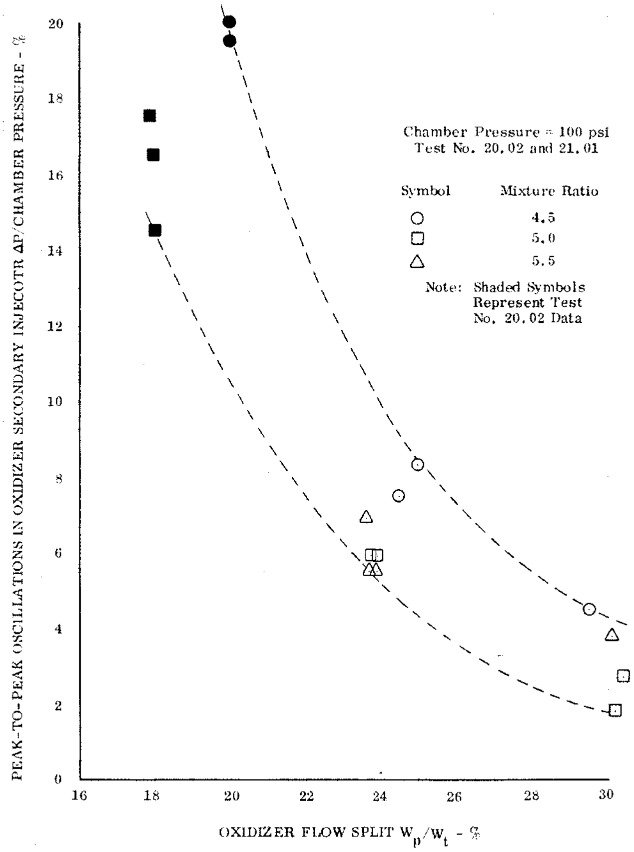

Figure 127. Variation of Peak-to-Peak Oscillations in Oxidizer Secondary Injector Pressure Drop with Flow Split DF 84971

The measured overall thrust chamber heat transfer and the ratio of the measured-to-predicted heat transfer values are shown in figure 128 for the three chamber pressures evaluated in the tests. In comparison to the fixed-thrust injectors, the dual orifice produces higher thrust chamber heat transfer. With the fixed-thrust injectors heat transfer was generally less than the predicted (theoretical) level established by the Bartz short form equation; however, with the dual orifice injector, heat transfer is generally above the theoretical level.

The data in the lower part of figure 128 show that the ratio of measured-to-predicted heat transfer increased as chamber pressure decreased. At mixture ratio of approximately 5.0 for example, the measured-to-predicted heat transfer ratio ranges from approximately 1.0 at 500-psia chamber pressure to 1.2 at 100-psia chamber pressure.

Figure 129 presents heat transfer data for the separate thrust chamber sections. The figure shows the measured rates to be greater than corresponding predicted levels in the spoolpiece, throat and nozzle sections but considerably less than predicted levels in the chamber section adjacent to the injector.

Table XXIV. Thrust Chamber Heat Transfer Data for Dual Orifice Injector Tests

TEST DESCRIPTION					TEST	CHAMBER SECTION							SPOOLPIECE SECTION							THROAT SECTION							ALTITUDE NOZZLE SECTION						
Test No.	Test Type	Chamber L*	Mixture Ratio	Coolant Inlet Temp.	Parameter	Stave No. 1	Stave No. 2	Stave No. 3	Stave No. 4	Stave No. 5	Stave No. 6	Stave Avg.	Stave No. 1	Stave No. 2	Stave No. 3	Stave No. 4	Stave No. 5	Stave No. 6	Stave Avg.	Stave No. 1	Stave No. 2	Stave No. 3	Stave No. 4	Stave No. 5	Stave No. 6	Stave Avg.	Stave No. 1	Stave No. 2	Stave No. 3	Stave No. 4	Stave No. 5	Stave No. 6	Stave Avg.
18.01	Altitude	52	3.94	528.	$\dot{w}$	1.439	1.398	1.417	1.379	1.390	1.422	1.407	1.546	1.453	1.444	1.453	1.444	1.453	1.465	---	---	---	---	---	---	1.302	1.575	1.561	1.554	1.602	1.576	1.590	1.575
					TBO	557	551	558	---	551	---	554	571	591	---	---	615	598	593	---	---	---	---	---	---	613	---	---	---	---	---	---	598
					TW2	---	---	---	---	---	---	---	---	---	---	---	---	---	---	838	891	1014	1128	---	---	912	---	---	---	---	---	---	---
					Q	40.43	31.70	41.56	---	30.56	---	35.20	64.80	89.79	---	---	124.24	100.18	94.78	---	---	---	---	---	---	110.24	---	---	---	---	---	---	109.55
18.01	Altitude	52	4.67	528.	$\dot{w}$	1.439	1.398	1.417	1.378	1.389	1.422	1.407	1.545	1.452	1.444	1.452	1.444	1.452	1.463	---	---	---	---	---	---	1.305	1.574	1.561	1.550	1.602	1.575	1.589	1.575
					TBO	566	557	565	---	553	---	560	600	626	---	---	624	598	612	---	---	---	---	---	---	636	---	---	---	---	---	---	622
					TW2	---	---	---	---	---	---	---	---	---	---	---	---	---	---	852	937	1027	1126	---	---	986	---	---	---	---	---	---	---
					Q	53.05	39.49	51.69	---	34.05	---	44.37	110.45	141.93	---	---	137.72	101.07	122.40	---	---	---	---	---	---	139.56	---	---	---	---	---	---	146.17
18.01	Altitude	52	5.18	528.	$\dot{w}$	1.439	1.397	1.417	1.378	1.389	1.422	1.407	1.545	1.452	1.444	1.452	1.444	1.452	1.463	---	---	---	---	---	---	1.298	1.574	1.561	1.553	1.601	1.575	1.589	1.575
					TBO	569	556	565	---	553	543	557	612	630	---	---	629	603	619	---	---	---	---	---	---	636	---	---	---	---	---	---	621
					TW2	---	---	---	---	---	---	---	---	---	---	---	---	---	---	840	918	1036	1085	---	---	970	---	---	---	---	---	---	---
					Q	57.71	37.95	51.63	---	33.08	19.48	39.74	128.71	146.44	---	---	144.48	108.02	131.33	---	---	---	---	---	---	139.82	---	---	---	---	---	---	145.96
18.01	Altitude	52	5.37	528.	$\dot{w}$	1.438	1.397	1.416	1.378	1.389	1.422	1.407	1.545	1.452	1.444	1.452	1.444	1.452	1.463	---	---	---	---	---	---	1.303	1.574	1.561	1.553	1.601	1.575	1.589	1.575
					TBO	570	557	563	---	552	540	556	615	631	---	---	628	604	620	---	---	---	---	---	---	636	---	---	---	---	---	---	621
					TW2	---	---	---	---	---	---	---	---	---	---	---	---	---	---	836	921	1039	1069	---	---	966	---	---	---	---	---	---	---
					Q	59.15	39.38	47.76	---	32.07	16.08	38.67	133.34	148.62	---	---	143.51	108.84	132.94	---	---	---	---	---	---	139.94	---	---	---	---	---	---	144.56
18.01	Altitude	52	5.63	528.	$\dot{w}$	1.439	1.398	1.417	1.379	1.389	1.422	1.407	1.545	1.452	1.444	1.452	1.444	1.452	1.463	---	---	---	---	---	---	1.302	1.575	1.561	1.554	1.602	1.575	1.590	1.575
					TBO	569	553	564	---	549	542	555	617	630	---	---	627	609	621	---	---	---	---	---	---	636	---	---	---	---	---	---	618
					TW2	---	---	---	---	---	---	---	---	---	---	---	---	---	---	835	890	1031	1085	---	---	958	---	---	---	---	---	---	---
					Q	58.10	33.59	48.99	---	27.14	18.14	36.95	135.38	146.44	---	---	140.83	116.81	134.20	---	---	---	---	---	---	139.99	---	---	---	---	---	---	140.44
19.01	Altitude	52	4.06	530.	$\dot{w}$	1.440	1.399	1.418	1.379	1.390	1.423	1.407	1.546	1.453	1.445	1.453	1.445	1.453	1.465	---	---	---	---	---	---	1.320	1.576	1.562	1.555	1.603	1.576	1.591	1.577
					TBO	557	557	555	571	---	542	556	557	598	600	---	581	583	584	---	---	---	---	---	---	587	---	---	---	---	---	---	576
					TW2	---	---	---	---	---	---	---	---	---	---	---	---	---	---	691	698	744	794	---	---	732	---	---	---	---	---	---	---
					Q	38.40	37.61	35.10	56.05	---	16.86	36.84	41.74	99.21	101.07	---	73.18	76.23	77.00	---	---	---	---	---	---	74.83	---	---	---	---	---	---	73.01
19.01	Altitude	52	4.67	530.	$\dot{w}$	1.440	1.398	1.418	1.379	1.390	1.423	1.407	1.546	1.453	1.445	1.453	1.445	1.453	1.465	---	---	---	---	---	---	1.322	1.576	1.562	1.554	1.603	1.576	1.591	1.577
					TBO	559	555	554	572	---	540	556	570	601	607	---	587	584	590	---	---	---	---	---	---	594	---	---	---	---	---	---	580
					TW2	---	---	---	---	---	---	---	---	---	---	---	---	---	---	698	716	742	804	---	---	740	---	---	---	---	---	---	---
					Q	41.38	36.15	34.45	57.24	---	14.55	36.79	62.36	103.03	110.99	---	81.52	78.88	87.59	---	---	---	---	---	---	84.32	---	---	---	---	---	---	78.52
19.01	Altitude	52	5.09	529.	$\dot{w}$	1.440	1.399	1.418	1.379	1.390	1.423	1.407	1.546	1.453	1.445	1.453	1.445	1.453	1.465	---	---	---	---	---	---	1.323	1.576	1.562	1.555	1.603	1.576	1.591	1.577
					TBO	559	555	554	571	---	539	556	576	601	606	---	588	585	591	---	---	---	---	---	---	594	---	---	---	---	---	---	580
					TW2	---	---	---	---	---	---	---	---	---	---	---	---	---	---	697	720	740	805	---	---	741	---	---	---	---	---	---	---
					Q	41.12	35.36	34.42	56.64	---	13.54	36.25	71.68	103.62	110.47	---	83.52	79.62	89.93	---	---	---	---	---	---	84.62	---	---	---	---	---	---	78.41
19.01	Altitude	52	5.36	530.	$\dot{w}$	1.439	1.398	1.417	1.379	1.390	1.423	1.407	1.546	1.453	1.445	1.453	1.445	1.453	1.465	---	---	---	---	---	---	1.320	1.575	1.562	1.554	1.602	1.576	1.590	1.575
					TBO	559	557	553	569	---	538	555	577	604	616	---	587	585	594	---	---	---	---	---	---	595	---	---	---	---	---	---	578
					TW2	---	---	---	---	---	---	---	---	---	---	---	---	---	---	694	723	739	797	---	---	738	---	---	---	---	---	---	---
					Q	41.34	37.96	32.74	54.07	---	11.58	35.57	72.05	107.36	124.50	---	81.96	79.46	93.25	---	---	---	---	---	---	85.13	---	---	---	---	---	---	75.42
19.01	Altitude	52	5.61	530.	$\dot{w}$	1.440	1.399	1.418	1.380	1.391	1.423	1.408	1.547	1.453	1.445	1.454	1.445	1.454	1.465	---	---	---	---	---	---	1.322	1.576	1.562	1.555	1.603	1.577	1.591	1.577
					TBO	559	563	553	569	---	535	556	580	607	620	---	589	588	597	---	---	---	---	---	---	594	---	---	---	---	---	---	573
					TW2	---	---	---	---	---	---	---	---	---	---	---	---	---	---	693	725	743	805	---	---	742	---	---	---	---	---	---	---
					Q	42.32	46.32	32.72	53.30	---	6.06	36.19	77.98	111.95	129.81	---	85.09	83.72	97.88	---	---	---	---	---	---	84.77	---	---	---	---	---	---	68.00
21.01	Altitude	52	4.45	528.	$\dot{w}$	1.44	1.40	1.42	1.38	1.39	1.42	1.407	1.55	1.45	1.45	1.45	1.45	1.45	1.465	---	---	---	---	---	---	1.313	1.58	1.56	1.56	1.60	1.58	1.59	1.577
					TBO	540	544	542	557	---	536	544	566	569	---	575	561	550	564	---	---	---	---	---	---	558	---	---	---	---	---	---	548
					TW2	---	---	---	---	---	---	---	---	---	---	---	---	---	---	595	609	629	638	---	---	618	---	---	---	---	---	---	---
					Q	15.73	20.97	18.58	39.38	---	10.59	21.12	58.35	58.82	---	66.69	46.71	30.50	52.06	---	---	---	---	---	---	38.70	---	---	---	---	---	---	30.03
21.01	Altitude	52	4.97	528.	$\dot{w}$	1.44	1.40	1.42	1.38	1.39	1.42	1.407	1.55	1.45	1.45	1.45	1.45	1.45	1.465	---	---	---	---	---	---	1.308	1.58	1.56	1.56	1.60	1.58	1.59	1.577
					TBO	540	544	541	558	---	536	544	569	569	---	573	559	549	564	---	---	---	---	---	---	559	---	---	---	---	---	---	550
					TW2	---	---	---	---	---	---	---	---	---	---	---	---	---	---	598	606	620	624	---	---	613	---	---	---	---	---	---	---
					Q	16.66	21.51	17.38	39.68	---	10.19	21.16	61.79	58.76	---	64.56	44.26	29.97	51.66	---	---	---	---	---	---	39.34	---	---	---	---	---	---	33.37
21.01	Altitude	52	5.59	528.	$\dot{w}$	1.44	1.40	1.42	1.38	1.39	1.42	1.407	1.55	1.45	1.45	1.45	1.45	1.45	1.465	---	---	---	---	---	---	1.320	1.58	1.56	1.56	1.60	1.58	1.59	1.577
					TBO	549	545	542	556	---	537	546	565	568	---	573	565	557	566	---	---	---	---	---	---	558	---	---	---	---	---	---	550
					TW2	---	---	---	---	---	---	---	---	---	---	---	---	---	---	592	601	624	626	---	---	611	---	---	---	---	---	---	---
					Q	28.43	22.40	19.11	36.91	---	11.33	23.64	55.58	56.86	---	64.09	52.14	41.31	53.89	---	---	---	---	---	---	38.00	---	---	---	---	---	---	33.50
21.01	Altitude	52	5.58	528.	$\dot{w}$	1.44	1.40	1.42	1.38	1.39	1.42	1.407	1.55	1.45	1.45	1.45	1.45	1.45	1.465	---	---	---	---	---	---	1.320	1.58	1.56	1.56	1.60	1.58	1.59	1.577
					TBO	553	546	541	565	---	539	549	567	560	---	571	562	561	564	---	---	---	---	---	---	556	---	---	---	---	---	---	554
					TW2	---	---	---	---	---	---	---	---	---	---	---	---	---	---	593	593	608	621	---	---	604	---	---	---	---	---	---	---
					Q	34.76	24.01	17.66	49.59	---	13.78	27.99	58.94	45.29	---	60.50	47.90	46.47	51.65	---	---	---	---	---	---	35.45	---	---	---	---	---	---	39.91
21.01	Altitude	52	5.02	528.	$\dot{w}$	1.44	1.40	1.42	1.38	1.39	1.42	1.407	1.55	1.45	1.45	1.45	1.45	1.45	1.465	---	---	---	---	---	---	1.320	1.58	1.56	1.56	1.60	1.58	1.59	1.577
					TBO	555	553	548	562	---	540	552	568	569	---	570	557	566	566	---	---	---	---	---	---	557	---	---	---	---	---	---	577
					TW2	---	---	---	---	---	---	---	---	---	---	---	---	---	---	593	603	612	625	---	---	608	---	---	---	---	---	---	---
					Q	37.19	34.06	26.85	46.42	---	15.30	31.97	60.27	58.37	---	59.47	40.32	53.51	54.23	---	---	---	---	---	---	36.98	---	---	---	---	---	---	75.83
21.01	Altitude	52	4.51	528.	$\dot{w}$	1.44	1.40	1.42	1.38	1.39	1.42	1.407	1.55	1.45	1.45	1.45	1.45	1.45	1.465	---	---	---	---	---	---	1.320	1.58	1.56	1.56	1.60	1.58	1.59	1.577
					TBO	558	551	547	560	---	543	552	566	566	---	569	562	566	566	---	---	---	---	---	---	554	---	---	---	---	---	---	582
					TW2	---	---	---	---	---	---	---	---	---	---	---	---	---	---	592	601	606	623	---	---	606	---	---	---	---	---	---	---
					Q	42.59	31.33	25.03	43.35	---	20.23	32.46	58.09	53.62	---	58.68	47.47	53.66	54.17	---	---	---	---	---	---	32.98	---	---	---	---	---	---	83.88

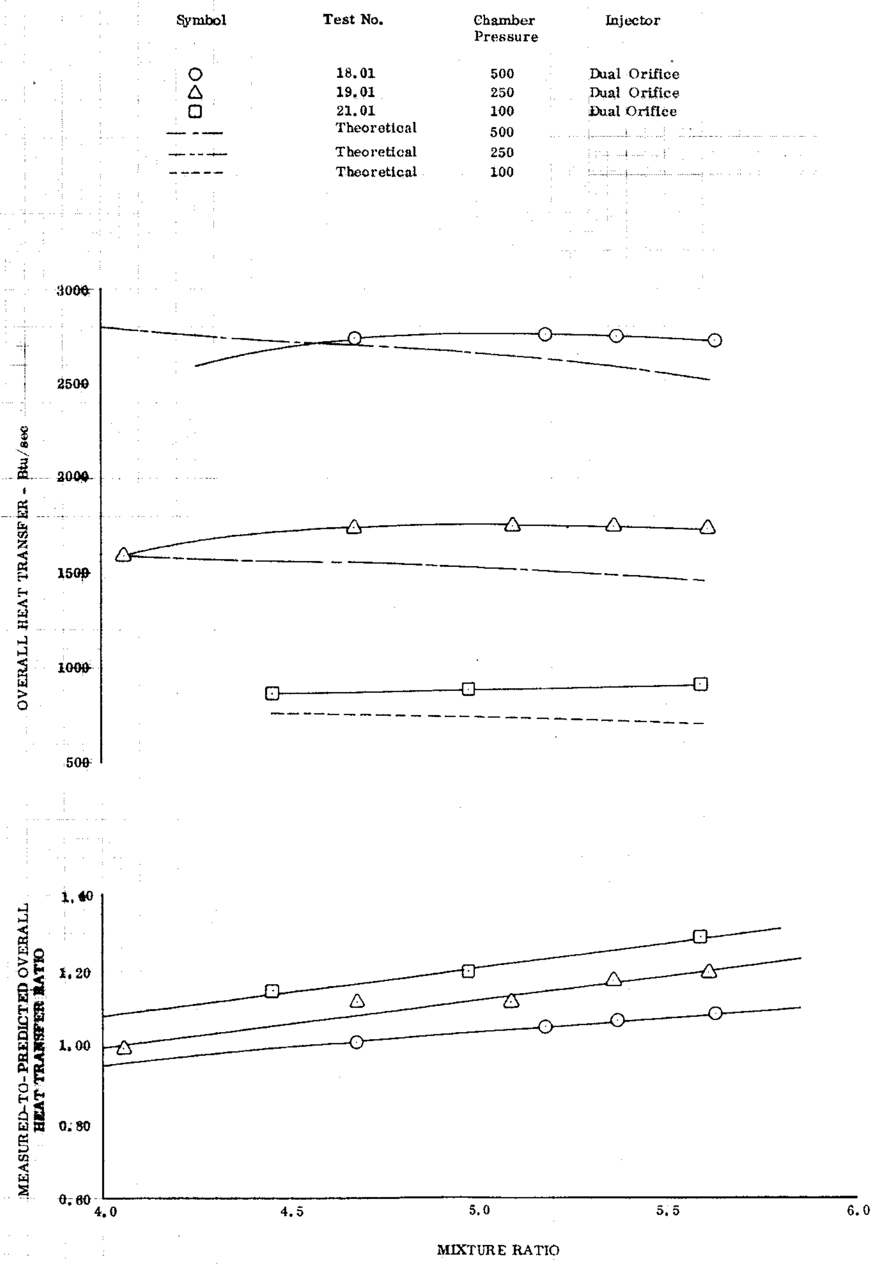

Figure 128. Overall Thrust Chamber Heat Transfer for Dual Orifice Injector

DF 84979

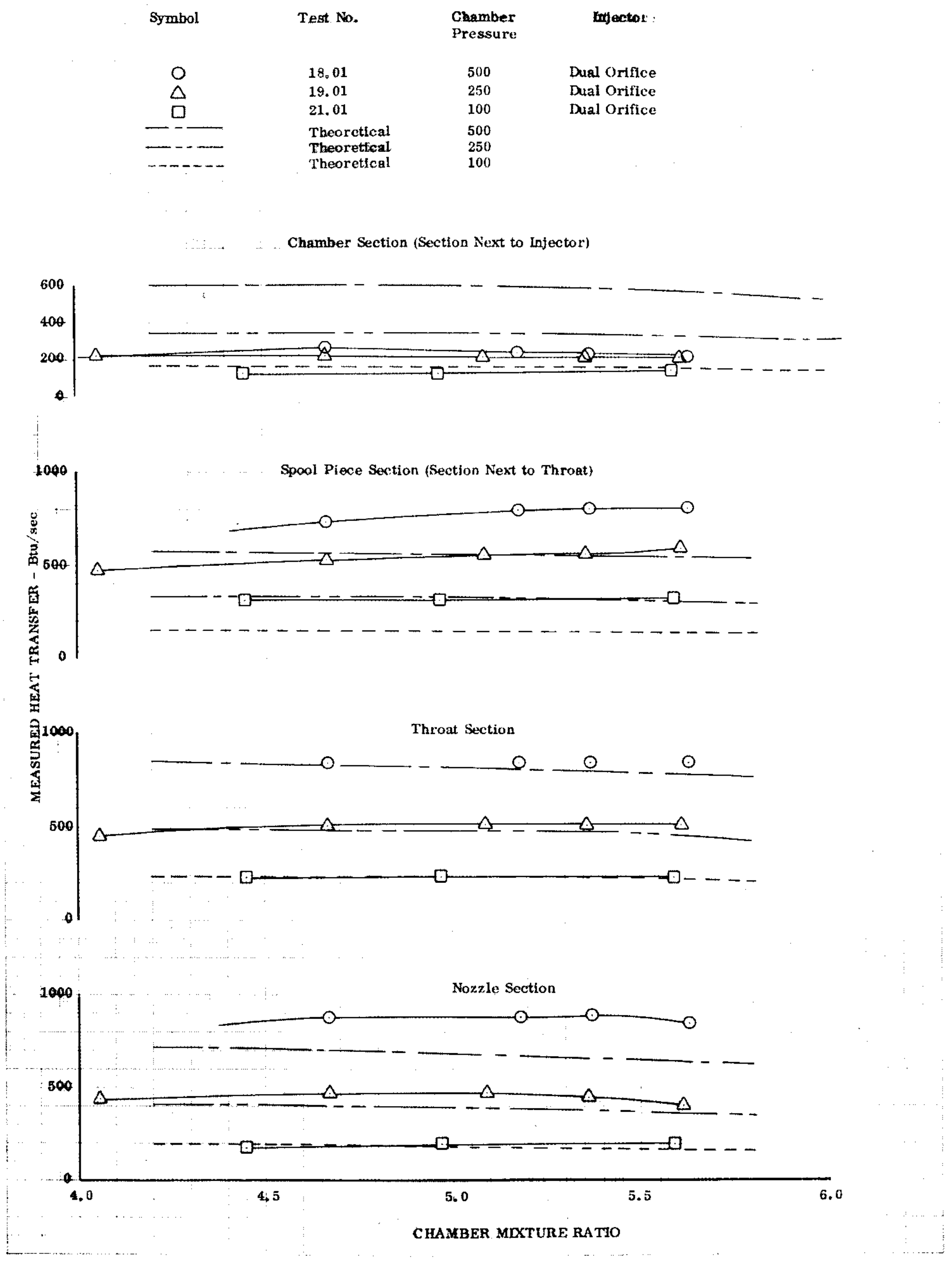

Figure 129. Thrust Chamber Section Heat Transfer For Dual Orifice Injector DF 84978

F. HARDWARE DURABILITY

The dual orifice injector demonstrated excellent durability. In tests 18.01 through 21.01, 295 sec of firing time was accumulated without damage. Figure 130 shows the injector after test 21.01.

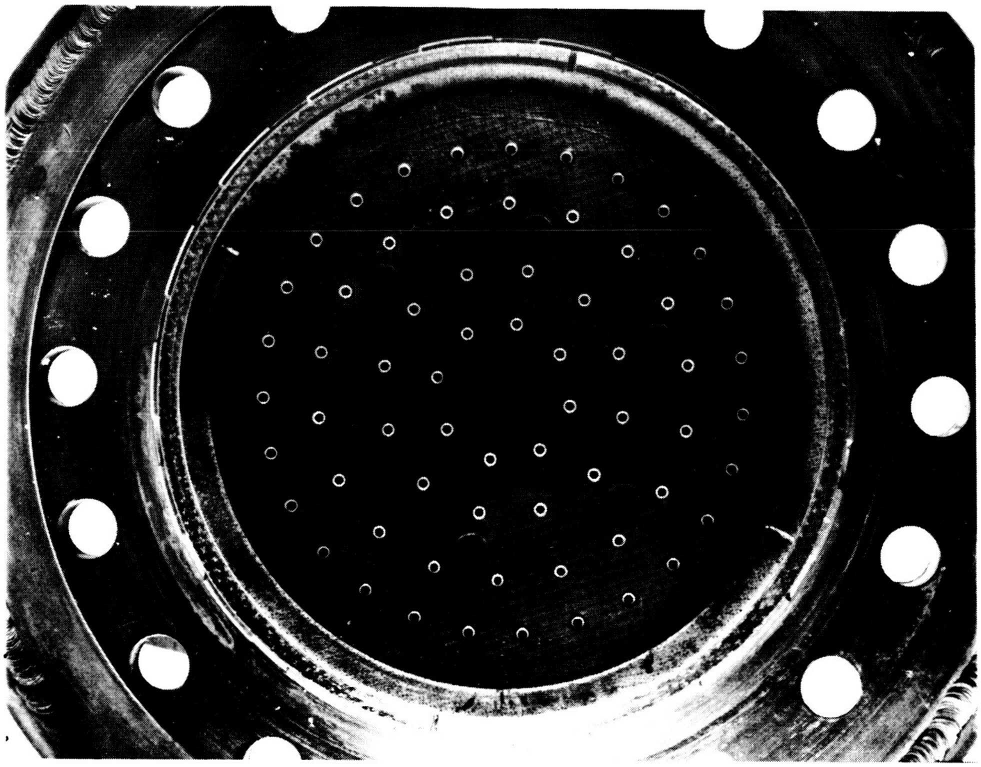

Figure 130. Dual Orifice Injector after Testing FE 104113

The throat section of the three piece regenerative chamber was used in the dual orifice tests. It was water-cooled and there was no damage. Figure 131 illustrates the post-run condition; the total firing time accumulated with this throat section in fixed-thrust and throttling injector tests is 419 sec.

The other chamber hardware provided acceptable durability. The 60 to 1 expansion ratio nozzle functioned without incident; however two minor problems were encountered with the combustion chamber sections. One of these occurred after test 19.01 when the spool section had to be replaced because a leak check of its cooling jacket revealed several small interior leaks between the staves in the area of the coolant exit manifold flange. A post-test inspection showed erosion in the same area. The erosion and leaks are attributed to overheating resulting from excessively long transverse land areas at the end of the spool-section cooling passages. The chugging-type combustion instability that prevailed in test 20.02 caused the other hardware problem. Approximately 25 sec into that test, two chamber pressure tap fittings and connecting instrumentation tubes were burned out. The test was terminated quickly enough after the burnouts occurred so that damage was confined to the chamber pressure taps and tubes. Subsequently the tubes were removed and the taps welded closed so that testing could be continued.

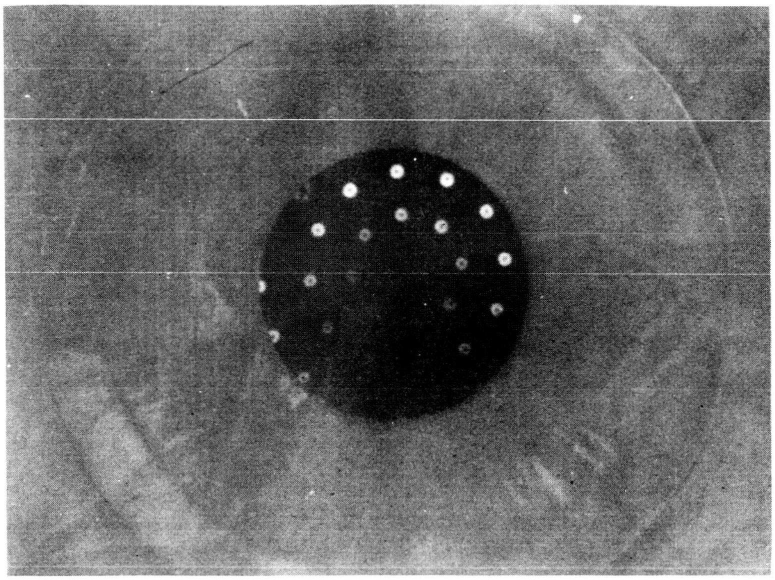

Figure 131. Throat Section from Three-Piece Regenerative Chamber after 419 Seconds Firing Time FD 48052

APPENDIX A
THRUST CHAMBER HEAT TRANSFER AND STRESS ANALYSIS

A. HEAT TRANSFER ANALYSIS

1. General

Analysis and design of the regenerative and water-cooled thrust chambers were similar. In both cases, the thrust chamber contour was preselected, and the objective was to determine the coolant passage configuration. For the regenerative thrust chamber, the passage configuration that provided tolerable wall temperatures with minimum coolant pressure loss was selected. The coolant passage geometry for the water-cooled chamber was selected so that the water coolant temperature rise was measurable and the wall temperatures acceptable.

For both chambers, candidate coolant passage configurations were evaluated with the aid of an IBM-360 computer until a preferred configuration was selected. Inputs and outputs for the computer program are given in table XXV. The analysis performed by the computer included an iterative stepwise solution of the continuity, energy, momentum, and state equations, solved together with a heat balance equation to determine the coolant conditions and wall temperatures along the thrust chamber contour.

Table XXV. Heat Transfer Computer Program Parameters

Known Parameters (Input)	Calculated Parameters (Output)
Combustion side heat transfer profile	Coolant conditions
Adiabatic wall temperature profile	Wall temperature profiles
Coolant passage configuration	Heat flux profile
Coolant flowrate and inlet conditions	
Coolant properties	

Before giving the equations used, several important aspects of the heat transfer analysis, including the selection of the combustion side and coolant side heat transfer coefficients, and the fin analysis employed for the web between passages are discussed.

In designing the water-cooled and regenerative cooled thrust chamber, different combustion side heat transfer coefficients were used. For the water-cooled chamber design, the simplified Bartz short form equation (reference 19) was used to compute the combustion side heat transfer coefficients. This equation was selected because it provides coefficients for flox/methane that closely agree with those computed using more rigorous boundary layer equations. It is also simple to apply because it is a closed-form equation. Use of the rigorous methods, which involves stepwise numerical integration of the open-form boundary layer equations, was not considered to be warranted because the injector design has such a significant effect on heat transfer that minor errors, introduced by use of the simplified Bartz equation, are small in comparison. For the regenerative cooled thrust chamber design, the coefficients derived from the water-cooled chamber test data for the highest performing injector (the converging fuel stream injector with a 40-scfm faceplate) were used. The coefficient profiles used in the design of the two chambers are compared in figure 132.

On the coolant side, the chemical machining process used to etch the passages in THERMAL SKIN ® chambers causes roughness of a sand-like nature that must be accounted for in the heat transfer calculations. Roughness measurements have been made for copper, nickel, Inconel, and stainless steel. For these materials the measured rms roughness values (ϵ) ranged from 90 to 150 μin. These values compare with rms roughness values of 60 or less for smooth surfaces. Because of the combined effect of this roughness and small coolant passages, the relative roughness (expressed as a ratio of the rms roughness value to the hydraulic diameter of the coolant passage, ϵ/D) is large and hence has an augmentation effect on the coolant side coefficient. The coolant coefficient equation of Dipprey and Sabersky (reference 20), was selected as the most representative for this application, since it was based upon experimental data obtained in tubes having various degrees of sand-grain roughness. The equation represents an extension of Nikuradse's classical work (reference 21), involving roughness and its effects on friction and velocity profiles, into the heat transfer area.

No enhancement factor for the coolant side coefficients to account for throat curvature was used because of a lack of published experimental data showing this to be a significant phenomenon for high Reynolds No. flow in noncircular, hydraulically rough passages of small hydraulic diameters.

The heat transfer conduction through the THERMAL SKIN wall was computed by treating the webs between the coolant passages as fins and applying a one-dimensional fin equation developed by Kraus (reference 22). This fin analysis assumes rectangular passages and a uniform temperature across the web (figure 133). In the combustion chamber and throat regions, where the heat fluxes were high, a two-dimensional heat transfer conduction analysis was used to determine wall temperatures. In these two-dimensional analyses, the actual passage shape, i.e., the corner passage radii, was analyzed.

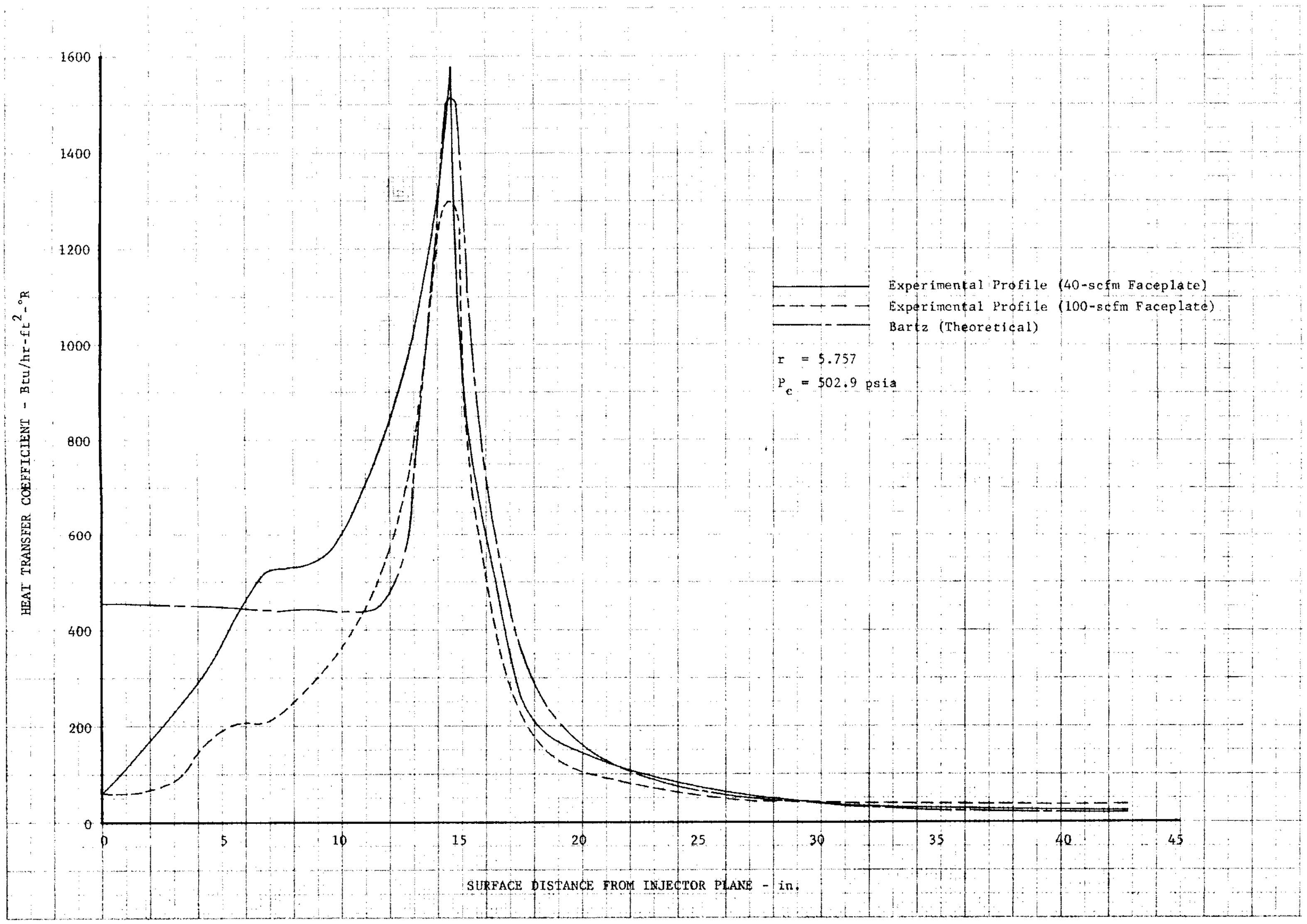

Figure 132. Combustion-Side Heat Transfer Coefficient Profiles

DF 68258

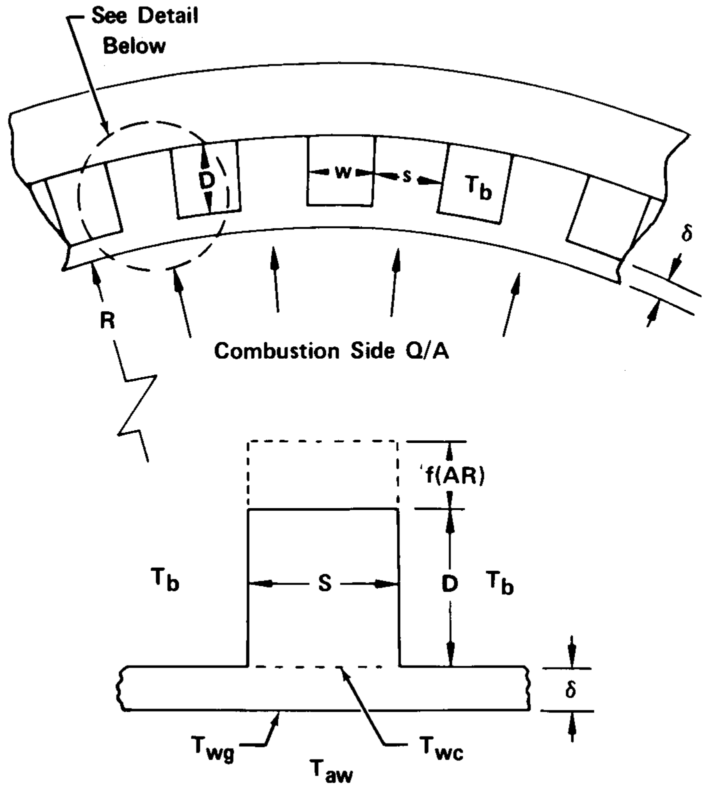

Figure 133. Equivalent Fin Based on Passage Web Dimensions FD 44523A

2. Analysis

The equations used in the heat transfer analysis are presented below. For an incremental section of a coolant passage, as shown in figure 134, the continuity, energy, momentum, and state equations can be written as follows:

Continuity equation

$$\dot{M} = \text{constant}$$

Energy equation

$$H_j = H_{j-1} + \frac{\Delta Q}{\dot{M}} + \left(\frac{dP}{dX}\right) \frac{\Delta X}{\bar{\rho}_b J}$$

Momentum equation

$$\frac{dP}{dX} = -\frac{4\bar{f}_h}{DH} \left(\overline{VH}\right) - \frac{\dot{M}\left(U_j - U_{j-1}\right)}{g_c \bar{A}\, \Delta X}$$

where

$$\overline{VH} = \left(\frac{\dot{M}}{\bar{A}}\right)^2 \frac{1}{2g_c \bar{\rho}_b}$$

and

$$f_h = f\left(\frac{\mu_w}{\mu_b}\right)^{40f} \sqrt{\frac{\rho_w}{\rho_b}}$$

State equation

$$P = P(T_b, \rho_b)$$

The bars over the parameters refer to average values for the increment ΔX.

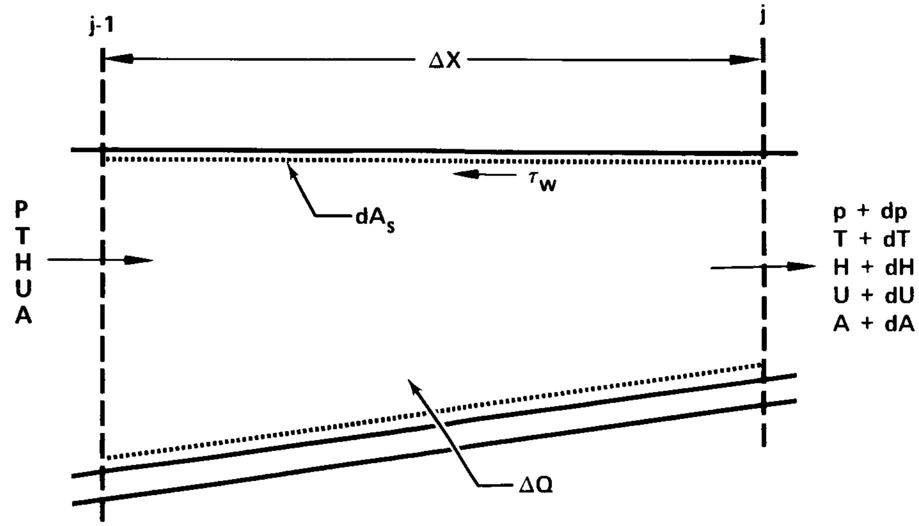

Figure 134. Coolant Flow Passage Element FD 23426A

The friction factor f_h is the isothermal friction factor corrected for heat transfer based on the work of reference 23. Pressure drops caused by sudden expansions and contractions in the flow area were treated by incompressible flow equations.

The transport and thermodynamic properties of the coolant required to solve the equations were "built" into the computer programs in the form of equations and tables. Properties of water were obtained from reference 24. Properties of methane used in the design of the regenerative cooled thrust chamber design were documented as part of the contracted program and given in the Interim Report, reference 1.

For each increment of the thrust chamber, a one-dimensional heat balance equation was solved to determine the wall temperatures, which can be written as:

$$\frac{q}{A} = (T_{Aw} - T_{wg})\, h_g = (T_{wg} - T_{wc})\, \frac{k_w}{\delta} = (T_{wc} - T_b)\, h_c A'$$

where

$$h_c = St \left(\frac{T_b}{T_{wc}}\right)^{0.55} C_{Pb} \left(\frac{\dot{M}}{N_s A}\right)$$

The Stanton number as mentioned earlier is based on the Dipprey and Sabersky equation. The constants in the equation were modified to correspond to those experimentally determined in reference 25. The Stanton number equation is:

$$St = \frac{f/2}{0.92 + \sqrt{f/2}\left[4.7(\epsilon^*)^{0.2} (Pr_b)^{0.44} - A(\epsilon^*)\right]}$$

where

$$\epsilon^* = Re_b \sqrt{f/2}\, (\epsilon/DH)$$

$$A(\epsilon^*) = \sqrt{2/f} + 2.5 \ln(2\epsilon/DH) + 3.75$$

The term ϵ in the equations is the measured passage surface roughness. The isothermal friction factor was obtained by performing iterative calculations for the function shown in figure 135. The dimensionless terms ϵ^* and $A(\epsilon^*)$ are used to correlate the friction factor data normally presented on a Moody Diagram.

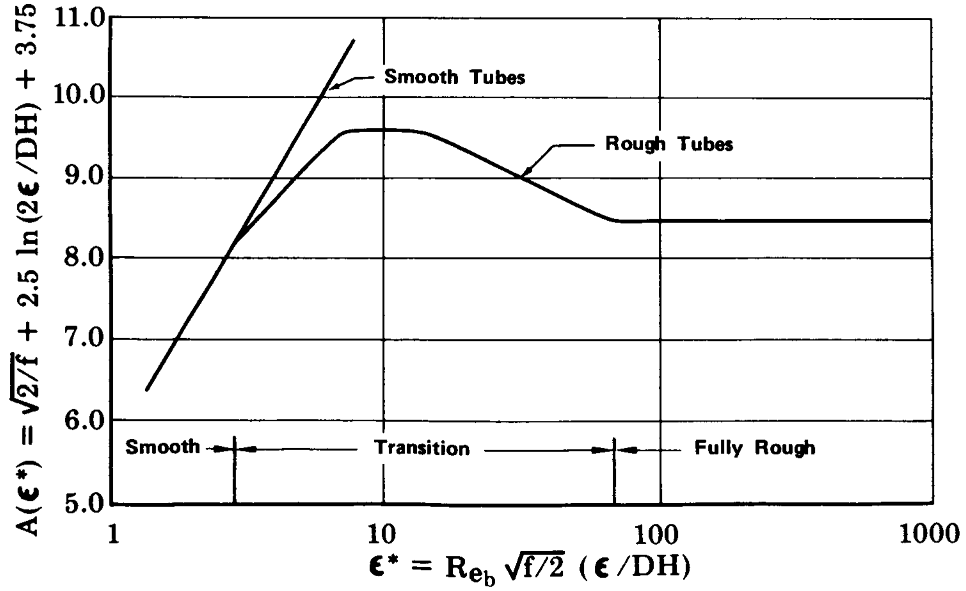

Figure 135. Friction Similarity Function FD 23422

The term, A', represents the ratio of the combustion side-to-coolant side heat transfer area. It accounts for the heat transfer effect due to the web between passages by employing Kraus' one-dimensional fin equation defined as follows:

$$A' = \frac{A_w + A_f \, \eta_{fin}}{A}$$

where

$$\eta_{fin} = \frac{\tanh M}{M}$$

$$M = \left[D + w(AR)\right]\sqrt{\frac{2h_c}{K_w S}}$$

$$A = 2\pi R$$

$$A_w = W \cdot N_s$$

$$A_f = 2\left[D + W\,(AR)\right] N_s$$

Figure 133 shows the equivalent fin geometry in terms of the above symbols. The term AR is used to control the amount of the passage back wall which effectively transfers heat. The value of this term is based upon two-dimensional studies and is a function of the conductivity of the back wall material. For low conductivity back wall materials such as stainless steel or Inconel, AR = 0 gives the best agreement with two-dimensional calculations.

B. COOLANT PASSAGE STRESS ANALYSIS

After the coolant passage geometry had been sized by heat transfer calculations, a stress analysis was performed. Stresses of concern were bending and shear stresses in the combustion side wall, the bond (or web) stress level and thermal stresses. Because the THERMAL SKIN chambers (the water-cooled as well as the regenerative cooled chambers) were of constant depth and constant hot wall designs, the stress analysis dictated the minimum land widths and the maximum passage widths.

The equation used in the analysis and the allowable stresses are as follows:

Bending Stresses

$$\sigma_B = \frac{Pw^2}{2\delta^2}\,; \qquad \sigma_B \leq \sigma_y \text{ for hot wall material}$$

where σ_y is the material yield strength.

Shear Stresses

$$\sigma_s = \frac{Pw}{2\delta} \;;$$

$\sigma_s \leq 0.57\, \sigma_u$ for hot wall material

where σ_u is the material ultimate strength.

Web Tensile Stresses

$$\sigma_T = \frac{Pw}{S} \;;$$

$\sigma_T \leq \sigma_y$ for hot wall material

also

$\sigma_T \leq$ braze and diffusion bond strength.

Thermal Stresses

$$\sigma_{TH} = \frac{\left[\alpha_1 (Tw_1) - \alpha_2 (Tw_2)\right] E_1}{1 + \dfrac{\delta_1 E_1}{\delta_2 E_2}}$$

The bending stress equation was derived from a fixed-end, uniform load beam analysis with bending about fixed ends. The shear and web tensile stress equations were derived considering the coolant pressure forces. The thermal stress equation is introduced because the back wall and the combustion side wall are not at the same temperature. All stresses were calculated assuming square corner passages. Because etched passages have rounded corners, this assumption yields a conservative design approach where maximum passage widths are set by bending stress considerations.

Allowable stress levels for bending, shear, and web stresses were established in a conventional manner. For bending stresses the allowable stress was taken to be the yield strength; the allowable shear stress was calculated as 57% of the ultimate strength; and the allowable web tensile stress corresponded to the lower value of either yield strength (for the combustion side material) or the bond strength.

Establishment of an allowable thermal stress was not straightforward. In the regenerative cooled chamber, the thermal stresses exceed the yield strengths for practially the entire chamber length because of the large temperature difference between the combustion side wall and the back wall. These thermal stresses will not necessarily cause failure, but the wall will be in the plastic region of the stress-strain curve. Hence, at these thrust chamber locations, another stress criterion was established for design. This was accomplished as follows: Because the wall is in the plastic region, it was assumed that the wall could not support a bending stress and, therefore, it deflects into a circular arc with the coolant pressure acting normal to it at every location. For this assumed plastic model a failure analysis was developed that relates the deflection angle of the plastic front wall to a pressure loading parameter given in figure 136. As noted in this figure, front wall failure occurs with this model at the pressure loading parameter value of X = 155 and deflection angle of θ = 132 deg. At this point, the front wall is no longer able to resist the pressure load because of the rapid thinning that occurs. Thus is proceeds to failure in a manner similar to hoop failure in a tube.

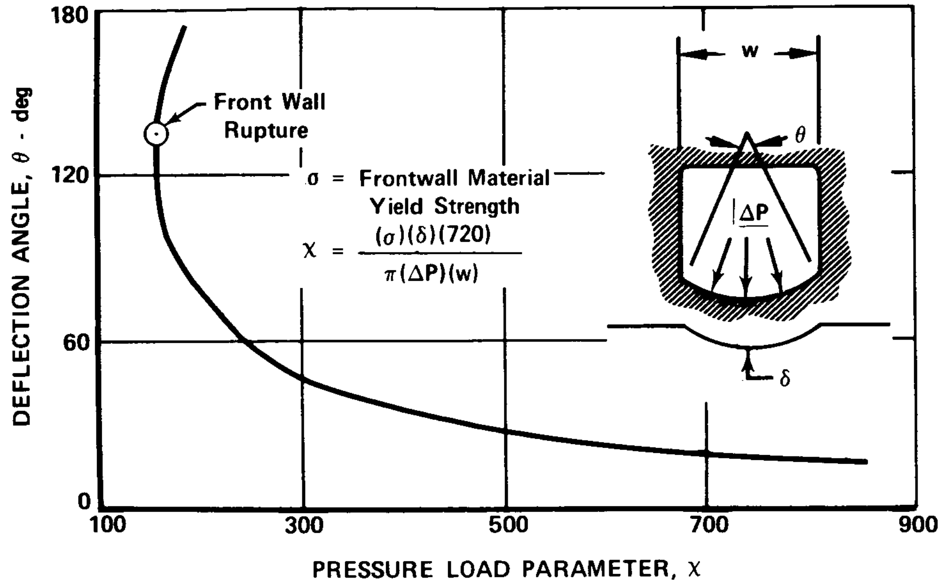

Figure 136. THERMAL SKIN® Hot Wall Plastic Deflection

FD 44522A

This analysis has been programmed as part of the heat transfer calculation and is currently employed in place of the bending and shear equations originally used. By incorporating this equation in the heat transfer calculation, it is possible to account for the reduction in coolant coefficient and resulting increase in wall temperature caused by the increased flow area in an unfailed but deflected passage.

Figure 137 is a plot of the resulting predicted passage failure pressure for Nickel 200, as a function of mean wall temperature and passage geometry.

In this analysis the passages are assumed to have square corners. This assumption results in pessimistic (large) deflections and hence the use of the analysis to determine maximum allowable passage width provides a conservative passage design.

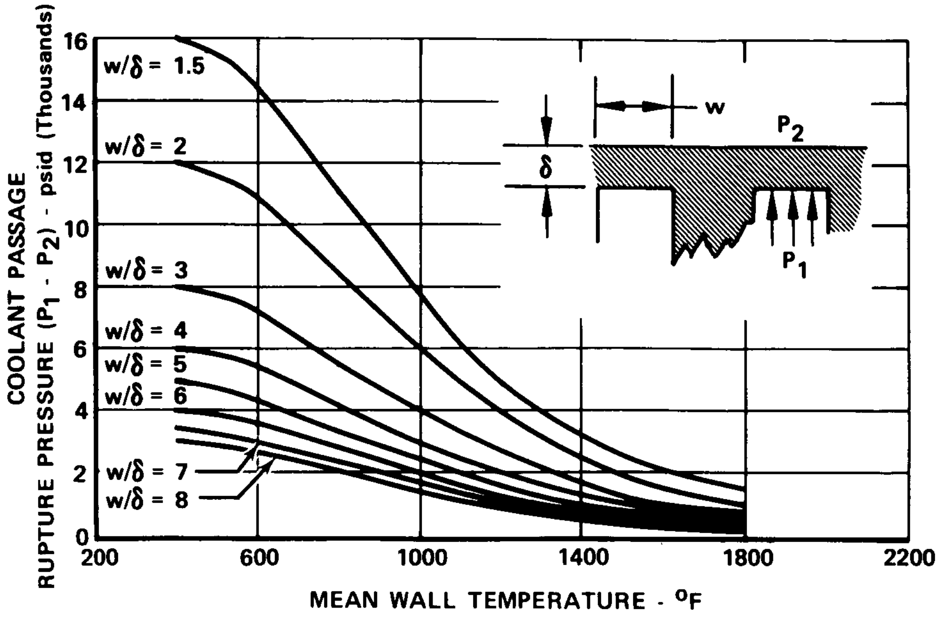

Figure 137. THERMAL SKIN® Combustion-Side Wall Rupture Limit FD 44529B

APPENDIX B
TEST FACILITIES AND PROPELLANT HANDLING

A. TEST FACILITIES

1. General

All combustion firing tests in the program were made in the Liquid Propellant Research Facility (LPRF). This facility is used for all testing operations at the Florida Research and Development Center requiring significant quantities of liquid fluorine or flox. The LPRF (figure 138) has four separate horizontal firing bays for 1000-, 5000-, 15,000-, and 50,000-lb_f thrust, and a component test loop. (See figure 139.)

The flox/methane thrust chamber tests conducted under the program were made in the 15,000-lb_f thrust firing bay. This bay and the 5000-lb_f thrust bay are connected to a continuous altitude-simulating, steam-driven ejector system. The system includes the following equipment: (1) supersonic exhaust diffusers located at the two firing positions which expel combustion products into a common crossover duct, (2) a tube-in-shell water-cooled heat exchanger that cools the combustion gases, (3) two steam ejectors that pump the gases to atmospheric pressure, and (4) a scrubber-condenser that condenses the steam and removes hydrogen fluoride. The capability of the ejector system to maintain exhaust pressure below 0.3 psia during hot testing assured full expansion of the 60 to 1 area ratio chambers tested in the program.

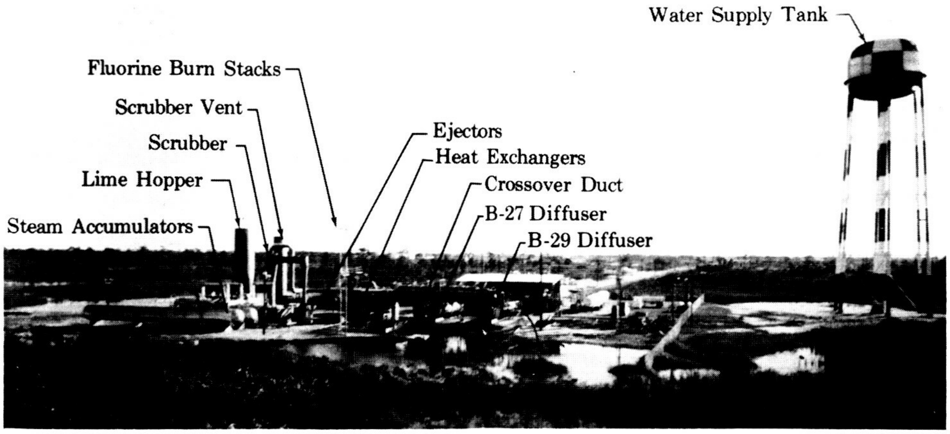

Figure 138. Liquid Propellant Research Facility FD 19750A

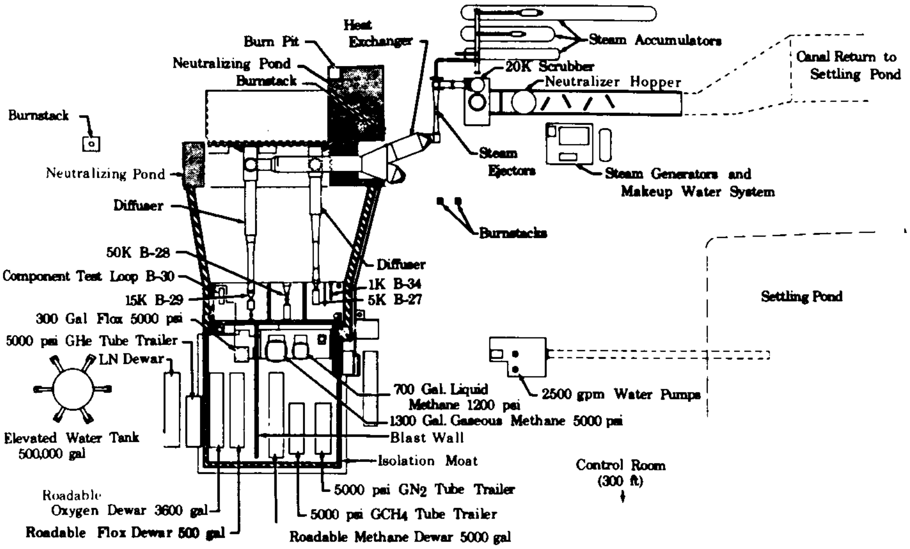

Figure 139. Liquid Propellant Research Facility Schematic FD 12808C

2. Test Stand Setup

a. Water-cooled Chamber Tests

(1) Fixed-Thrust Injectors

The test stand setups for the water-cooled chamber tests made with the fixed-thrust injectors are shown in figure 140. Both sea level and altitude tests were made; the setups were identical except that in the sea level tests, the 60 to 1 nozzle extension and its associated water supply manifolds were not used. Propellants and the water coolant were pressure-fed to the test rig. Flox was supplied from a 300-gal. oxidizer run tank. Ambient temperature methane gas was supplied from a 1300-gal. fuel run tank, which was backed up by a 1475-gal. tube trailer. The methane gas was heated to approximately 840° R in a steam heat exchanger, located in the fuel run line just upstream of the injector.

The chamber cooling water was supplied from a 700-gal. tank. The water flow was split and metered by calibrated cavitating venturis located in the inlet lines to each thrust chamber section. Six venturis were used with each section. Because the venturis were supplied from the same tank at approximately 1000 psia, the venturis were of different sizes to provide the required coolant flowrates to the chamber, throat, and nozzle stave segments. The venturi sizes and flowrates were as follows:

	Venturi, Throat Diameter, in.	Average Stave Flowrate, lb_m/sec	Total Section Flowrate, lb_m/sec
Chamber	0.098	1.01	6.06
Throat	0.120	1.43	8.58
Nozzle	0.106	1.15	6.90

Orifices were used in the coolant exit manifold to provide a back pressure of approximately 600 psia, which was high enough to prevent film boiling in the coolant passages, but low enough to provide an adequately high pressure drop across the venturis to ensure cavitation.

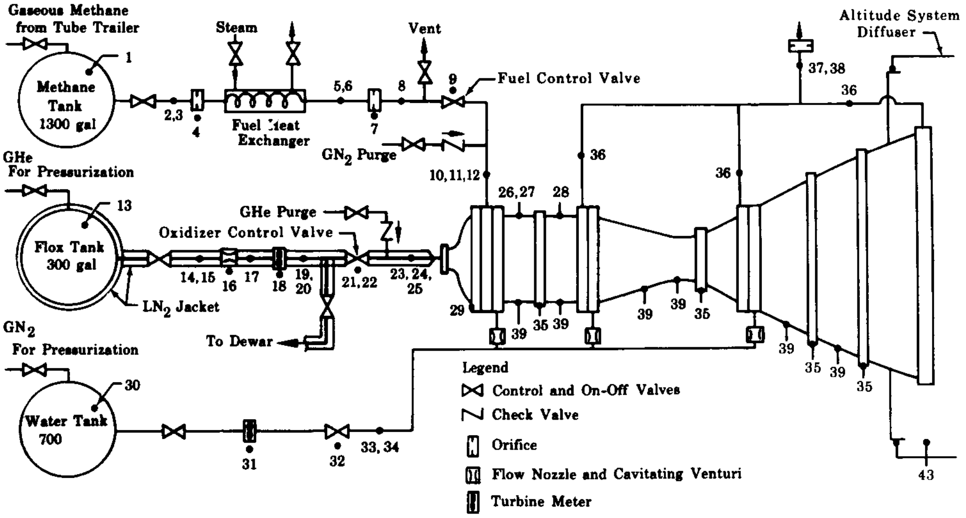

Figure 140. Test Stand Schematic for Fixed-Thrust Injector, Water-Cooled Chamber Tests

FD 23893B

(2) Throttling Injector

In the dual orifice injector tests, the stand setup was slightly different than that used with the fixed-thrust injectors, as indicated in figure 141. Methane was supplied directly from a tube trailer while the 1300-gal. tank was used for the water supply. The most significant difference was in the oxidizer injector supply where a flow divider valve was installed to vary the dual orifice injector primary-to-secondary flow split. Water flowrates were increased for the tests by enlarging the cavitating venturis and by raising the water tank pressure to 1200 psia. Because the throat section of the 3-piece regenerative chamber was used in the tests and because it did not have provisions for separately supplying its six staves, cavitating venturis were not used for the throat. The cavitating venturi sizes and flowrates used with the chamber and nozzle sections were as follows:

Section	Venturi Throat Diameter, in.	Stave Flowrate, lb_m/sec	Total Section Flowrate, lb_m/sec
Chamber (2 required)	0.122	1.41	8.46
Nozzle	0.120	1.59	8.54

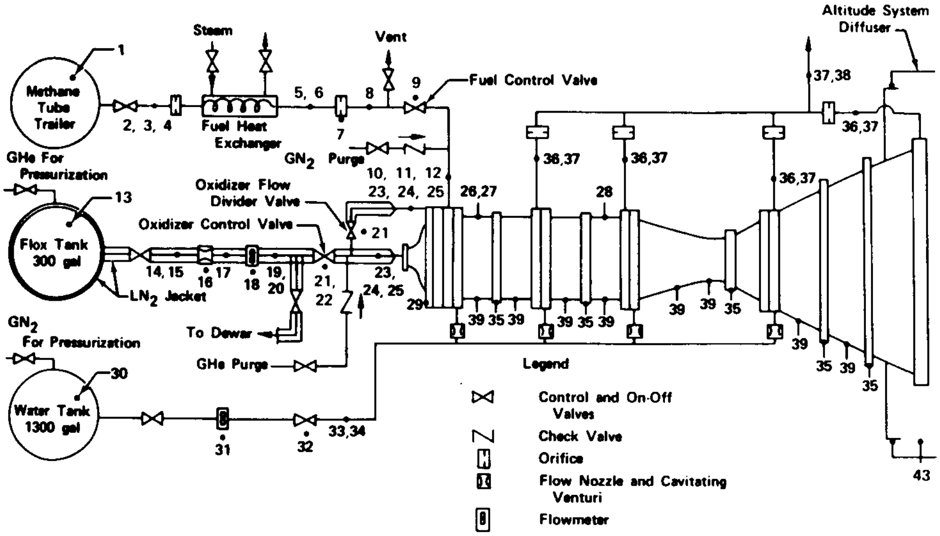

Figure 141. Test Stand Schematic for Dual Orifice Injector, Water-Cooled Chamber Tests

FD 23893D

b. Regenerative Chamber Test Setups

The test stand piping arrangements for the separately cooled methane and regeneratively cooled chamber tests are shown in figures 142 and 143. The oxidizer supply system was identical in all arrangements and the same as that used in water-cooled chamber tests. In separately cooled chamber tests at sea level and altitude conditions, liquid methane for cooling the thrust chamber was supplied from a 1300-gal. run tank. The methane coolant was vented downstream of the chamber. Gaseous methane fuel, heated to approximately 840°R in the steam heat exchanger, was separately supplied to the injector from a high pressure tube trailer.

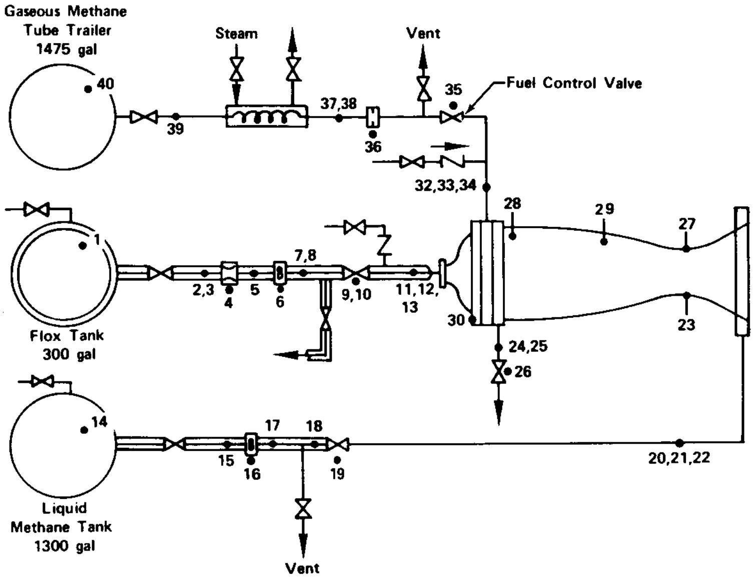

a. Sea Level

FD 27944A

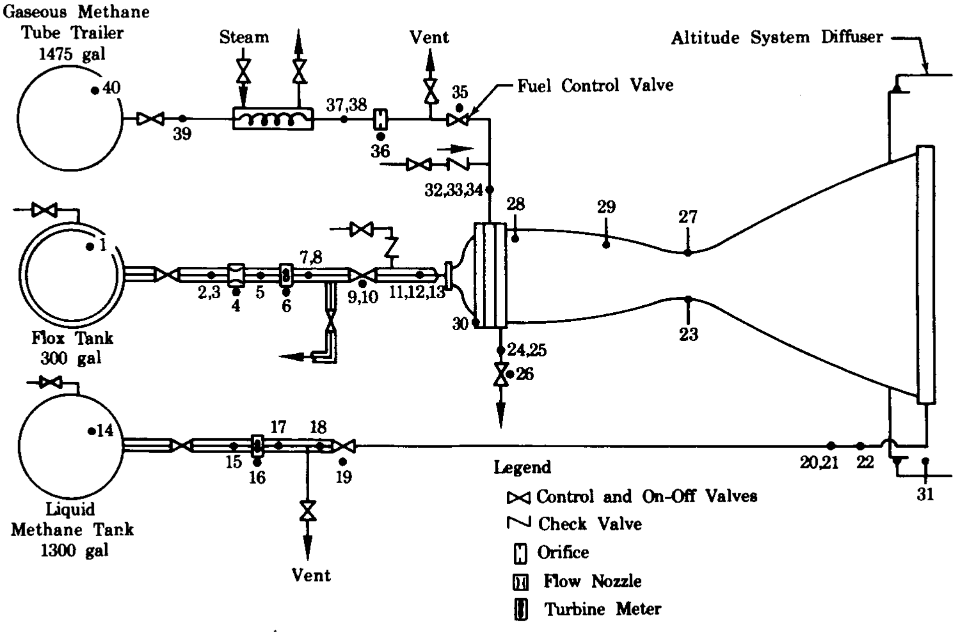

b. Altitude

FD 27944

Figure 142. Test Stand Schematics for Methane Separately Cooled Tests

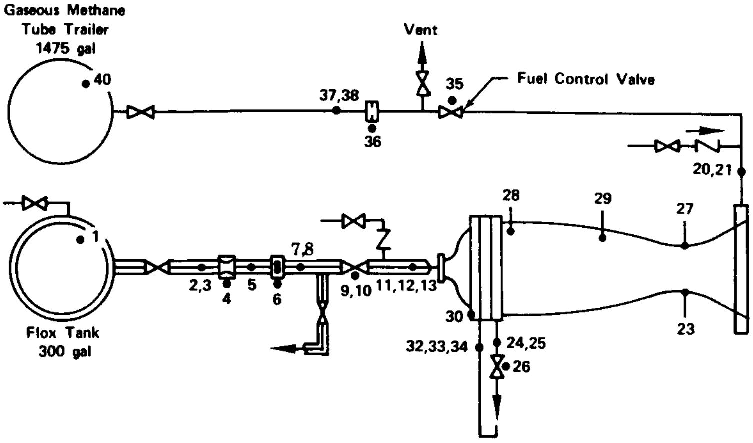

a. Sea Level FD 27944B

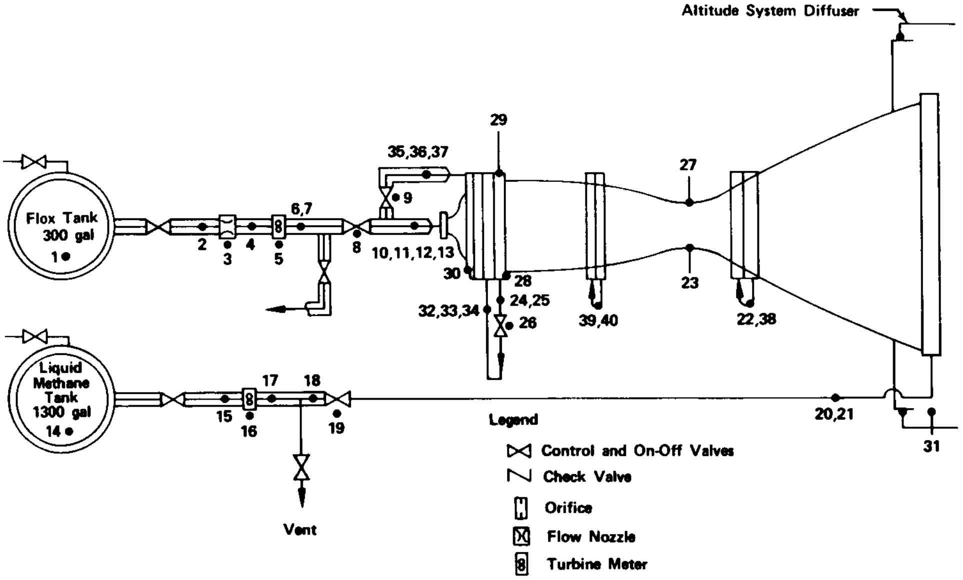

b. Altitude FD 27945A

Figure 143. Test Stand Schematics for Regeratively Cooled Chamber Tests

In the regenerative tests with the full length thrust chamber, liquid methane was supplied to the thrust chamber, while in the sea level regenerative tests, ambient temperature methane gas was provided to the chamber as coolant. In both cases, the separate injector fuel supply was deleted and methane was fed to the injector from the thrust chamber cooling jacket.

3. Test Stand Controls

An automatic closed-loop control system consisting of an analog computer, digital sequencer, and the test stand-mounted electro-hydraulic valves, was used for control of test firing events. Figure 144 is a partial view of the LPRF control room showing the analog computer. Using various control references such as flowrate, chamber pressure, and mixture ratio, the computer can control up to 10 functions. The sequencer has capabilities for operating up to 40 relay channels in 1-msec increments over a time interval of 2000 sec.

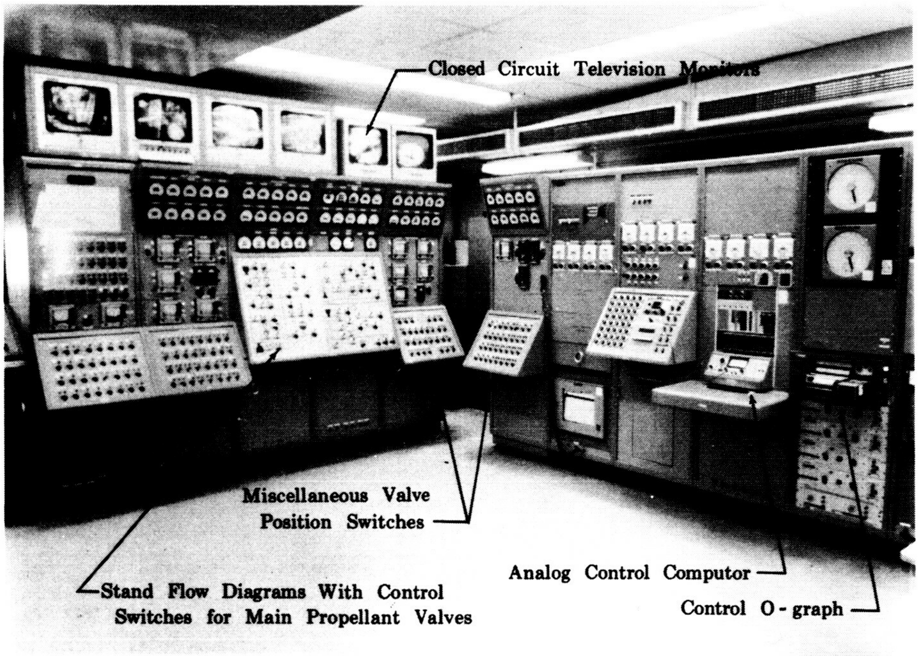

Figure 144. LPRF Control Room FD 19756

Control sequencing for each of the various types of tests was established during cold flow tests using the actual fuel (methane), but with liquid nitrogen substituted for the oxidizer. The control modes used in water-cooled chamber tests with the fixed-thrust and dual orifice injectors are shown in figures 145 and 146, respectively. The tests were similar except for the sequencing of the flow divider valve in the dual orifice tests. This valve was on position control during the tests. It was preset for test startup and during a given test, the flow split between the primary and secondary injector were varied by changing its position.

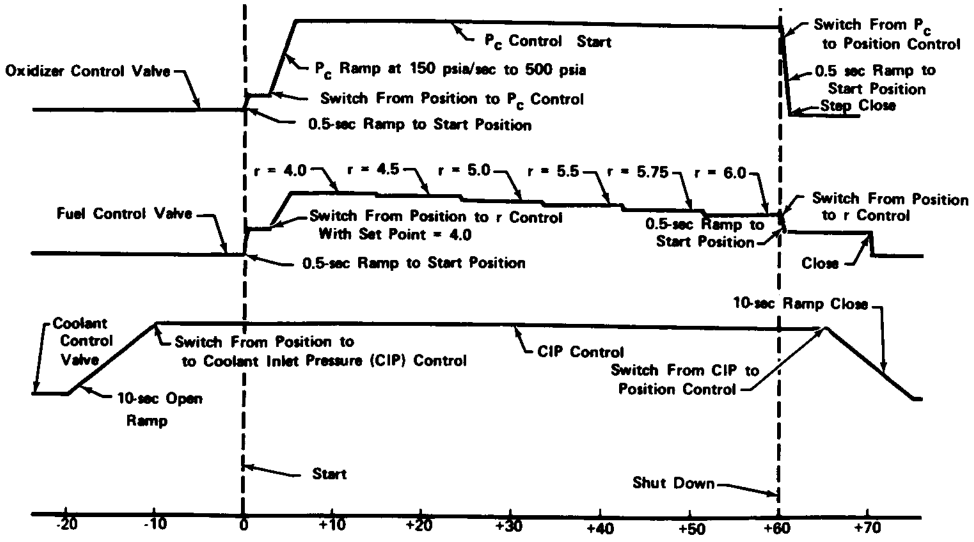

Figure 145. Sequence of Test Events for Water-Cooled Chamber Tests with Fixed-Thrust Injectors

FD 44524

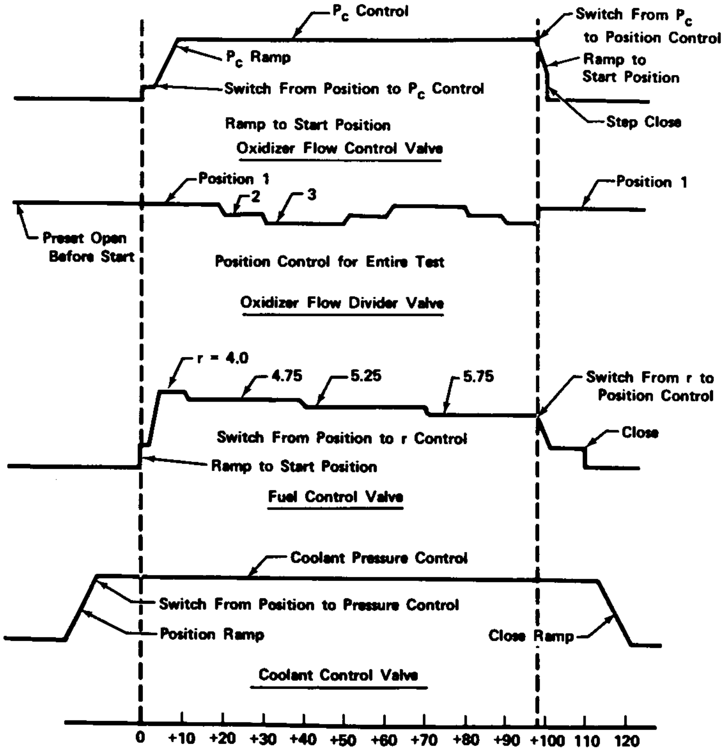

Figure 146. Sequence of Events for Water-Cooled Chamber Tests with Dual Orifice Injector

FD 43164

In both the fixed-thrust and dual orifice injector tests the water coolant flow was started approximately 20 sec before start of the propellant flows. The oxidizer and fuel control valves were ramped on position control modes at startup to set points that provided a mixture ratio of 4.0 at approximately 100-psia chamber pressure. Both valves remained in their respective positions until a flow of liquid oxidizer was established at the injector. Then the control system was switched to a chamber pressure-mixture ratio control mode and chamber pressure was ramped at approximately 150 psia/sec to the desired level while maintaining the mixture ratio at 4.0. The oxidizer valve controlled chamber pressure and the fuel valve controlled mixture ratio. The mixture ratio set point was changed in steps during the tests so that data were obtained over approximately a 4 to 6 mixture ratio range.

In separately cooled methane tests, jacket coolant flow was established at the steady-state level before propellants were supplied to the injector. For tests with the full length chamber, cold flow tests were conducted with the objective of determining a sequence that would initiate injector flow after stable coolant flow was attained, but before the cooling jacket contained a significant amount of liquid, to avoid a significant upset of the coolant conditions at startup from the rapid application of heat flux. The coolant inlet valve controlled flowrate and the coolant discharge valve controlled jacket exit pressure at a preset level. The injector propellant control scheme used for the separately cooled tests was almost identical to that described for the water-cooled tests (figure 147a).

In regenerative tests, a fuel lead was used. The inlet fuel valve was opened to establish a low level fuel flow through the chamber and the injector before the oxidizer control valve was opened. Other control modes used in the regenerative tests were similar to those of the water-cooled and separately cooled chamber tests (figure 147b). The fuel lead was 8 and 2 sec in the altitude and sea level tests respectively.

The test stand sequencer was used in all tests to schedule the control system computer and to provide automatic go/no-go checks of critical parameters. The go/no-go checks consisted of either continuous or intermittent sampling of critical parameters to determine if the test could be continued safely or if it should be advanced to shutdown. Examples of these checks are given below.

1. To verify ignition early in each test, the continuity of a weighted wire hanging in the center of the exhaust nozzle was checked. The time required for the wire to burn through was known and therefore provided a repeatable verification of timely ignition.

2. After stable operation had been attained, chamber pressure was sampled continuously to ensure that it was above a minimum level which would result if severe test rig damage or a facility malfunction occurred.

3. The electrical continuity of a leak detection system that was used to provide an instant indication of leaks in the test stand or test rig fluorine plumbing, was continuously monitored.

4. For simulated altitude tests, a check of maximum diffuser pressure was used to ensure that the exhaust pressure did not exceed the incipient separation level of the 60 to 1 area ratio nozzles.

5. In the regenerative tests, the fuel injector pressure drop was sampled prior to opening the oxidizer valve to ensure flow through the coolant jacket at start.

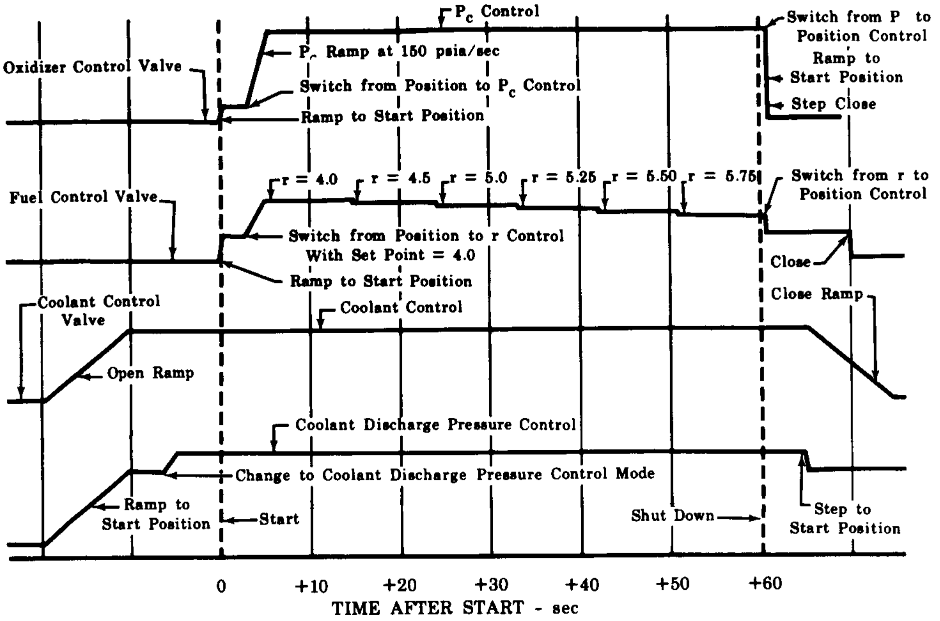

a. Separately Cooled FD 27946

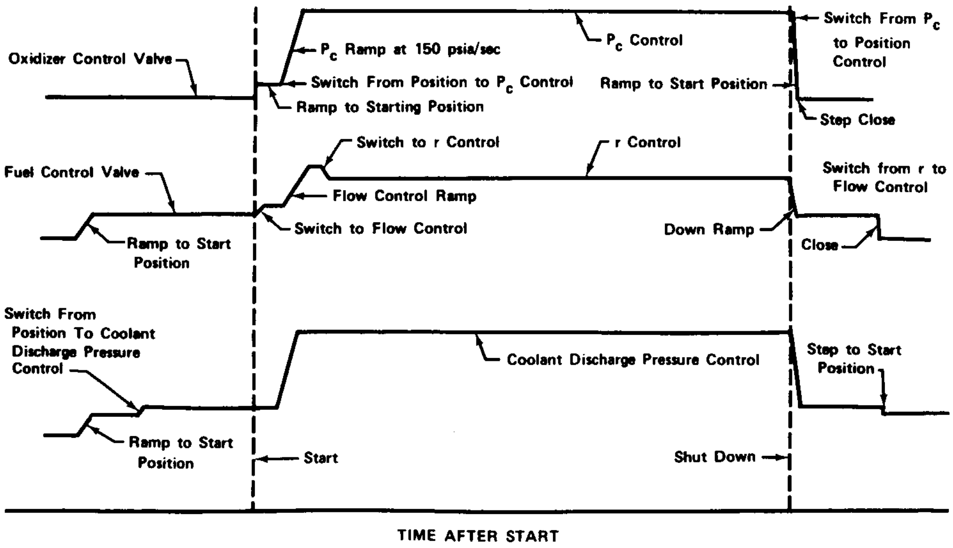

b. Regeneratively Cooled FD 44537

Figure 147. Sequence of Events for Regenerative Chamber Tests

A number of purges were used to prevent contamination of the test rig prior to test and to ensure clearing of propellants at shutdown. With the exception of those for the injector, the purges were controlled by valves that were sequenced off during the starting transient and were opened as the run valves were closed.

Injector purges remained on throughout the test and relied on redundant check valves to prevent backflow. This technique permitted continuous, high volumetric purge flows through the injector to prevent aspiration of combustion products into the injector manifolds during normal test transients and unexpected emergency shutdowns. Helium and nitrogen were used as purges for the oxidizer and fuel injectors respectively.

4. Data Acquisition

The LPRF central data acquisition system (figure 148) is capable of recording the outputs of up to 135 measurement channels from either of the four firing bays. Excellent recording accuracy and response are available through a 100-channel, low level input, analog-to-digital converter. The converter feeds a magnetic tape system at sampling rates of 80 scans/sec to provide a data sample from each channel every 0.0125 sec. The records from the digital recorder were used for performance determination. Two 18-channel oscillographs and 14 channels of direct-inking strip charts are also available and were used primarily for monitoring critical parameters during tests and analysis of transient behavior. To protect the regenerative chamber, selected wall temperatures were monitored on strip charts during testing. Several tests were advanced to shutdown when wall temperatures exceeded a predetermined safe value.

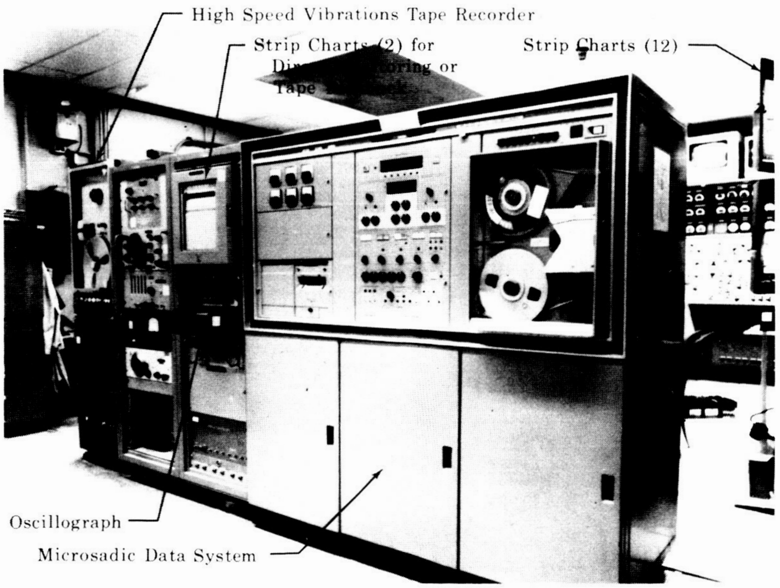

Figure 148. LPRF Data Recording Equipment FD 19757A

Tables XXVI and XXVII give the instrumentation and the recording methods used in the tests. The locations of the instrumentation for the various test configurations are shown on figures 140 through 143.

Continuous remote test observation was possible through the use of six closed-circuit television channels with individual monitors; color film coverage was provided by three high speed cameras.

B. PROPELLANT HANDLING

1. Flox

The oxidizer in this program was liquid flox with a nominal fluorine concentration of 82.6%. The same procedures used for operation with liquid fluorine were used in handling the flox mixtures. Detailed descriptions of fluorine handling procedures used by P&WA are presented in references 5 and 26.

The LPRF, where all large scale liquid fluorine and flox operations at the Florida Research and Development Center are conducted, is west of all other test facilities and takes advantage of the prevailing easterly winds to carry fluorine vapors and reaction products away from inhabited areas.

Transfers of fluorine or flox at the LPRF are accomplished remotely from the control room, which is located about 300 ft east of the test stands. Except for the supplier delivery vehicles which are equipped with manual valves, all fluorine systems, including the roadable Dewars used for storage, are equipped with remotely operated valves.

In the LPRF, rigorous standards of materials selection, fabrication, cleaning, passivation, and leak detection are followed for fluorine test facility design and operations. Metals of proven fluorine compatibility are used. Full penetration welds are employed wherever possible in lieu of mechanical joints. Facility valves are of the top entry, solid body type, having copper braid rings and Teflon chevron stem packings arranged as shown in figure 149. Test stand fluorine systems are cleaned after installation and or modifications by flushing with an acidic solvent followed by demineralized water and vacuum drying. After cleaning, the systems are passivated using gaseous fluorine. Subsystems and components, such as instrumentation transducers, are individually passivated before installation. In addition, prior to each test the facility was passivated using gaseous fluorine at 15 psig. During this passivation, a complete sniff check was made on all fluorine joints and valve stems.

Table XXVI. Instrumentation for Water-Cooled Chamber Tests

No.	Item	Digital Recorder	Oscillograph	Strip Chart	Gage
1*	Fuel Run Tank Pressure				X
2	Fuel Orifice Upstream Pressure	X			
3	Fuel Orifice Upstream Temperature (CC)**	X			
4	Fuel Orifice Differential Pressure	X(2)			
5	Fuel Heat Exchanger Exit Temperature (CA)**	X	X	X	
6	Fuel Heat Exchanger Exit Pressure	X	X		
7	Fuel Orifice Differential Pressure	X(2)	X		
8	Fuel Control Valve Inlet Pressure	X			
9	Fuel Control Valve Position	X			
10	Fuel Injector Inlet Pressure	X	X		
11	Fuel Injector Inlet Temperature (CA)	X			
12	Fuel Injector Differential Pressure	X	X		
13	Oxidizer Run Tank Pressure				X
14	Oxidizer Flow Nozzle Inlet Pressure	X			
15	Oxidizer Flow Nozzle Inlet Temperature (R)	X			
16	Oxidizer Flow Nozzle Differential Pressure	X(2)	X	X	
17	Oxidizer Flow Nozzle Exit Temperature (R)	X	X		
18	Oxidizer Volumetric Flowrate	X(2)		X	

*Numbers refer to locations shown on test stand schematic

**CC = Copper-Constantan thermocouples; CA = Chromel-alumel thermocouples; R = Resistance-type temperature probe

Table XXVI. Instrumentation for Water-Cooled Chamber Tests (Continued)

No.	Item	Digital Recorder	Oscillograph	Strip Chart	Gage
19	Oxidizer Turbine Meter Exit Temperature (R)	X			
20	Oxidizer Control Valve Inlet Pressure	X			
21	Oxidizer Control Valve Position	X			
22	Oxidizer Control Valve Body Temperature (CC)	X			
23	Oxidizer Injector Inlet Temperature (R)	X	X		
24	Oxidizer Injector Inlet Pressure	X			
25	Oxidizer Injector Differential Pressure	X			
26	Chamber Pressure - Upstream Taps	X(2)	X	X	
27	Chamber Pressure - High Frequency Transducer	X(2)	Tape Recorder		
28	Chamber Pressure - Downstream Taps	X(2)			
29	Thrust	X(2)	X		
30	Coolant Tank Pressure				X
31	Coolant Flowrate	X(2)	X		
32	Coolant Control Valve Position	X			
33	Coolant Inlet Manifold Pressure	X	X	X	
34	Coolant Inlet Manifold Temperature (CC)	X			
35	Coolant Bulk Temperature (CC)	X(12)			
36	Coolant Exit Stave Temperatures (CC)	X(18)			
37	Coolant Exit Manifold Temperature (CC)	X	X	X	
38	Coolant Exit Manifold Pressure	X		X	

Table XXVI. Instrumentation for Water-Cooled Chamber Tests (Continued)

No.	Item	Digital Recorder	Oscillograph	Strip Chart	Gage
39	Chamber Hot-Wall Temperatures (CA)	X(12)		X(12)	
40	Calculated Fuel Flow (From Control System)	X		X	
41	Calculated Mixture Ratio (From Control System)	X		X	
42	Sequencer Time	X	X		
43	Nozzle Exit Pressure	X(4)	X	X	

Table XXVII. Instrumentation for Regenerative Chamber Tests

No.	Item	Digital Recorder	Oscillograph	Strip Chart	Gage
1*	Oxidizer Run Tank Pressure				X
2	Oxidizer Flow Nozzle Inlet Pressure	X			
3	Oxidizer Flow Nozzle Inlet Temperature (R)**	X			
4	Oxidizer Flow Nozzle Differential Pressure	X(2)			
5	Oxidizer Flow Nozzle Exit Temperature (R)	X			
6	Oxidizer Volumetric Flowrate	X(2)	X	X	
7	Oxidizer Turbine Meter Exit Temperature (R)	X			
8	Oxidizer Supply Line Temperature (R)				X
9	Oxidizer Control Valve Position	X	X		
10	Oxidizer Control Valve Body Temperature (CC)	X			
11	Oxidizer Injector Inlet Temperature (R)	X	X		

*Numbers refer to locations shown on test stand schematics.

**R = Resistance-type temperature probe; CC = Copper-constantan thermocouples; CA = Chromel-alumel thermocouples

Table XXVII. Instrumentation for Regenerative Chamber Tests (Continued)

No.	Item	Digital Recorder	Oscillograph	Strip Chart	Gage
12	Oxidizer Injector Inlet Pressure	X			
13	Oxidizer Injector Differential Pressure	X	X	X	
14	Coolant Tank Pressure				X
15	Coolant Turbine Meter Inlet Pressure	X		X	
16	Coolant Volumetric Flow	X(2)	X		
17	Coolant Turbine Meter Outlet Temperature (R)	X			
18	Coolant Control Valve Inlet Temperature (R)	X			
19	Coolant Control Valve Position	X	X		
20	Coolant Inlet Manifold Pressure	X		X	
21	Coolant Inlet Manifold Temperature (R)	X	X	X	
22	Instrumented Passage Flow Orifice ΔP	X(3)			
23	Coolant Bulk Temperature (CA)	X(36)***			
24	Coolant Outlet Manifold Temperature (CA)	X	X	X	
25	Coolant Outlet Manifold Pressure	X	X	X	
26	Coolant Outlet Control Valve Position	X			
27	Chamber Wall Temperature (CA)	X(36)***		X(6)	
28	Chamber Pressure - Upstream Taps	X(2)	X	X	
29	Chamber Pressure - Downstream Taps	X(2)	X		

***These totals are the number of T.C.'s available; not all of these were recorded in each test because of data system limitations.

Table XXVII. Instrumentation for Regenerative Chamber Tests (Continued)

No.	Item	Digital Recorder	Oscillograph	Strip Chart	Gage
30	Thrust	X(2)	X		
31	Nozzle Exit Pressure	X(4)	X	X	
32	Fuel Injector Differential Pressure	X			
33	Fuel Injector Inlet Temperature (CA)	X			
34	Fuel Injector Inlet Pressure	X			
35	Fuel Control Valve Position	X	X		
36	Fuel Orifice Differential Pressure	X(2)	X		
37	Fuel Orifice Inlet Pressure	X	X		
38	Fuel Orifice Inlet Temperature (CA)	X			
39	Fuel Heat Exchanger Inlet Temperature (CC)	X			
40	Fuel Tube Trailer Pressure				X
41	Fuel Weight Flow (calculated)	X			
42	Mixture Ratio (calculated)	X		X	

For use in the program, flox was obtained premixed and by mixing at FRDC. One 5000-lb batch of premixed flox was received; however, flow samples taken at FRDC revealed that the fluorine concentration was excessively high, so lox had to be added at FRDC to bring it within acceptable limits (82.6% ± 0.5%). At FRDC liquid flox was prepared in a nitrogen-jacketed roadable dewar by adding liquid oxygen and liquid fluorine while the dewar was mounted on load cells. The weight of each constituent added was determined from total dewar weight monitored and recorded in the control room. The concentration established by weighing was then verified by chemical analyses. Samples for analysis were taken after the entire flox batch was transferred to the oxidizer run tank and twice recirculated back to the roadable vessel to ensure a uniform mixture. Samples were obtained by trapping liquid flox in a nitrogen-jacketed chamber. After trapping the liquid sample, the nitrogen flow to the jacket was secured, a valve to an evacuated bottle was opened, and the sample was permitted to warm and evaporate until the system came to equilibrium.

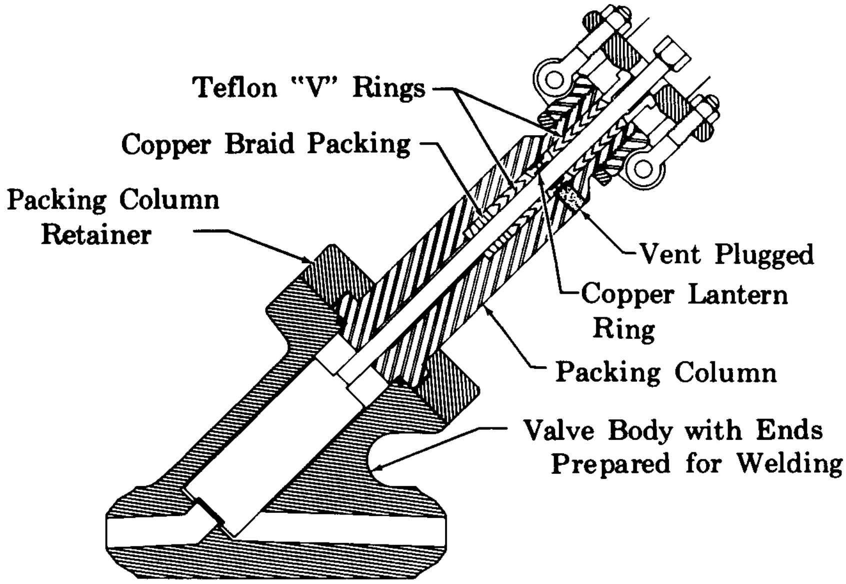

Figure 149. Liquid Fluorine Facility Valve FD 25686

Flox concentration of the vaporized sample was determined by laboratory analysis using the wet chemistry, mercury absorption technique. This method of analysis is one of the oldest techniques for the determination of fluorine concentration. It is based upon the rapid absorption of fluorine gas by elemental mercury to reduce the pressure of a gaseous sample. The quantity of fluorine absorbed is determined by measurement of the pressure and volume of the sample before and after absorption.

The mercury-absorption apparatus developed and used at FRDC is shown schematically in figure 150. It uses a fluorine compatible pressure transducer to automatically record the pressure of the sample within a constant volume system. In operation, a portion of the vaporized flox sample was transferred into the evacuated reaction chamber. The reference initial pressure was established at this point and the recorder was set at 100%. A measured quantity of mercury was then allowed to flow into the reaction chamber. The pressure immediately decayed as the fluorine was absorbed by the mercury. A magnetic stirrer for the mercury was provided to disperse the inert interface of mercury fluoride, which forms on the mercury surface, and thereby to assure complete absorption. When complete absorption was indicated (by a leveling of the pressure trace on the recorder), the reaction flask was opened to an evacuated expansion coil having a volume equal to the volume of the mercury added; thus the system was returned to its original volume. The pressure recorder then indicated directly the percentage of sample that was not absorbed. With this apparatus, duplicate analyses of samples in the range of 63%-93% fluorine have shown a repeatability of 0.23%.

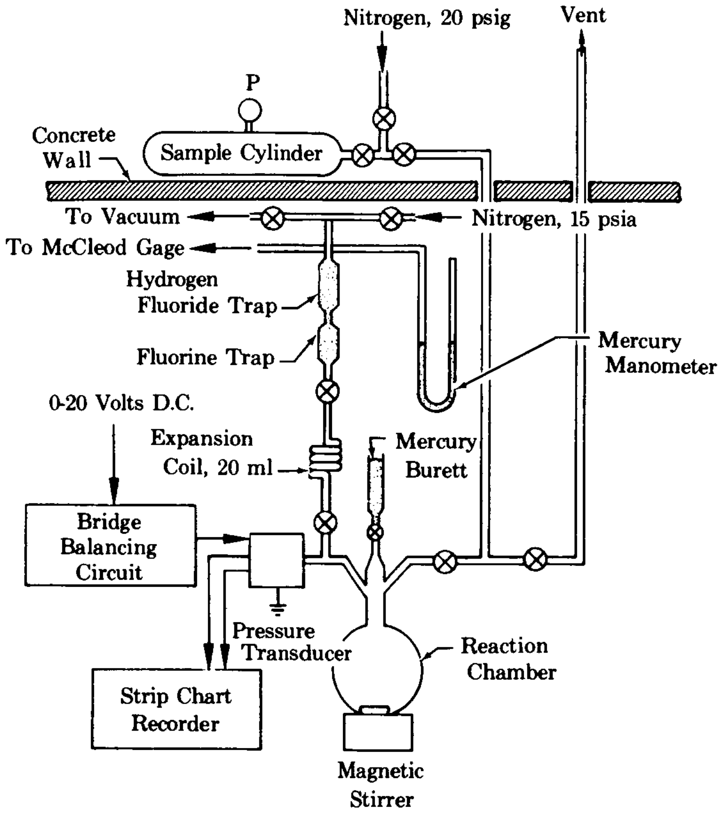

Figure 150. Schematic Diagram of Mercury Absorption Apparatus FD 19753

2. Methane

Methane was purchased as a liquid in vacuum-jacketed roadable dewars. Gaseous methane was made from the liquid as required. Methane presented no unusual handling problems, so methods commonly used for flammable gases and cryogenic liquids were used.

APPENDIX C
DATA REDUCTION AND PERFORMANCE CALCULATIONS

A. DATA ACQUISITION

The low-level input digital recording system at the Liquid Propellant Research Facility was used during tests to obtain magnetic tape records of all measured parameters at a scanning interval of 0.0125 seconds. A high speed IBM System 360-Model 65 digital computer was used to reduce the recorded data to engineering units and to calculate the time-based averages that are used for steady-state performance determination. Maximum, minimum, and 3σ levels of the recorded data within the period of the average are printed out concurrently with the average to provide a convenient reference for critical review of parameter stability. Oscillograph, strip chart, and scan-to-scan digital data are also reviewed to ensure parameter stability.

B. PERFORMANCE ANALYSIS

Performance parameters not directly measured and the methods used for their determination are described in the following paragraphs.

1. Thrust

a. Sea Level Thrust Chamber Tests

Vacuum thrust for chambers tested at sea level conditions was determined from measured thrust using the relation:

$$F_{vac} = F_{meas} + P_a A_e$$

b. Altitude Thrust Chamber Tests

The supersonic diffuser described in Appendix B was used to simulate altitude conditions in all tests of the 60:1 expansion ratio thrust chambers. The altitude test thrust chambers were mounted so that a portion of the expansion nozzle projected into the diffuser (figure 151). A low leakage slip seal was provided at the diffuser entrance to allow free axial nozzle translation. For tests in the altitude system, the vacuum thrust equation was as follows:

$$F_{vac} = F_{mea} - P_{diff} (A_s - A_e) + P_a A_s$$

2. Thrust Chamber Throat Total Pressure

Throat total pressures were determined from an injector face tap and a chamber tap located just upstream of the throat. Determination of throat total pressures from the two taps involved different methods. For the downstream tap, the measured value corresponds to a static pressure which was converted to a total pressure by multiplying by 1.015 (the total-to-static pressure ratio from one-dimensional isentropic flow relationships for the chamber contraction ratio of 4). The pressure measurement at the injector face tap represents a total pressure before combustion. It was reduced to a throat total pressure by multiplying by 0.9862 to account for a momentum loss of 1.38% determined from reference 14.

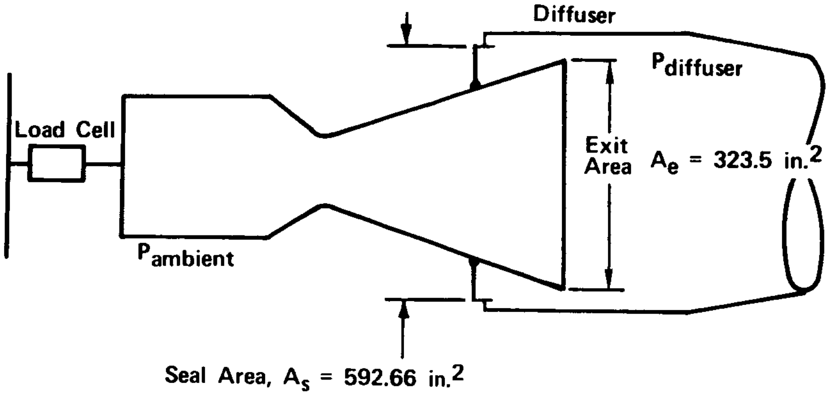

Figure 151. Schematic Diagram of Chamber-Diffuser Installation FD 25688C

3. Performance Parameters

Vacuum thrust and throat total pressure (P_t), determined as outlined in paragraphs 1 and 2 above, were used to calculate the normal thrust chamber and engine performance parameters:

Vacuum Specific Impulse

$$I_{vac} = \frac{F_{vac}}{\dot{w}_o + \dot{w}_f}$$

Characteristic Exhaust Velocity

$$c^*_{(P_c)} = \frac{P_t C_D A_t g_c}{\dot{w}_o + \dot{w}_f}$$

Vacuum Thrust Coefficient

$$C_{F_{vac}} = \frac{F_{vac}}{P_t C_D A_t} = \frac{I_{vac} g_c}{c^*_{(P_c)}}$$

4. Theoretical Performance Parameters

Performance efficiencies were determined using full shifting equilibrium performance values, calculated with thermochemical data published by the Joint Army-Navy-Air Force (JANAF) Thermochemical Panel. Because propellant performance is a function of chamber pressure, mixture ratio, expansion ratio, propellant inlet energy and heat loss to the thrust chamber coolant, curve fits of the theoretical data were stored as permanent data in the computer program employed for performance calculations. The theoretical performance parameters are:

Theoretical Vacuum Specific Impulse

$$I'_{vac} = f_1 \left[P_t,\ r,\ \epsilon,\ \Delta H_i,\ Q \right]$$

and

Theoretical Characteristic Exhaust Velocity

$$c^{*\prime} = f_2 \left[P_t,\ r,\ \Delta H_i,\ Q_c \right]$$

In these equations, P_t, r, and ϵ are the throat total pressure, mixture ratio and expansion ratio respectively; ΔH_i, Q and Q_c are factors which correct the theoretical values to the actual test conditions. The first term, ΔH_i, was used to correct for deviations of the actual injector inlet conditions from the reference normal boiling point liquid inlet state.

The term, Q, in the theoretical impulse equation, represents the heat transferred to the thrust chamber coolant. In water-cooled and separately cooled methane tests, Q was equal to the measured heat loss to thrust chamber coolant. In regenerative tests, Q was also made equal to the heat loss of the fuel coolant; however, since the I_{vac} was based on fuel injector inlet conditions, the resulting value was equivalent to that computed for $Q = O$, but using the thrust chamber inlet fuel temperature as the basis for I_{vac}.

The term, Q_c, in the theoretical c* equation, corresponds to the heat transferred to the combustion chamber wall. In all tests, the measured heat loss to the coolant between the throat and the injector was used as Q_c.

Thus in all cases, the theoretical I'_{vac} and $c^{*\prime}$ values represented values based on injector inlet conditions and were adjusted downward for appropriate heat losses.

5. Performance Efficiencies

The theoretical and measured performance parameters were used to compute the following efficiencies:

Ideal Specific Impulse Efficiency

$$\eta_{I_{vac}} = \frac{I_{vac}}{I'_{vac}} \times 100$$

The discharge coefficient (C_D) used in these equations was established from the curve shown in figure 152. As noted in the figure, the value is equal to 0.985 for the geometry of the 5K thrust chambers. The curve in this figure is from reference 27.

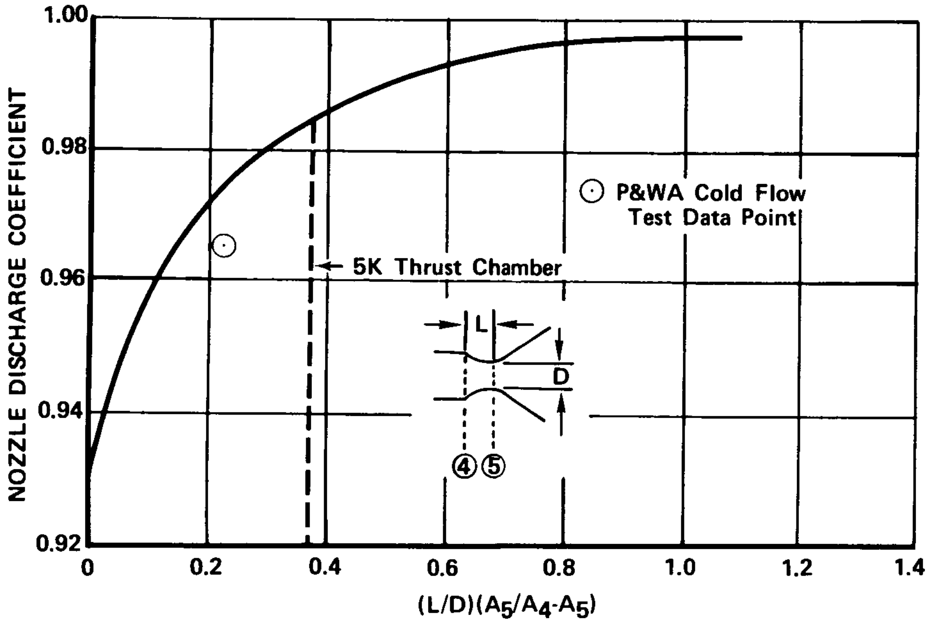

Figure 152. Throat Discharge Coefficient as a Function of the Thrust Chamber Dimensions FD 20974A

The throat area (A_t) used in the calculations represented the measured value corrected for expansion at operating temperatures. In the water-cooled chamber tests, the expansion of the throat was negligible because the backwall of the THERMAL SKIN chamber was very nearly ambient temperature. In the regenerative tests, however, the throat station backwall temperature was appreciably different from ambient (as much as 975°R) and, therefore, the measured throat area was corrected upwards to account for thermal expansion; the maximum correction to the throat area amounted to 0.73%.

Characteristic Exhaust Velocity Efficiency

$$\eta_{c^*_{(P_c)}} = \frac{c^*_{(P_c)}}{c^{*\prime}} \times 100$$

Vacuum Thrust Coefficient Efficiency

$$\eta_{C_{F_{vac}}} = \frac{\eta_{I_{vac}}}{\eta_{c^*_{(P_c)}}} \times 100$$

In the sea level tests, a c* efficiency was calculated from thrust measurements to provide an independent check on chamber pressure based values. It was calculated from the following equation:

$$\eta_{c^*_{(F)}} = \frac{\eta_{I_{vac}}}{C_s}$$

In this equation, ηI_{vac} and C_s are the measured vacuum impulse and the calculated stream thrust coefficient, respectively, for the low expansion ratio (6.5 to 1) nozzles. The C_s value was computed using the method of characteristics and accounts for the effects of wall friction and exit divergence (reference 28).

C. EXPERIMENTAL DATA ERROR ANALYSIS

To validate the experimental performance data, a statistical error analysis was made for a typical injector/chamber test. Estimates of performance data uncertainty were obtained by combining the precision and bias estimates for the individual parameters using a statistical variation analysis (reference 29). Basically, the precision error of a function may be estimated by combining the precision errors of the independent variables of that function in the following manner:

$$S_\phi^2 = \sum_{i=1}^{n} \left(\frac{\partial \phi}{\partial x_i}\right)^2 \left(S_{x_i}\right)^2$$

where:

S_ϕ = estimate of the precision error for the parameter (would be 1σ precision for infinite sample)

$\frac{\partial \phi}{\partial x_i}$ = the partial derivative of the function with respect to the ith variable

S_{x_i} = the precision error estimate value associated with the ith variable.

For example, in calculating characteristic exhaust velocity based on chamber pressure

$$c^*_{(P_c)} = \frac{A_t g_c P_t}{\dot{w}_p}$$

The precision error estimate, S_{c*}, is given by:

$$(S_{c*})^2 = \left(\frac{\partial c*}{\partial A_t}\right)^2 (S_{A_t})^2 + \left(\frac{\partial c*}{\partial P_t}\right)^2 (S_{P_c})^2 + \left(\frac{\partial c*}{\partial \dot{w}_p}\right)^2 (S_{\dot{w}_p})^2$$

where:

$$\left(\frac{\partial c*}{\partial A_t}\right) = \frac{g_c P_t}{\dot{w}_p}$$

$$\left(\frac{\partial c*}{\partial P_c}\right) = \frac{A_t g_c}{\dot{w}_p}$$

$$\left(\frac{\partial c*}{\partial \dot{w}_p}\right) = \frac{A_t g_c P_t}{(\dot{w}_p)^2}$$

The bias limit associated with each function is estimated from identical equations, but substituting the bias limit of each parameter for the precision error. Using the methods suggested by the ICRPG Experimental Measurements Committee (reference 30), the uncertainty of each parameter was calculated from

$$U_\phi = \pm \left[B_\phi + 2S_\phi\right]$$

where B_ϕ is the bias limit and S_ϕ is the precision. The $2S_\phi$ value of the uncertainty, U_ϕ, implies that a 95%-confidence-interval estimate is used to represent the precision portion of uncertainty. U_ϕ therefore represents the limits around the true value beyond which no data would reasonably be expected to fall.

The uncertainty estimates for the engine performance parameters are given in table XXVIII. The uncertainty estimates presented are somewhat pessimistic because, while they reflect the increased accuracy from redundant measurements, they do not reflect the improvement obtained by time averaging.

Table XXVIII. Experimental Error Analysis - Regenerative Chamber Test No. 14.05

Parameter	Units	Nominal	Bias Limit (% of Nominal)	Precision 2S-95% Confidence (% of Nominal)	Uncertainty (% of Nominal)
P_c	$lb_f/in.^2$	494.7	±0.24	±0.15	±0.39
F_{vac}	lb_f	5027	±0.60	±0.54	±1.14
$\dot{w}_o$	lb_m/sec	10.99	±1.02	±0.82	±1.84
$\dot{w}_f$	lb_m/sec	2.19	±1.52	±1.28	±2.80
$\dot{w}_p$	lb_m/sec	13.18	±0.91	±0.68	±1.59
I_{vac}	lb_f-sec/lb_m	381.5	±1.08	±0.90	±1.98
c*	ft/sec	6674	±1.36	±0.73	±2.09
$C_{F\ vac}$	----	1.84	±1.19	±0.56	±1.75

APPENDIX D
REFERENCES

1. "Space Storable Regenerative Cooling Investigation - Interim Report," Pratt & Whitney Aircraft FR-2552, NASA CR-72341, Contract NAS3-11190, 26 July 1968.

2. "Flox/Methane Pump-Fed Engine Study - Final Report," Pratt & Whitney Aircraft FR-3040, NASA CR-72485, Contract NAS3-7950, 10 May 1969.

3. Bittker, David A., "An Analytical Study of Turbulent and Molecular Mixing in Rocket Combustion," NASA TN-4321, September 1958.

4. "Investigation of Light Hydrocarbon Fuels with Flox Mixtures as Liquid Rocket Propellants - Final Report," Pratt & Whitney Aircraft FR-1433, NASA CR-54445, Contract NAS3-4195, 1 September 1965.

5. "Investigation of Light Hydrocarbon Fuels with Fluorine-Oxygen Mixtures as Liquid Rocket Propellants - Final Report," Pratt & Whitney Aircraft FR-2227, NASA CR-72147, Contract NAS3-6296, 15 September 1967.

6. "Investigation of Light Hydrocarbon Fuels with Fluorine-Oxygen Mixtures as Liquid Rocket Propellants - Final Report," Pratt & Whitney Aircraft FR-2872, NASA CR-72425, Contract NAS3-10294, 28 June 1968.

7. "High Energy Advanced Throttling Concept Study - Final Report," Pratt & Whitney Aircraft FR-1573, AFRPL-TR-66-43, Contract AFO 4(611) - 9965, March 1966 (Confidential).

8. "High Energy Advanced Throttling Concept Study - Final Report," Pratt & Whitney Aircraft FR-2366, AFRPL-TR-67-140, Contract AFO 4(611)-11611, May 1967 (Confidential).

9. "Hydrogen-Fluorine Engine Evaluation - Final Report," Pratt & Whitney Aircraft FR-3030, NASA CR-72481, Contract NAS3-7991, December 1968 (Confidential).

10. Priem, R. J. and M. F. Heidmann, "Propellant Vaporization as a Design Criterim for Rocket-Engine Combustion Chambers," NASA TR R-67, 1969.

11. "Users Manual for Chemical Kinetic Analysis (Deck 2)," PWA FR-2888 Supplement 2, Prepared under Contract AF 33 (165)-3128.

12. Ahlberg, J. H., Hamilton, S., Migdol, D., and Nilson, E. N., "Truncated Perfect Nozzles in Optimum Nozzle Design," ARS Journal, May 1961, pp. 614-620.

13. Tong, L. S., Boiling Heat Transfer and Two-Phase Flow, John Wiley and Sons, N. Y., N. Y.

14. Sutton, George P., "Rocket Propulsion Elements," Third Edition, John Wiley and Sons, New, 1964.

15. Schmidt, H. W., "Handling and Use of Fluorine and Fluorine-Oxygen Mixtures in Rocket Systems," NASA SP 3037, 1967.

16. "Final Report of Advanced Throttling Concept Study," Contract AF 04(611)-9575, AFRPL-TR-65-98 and PWA FR 1279, 19 March 1965.

17. "Space Storable Engine Characterization - Final Report," Pratt & Whitney Aircraft FR-3169, NASA CR-72552, Contract NAS3-12010, 24 November 1969.

18. Dankoff, W. E., Johnson, I. A., Conrad, E. W. and Tomazic, W. A., "M-1 Injector Development - Philosophy and Implementation," NASA TN D4730, August 1968.

19. Bartz, D. R., "A Simple Equation for Rapid Estimation of Rocket Nozzle Convective Heat Transfer Coefficients," Jet Propulsion, 27, (49), 1937.

20. Dipprey, Duane F. and Rolf H. Sabersky, "Heat and Momentum Transfer in Smooth and Rough Tubes at Various Prandtl Numbers," CIT, JPL Report No. 32-269, 6 June 1962.

21. Nikuradse, J., "Laws for Flow in Rough Pipes," VDI - Forschungshelf 361, Series B, Vol. 4 (1933); Translation, Brielmaier, A. A., NACA TM 1292 (1950).

22. Kraus, A. D., "Heat Flow Theory and Extended Surfaces for Heat Transfer," C-M Technical Publication Corporation, New York 17, New York, 1961.

23. Maurer, G. W. and B. W. LeTourneau, "Friction Factors for Fully Developed Turbulent Flow in Ducts With and Without Heat Transfer," ASME Paper No. 63-WA-98.

24. Keenan, J. H. and F. G. Keyes, "Thermodynamic Properties of Steam," John Wiley and Sons, New York, New York.

25. "Investigation of Cooling Problems at High Chamber Pressures - Final Report," R-6529, Contract NAS8-20225, 15 September 1966.

26. "Resarch on a Hydrogen-Fluorine Propulsion System - Final Report," Pratt & Whitney Aircraft FR-1585, NASA CR-72074, Contract NASw-754, 21 October 1966, CONFIDENTIAL (Title Unclassified).

27. "Performance Characteristics of Compound A/Hydrazine Propellant Combinations," Rocketdyne Report TR-65-107, prepared under Contract AF04(611)-9573, May 1963 (Confidential).

28. "Digital Computer Programs for Rocket Nozzle Design and Analysis - Volume II - Bell Nozzle Design," Pratt & Whitney Aircraft, FR1021, pepared under Contract NAS9-2487, 26 June 1964.

29. Colbert, D. L., "Use of Partial Deviation in Variation Analysis," Pratt and Whitney Aircraft, FR1993, 30 September 1966.

30. "ICRPG Handbook for Estimating the Uncertainty in Measurements Made with Liquid Propellant Rocket Engine Systems," CPIA Publication, No. 180, prepared by Pratt & Whitney Aircraft for the ICRPG Performance Standardization Working Group, May 1969.

APPENDIX E
DISTRIBUTION LIST FOR FINAL REPORT
NASA CR-72704

Report Copies			
R	D	Recipient	Designee
		National Aeronautics & Space Administration Lewis Research Center 21000 Brookpark Road Cleveland, Ohio 44135	
1		Attn: Contracting Officer, MS 500-313	
5		Liquid Rocket Technology Branch, MS 500-203	
1		Technical Report Control Office, MS 5-5	
1		Technology Utilization Office, MS 3-16	
2		AFSC Liaison Office, MS 501-3	
2		Library, MS 60-3	
1		Office of Reliability & Quality Assurance MS 500-111	
1		D. L. Nored, Chief, LRTB, MS 500-203	
3		J. W. Gregory, Project Manager, MS 500-209	
1		E. W. Conrad, MS 500-204	
1		N. P. Hannum, MS 500-204	
1		R. H. Knoll, MS 501-2	
1		W. A. Tomazic, MS 500-204	
		National Aeronautics & Space Administration Washington, D. C. 20546	
2		Attn: Chief, Liquid Experimental Engineering, RPX, Office of Advanced Research & Technology	
2		Chief, Liquid Propulsion Technology, RPL, Office of Advanced Research & Technology	
1		Director, Launch Vehicle & Propulsion, SV, Office of Space Science & Applications	
1		Chief, Environmental Factors & Aero., RV-1, Office of Advanced Research & Technology	
1		Director, Advanced Manned Missions, MT	
1		Director, Technology Utilization Office, KT	
1		Chief, Space Vehicles Structures (OART)	
6		NASA Scientific & Technical Information Facility P. O. Box 33 College Park, Maryland 20740	

Report Copies			
R	D	Recipient	Designee
1		National Aeronautics & Space Administration Ames Research Center Moffett Field, California 94035 Attn: Library	Hans M. Mark Mission Analysis Division
1		National Aeronautics & Space Administration Flight Research Center Greenbelt, Maryland 20771 Attn: Library	Merland L. Moseson Code 620
1		National Aeronautics & Space Administration John F. Kennedy Space Center Cocoa Beach, Florida 32931 Attn: Library	Dr. H. Kurt Debus
1		National Aeronautics & Space Administration Langley Research Center Langley Station Hampton, Virginia 23365 Attn: Library	E. Cortright Director
1		National Aeronautics & Space Administration Manned Spacecraft Center Houston, Texas 77001 Attn: Library	J. Thibodaux, Jr. Chief, Propulsion & Power Division
1		National Aeronautics & Space Administration George G. Marshall Space Flight Center Huntsville, Alabama 35812 Attn: Library	Hans G. Paul L. J. Hastings James Thomas D. L. Burrows I. C. Yates C. D. Nevins J. F. Blumrich
1		Office of the Director of Defense Research and Engineering Washington, D. C. 20301 Attn: Office of Assistant Director (Chemical Technology)	
1		Jet Propulsion Laboratory 4800 Oak Grove Drive Pasadena, California 91103 Attn: Library	Henry Burlage, Jr. Duane Dipprey

Report Copies		Recipient	Designee
R	D		
1		Defense Documentation Center Cameron Station, Building 5 5010 Duke Street Alexandria, Virginia 22314 Attn: TISIA	
1		RTD (RTNP) Bolling Air Force Base Washington, D. C. 20332	
1		Arnold Engineering Development Center Air Force Systems Command Tullahoma, Tennessee 37389 Attn: Library	Dr. H. K. Doetsch
1		Advanced Research Projects Agency Washington, D. C. 20525 Attn: Library	
1		Aeronautical Systems Division Air Force Systems Command Wright-Patterson Air Force Base Dayton, Ohio Attn: Library	D. L. Schmidt Code: ARSCNC-2
1		Air Force Missile Test Center Patrick Air Force Base, Florida Attn: Library	L. J. Ullian
1		Air Force Systems Command Andrews Air Force Base Washington, D. C. 20332 Attn: Library	Capt. S. Bowen SCLT
1		Air Force Rocket Propulsion Laboratory (RPR) Edwards, California 93523 Attn: Library	
1		Air Force Rocket Propulsion Laboratory (RPM) Edwards, California 93523 Attn: Library	
1		Air Force FTC (FTAT-2) Edwards Air Force Base, California 93523 Attn: Library	Donald Ross
1		Air Force Office of Scientific Research Washington, D. C. 20333 Attn: Library	Dr. J. F. Masi SREP

Report Copies		Recipient	Designee
R	D		
1		Space & Missile Systems Organization Air Force Unit Post Office Los Angeles, California 90045 Attn: Technical Data Center	
1		Office of Research Analyses (OAR) Holloman Air Force Base, New Mexico 88330 Attn: Library RRRD	
1		U. S. Air Force Washington, D. C. Attn: Library	Col. C. K. Stambaugh Code: AFRST
1		Commanding Officer U. S. Army Research Office (Durham) Box CM, Duke Station Durham, North Carolina 27706 Attn: Library	
1		U. S. Army Missile Command Redstone Scientific Information Center Redstone Arsenal, Alabama 35808 Attn: Document Section	Dr. W. Wharton
1		Bureau of Naval Weapons Department of the Navy Washington, D. C. Attn: Library	J. Kay Code: RTMS-41
1		Commander U. S. Naval Missile Center Point Mugu, California 93041 Attn: Technical Library	
1		Commander U. S. Naval Weapons Center China Lake, California 93557 Attn: Library	
1		Commanding Officer Naval Research Branch Office 1030 E. Green Street Pasadena, California 91101 Attn: Library	

Report Copies			
R	D	Recipient	Designee
1		Director (Code 6180) U. S. Naval Research Laboratory Washington, D. C. 20390 Attn: Library	H. W. Carhart J. M. Krafft
1		Picatinny Arsenal Dover, New Jersey 07801 Attn: Library	I. Forsten
1		Air Force Aero Propulsion Laboratory Research & Technology Division Air Force Systems Command U. S. Air Force Wright-Patterson AFB, Ohio 45433 Attn: APRP (Library)	R. Quigley C. M. Donaldson
1		Electronics Division Aerojet-General Corporation P. O. Box 296 Azusa, California 91703 Attn: Library	W. L. Rogers
1		Space Division Aerojet-General Corporation 9200 East Flair Drive El Monte, California 91734 Attn: Library	S. Machlawski
1		Aerojet Ordnance and Manufacturing Aerojet-General Corporation 11711 South Woodruff Avenue Fullerton, California 90241 Attn: Library	
1		Aerojet Liquid Rocket Company P. O. Box 13222 Sacramento, California 95813 Attn: Technical Library 2484-2015A	R. Stiff
1		Aeronutronic Division of Philco Ford Corporation Ford Road Newport Beach, California 92663 Attn: Technical Information Department	Dr. L. H. Linder
1		Aerospace Corporation 2400 E. El Segundo Blvd. Los Angeles, California 90045 Attn: Library - Documents	J. G. Wilder

Report Copies			
R	D	Recipient	Designee
1		Aerojet Liquid Rocket Company P. O. Box 13222 Sacramento, California 95813 Attn: Technical Library 2484-2015A	R. Stiff
1		Aeronutronic Division of Philco Ford Corporation Ford Road Newport Beach, California 92663 Attn: Technical Information Department	Dr. L. H. Linder
1		Aerospace Corporation 2400 E. El Segundo Blvd. Los Angeles, California 90045 Attn: Library - Documents	J. G. Wilder
1		Arthur D. Little, Inc. 20 Acorn Park Cambridge, Massachusetts 02140 Attn: Library	A. C. Tobey
1		Astropower Laboratory McDonnell-Douglas Aircraft Company 2121 Paularino Newport Beach, California 92163 Attn: Library	
1		ARO, Incorporated Arnold Engineering Development Center Arnold AF Station, Tenneessee 37989 Attn: Library	
1		Susquehanna Corporation Atlantic Research Division Shirley Highway & Edsall Road Alexandria, Virginia 22314 Attn: Library	
1		Beech Aircraft Corporation Boulder Facility Box 631 Boulder, Colorado Attn: Library	Douglas Pope
1		Bell Aerosystems, Inc. Box 1 Buffalo, New York 14240 Attn: Library	T. Reinhardt W. M. Smith

Report Copies		Recipient	Designee
R	D		
1		Instruments & Life Support Division Bendix Corporation P. O. Box 4508 Davenport, Iowa 52808 Attn: Library	W. M. Carlson
1		Bellcomm 955 L'Enfant Plaza, S. W. Washington, D. C. Attn: Library	H. S. London
1		Boeing Company Space Division P. O. Box 868 Seattle, Washington 98124 Attn: Library	J. D. Alexander C. F. Tiffany
1		Boeing Company 1625 K. Street, N. W. Washington, D. C. 20006	
1		Boeing Company P. O. Box 1680 Huntsville, Alabama 35801	Ted Snow
1		Chemical Propulsion Information Agency Applied Physics Laboratory 8621 Georgia Avenue Silver Spring, Maryland 20910	Tom Reedy
1		Chrysler Corporation Missile Division P. O. Box 2628 Detroit, Michigan Attn: Library	John Gates
1		Chrysler Corporation Space Division P. O. Box 29200 New Orleans, Louisiana 70129 Attn: Librarian	
1		Curtiss-Wright Corporation Wright Aeronautical Division Woodridge, New Jersey Attn: Library	G. Kelley

Report Copies		Recipient	Designee
R	D		
1		University of Denver Denver Research Institute P. O. Box 10127 Denver, Colorado 80210 Attn: Security Office	
1		Fairchild Stratos Corporation Aircraft Missiles Division Hagerstown, Maryland Attn: Library	
1		Research Center Fairchild Hiller Corporation Germantown, Maryland Attn: Library	Ralph Hall
1		Republic Aviation Fairchild Hiller Corporation Farmington, Long Island New York	
1		General Dynamics/Conviar P. O. Box 1128 San Diego, California 92112 Attn: Library	Frank Dore
1		Missiles and Space Systems Center General Electric Company Valley Forge Space Technology Center P. O. Box 8555 Philadelphia, Pennsylvania 19101 Attn: Library	A. Cohen F. Schultz
1		General Electric Company Flight Propulsion Laboratory Department Cincinnati, Ohio Attn: Library	D. Suichu
1		Grumman Aircraft Engineering Corporation Bethpage, Long Island, New York Attn: Library	Joseph Gavin
1		Hercules Powder Company Allegheny Ballistics Laboratory P. O. Box 210 Cumberland, Maryland 21501 Attn: Library	

Report Copies			
R	D	Recipient	Designee
1		Honeywell, Inc. Aerospace Division 2600 Ridgeway Road Minneapolis, Minnesota Attn: Library	
1		IIT Research Institute Technology Center Chicago, Illinois 60616 Attn: Library	C. K. Hersh
1		Kidde Aero-Space Division Walter Kidde & Company, Inc. 567 Main Street	R. J. Hanville
1		Ling-Temco-Vought Corporation P. O. Box 5907 Dallas, Texas 75222 Attn: Library	
1		Lockheed Missiles & Space Company P. O. Box 504 Sunnyvale, California 94087 Attn: Library	
1		Lockheed Propulsion Company P. O. Box 111 Redlands, California 92374 Attn: Library, Thackwell	H. L. Thackwell
1		Marquardt Corporation 16555 Saticoy Street Box 2013 - South Annex Van Nuys, California 91409	L. R. Bell, Jr.
1		Martin-Marietta Corporation (Baltimore Division) Baltimore, Maryland 21203 Attn: Library	
1		Denver Division Martin-Marietta Corporation P. O. Box 179 Denver, Colorado 80201 Attn: Library	Dr. Morganthaler F. Schwartzberg

Report Copies R	D	Recipient	Designee
1		Orlando Division Martin-Marietta Corporation Box 5827 Orlando, Florida Attn: Library	J. Fern
1		Western Division McDonnell-Douglas Astronautics 5301 Bolsa Avenue Huntington Beach, California 92647 Attn: Library	R. W. Hallet G. W. Burge P. Klevatt
1		McDonnell Douglas Aircraft Corporation P. O. Box 516 Lambert Field, Missouri 63166 Attn: Library	R. A. Herzmark
	1	Rocketdyne Division North American Rockwell Inc. 6633 Canoga Avenue Canoga Park, California 91304 Attn: Library, Dept. 596-306	Dr. R. J. Thompson
1			S. F. Iacobellis
1			R. Pauckert
1		Space & Information Systems Division North American Rockwell 12214 Lakewood Blvd. Downey, California Attn: Library	
1		Northrop Space Laboratories 3401 West Broadway Hawthorne, California Attn: Library	Dr. Wm. Howard
1		Purdue University Lafayette, Indiana 47907 Attn: Library (Technical)	Dr. B. Reese
1		Radio Corporation of America Astro-Electronics Products Princeton, New Jersey Attn: Library	
1		Rocket Research Corporation Willow Road at 116 Street Redmond, Washington 98052 Attn: Library	F. McCullough, Jr.

Report Copies		Recipient	Designee
R	D		
1		Stanford Research Institute 333 Ravenswood Avenue Menlo Park, California 94025 Attn: Library	Dr. G. Marksman
1		Thiokol Chemical Corporation Redstone Division Huntsville, Alabama Attn: Library	John Goodloe
1 1		TRW Systems Inc. 1 Space Park Redondo Beach, California 90278 Attn: Tech. Lib. Doc. Acquisitions	D. H. Lee H. Burge
1		United Aircraft Corporation Corporation Library 400 Main Street East Hartford, Connecticut 06108 Attn: Library	Dr. David Rix Erle Martin Frank Owen Wm. E. Taylor
1		United Aircraft Corporation United Technology Center P. O. Box 358 Sunnyvale, California 94038 Attn: Library	Dr. D. Altman
1		Vickers, Inc. Box 302 Troy, Michigan	
1		Vought Astronautics Box 5907 Dallas, Texas Attn: Library	